SYNTHESES OF DERIVATIZED CAPPED IRON(II) PORPHYRIN COMPLEXES AND THEIR INTERACTION WITH CO AND O_2

by

Hang Tang

B. Sc., Peking University, P.R. China, 1982

A THESIS SUBMITTED IN PARTIAL FULFILMENT OF

THE REQUIREMENTS FOR THE DEGREE OF

DOCTOR OF PHILOSOPHY

IN

THE FACULTY OF GRADUATE STUDIES

DEPARTMENT OF CHEMISTRY

WE ACCEPT THIS THESIS AS CONFORMING

TO THE REQUIRED STANDARD

THE UNIVERSITY OF BRITISH COLUMBIA
AUGUST, 1990

In presenting this thesis in partial fulfilment of the requirements for an advanced degree at the University of British Columbia, I agree that the Library shall make it freely available for reference and study. I further agree that permission for extensive copying of this thesis for scholarly purposes may be granted by the head of my department or by his or her representatives. It is understood that copying or publication of this thesis for financial gain shall not be allowed without my written permission.

Department of chemistry

The University of British Columbia
Vancouver, Canada

Date Oct. 11, 1990

DE-6 (2/88)

Abstract

The affinity of hemoglobin for CO relative to O_2 is decreased compared to simple iron-porphyrin systems mainly due to electronic effects. Hydrogen-bond formation with the His E7 residue of hemoglobin has been revealed to stabilize the bound dioxygen. This thesis describes the development of a series porphyrin models, benzene-4/4 (**49a**), benzene-5/5 (**49b**), amidobenzene-4/4 (**49c**) and amidobenzene-5/5 (**49d**) capped porphyrins, which serve as simple models to imitate the hydrogen bonding in hemoglobin.

The chain linked bis pyrroles **38** were synthesized by Friedel-Crafts acylation of the benzene and nitrobenzene diacid chain derivatives with two equivalents of the β-unsubstituted pyrrole **36**, followed by diborane reduction of the ketonic groups. After the nitro functions were transformed to the acetamides, modification of the ethyl ester functions of **38a**, **38b** and **39** via the benzylesters **40**, the carboxypyrroles **41** and the α-unsubstituted pyrroles **42** afforded the important bis formyl pyrroles **43**. The cyanoacrylate protected formyl pyrrole derivatives **44** were subjected to monochlorination at the α-methyl groups followed by condensation with two equivalents of the α-unsubstituted pyrrole **46** to give dipyrromethane dimers **47**. Strong aqueous alkali caused saponification of the two ester groups and deprotection of the formyl functions to give **48**. The α-formyl-α′-unsubstituted dipyrromethane dimer, resulting from the thermal decarboxylation of **48**, was cyclized to produce the porphyrin **49** in acidic medium.

The interactions of CO and O_2 with the heme derivatives, Fe^{II}(porphyrin)(DcIm), have been studied. The CO binding constant of the amide substituted heme is two fold

larger than that of the non-amide substituted heme. In contrast, the low temperature (-45°C) O_2 binding constants of the hemes have shown a 6-8 fold increase from nonamide to amide substituted hemes, probably because of a hydrogen bonding between the amide function and bound dioxygen similar to the hydrogen bonding in hemoglobin.

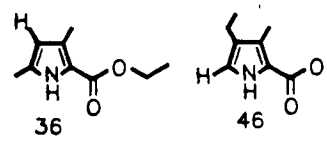

36 46

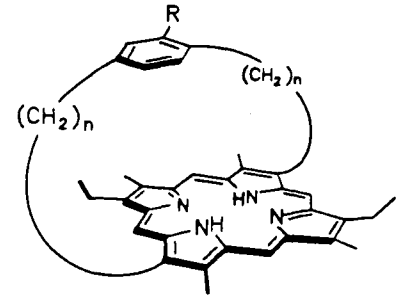

49a n=4, R=H
49b n=5, R=H
49c n=4, R=NHCOCH$_3$
49d n=5, R=NHCOCH$_3$

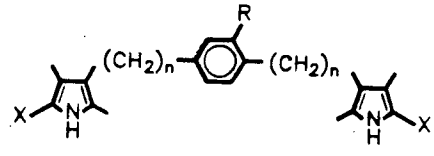

38 X=CO_2Et
39 X=CO_2Et
40 X=CO_2CH_2Ph
41 X=CO_2H
42 X=H
43 X=CHO
44 X=C(H)=C(CN)CO_2CH_3

a n=4, R=H
b n=5, R=H
c n=4, R=NO_2(38) or NHCOCH$_3$(39, 40, 41, 42, 43, 44)
d n=5, R=NO_2(38) or NHCOCH$_3$(39, 40, 41, 42, 43, 44)

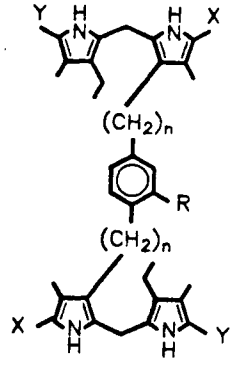

	X	Y
47	C(H)=C(CN)CO_2CH_3	CO_2Et
48	CHO	CO_2H

a n=4, R=H
b n=5, R=H
c n=4, R=NHCOCH$_3$
d n=5, R=NHCOCH$_3$

Table of Contents

List of Tables

List of Figures

List of Abbreviations

atm	atmosphere
B	base
DcIm	1,5-dicyclohexylimidazole
diglyme	dimethylether of diethylene glycol
DMF	N,N-dimethylformamide
DMSO	dimethyl sulfoxide
DPG	2,3-diphosphoglycerate
ESR	electron spin resonance
FAB	fast atom bombardment
Hb	hemoglobin
HbO_2	oxyhemoglobin
His	histidine
^{1}H-nmr	proton nuclear magnetic resonance
IHP	inositol hexaphosphate
k_{off}	dissociation rate constant
k_{on}	association rate constant
L	ligand: CO or O_2
Mb	myoglobin
MbO_2	oxymyoglobin
MeIm	1-methylimidazole
MO	molecular orbital

M. P.	melting point
N_{porph}	pyrrole nitrogens
Por	porphyrin
t-bu	tert-butyl
TFA	trifluoroacetic acid
THF	tetrahydrofuran
TLC	thin layer chromatography
TMS	tetramethylsilane
TPP	meso-tetraphenylporphyrin
$T_{piv}PP$	tetra(α,α,α,α-o-pivalamidophenyl)porphyrin
Val	valine

Abbreviations in UV/visible and nmr assignments

br	broad rise	λ(nm)	wavelength in nanometers
bs	broad singlet	A	absorbance
d	doublet	ε	extinction coefficient
m	multiplet	sh	shoulder
q	quartet		
s	singlet		
t	triplet		

Acknowledgements

I wish to express my sincere gratitude to Professor David Dolphin for his guidance and encouragement throughout this work.

I would like to extend special thanks to Dr. Tilak Wijesekera for his many invaluable suggestions and discussions during the synthetic work, and for his assistance with the preparation of this thesis.

Thanks are due to Professor Brian R. James for helpful discussions on binding studies.

Finally, I would like to take this opportunity to thank all the members of Professor Dolphin's research group, over the years, for making my stay at U. B. C. a pleasant one.

Chapter 1

Introduction

1.1.1 The porphyrin macrocycle[1]

All porphyrins are derived from porphin (**1**) by substitution of peripheral H atoms with side chains. In the Fischer system of nomenclature, the peripheral positions are

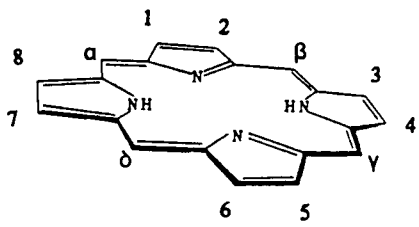

1

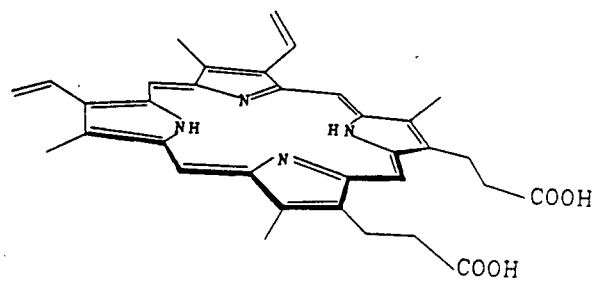

2

numbered 1 - 8 and the methine (meso) positions are designated α, β, γ and δ. Various substitution patterns at the periphery give rise to several naturally occurring porphyrins. The iron complex of protoporphyrin-IX (**2**) is the prosthetic group of hemoglobin, myoglobin, peroxidases, oxidases and many cytochromes.[2]

The heterocyclic ring of a porphyrin contains 24 atoms forming a highly aromatic system with 18 conjugated π electrons. Unlike smaller aromatics, however, highly distorted porphyrin systems do exist.[3] Skeletal distortion occurs in two ways: ruffling and doming. Doming of a porphyrin occurs when all of four pyrrole nitrogens are out of the porphyrin plane on the same side. Ruffling of a porphyrin results when opposite

pyrrole nitrogens are out of the porphyrin plane on the same side and adjacent pyrrole nitrogens are out of the plane on the opposite sides. These deformations tend to minimize angular bond strain at α, β, γ and δ meso positions. However, there is little loss in aromatic stabilization since individual pyrrole rings tend to remain planar.

The two protons attached to the nitrogens in a porphyrin are readily ionizable resulting in the porphyrin dianion. These dianions are very stable tetradentate ligands towards a variety of metal ions. Due to the high degree of electron delocalization, both porphyrins and metalloporphyrins are highly colored compounds with characteristic spectra in the UV/visible range.

1.1.2 Iron spin state and geometry[4]

The neutral four-coordinate Fe(II)-porphyrin moiety can coordinate a variety of ligands in the remaining two axial positions. The ligands include species bearing lone pair electrons for donation to the metal center. The ferrous ion contains six d-electrons which can populate the orbitals as shown in Fig. 1.1. It can exhibit three spin states: S = 0, low spin; S = 1, intermediate spin; and S = 2, high spin state. The spin state and stereochemistry of the iron(II) center is controlled almost entirely by the nature and number of axial ligands. The coordination of strong field ligands such as imidazole, CO and O_2 leads to low spin six-coordinate hemes. Weaker field ligands, typically anionic ones such as chloride and azide, lead to five-coordinate high spin derivatives.

The d-orbital populations for the five and six-coordinate states seen in hemoproteins are shown in Fig. 1.1. When ferrous heme is coordinated by only one imidazole, it is high spin and out of plane towards the imidazole yielding a roughly square pyramidal bonding geometry. When coordinated by two imidazoles or an imidazole and CO, the iron is low spin and located much closer to or within the

porphyrin plane to form an octahedral type complex.

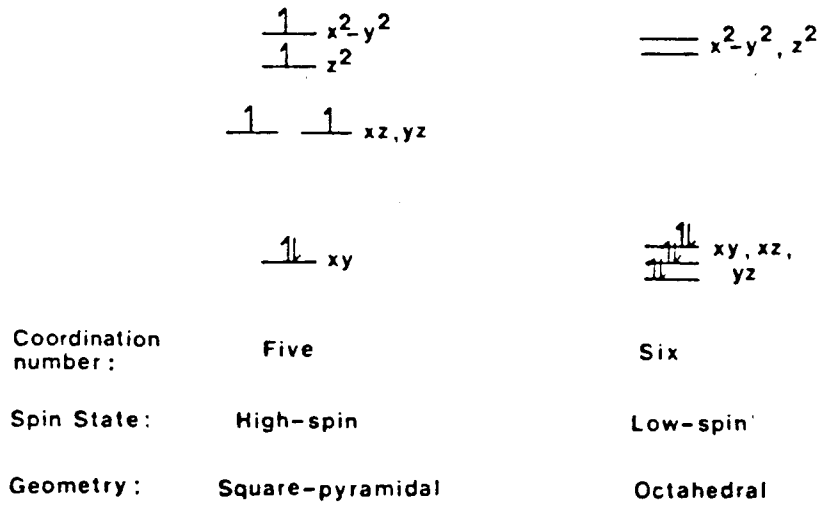

Fig. 1.1 d-orbital populations for five and six-coordinate (d^6)Fe(II)

1.2 The structure and functions of hemoglobin

1.2.1 Hemoglobin structure and cooperativity

Hemoglobins are essential to the life of all vertebrates; they also occur in some invertebrates and in the root nodules of leguminous plants. The main task of hemoglobin is to convey oxygen from the lungs to the tissues and facilitate the return of carbon dioxide from the tissues back to the lungs. Another hemoprotein in the muscle, monomeric myoglobin, combines with the oxygen released by hemoglobin, stores it and transports it to mitochondria, where the oxygen generates chemical energy by the "combustion" of glucose to carbon dioxide and water.

Hemoglobin is a tetramer of molecular weight 64,500 and consists of four polypeptide chains; two α chains each containing 141 amino acid residues and two β chains each containing 146 amino acid residues. Each chain has a prosthetic heme

group (the active site), iron(II) protoporphyrin IX. The α and β chains (subunits) have different sequences of amino acids but fold up to form similar three-dimensional structures. Each α subunit is linked to a β unit to give two sets of dimers, α1β1 and α2β2. These dimers are in turn held together so as to form α1β2 and α2β1 contacts which make up the overall quaternary structure of the tetramer.[5]

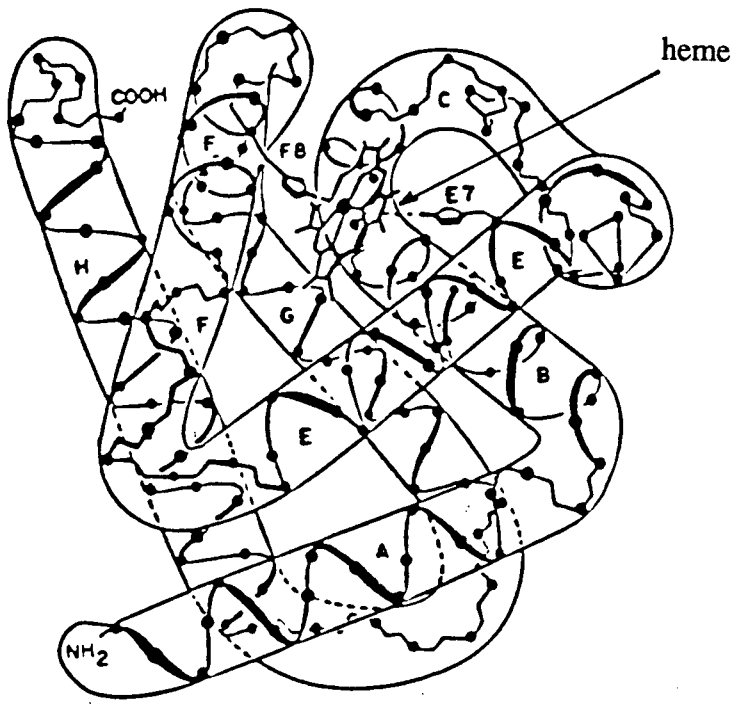

Fig. 1.2 Tertiary structure surrounding the heme prosthetic group of hemoglobin subunits[5]

The hemes in Hb are held separately in protein pockets formed by several helical and non helical segments (Fig. 1.2). Helices E and F constitute the "distal" and "proximal" sides of the heme, respectively. The iron of the heme is 5-coordinated to the four porphyrin nitrogens (N_{porph}) and N_ϵ of the proximal histidine F8 which is the only covalent linkage between the heme and the protein. The porphyrin is in van der Waals contact with another histidine on the distal side (E7) and also makes contact

with 18 other amino acid side chains, most of which are nonpolar.

The oxygen transport property of hemoglobin is dependent upon the ability of its ferrous iron binding O_2 reversibly instead of being irreversibly oxidized. Hemoglobin binds oxygen cooperatively[5] with a free energy of cooperativity of 3.5 kcal/mol under physiological conditions, this corresponds to the rise in O_2 affinity between zero and full oxygen saturation being about 500-fold.[6]

The cooperative binding of dioxygen by hemoglobin is manifested by its sigmoidal equilibrium curve[7] (Fig. 1.3). It ensures uptake and release of dioxygen over

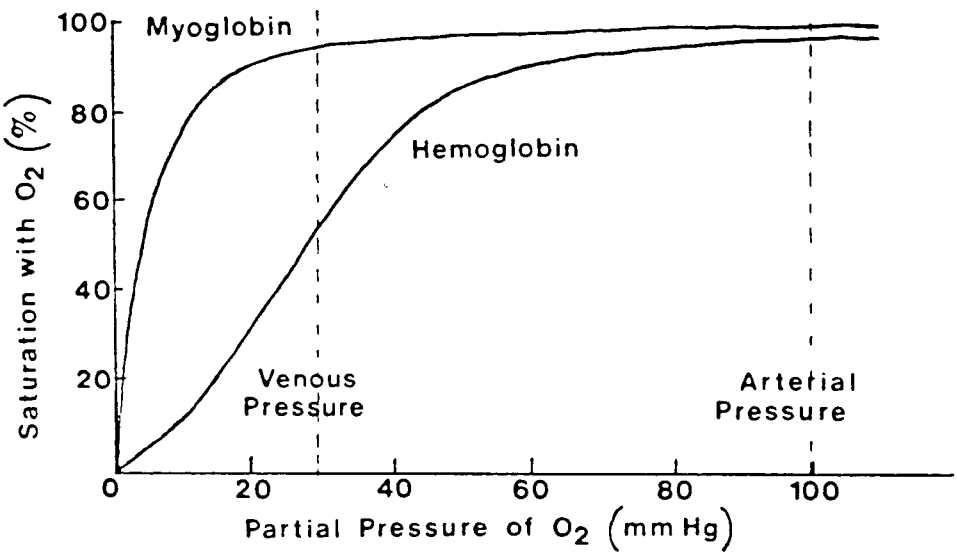

Fig. 1.3 Saturation curves for dioxygen binding to hemoglobin and myoglobin

the comparatively narrow range of partial O_2 pressures that distinguish the lungs (Po_2 ~100 mm Hg) from the tissues (Po_2 ~30-40 mm Hg). The oxygen equilibrium curve of single chain hemoglobin, such as the one found in myoglobin, is hyperbolic.[7]

The oxygen affinity of hemoglobin rises with increasing oxygen binding so that a sigmoidal oxygen equilibrium curve results. Initially, hemoglobin is reluctant to take up

oxygen, but its affinity increases with oxygen uptake. At arterial oxygen pressure, both myoglobin and hemoglobin are nearly saturated. But at venous pressure, myoglobin gives up only about 10 percent of its oxygen, whereas hemoglobin releases roughly half. At any partial pressure of O_2, myoglobin has a higher O_2 affinity than hemoglobin, which allows oxygen to be transferred from the blood to the muscle.

Studies on ligation to myoglobin[7] indicate a first order dependence on oxygen

$$Mb + O_2 \underset{}{\overset{K_{Mb}^{O2}}{\rightleftharpoons}} MbO_2$$

concentration, where the equilibrium constant is defined by:

$$K_{Mb}^{O2} = \frac{[MbO_2]}{[Mb][O_2]}$$

The sigmoidal curve of hemoglobin[7] bearing four active sites indicates a greater than first order dependence on oxygen concentration,

$$(Hb)_n + nO_2 \underset{}{\overset{K_{Hb}^{O2}}{\rightleftharpoons}} (HbO_2)_n$$

With the affinity constant defined by:

$$K_{Hb}^{O2} = \frac{[HbO_2]_n}{[Hb]_n[O_2]^n}$$

Hill's equation fits the experiment best for a Hill's constant n ~2.7.

The oxygen affinity of hemoglobin is also modulated by protons, chloride ions, 2,3-diphosphoglycerate (DPG) and inositol hexaphosphate (IHP), known collectively as the heterotropic ligands.[8, 9] Increasing the concentration of any one of the heterotropic ligands shifts the oxygen equilibrium curve of the hemoglobin to the right, towards lower oxygen affinity, and a more sigmoidal oxygen equilibrium curve results.

The cooperative effects of hemoglobin are due to an equilibrium between two alternative quaternary structures of the tetramer, the deoxy or T and the oxy or R structure. Owing to the ingenious and laborious work of Kendrew *et al.*[10] and Perutz,[5] we now have clear structural pictures of hemoglobin and myoglobin. Crystallographic analyses of deoxy- and oxyhemoglobin have revealed differences in their structures and therefore made it possible to investigate the mechanism of cooperativity. The arrangement of the subunits (quaternary structure) and the conformation of the subunits (tertiary structure) of R and T states have been found to be different. The quaternary T→R transition consists of a rotation of the dimer $\alpha 2\beta 2$ relative to $\alpha 1\beta 1$ by 12 - 15° and a translation of one dimer relative to the other by 0.8 Å[11] (Fig. 1.4).

In deoxyhemoglobin,[12] the iron is high-spin ferrous (S = 2) and five-coordinate. The iron atoms of the α and β hemes are displaced from the mean planes of N_{porph} resulting in the doming of the porphyrins towards the proximal histidine F8. The imidazole ring of the proximal histidine F8 is in an asymmetric position with respect to the porphyrin nitrogens of the heme (Fig. 1.5).[11, 12] Quantitative energy calculations[13] have indicated that the steric repulsion between the asymmetric axial imidazole and the porphyrin ring causes the doming of Fe towards the proximal imidazole. Studies by crystallography[14, 15] have revealed that the tight packing of the heme and the intersubunit contacts inhibit the iron from assuming symmetrical R-like coordination and the heme from becoming planar. However, there is little strain on the heme in deoxyhemoglobin.

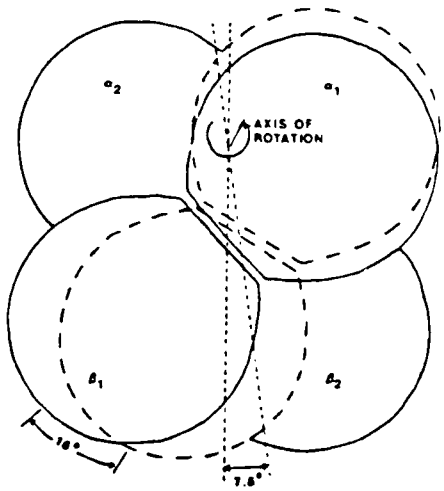

Fig. 1.4 Changes of quaternary structure of hemoglobin on transition from T (full lines) to R (broken lines)[5(c)]

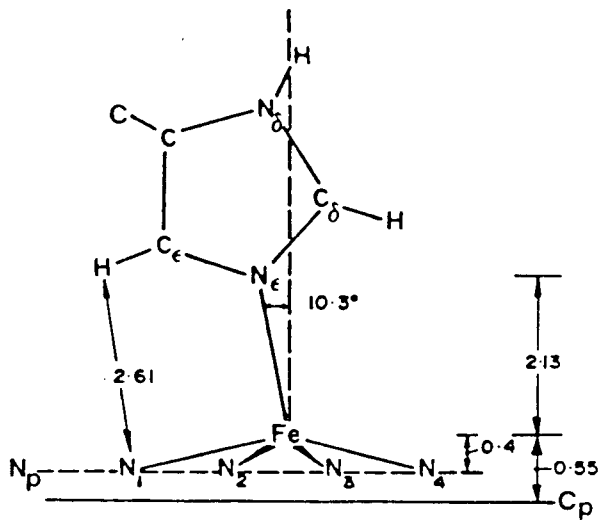

Fig. 1.5 Proximal environment of deoxy-hemoglobin, the distances are measured in Å[6]

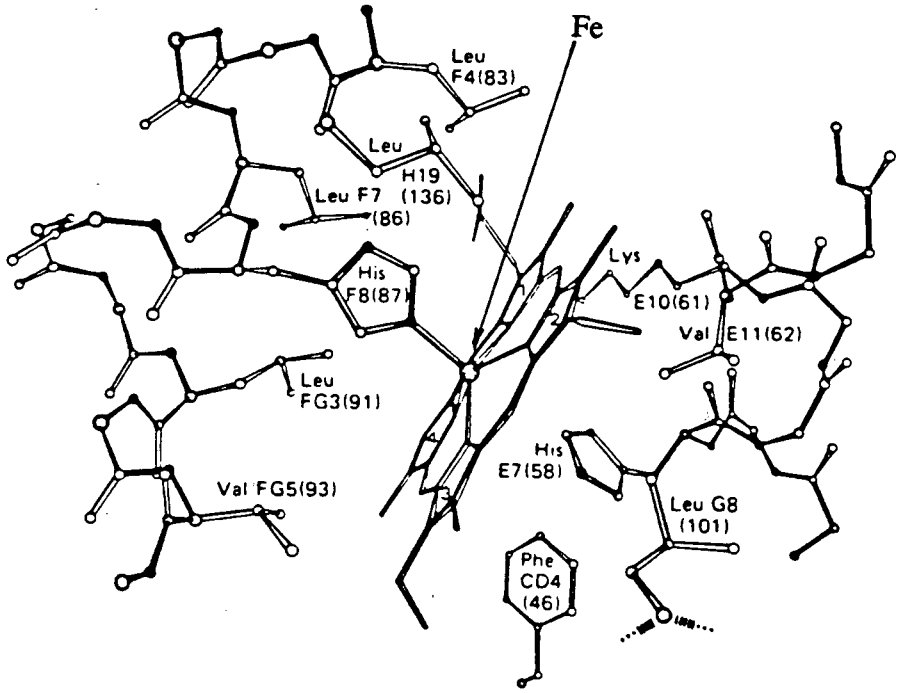

Fig. 1.6 Protein residues that comprise the proximal and distal environments of the heme[13(a)]

On the distal side of the β subunit, valine E11, histidine E7, and phenylalanine CD4 residues are in close proximity to the heme, and occupy the space that would be required for a sixth ligand to coordinate (Fig. 1.6).

In the relaxed (R) oxyhemoglobin,[16] the iron atoms become low-spin (S = 0) and six-coordinate. The heme group appears to be nearly planar in the α subunit but ruffled in the β subunit, and the iron atom has moved towards the porphyrin plane. As a result the proximal histidine comes closer to the porphyrin plane in oxy- than in deoxyhemoglobin. The position of His F8 relative to the heme becomes more symmetric, the geometry of which reduces steric repulsions between the imidazole and porphyrin nitrogens.[11] On the distal side of the β subunit, the Val E11 side chain

whose presence hinders ligand binding in deoxyhemoglobin has shifted away.

1.2.2 Role of the distal residues

Free ferrous porphyrins are rapidly oxidized by oxygen, and their affinity for oxygen is several thousand times less than for carbon monoxide. Globin keeps iron from being oxidized, which is necessary because only ferrous iron combines reversibly with oxygen, and also discriminates in favor of oxygen against carbon monoxide.

Stabilization of the bound dioxygen moiety via hydrogen-bonding with the His E7 residue was first suggested in view of the electronic picture of an end-on coordinated geometry in the distal pocket by Pauling.[17] Infrared[18] and resonance Raman[19] appear to support this hypothesis indirectly. Kinetic studies[20] of the O_2, CO and isocyanide binding properties of a variety of vertebrate and invertebrate heme proteins have indicated that the distal histidine is capable of forming a hydrogen bond with bound dioxygen molecules. The strength of this hydrogen bond was estimated to be 2 and 1 kcal/mol for mammalian myoglobin and hemoglobin, respectively. ESR spectra[21-23] of some myoglobins and hemoglobins have also provided more direct evidence for such H-bonding.

The first direct evidence of the H-bonding was provided by a neutron diffraction study of oxymyoglobin that yielded the N···O_2 distance of 2.97 Å[24] (Fig. 1.7). This was followed by X-ray analysis of oxyhemoglobin which gave the N···O_2 distances of 2.7 and 3.2-3.4 Å for the α and β subunits, respectively.[16, 25] Therefore, in the α subunits of hemoglobin, N_ε of the distal histidine forms a hydrogen bond with the terminal oxygen atom and stabilizes O_2 bound to the heme iron. In the β subunit, the distal histidine N_ε-H is further away and equidistant from both O atoms suggesting a weaker interaction with either or both O atoms. The absence of such H-bonding to the

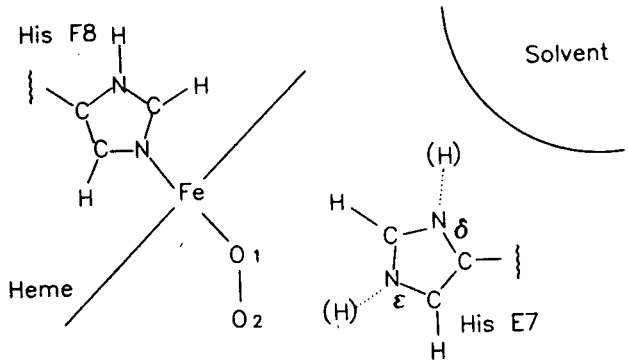

Fig. 1.7 The environment of the bound O_2 in hemoglobin, possible hydrogen bonding with the His E7

oxygen in CO of carbonmonoxyhemoglobin is consistent with electroneutrality of the Fe-C-O unit.[26]

Olson *et al.*[27] have replaced the distal histidines in myoglobin and hemoglobin by glycine, which opened an access to the heme pocket. It left the oxygen affinity and kinetic constants of the β-subunits unchanged, but diminished the oxygen affinity of the α-subunits 8-fold. The reduction in the oxygen affinity was brought about by a 60-fold increase in the dissociation (off) rate that more than compensates the 10-fold increase in associate (on) rate due to the opening of the heme pocket. Thus, it has confirmed further that in both myoglobin and α hemoglobin, His E7 stabilizes bound O_2 by H-bonding.

In synthetic model compounds which offer no steric hindrance to the ligands, oxygen binds with an Fe-O-O angle of 120°, while CO lies on the heme axis perpendicular to the heme plane. The heme pockets of myoglobin and hemoglobin seem to be tailored to accommodate the bent oxygen and force the CO off the heme axis, which might have accounted for their low CO affinity. However, X-ray crystallographic study of human carbonmonoxyhemoglobin at 2.2 - 2.3 Å resolution[28]

has shown a very small inclination, but the porphyrins are ruffled. X-ray analysis[29] of a synthetic "hindered pocket" iron porphyrin having a lower CO affinity than that of the unhindered "picket fence" iron porphyrin shows similar geometry. Fe-C-O is slightly but detectably bent and tilted off the axis normal to the porphyrin plane. This modest distortion of the carbonyl unit is accompanied by considerable ruffling of the porphyrin periphery. It may be concluded from these experimental data that in both the "hindered pocket" porphyrin and in hemoglobin, the strain energy responsible for the low CO affinity is from a combination of structural changes involving both ligand distortions and overall porphyrin skeletal deformations.

Springer *et al.*[30] have studied the protection of the heme iron from oxidation by replacing the distal histidine in sperm-whale myoglobin by ten different amino acid residues. The replacements reduced the oxygen affinity and accelerated autoxidation. Usually oxidation occurs in the fraction of molecules which are deoxygenated. The faster autoxidation is therefore partly attributed to the decreased oxygen affinity. Furthermore, Perutz[31] has suggested that the distal histidine protects the ferrous heme iron by acting as a proton trap since autoxidation is catalysed by protons. At neutral pH, the distal histidine is protonated only at N_δ which faces the solvent (Fig. 1.7). Any proton entering the heme pocket of deoxymyoglobin would be bound by N_ε, and simultaneously N_δ would release its proton to the solvent. When the histidine side-chain swings out of the heme pocket, the protons would interchange, restoring the previous state.

1.3 The nature of O_2 and bound O_2

Molecular oxygen is a paramagnetic molecule with a formal bond order of two.

It has a triplet ground state with two unpaired electrons. This is explained readily by simple molecular orbital theory (Fig. 1.8A). The MO description for molecular dioxygen shows vacancies for the addition of a single electron in both of the antibonding 2p π_g^* orbitals. The addition of one or two electrons to a neutral dioxygen molecule results in the formation of the superoxide (O_2^-) and peroxide (O_2^{2-}) anions respectively, leaving superoxide with a bond order of 1.5 and peroxide O-O link a bond order of one. The reduction in bond order is associated with an increase in O-O bond length and a decrease in the stretching frequency, $\upsilon_{O\text{-}O}$, all of which are useful guides to the assessment of the properties of O_2-metal complexes (Table 1.1).

The nature of iron-oxygen bonding in hemoglobin has been the subject of much discussion. There have been three major proposals on the electronic nature of the O_2-

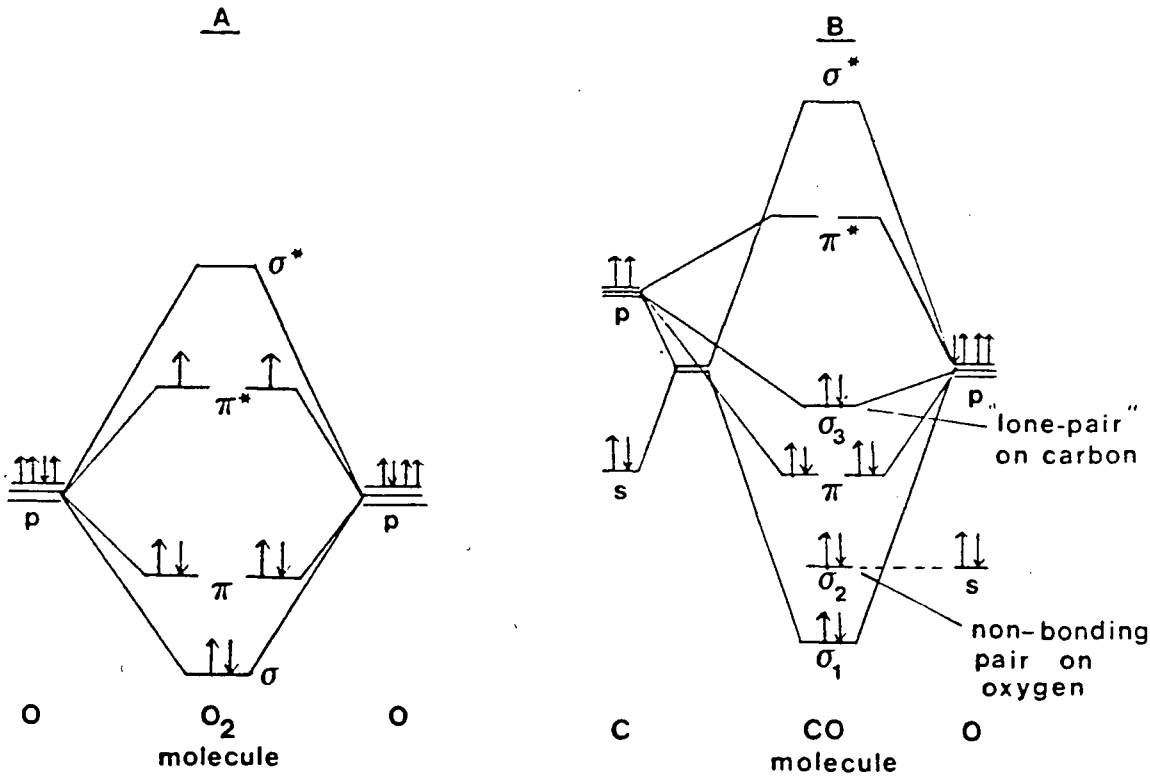

Fig. 1.8 Molecular orbital diagrams for O_2 (A) and CO (B)

Table 1.1 Properties of the dioxygen moiety

Species	Bond Order	Compound	O-O Distance (A)	Bond Energy (kcal/mol)	ν(O-O) cm^{-1}
O_2^+	2.5	O_2AsF_6	1.123	149.4	1858
O_2	2	O_2	1.207	117.2	1554.7
O_2^-	1.5	KO_2	1.28	—	1145
O_2^{2-}	1	Na_2O_2	1.49	48.8	842

metal moiety.

Pauling's model[17] is as follows: approach of dioxygen to the Fe center leads to spin pairing of the electrons in the π^* orbitals, following their loss of degeneracy. The Fe-O_2 bond then involves σ donation from dioxygen into empty d_z^2 orbital of Fe, which is balanced by d-π back donation from Fe into the antibonding molecular orbitals of O_2. This model postulates low-spin Fe(II) with neutral dioxygen, which must be in a singlet state to account for the overall diamagnetism of the system.[32] In contrast, Weiss[33] has put forward a scheme in which electron transfers to dioxygen from iron has taken place, giving $Fe^{3+}(O_2^-)$. The diamagnetism then results from strong antiferromagnetic interaction between low-spin iron(III) and superoxide ion. Infrared[18(a)] and flash photolysis[34] have shown support for this Fe(III)-superoxide species. X-ray fluorescence has also pointed to the presence of unpaired electron density on the iron atom.[35]

Another molecular orbital calculation favors a model based on the electronic structure of ozone.[36] It suggests that the similarity of the infrared O-O stretching

frequencies of MbO_2 and superoxide anion, used as evidence for the Weiss' model, may be coincidental, and there is little electron transfer from Fe to O_2. In this model, low spin Fe(II) is considered to exist in an excited state while dioxygen retains a triplet configuration. Excitation of one electron from the d_{xz} into d_z^2 orbital of Fe(II), pointing towards the triplet dioxygen, leads to a σ bond, while the interaction between the remaining electron in the d_{xz} orbital and π-system of the O_2 forming a three center, four electron π bond. This model is consistent with a diamagnetic Fe-O_2. The facile formation and dissociation of the Fe-O_2 bond is easily rationalized in this model since the O_2 always retains its triplet ground state character in the system. The high resolution ^{17}O-nmr spectrum of the FeO_2 linkage of a dioxygen-imidazole-iron(d^6) porphyrin complex[37] has given a spectrum pattern similar to ozone.[38]

The crystal structures of MbO_2[39] and HbO_2[16] have shown that the Fe-O-O has a bent, end-on geometry, as predicted by Pauling.[17] The angle of Fe-O-O is 115° in oxymyoglobin, 153° in α oxyhemoglobin and 159° in the β oxyhemoglobin. The oxygen molecule forms a hydrogen bond with N_ε of His E7 in the α, but either none or a weak one in the β subunit.

1.4 Carbon monoxide binding in hemoproteins

Carbon monoxide with a bond order of three (Fig. 1.8B) binds with a ferrous heme with much higher affinity than oxygen. The bonding of CO to ferrous ion can be regarded as follows:[40] overlap of a filled carbon σ-type orbital on the metal atom is enhanced by π back donation from Fe to CO, which is maximized at an angle of 180°. Thus, the resultant Fe-C-O unit is linear and with near electrical neutrality.

Whereas CO is bound to ferrous ion and simple porphyrin Fe(II) in a linear

manner,[41] the crystal structure determination has indicated that the CO lies off the heme axis in both α and β subunits of carbonmonoxyhemoglobin and myoglobin.[26, 42, 43] This has implied the distal residues as the source of the distortion.

1.5 Studies of hemoprotein distal electronic effects with model compounds

Although the reversible binding of O_2 and CO to heme proteins occurs at the iron atom, the steric and electronic controls provided by the protein play major roles. The crystal structure determinations of various hemoglobins (oxy or deoxy) and myoglobins (oxy or deoxy) have shown that the most important changes on ligand binding involve the changes in the immediate vicinity of the heme (Section 1.2). In the aspect of distal side effects, the steric obstruction may serve to lower the affinity for the sixth ligand (*e.g.* CO),[42] and hydrogen bonding[24] between dioxygen and the distal residue may electronically stabilize the O_2-complex. On the proximal side, non-bonded globin constrains can prevent the required movement of the iron into the porphyrin ring on ligand binding.[13-15] In addition, electronic interactions (hydrophobic or polar) between the porphyrin ring and protein residues in close proximity could alter electron density of the heme moiety.[44]

Heme proteins have complex structures and their dynamic equilibrium studies are extremely complicated due to the influence of both tertiary and quaternary changes on ligand binding. Theoretical studies of CO and O_2 binding to myoglobin[45] have indicated that approach of a ligand to the heme is controlled by successive barriers, in addition to the most inner barrier of Fe-ligand bond formation. In order to evaluate the influence of the immediate protein environment (heme pocket) on the ligand binding, it is necessary to construct models with the minimum of added molecular structure necessary

to mimic the active site behavior of a hemoprotein. These synthetic iron-containing oxygen carriers are more readily characterized than the hemoproteins. A more accurate X-ray crystal structure can be obtained than for the much larger, more complicated hemoprotein. By designing different model compounds, it is possible to investigate separately the effects of the heme environment on heme binding reactivity.[46]

1.5.1 Requirements for the model compounds[46]

A synthetic model compound contains an active heme site in which a ferrous atom is bound to give a complex which is then able to combine reversibly with dioxygen. But, difficulty arises with obtaining porphinatoiron-dioxygen complexes. Simple ferrous porphyrins, in the absence of large excess of base **B**, undergo rapid and irreversible oxidation by molecular oxygen to yield the μ-oxo dimer:

$$Fe^{II}(Por)(B)_2 \rightleftharpoons Fe^{II}(Por)(B) + B$$

$$Fe^{II}(Por)(B) + O_2 \rightleftharpoons Fe(Por)(B)(O_2)$$

$$Fe(Por)(B)(O_2) + Fe^{II}(Por)(B) \rightleftharpoons (B)(Por)Fe^{III}\text{-}O_2\text{-}Fe^{III}(Por)(B)$$

$$(B)(Por)Fe\text{-}O_2\text{-}Fe(Por)(B) \xrightarrow{\text{rapid}} 2Fe^{IV}(Por)(B)(O^{2-})$$

$$Fe^{IV}(Por)(B)(O^{2-}) + Fe^{II}(Por)(B) \xrightarrow{\text{rapid}} (Por)Fe^{III}\text{-}O\text{-}Fe^{III}(Por) + 2B$$

Autoxidation proceeds via formation of the monomeric iron-dioxygen adduct $Fe(Por)(B)(O_2)$, followed by formation of a μ-peroxo-dimer, $(B)(Por)Fe\text{-}O_2\text{-}Fe(Por)(B)$. Then, experimental data indicate that this peroxo-bridged complex decomposes via the formation of a presumed ferryl, $Fe(IV)(Por)(B)(O^{2-})$ intermediate to give the μ-oxo

dimer.[46, 47] This reaction does not occur in hemoproteins because the polypeptide chain surrounding the heme prevents the close approach of two hemes and the subsequent oxidation.

Another major difficulty encountered is that the simple ferrous porphyrins in solution, in the presence of strongly coordinating N-donor ligands, tend to form a six-coordinate complex:

$$Fe^{II}(Por) + B \overset{K_1}{\rightleftharpoons} Fe^{II}(Por)(B) + B \overset{K_2}{\rightleftharpoons} Fe^{II}(Por)(B)_2$$

Often in such systems $K_2 > K_1$, making $Fe^{II}(Por)(B)_2$ the dominant species in solution. This can be largely understood in terms of the ligand field stabilization energy that results from the spin state change in going from 5-coordinate high spin to 6-coordinate low spin.

In order to overcome these difficulties, three strategies have been devised: (1) steric - in this case the dimerization and 6-coordination of the base are inhibited; (2) low temperature - to slow down the reactions leading to dimerization; (3) rigid surfaces - iron-porphyrins in this case are attached to the surface (polymer) in such a way as to prevent dimerization and six-coordination.

Several hemoglobins and myoglobins are known to undergo autoxidation reactions promoted by anions. This autoxidation is known to proceed in the presence of protons.[48] Formation of superoxide ion (or the hydroperoxyl radical $HO_2^{\cdot}$) has been implicated in this oxidation. In a recent ^{17}O-nmr study[49] of a "basket handle" porphinatoiron dioxygen adduct, $H_2{}^{17}O$ and $H_2{}^{17}O_2$ species have been detected in the autoxidation process, strongly supporting the implication of superoxide (or the hydroperoxyl radical $HO_2^{\cdot}$) in the reaction. The hydrophobic environment for the heme center in hemoglobin and myoglobin is very important to prevent this kind of

autoxidation. Therefore, experiments with model systems of heme oxygen carriers are generally conducted in nonaqueous media.

1.5.2 Model compounds

Continued efforts to overcome the problems associated with synthetic oxygen carriers have led to the development of various elaborate model hemes. These model compounds with different structures have provided much information about the effects of the protein environment on ligand binding. The mechanism of ligand binding by heme proteins has been established based partly on model studies.

This section mainly deals with the model studies relevant to distal electronic effects - hydrogen bonding between bound dioxygen and His E7 residue. A detailed discussion about the distal steric effect of the hemoproteins is available.[50]

CO and O_2 binding experiments of heme proteins and synthetic analogues have indicated the importance of the local polarity at the binding site to the differential binding of CO and O_2. Direct evidence such as from neutron diffraction and X-ray analysis studies (Section 1.2.2) of oxymyoglobin and oxyhemoglobin has left little doubt that heme-bound dioxygen has a tendency to form a hydrogen bond with His E7. However, quantitative estimations of the energetic contribution of this interaction to the overall stability of the metal-oxygen complex still depend on the model binding studies. By using a cobalt salicylidenimine complex, Drago *et al.*[51] observed a 400 fold increase in oxygen affinity when trifluoroethanol was added to a CH_2Cl_2 solution, suggesting intermolecular hydrogen bonding. More sophisticated porphyrin models[53, 54, 57, 58, 60] with amide substitution have exhibited intramolecular hydrogen bonding quite similar to natural heme proteins, however, in no cases has such hydrogen bonding been confirmed by X-ray structural analysis.

(i) Picket-Fence systems

Synthetic analogues of dioxygen-carrying complexes with amide substituents in the distal protected pocket have the potential to form hydrogen bonds between the NH and bound dioxygen. One of them, the "picket fence" porphyrin: tetra(α,α,α,α-o-pivalamidophenyl)porphinatoiron (3)[52] was the first synthetic model capable of binding dioxygen reversibly at room temperature. This compound has steric bulkiness

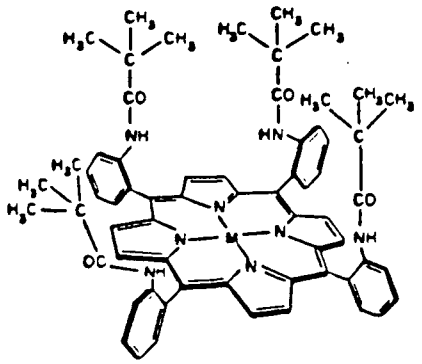

3 $T_{piv}PP$

a M=2H

b M=Fe

constructed with the pivalamido groups on one side of the porphyrin plane and leaves the other side unencumbered. An imidazole ligand is allowed to coordinate to the unhindered side of the porphinatoiron, while the other side remains as a pocket for oxygen-binding. Moreover, the fence discourages dimerization to a μ-oxo dimer.

Since this compound has polar amide substituents in the distal pocket, much work has been carried out to investigate the possible interactions between coordinated dioxygen and carbon monoxide with the amides. Single crystal X-ray analysis data[53, 54] have shown a suitable geometry for such hydrogen-bonding. The terminal oxygen atom and the N-H group point towards each other. The shorter N(H)···O separations of 3.88

and 4.19 Å in the picket fence O_2-complex can be compared to typical values of 2.94 Å for primary amides[55] and 2.85 Å for secondary amides[56] where strong hydrogen-bonding interactions exist. The separations in the model O_2-adduct are ~1 Å longer, suggesting a weaker hydrogen bond. Calculation[54] has suggested significant enthalpic stabilization due to this hydrogen bond.

ESR studies[22] of mono-ortho and para acetamido derivatives of cobalt(II)TPP [(o-$NHCOCH_3$)TPPCo and (p-$NHCOCH_3$)TPPCo], in the presence of N-methylimidazole and molecular oxygen, have provided information concerning the dynamics of bound oxygen: when hydrogen bonding is possible (from the N-H of the ortho acetamide), the ESR spectra of the dioxygen adduct, like oxymyoglobin, are not motionally averaged as they are for the para acetamide. The motion of the (p-$NHCOCH_3$)TPPCo as shown in the averaging of the ESR signals in solution originates from the rotation of the dioxygen moiety about the Co-O bond in the absence of a hydrogen bond.

(ii) Substituted "chelated" porphyrins

Chang and co-workers[57] have made a model system consisting of a series of 5-coordinate heme compounds (**4**) differing principally in the dipole moment of the

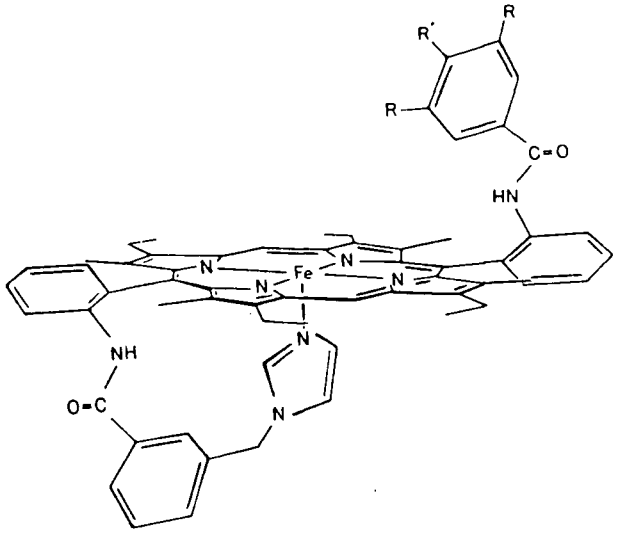

4a	R=H	R′=t-Bu
4b	R=CH_2OMe	R′=H
4c	R=CH_2OH	R′=H
4d	R=$CO_2C_4H_9$	R′=H
4e	R=$CONHC_4H_9$	R′=H
4f	R=$CONEt_2$	R′=H
4g	R=$CONi\text{-}Pr_2$	R′=H

phenyl substituents above the O_2 binding site. Binding studies on these complexes revealed that the polar groups in near proximity to the binding site of the CO or O_2, dramatically affect k_{off} for O_2 but not for CO (CO binding kinetics appear to be only affected by steric interactions). From Table 1.2, it is apparent that compound **4e** with a secondary amide substituent has a much stronger O_2-affinity than the other hemes. Its O_2 dissociation rate is much slower than for the other hemes due to H-bonding.

The other two compounds **5a** and **5b** have a polar acetamido group either on the same or the opposite side of the O_2/CO binding site. The binding data suggested that enhanced O_2 affinity of **5b** relative to **5a** must be due to a favorable interaction of the Fe-OO and amide dipoles. It was concluded that this enhanced affinity is derived from a non-bonding dipole-dipole interaction and not from direct hydrogen bonding (too distant for effective H-bonding compared with a typical peptide H-bonding distance of (2.8 - 3 Å).

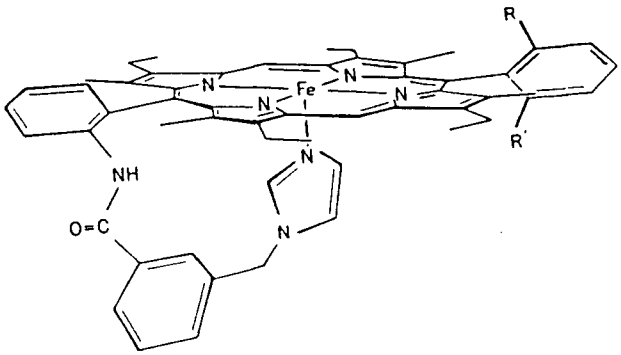

5a R=H R′=$NHCOCH_3$

5b R=$NHCOCH_3$ R′=H

Co^{II} 1-naphthyl porphyrins (**6**)[58] substituted with amido, carboxy and hydroxyl

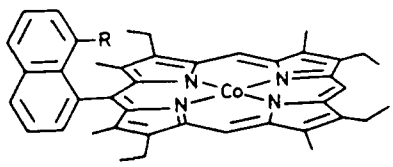

6a R=H

6b R=CO_2H

6c R=$CONH_2$

6d R=CH_2OH

Table 1.2 CO & O_2 binding constants of **4** & **5** in toluene at 20 - 22°C[57]

Compound	k^{O2} $M^{-1}s^{-1}$	k^{-O2} s^{-1}	$P^{O2}_{1/2}$ torr	k^{CO} $M^{-1}s^{-1}$	k^{-CO} s^{-1}	$P^{CO}_{1/2}$ torr
4a	$4.7x10^7$	15,500	33	$2.5x10^6$	0.14	0.0057
4b	$2.6x10^7$	9,900	38	$1.1x10^6$	0.028	0.0075
4c	$2.3x10^7$	2,900	13	$1.2x10^6$	0.090	0.0075
4d	$2.2x10^7$	11,000	48	$1.5x10^6$	0.13	0.0086
4e	$1.3x10^7$	300	2.3	$1.3x10^6$	0.042	0.0032
4f	$1.4x10^7$	4,750	34	$0.59x10^6$	0.048	0.0081
4g	$1.3x10^7$	9,300	72	$0.47x10^6$	0.053	0.011
5a	$3x10^7$	38,000	126	$2.3x10^6$	0.12	0.0054
5b	$2.6x10^7$	4,100	16	$1.6x10^6$	0.072	0.0045

groups at the 8-naphthyl positions display significant enhancements in O_2 affinity which correlates well with H-bond strength (Table 1.3). The data clearly demonstrate that the presence of a protic group near the dioxygen binding site drastically increases the Co-O_2 formation constant, achieving a free energy gain between 3 kcal/mol for **6b** and 1.1 kcal/mol for **6d**, with reference to **6a** in DMF at -42°C. The enthalpy change for these intramolecular H-bonded dioxygen complex formations also increases significantly. Compared to literature thermodynamic parameters of hydrogen-bonding,[59] the large gain in enthalpy for the models is attributed to the intramolecular H-bond. The large negative entropy is also consistent with the loss of rotational degrees of freedom of the metal-bound O_2 due to the hydrogen bonding.

(iii) "Basket Handle" models

Momenteau *et al.*[60] were the first to show the dramatic differences in oxygen binding to a heme equipped with amido groups versus a heme with less polar ether groups on their distal side. These "basket handle" porphyrins contain one strapping group with a pyridine as the axial ligand of the parent porphinatoiron and the other strapping group consists of a simple alkyl chain bridging over the oxygen-binding site. The distal cavity size in both hemes is considered to be very similar with only slight differences in shape owing to the more rigid amide linkages. Two of these "basket handle" porphyrins, **7a** and **7b**, include the long aliphatic C_{12} chain which maybe expected to introduce little, if any, steric interference. The CO affinities of these 5-coordinate systems are nearly identical with k^{+CO} and k^{-CO} are simultaneously decreased by a factor of 2. K^{O2} is ten times larger for compound **7b** than for compound **7a** (Table 1.4). The change of K^{O2} is found to result exclusively from a ten fold reduction of the oxygen dissociation rate in compound **7b**. Thus the presence of the NH (amide)

Table 1.3 Thermodynamic properties for O_2 binding to cobalt porphyrins[58]

Compound	Solvent	T(°C)	$P_{1/2}$(torr)	ΔH(kcal/mol)	ΔS(e.u.)*
6a	DMF	-42	21	-11±0.4	-52±2
		-30	70		
6b	DMF	-42	0.028		
		-30	0.73	-22±1	-88±5
		0	49		
6c	DMF	-42	0.30		
		-30	4.0	-16±2	-70±7
		0	91		
6d	DMF	-42	2.00		
		-30	4.9	-13±1	-56±4
		0	100		
CoMb(sperm whale)		25	57	-13.3	-53
CoMb(horse)		25	57	-11.3	-46
CoHbα-SH		15	24.3	-13.9	-54.4
CoHbβ-SH		15	24.5	-16.5	-63.8

* The entropy units are $J \cdot mol^{-1}K^{-1}$

group in **7b** strongly increases the intrinsic stability of the oxy derivative. Proton nmr[61] spectroscopy has indicated that the bridged chain pulls the amide protons towards the center of the porphyrin as shown by the high field shift (up to 3 ppm) of the corresponding resonances in the Zn(II) or in the carbon monoxide iron(II) complexes

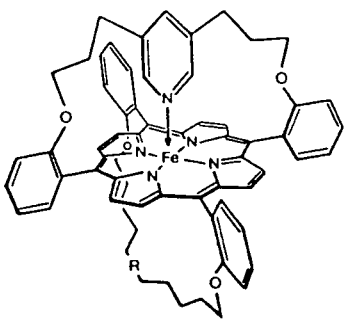

7a $R=(CH_2)_{12}$

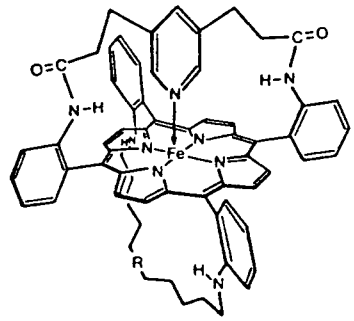

7b $R=CO(CH_2)_{10}CO$

relative to aromatic amides. Ring current shift calculations have estimated that the distance between one of the amide nitrogen atom and the terminal O atom in a bent configuration may be close to 3 Å, consistent with an intramolecular hydrogen bond.

Table 1.4 Kinetic rate parameters & equilibrium constants for the binding of CO & O_2 with basket-handle porphyrins (Solvent: toluene; temperature: 20°C)[60]

Heme	**7a**	**7b**
$10^{-7}xk^{CO}$ ($M^{-1}s^{-1}$)	6.8	3.5
$10^{3}xk^{-CO}$ (s^{-1})	69	30.4
$10^{-8}xK^{CO}$ (M^{-1})	9.9	11.5
$10^{-7}xk^{O2}$ ($M^{-1}s^{-1}$)	30	36
$10^{-3}xk^{-O2}$ (s^{-1})	40	5
$10^{-3}xK^{O2}$ (M^{-1})	7.5	70

All of the above model studies have provided evidence that the polar functions in the heme distal side can increase the O_2 affinity greatly, this is possibly due to the hydrogen bonding stabilization of O_2-complex.

1.6 Brief overview of porphyrin synthesis

There have been several reviews[62 - 65] dealing with porphyrin synthesis. This section gives only a brief summary of the topic.

The porphyrin macrocycle can be constructed in essentially three different ways. They are:

(i) "one-pot" condensation of monopyrroles[62(a)]

(ii) "2+2" addition of dipyrrolic precursors[62(b)]

(iii) intramolecular cyclization of linear tetrapyrroles[62(c), 65]

The first method has very limited synthetic value since it is useful only for the synthesis of symmetrically substituted porphyrins and some "meso" substituted porphyrins. The synthesis of the well-known meso-tetraphenylporphyrin (TPP)[66] is an example of this method.

The "2+2" coupling of dipyrrolic intermediates can provide porphyrins with varied peripheral substitution of certain symmetries. In order to obtained a single porphyrin product, one of the two dipyrrolic intermediates should be symmetrical. The most useful dipyrrolic intermediates are dipyrromethanes and dipyrromethenes. A dipyrromethane is prepared by the condensation of an α-free pyrrole with a pyrrylcarbinyl cation **9** (Fig. 1.9), derived from the precursor **8**, in an acidic medium. The porphyrin formation from dipyrromethanes involves the acid-catalyzed coupling of 5,5′-diformyldipyrromethane with 5,5′-diunsubstituteddipyrromethane (or self-

condensation of 5′-unsubstituted-5-formyldipyrromethane) to produce a porphodimethene intermediate which is further oxidized to the porphyrin.

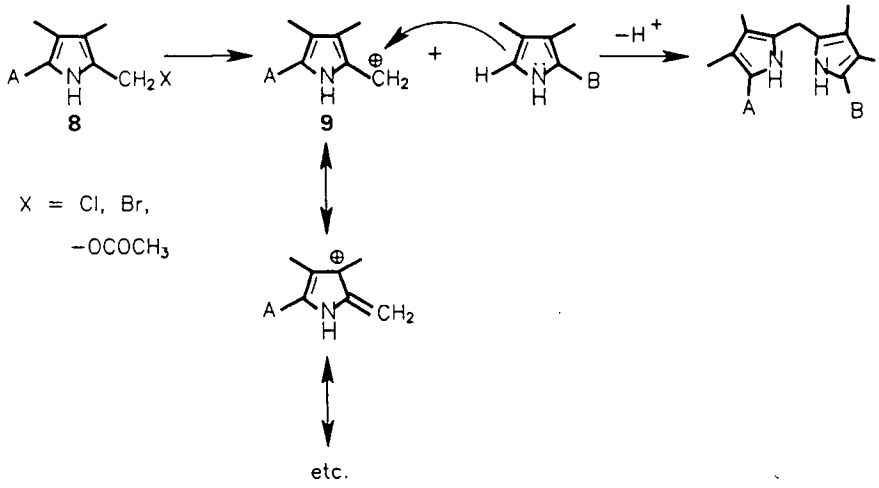

Fig. 1.9 Formation of a dipyrromethane from pyrrole precursors

Dipyrromethenes are relatively strong bases and are best handled in their more stable protonated forms, the dipyrromethenium salts. A general synthesis of dipyrromethenes involves the condensation of an α-formylpyrrole with an α-free pyrrole in the presence of strong acid (Fig. 1.10). There are also some specialized syntheses of dipyrromethenes. Solvolysis of a variety of monopyrroles in a hot solution of hydrobromic acid and formic acid leads to dipyrromethenes of head-to-head symmetry. In the presence of bromine, α-methyl-α′-unsubstitutedpyrroles condense in a head-to-tail fashion, giving a mixture of dipyrromethenes. Porphyrins can be made from dipyrromethenes in acidic media.

Intramolecular cyclization of a linear tetrapyrrole is a very useful way to make porphyrins with unsymmetrically arranged β-substituents. It involves the coupling of the individual pyrrole in an unambiguous manner, utilizing stable intermediates leading to a linear tetrapyrrolic compound, which in the final step is cyclized in a head-to-tail

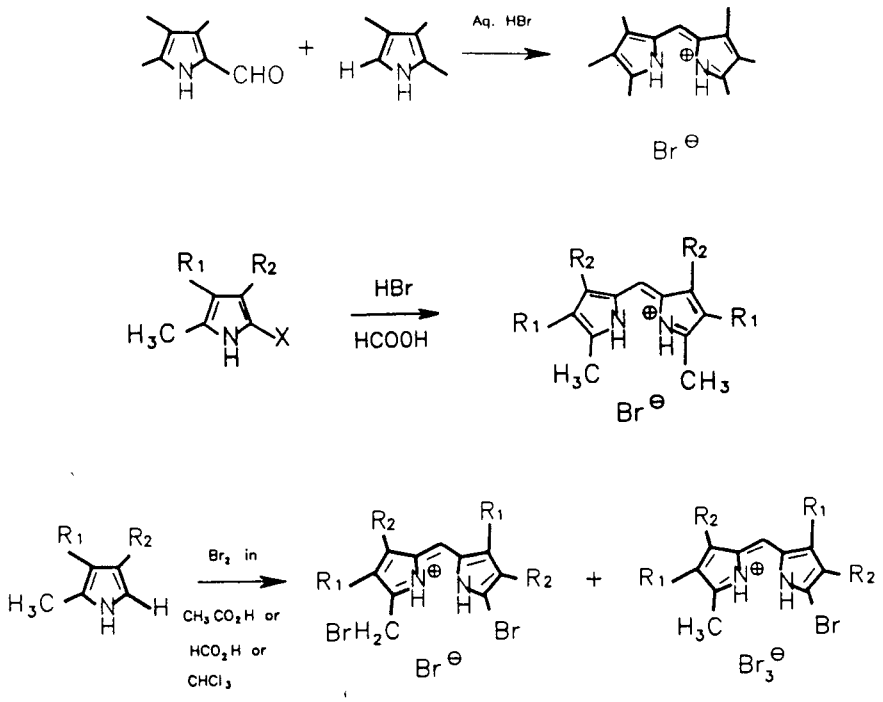

Fig. 1.10 Formation of dipyrromethenes from pyrrole precursors

fashion to the required porphyrin. Biladiene-ac **10** (Fig. 1.11) is the most common used tetrapyrrolic precursor in porphyrin synthesis. It can be synthesized from either dipyrromethanes or dipyrromethenes. The acid-catalyzed condensation of two equivalents of 2-formyl-5-methylpyrrole with dipyrromethane-5,5′-dicarboxylic acid, or alternatively of 5-unsubstituted-2-methylpyrrole with 5,5′-diformyldipyrromethane gives the 1,19-dimethylbiladiene-ac which can be cyclized in the presence of cupric salts to give the Cu complex of the porphyrin (Fig. 1.11). Instead of condensing with two equivalents of the same monopyrrole, a stepwise condensation of dipyrromethane with different mono pyrroles leads to a completely unsymmetrical porphyrin. Coupling of two dipyrromethenes, 5′-bromo-5-bromomethyldipyrromethene and 5′-unsubstituted-5-methyldipyrromethene gives 1-bromo-19-methylbiladiene-ac (Fig. 1.12). This

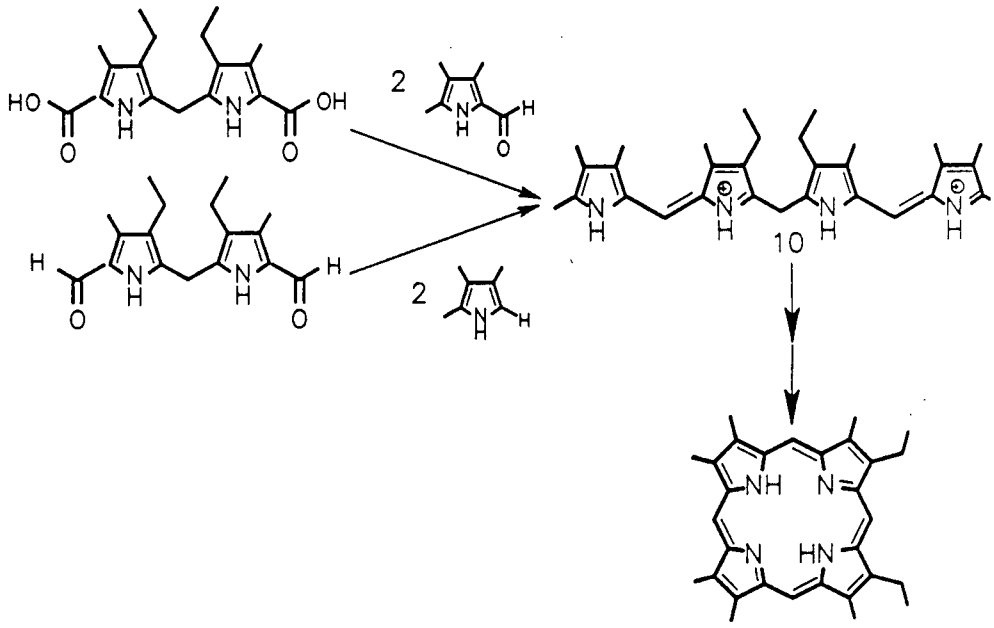

Fig. 1.11 Synthesis of porphyrins from dipyrromethanes

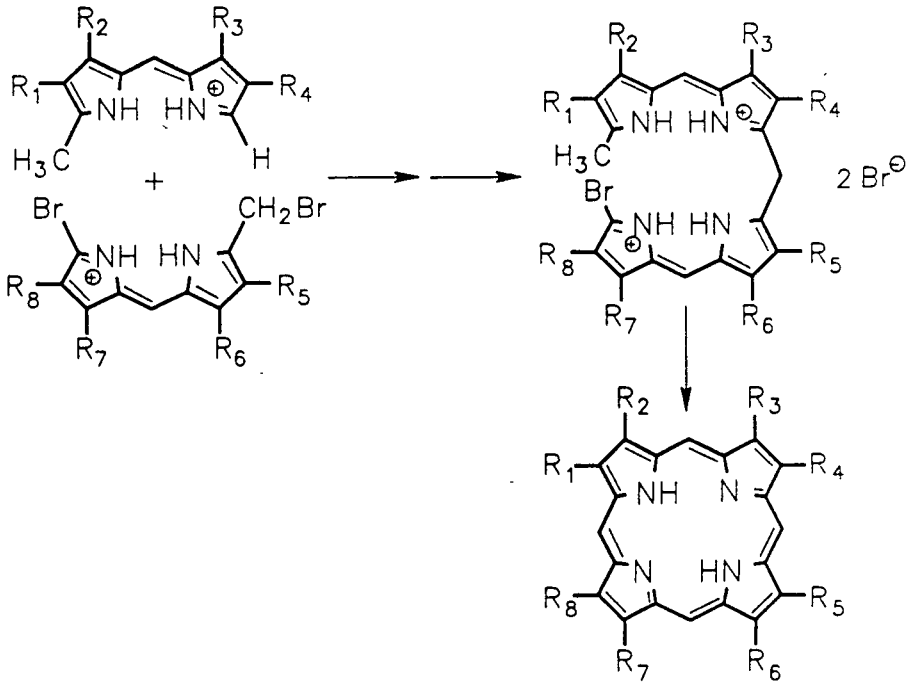

Fig. 1.12 Synthesis of porphyrins from dipyrromethenes

tetrapyrrolic precursor can be cyclized to the corresponding porphyrin by simply heating in o-dichlorobenzene or leaving in DMSO/pyridine at room temperature for several days. In a recent report,[65] Wijesekera and Dolphin have described the development of various monopyrroles and dipyrromethenes. These dipyrromethenes make it possible to construct very useful biladienes which lead to various porphyrins.

Chapter 2

Results and discussion of the porphyrin syntheses

2.1 Synthetic objective

Differentiation of CO and O_2 binding in model systems of oxygen binding heme proteins may arise from electronic and/or steric effects (Section 1.2.2). On the distal side of the heme, steric interplay with amino acids can influence the orientation of bound dioxygen or induce tilting of carbon monoxide. Alternatively, electronic interactions may stabilize or destabilize the bound moiety. There has been a simple reference series developed in this group, the durene capped hemes, **11**, **12** and **13**, where the influence of distal steric effects on CO and O_2 binding has been examined in

11, Durene-4,4, n=4

12, Durene-5,5, n=5

13, Durene-7,7, n=7

a, M=2H **b**, M=Fe

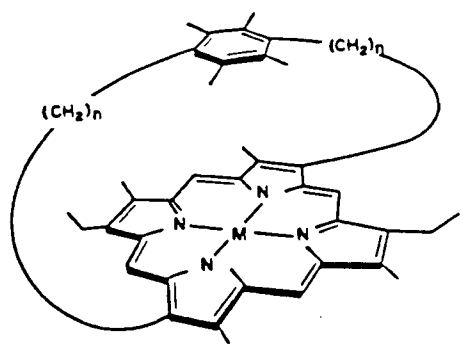

the absence of stabilizing electronic interactions.[50] The study of CO and O_2 binding within the completely hydrophobic distal cavity of the durene capped porphyrin series has revealed the relative contribution of steric effects, both proximal and distal, for R- and T- state heme systems.

Introduction of a polar factor to such heme model systems may help to understand the contribution of electronic effects to the discriminatory binding of CO and O_2. Neutron diffraction data[24] have indicated that a strong hydrogen bond exists between the terminal oxygen and the distal histidine E7 residue in the binding pocket of MbO_2 and α subunit of HbO_2, an interaction that is thought to stabilize the bound O_2. An amide substituted benzene capped porphyrin model may well help in understanding the nature of this hydrogen bond if the conformational requirement, *i.e.*, the direction in which the polar amide function points within the distal cavity, for such an interaction is satisfied. A hydrogen bond with bound O_2 then would be realized and thus increase the stability of the O_2-complex. The cap sizes chosen in this study were 4/4 and 5/5 methylene groups because from the previous study of the durene analogues,[50] it was known that the CO and O_2 binding constants of the 7/7 methylene system were very similar to those of the 5/5 methylene system. Therefore, one may not be able to see a significant difference in these two hemes. Synthesizing the 4/4 and 5/5 methylene chain amide substituted benzene capped porphyrins **49c** and **49d** was considered to be sufficient to investigate the electronic effects of the binding properties of this system. For the purpose of comparison, the benzene capped porphyrins **49a** and **49b** were also synthesized and studied.

a, Benzene-4,4, n=4, R=H

b, Benzene-5,5, n=5, R=H

c, Amidobenzene-4,4, n=4, R=$NHCOCH_3$

d, Amidobenzene-5,5, n=5, R=$NHCOCH_3$

49, M=2H, **50**, M=Fe

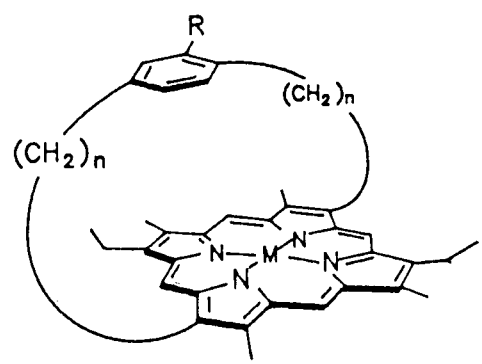

2.2 Synthetic plan

The synthetic strategy for the hydrocarbon chain strapped porphyrins and the durene capped porphyrins were developed in this group by Wijesekera[63] for the purposes of distorting the porphyrin mean plane, and making a myoglobin model with a fully hydrophobic distal cavity, respectively. The "retrosynthetic" analysis of the target molecule via dipyrromethane dimers has previously been described[63] (Fig. 2.1). The first disconnection of the target molecule **14** leads to the most crucial intermediate, **15**, of the entire synthetic scheme. With the peripheral substituents chosen as R_1=R_4, R_2=R_5 and R_3=R_6, the double disconnection leads to a symmetric dipyrrolic intermediate already carrying the chain. The reverse of this disconnection is a simple acid catalyzed reaction of an α-unsubstitutedpyrrole with an α-formylpyrrole to produce a methene link. In order to prepare this bis α-formylpyrrolic derivative, the hydrocarbon and the durene chains are made first and are then attached to two β-free pyrroles by two simultaneous Friedel-Crafts acylation reactions. Reduction of the carbonyl group followed by modification of the ethyl ester groups at positions 5 to formyl groups gives a derivative which is ready to be transformed to dipyrromethane dimers via coupling of a second pyrrole unit. However, before doing so, the formyl functions are protected as dicyanovinyl groups. The dipyrromethane dimers, after deprotection and decarboxylation are subjected to acid-catalysed intramolecular 2+2 coupling to give the desired porphyrins.

It was anticipated that this strategy could be used to construct the amide substituted benzene-capped porphyrins. Since the two porphyrins **49a** and **49b** without amide groups on the benzene cap are quite similar to the durene-capped porphyrins, no special problems were anticipated. However, for the porphyrins with the amide

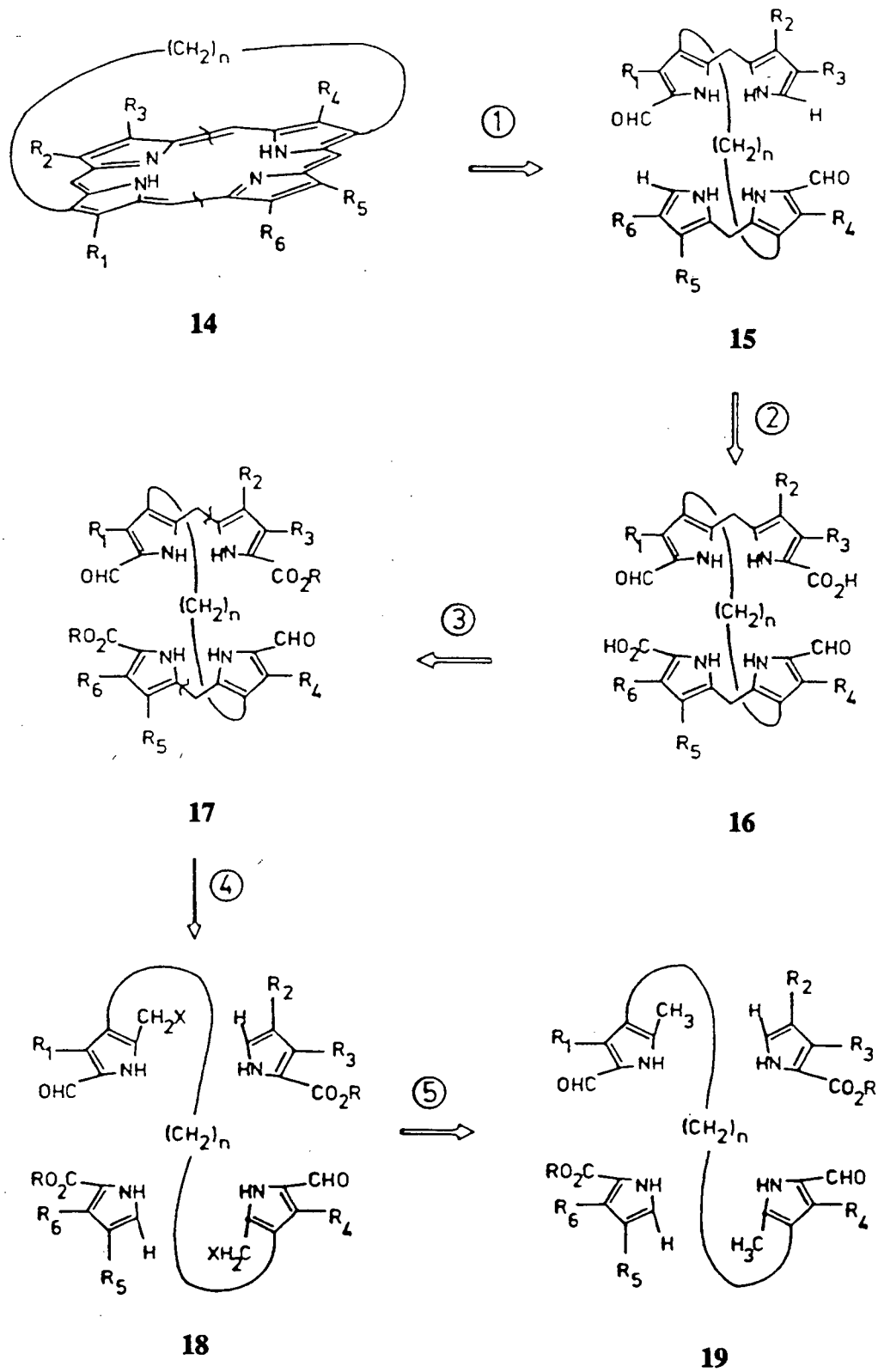

Fig. 2.1 A retrosynthetic analysis of the strapped porphyrin, after Wijesekera *et al.*[63]

functionality, it was necessary to consider the best stage to introduce the sensitive functional group, since although the hydrocarbon strap of other porphyrins survived the entire reaction sequence, the amide was not expected to. Therefore, it was considered appropriate to introduce the polar functionality to the molecules as late as possible, and utilize the previous developed synthetic route to the greatest extent.

Generally, an aromatic amide can be obtained by reducing the corresponding nitro compound. This raised the question as to how and when the nitro group should be introduced. Of course, if the nitro group could be introduced into the benzene-capped porphyrins, it would save time and avoid possible complications. However, because the porphyrin ring system itself is highly aromatic, there was no reason to expect that nitration would occur only on the appended benzene ring but not on the porphyrin periphery. Classical nitration procedures require the use of acidic reagents, and the resulting N,N′-diprotonated porphyrins are less nucleophilic, a feature that would have shown some advantage in this strategy. Protonation of a porphyrin with the acidic nitration medium would deactivate the porphyrin periphery and therefore nitration of the benzene ring be preferred. Thus, the porphyrins with benzene cap, **49a** and **49b**, were made and nitration was examined. The benzene capped porphyrin 5/5 **49b** was stirred with a mixture of acetic acid, sulphuric acid and nitric acid at room temperature for two hours. The brown-black solid obtained after work-up showed a characteristic UV/visible spectrum of a porphyrin. However, the mass spectrum showed only dinitrated and trinitrated compounds and no mononitrated product or unreacted starting material. Even by lowering the reaction temperature to 0°C, no mononitrated product was obtained. Since the meso positions of the porphyrin were unsubstituted, they should be ideal places for electrophilic attack of the nitrating agent, nitronium ion, NO_2^+. The deactivating factor was not sufficient to prevent the nitration of the porphyrin

periphery. There have been examples of porphyrin peripheral nitration even under very mild conditions.[67] This led us to the conclusion that the nitro functionality had to be introduced before the formation of the benzene-strapped porphyrin.

The aromatic nitro group is one of the most active towards catalytic hydrogenation and it might not be expected to survive such conditions which were necessary for some steps in the synthesis. Therefore, nitration was postponed until after protection of the α-formyl function, by conversion to a dicyanovinyl derivative, because this compound was relatively stable, and no further catalytic hydrogenation was required beyond this stage. The dicyanovinyl derivative prepared during the synthesis of the benzene-capped porphyrin 4/4 (**49a**) was used for nitration studies. The lemon yellow 1,4-bis{4-[5-(2,2-dicyanovinyl)-2,4-dimethylpyrrol-3-yl]butyl}benzene was stirred with an excess of nitronium tetrafluoroborate, a reagent which efficiently nitrates aromatics at low temperature. The common solvent for this reaction, sulfolane, was used because of its ability to solubilize both inorganic salts and organic compounds. The resulting reddish-brown solution was allowed to stir for one hour and the mixture was diluted with water and methylene chloride. The disappearance of the characteristic lemon yellow color of the starting material implied that the starting material had been destroyed. NMR and mass spectra of the isolated material confirmed the conclusion. It suggested that the pyrrole nucleus, sensitive to oxidizing agents, had been attacked by strong oxidizing species of the nitrating agent. Therefore, a simple pyrrole, 2-ethoxy carbonyl-3,4,5-trimethylpyrrole, was examined with nitronium tetrafluoroborate in methylene chloride at -80°C. Even at such a low temperature, the pyrrole was destroyed. It was concluded that nitration could only be achieved before the pyrroles were attached to the chain.

Nitration was then investigated at several stages: dicyanide **26**, dibromide **25**,

diester **23** and diester **28**. Except for the dibromide **25**, the other three compounds could be nitrated. Since the diester **28** is the step just before the coupling of the pyrroles, it was decided that nitration should be carried out at this stage.

However, problems arose from this early stage nitration. In the synthetic sequence, transbenzylation and debenzylation were necessary to make a clean, high yield α-free pyrrolic derivative. The nitro function is very sensitive to the catalytic hydrogenolysis conditions of debenzylation. Possible discrimination of such reaction conditions towards the reduction of a nitro group relative to debenzylation was examined. A THF solution of nitrotoluene and 2-benzyloxycarbonyl-4-ethyl-3,5-dimethylpyrrole (1:1 ratio) was stirred under hydrogen in a hydrogenator in the presence of Pd/C catalyst. Within 10 min, more than half of the total material had been reduced. It indicated that no discrimination existed. It was therefore decided that the catalytic debenzylation step should be eliminated by saponifying the ethyl ester **38** directly instead of the indirect transbenzylation-debenzylation sequence.

2.3 Benzene and nitrobenzene diacid chain derivatives

The synthetic scheme for the chain derivatives is shown in Fig. 2.2.

The commercially available terephthaldehyde **20** was reacted with malonic acid by Knoevenagel reaction[68] to form the diacid **21**. Pyridine and piperidine were used as the catalysts. An excess of malonic acid (>2:1) was used to obtain a high yield. The accompanying decarboxylation was observed during the condensation of the aldehyde with malonic acid (evolution of carbon dioxide).

The double bonds of compound **21** were then subjected to reduction. Two methods were tried, both being successful. The diacid **21** was first esterified to its

ethyl ester, and then reduced by hydrogenation using 10% Pd/C as the catalyst. The product was very clean and obtained in almost quantitative yield. But, with such a large quantity of the starting material (around 0.5 mol), a large volume of hydrogen (22.4 L) had to be absorbed to accomplish the reduction. The reduction took a long time (2 days) to consume the hydrogen and fresh catalyst had to be used several times during the reaction. Therefore, an easier and faster method was sought.

The diacid **21** was reduced directly by Raney Nickel-Aluminium alloy[69] using a low pressure catalytic hydrogenation. To the warm aqueous KOH solution of the diacid **21**, small portions of Raney Nickel-Aluminium alloy were added. The hydrogen liberated from the reaction of aluminium with strongly basic solution was adsorbed on the surface of the newly formed Raney nickel catalyst to perform the reduction. The product obtained by this method was very pure and the reaction was faster.

In order to increase the chain length by two carbons, the next step was to transform the acid group to some active functionality for further extension of the chain. The reduction of the acid to an alcohol was chosen. The commonly used reagent for this purpose is diborane. Even though carboxylic acids are generally more active towards diborane reduction than their ester derivatives, it was impossible to reduce compound **22** completely using diborane because of its low solubility in THF; only partial reduction could be achieved. Therefore, this reduction was carried out on the diester **23** which is significantly more soluble in the same solvent.

The esterification was first attempted in toluene and ethanol using a Dean-Stark apparatus. After being refluxed with p-toluene-sulphonic acid for two days, much of the solid diacid was remaining. Therefore the ester had to be prepared via the acid chloride, though it was not as clean a reaction as direct esterification. The dark brown acid chloride prepared by the reaction of **22** with thionyl chloride was used directly

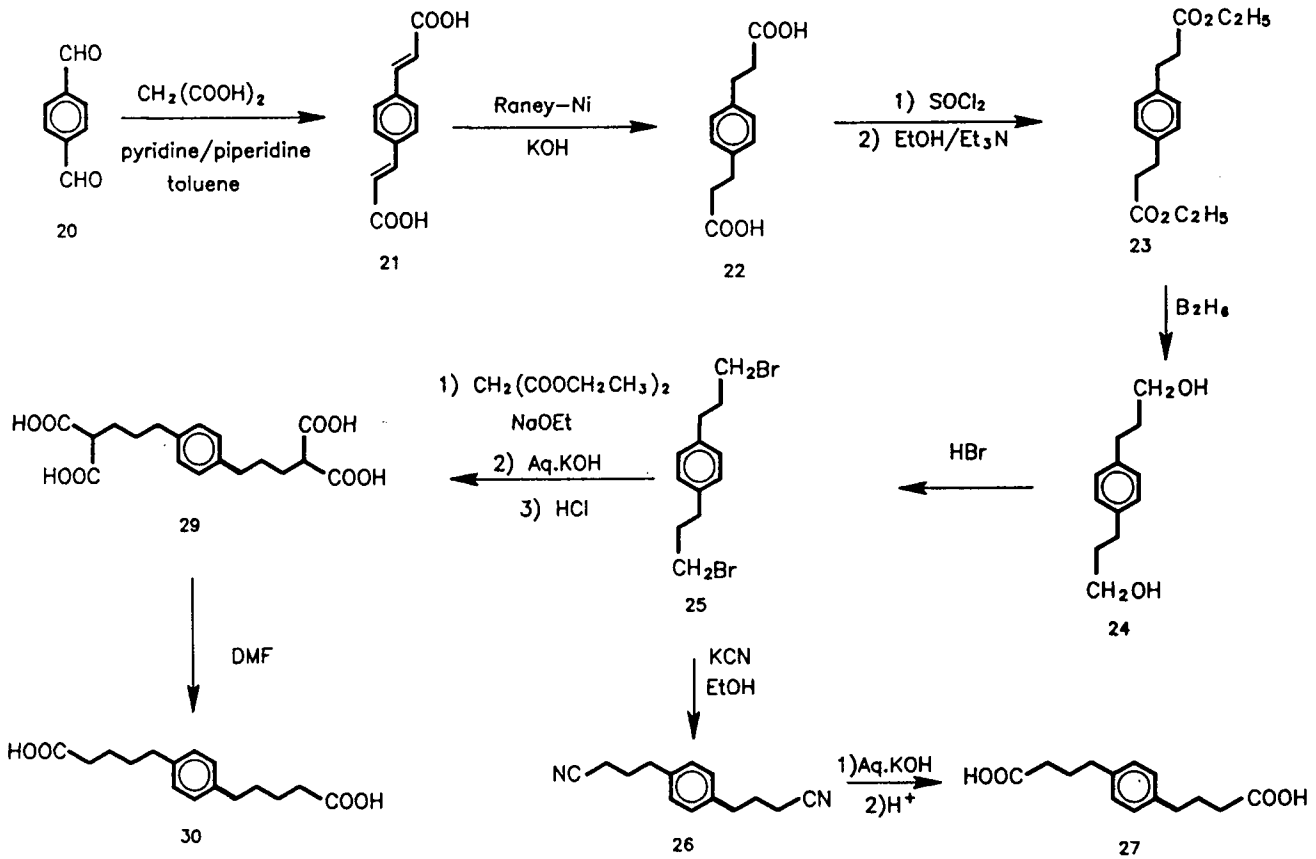

Fig. 2.2(a) Synthetic scheme for the chain derivatives

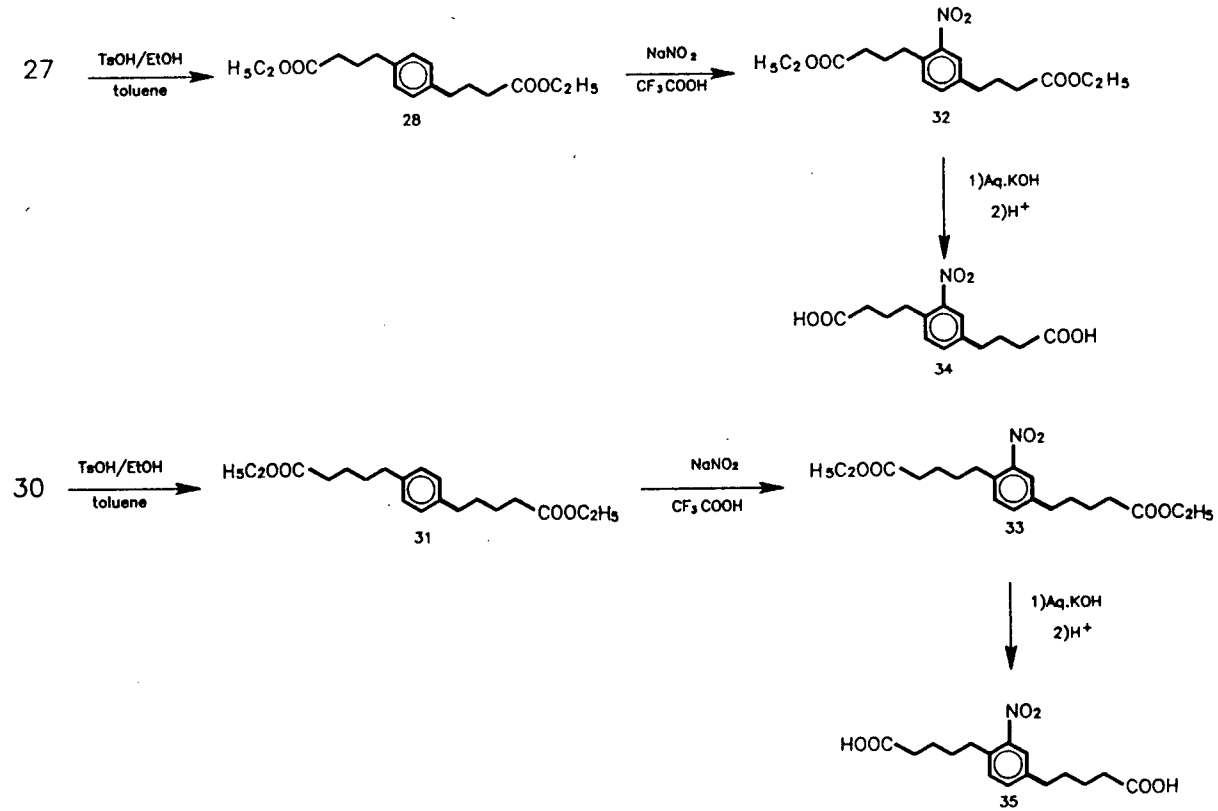

Fig. 2.2(b) Synthetic scheme for the chain derivatives

without purification. The crude diester **23** was washed with methanol until the filtrate was colorless, to give a white crystalline solid of analytical purity in 84% yield.

The diester **23** was then subjected to diborane reduction. To a THF solution of **23** and sodium borohydride, boron trifluoride etherate was added dropwise, and the reaction mixture was allowed to stir for four hours, before being quenched by the addition of acetic acid. Crystallization of the product was attempted and failed, which made purification by chromatography necessary. As the product bore two hydroxyl groups, it was very polar and did not move well on silica gel. Thus, the product **24** could only be collected as an impure brown liquid and this caused problems in the next few reactions. In order to avoid this, diborane was produced externally instead. In this case, diborane was conveniently prepared by the reaction of boron trifluoride etherate with sodium borohydride in dimethylether of diethylene glycol (diglyme). It was then distilled into the THF solution containing the starting material **23** by a small stream of nitrogen. The reduction took place smoothly and after work-up, the white slurry was dried in a vacuum desiccator giving an analytically pure product.

The next step was to convert the alcoholic groups in **24** to good leaving groups for further extension of the carbon chain. The readily prepared dibromide **25** was chosen for this purpose.

The preparation of the diacid **27** required the extension of the methylene side chain by only one carbon. This was easily achieved by the preparation of the nitrile **26** from the dibromide **25** using potassium cyanide. The nitrile **26** was readily hydrolysed in basic medium to give the corresponding pure diacid **27** in a yield greater than 90%.

To extend the methylene side chain by two carbons, a malonate synthesis was employed. The reaction was carried out in anhydrous ethanol with sodium ethoxide as the base. A common difficulty encountered in the alkylation of active CH_2 compounds

is the formation of unwanted dialkylated products. Since the reaction was carried out in ethanol, during the alkylation of diethyl sodiomalonate, the monoalkyl derivative initially formed is in equilibrium with its anion as indicated below:

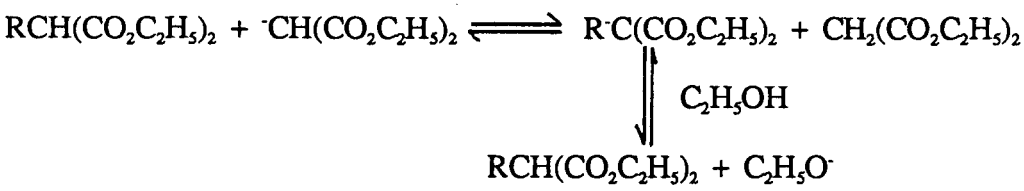

However, dialkylation does not take place to any appreciable extent because ethanol is sufficiently acidic to reduce the concentration of the anion of the monoalkyl derivative to a low value.[70] Nevertheless, to avoid possible dialkylation, an excess of diethyl malonate (4:1) was used. After 30 min reflux, some white solid came out of the solution which was believed to be sodium bromide. With 2 hours reflux, TLC indicated that no starting material remained. The tetraester was not isolated, but saponified *in situ* directly to the tetracid **29**.

Usually such tetracarboxylic acids are unstable and lose CO_2 spontaneously on heating to produce the dicarboxylic acid. However, effervescence upon addition of concentrated hydrochloric acid was mistakenly thought to be the indication of decarboxylation. Characterization of the acid prepared above indicated that no decarboxylation had occurred. Instead, effervescence originated from malonic acid which was produced by saponification of the excess diethyl malonate. Decarboxylation of tetracid **29** was then effected in DMF to give the white analytically pure product **30**.

With the diacids **27** and **30** in hand, the next consideration was to introduce a nitro function onto the benzene moiety. Although aromatic nitration has been studied extensively and there are many nitration methods available, our starting material was

such that the strong nitration conditions may affect other parts of the molecule. Direct nitration of the diacid **27** was tried first, but it proved not to be a good method. It was very difficult to determine if the reaction was complete and separation of the product from the unreacted starting material and the other impurities was difficult. Therefore, it was considered better to nitrate the ester of the diacid and obtain the nitro-diacid later by saponification.

Since there are a wide range of nitrating agents available,[71] nitration of these diesters seemed to be easy at the beginning. Firstly, the most common nitrating reagent, a mixture of concentrated nitric acid and sulphuric acid, was examined. To a mixture of concentrated nitric acid and sulphuric acid at room temperature, the diester **28** was added, and upon warming the mixture to 85°C for 20 min, some solid precipitated out. Work-up gave decomposed materials. The powerful oxidizing components in the solution might have been too violent at high temperature for the active benzylic positions. Thus, the use of a nitronium salt, nitronium tetrafluoroborate,[72] was examined. It is one of the most powerful nitrating agents and is preferred for nitrating aromatic compounds which are susceptible to acid-catalyzed hydrolysis. It also gives high yields at low temperatures[73] which can prevent oxidation of the substrates. The common solvents for this nitration are aprotic solvents such as sulfolane. However, sulfolane has a high boiling point (285°C) and is miscible with water and organic solvents. It is therefore difficult to separate the solvent and the product after reaction. Moreover, crystallization of the product might not be possible because the nitroester product might be a liquid. Fortunately, methylene chloride can dissolve nitronium tetrafluoroborate at a low concentration. A simple analogue of the starting material, toluene, was examined first with this solvent. At -80°C, toluene could be nitrated with nitronium tetrafluoroborate in methylene chloride without complication.

Therefore, nitration was tried with the diester **28** at different temperatures. The starting material in methylene chloride was stirred with nitronium tetrafluoroborate (1.1 equivalent) in an acetone-dry ice bath at -65°C for six hours, the nmr spectrum indicated that no nitration occurred and the clean starting material recovered. The temperature was raised gradually to -45°C, -30°C, -20°C and then 0°C. At this temperature, some reaction took place and a mixture of the starting material and the product resulted. The nmr spectrum of this material in the range of 7.0-8.0 ppm exhibited some new peaks at 7.32, 7.40 and 7.76 ppm in addition to the strong starting peak at 7.03 ppm. Raising the reaction temperature to 25°C gave more product but still a significant amount of the starting material remained. The starting material and the product had very similar R_f values on TLC so that it was not easy to separate them. To overcome this obstacle, nitration had to be driven to completion.

At the same time, testing of trifluoroacetic acid with sodium nitrite for nitration[74] was underway. At 0°C, a mixture of the starting material and the product was obtained. At 25°C, TLC analysis showed that there was more product than at 0°C, but more by-product with a slightly lower R_f value and more impurities at origin. In order to avoid decomposition of the compound and push the reaction towards the product, a lower temperature (0°) and more sodium nitrite were found to be useful. However, scale-up of the reaction caused problems. With 10 g of the starting material, more decomposition and more by-product resulted, and only a 40% yield of the product obtained. Therefore, the reaction was finally carried out in several small batches (5 g of the starting material). Because of the solubility problem of nitronium tetrafluoroborate in methylene chloride, the trifluoroacetic acid-sodium nitrite method was eventually employed in the synthesis.

TLC of the reaction mixture after work-up showed three very close spots: the

fastest moving one was the unreacted starting material, the middle one was believed to be the product and the one with the lowest R_f value, bright yellow in color, was a major by-product. Since the starting material, the product and the by-product were quite close on a TLC plate, it was very difficult to separate them. To purify the product, a column chromatographic separation had to be performed. Firstly, methylene chloride alone was used to elute out any possible unreacted starting material. Then, 1% methanol/methylene chloride was used to elute two bands, the faster moving one was the product and the other the by-product. Characterization of the product was mainly achieved by proton nmr and mass spectrometry. Since a nitro group exerts inductive, resonance and magnetic anisotropy effects on the benzene moiety, it causes a deshielding effect on the benzene protons. The usual chemical shifts of the protons of nitro benzene with respect to benzene are: δ_{ortho} = 0.92, δ_{meta} = 0.25, δ_{para} = 0.38 ppm downfield. The proton nmr [Fig. 2.3(b)] obtained from the nitrobenzene derivative **33** was in agreement with such a resonance pattern. The doublet at 7.28 ppm was assigned to the proton meta to NO_2. The doublet at 7.35 ppm was due to the proton para to NO_2 and the most downfield singlet at 7.72 ppm due to the proton ortho to NO_2. The proton nmr in the range 1-4 ppm also reflected the asymmetry caused by nitration, *e.g.* the triplet from the benzylic position, now split into two triplets. In the mass spectrum, the parent peak was not seen but a parent-45 corresponding to the loss of OCH_2CH_3 was observed. But, it was also the mass for the parent peak of the starting material. This was checked by high resolution mass spectrometry. For the nitrodiester **32**, the peak at mass 306 was examined. From calculation, the starting material should have the mass of 306.1831 and the product minus OCH_2CH_3 of 306.1342. The high resolution mass spectrum showed that the 306 peak (306.1352) was from the product instead of the starting material. This characterization was further

confirmed by elemental analysis.

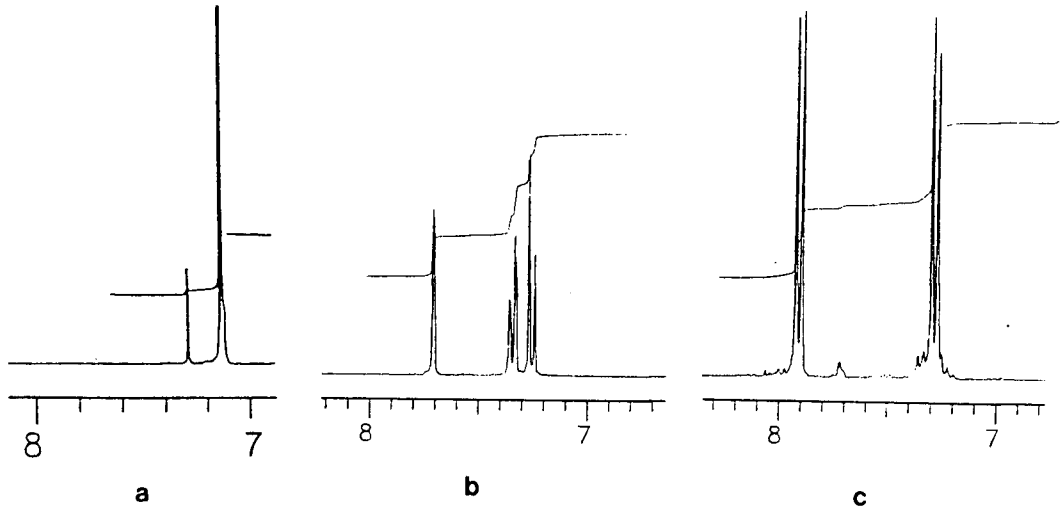

Fig. 2.3 NMR Spectra at 7.0-8.0 ppm range: (a) starting material; (b) nitro-product; (c) by-product

The bright yellow by-product was separated and fully characterized. Its proton nmr spectrum showed two doublets in the 7-8 ppm range each accounting for two protons [Fig. 2.3(c)]. This implied that something must have happened to the side chain instead of the benzene ring itself. The peaks assigned to the benzylic positions accounted for only two protons and the others were unchanged. The peaks from the 2,2′-positions had split into two sets. Therefore, only one benzylic position had been affected causing the asymmetry. The mass spectrum gave a parent peak amounting to the parent(the starting material)+O-2H which suggested that one of the benzylic positions had been oxidized to carbonyl function during the reaction. The nmr spectra comparison of this material to the known compound (4′-ethylacetophenone)[75] revealed a similarity. Thus the structure below was proposed for the by-product:

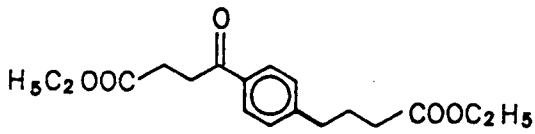

The structure was in agreement with the proton nmr and mass spectra of the by-product and was further confirmed by high resolution mass spectrometry and carbon-13 nmr. The carbon-13 nmr spectrum showed three typical carbonyl signals at 172, 173 and 197 ppm which were from two carbonyls of the chain terminal ester and a benzylic carbonyl. The conclusion was manifested by the mechanism of the reaction proposed by Uemura *et al.*[76] The following reactions were involved in the reaction solution:

$$NaNO_2 + CF_3COOH \rightleftharpoons HNO_2 + CF_3COONa \quad (1)$$

$$2HNO_2 \rightleftharpoons N_2O_3 + H_2O \quad (2)$$

$$HNO_2 + H^+ \rightleftharpoons NO^+ + H_2O \quad (3)$$

$$N_2O_3 \rightleftharpoons NO + NO_2 \quad (4)$$

$$N_2O_3 \rightleftharpoons NO^+ + NO_2^- \quad (5)$$

$$2NO_2 \rightleftharpoons N_2O_4 + H^+ \rightleftharpoons NO_2^+ + HNO_2 \quad (6)$$

The nitronium ion (NO_2^+) for aromatic nitration could be formed by reaction (6).

For the formation of aromatic ketones from alkylbenzenes with labile hydrogens (benzylic hydrogens), hydrogen abstraction by radical species (NO or NO_2) to give a benzylic radical is possible. This radical forms a hydroperoxide and the alkoxyl radical breaks down to form a ketone, or dimerizes to dialkyl oxide[77] (Fig. 2.4). It is interesting to note, however, that an appreciable amount of ketone was obtained even at low temperature (0°C, gave 30% of the total material) in our case.

The two nitrodiesters were saponified in aqueous KOH-ethanol solution under

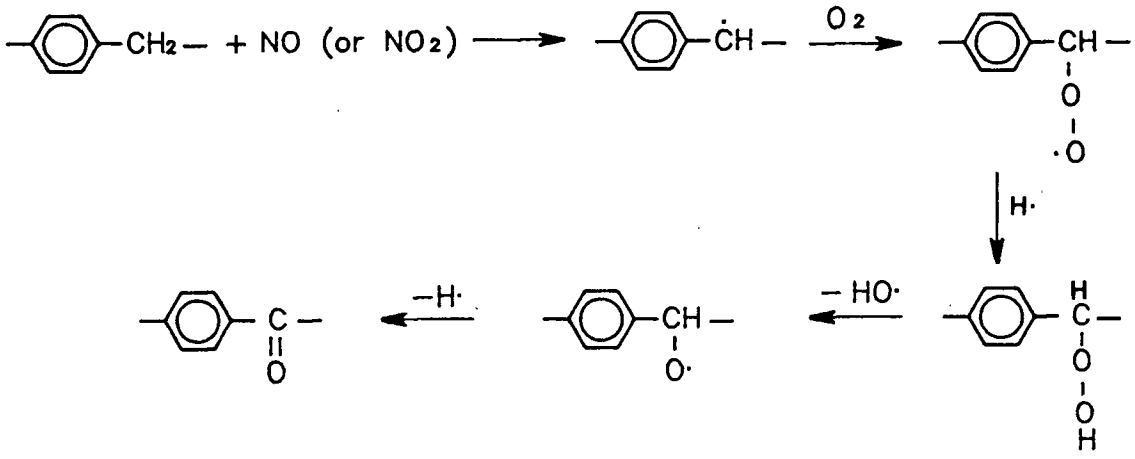

Fig. 2.4 Possible mechanism for the formation of the ketone by-product

nitrogen. The mass spectrum did not show the parent peak but a very strong parent-18. High resolution mass spectrometry indicated that it originated from the loss of one molecule of water to give, presumably the intramolecular anhydride. Thus, with the desired diacids **27**, **30**, **34** and **35** in hand, the pyrrole coupling reactions were studied.

2.4 Chain linked bis pyrroles

The first step towards dipyrromethane dimers was to convert the diacid chain to the chain linked dipyrrolic intermediate by a Friedel-Crafts reaction (Fig. 2.5). It was successfully achieved by reacting two moles of the β unsubstituted pyrrole with the diacids **27**, **30**, **34** and **35**.[78] There were two choices for the appropriate β-free pyrroles: 2-ethoxycarbonyl-3,5-dimethylpyrrole or 2-benzyloxycarbonyl-3,5-dimethyl

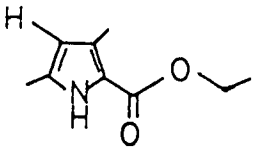

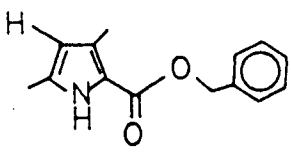

pyrrole. The latter appeared to be better because it would not only save a step, but would also bypass the high temperature transbenzylation. However, acylation with 2-benzyloxycarbonyl-3,5-dimethylpyrrole was examined and the benzylester pyrrole was found to be sensitive to the acylation conditions. By changing reaction conditions such as temperature, quantity of the catalyst used and solvent proportions, the reaction gave some product heavily contaminated by decomposed material. TLC of the reaction mixture showed a small spot with a lower R_f value and another faint spot with higher R_f value. These materials were postulated as being the half-acylation product and a very small amount of the product. Because of the insolubility of both starting material and product, it was impossible to purify and characterize them. The ethyl ester analogue **36** was therefore used in the reaction.

The coupling, carried out in two stages, involves the initial formation of the acid chloride from the diacid, which is subsequently acylated in the presence of stannic chloride, in a mixture of methylene chloride and nitromethane. Four equivalents of stannic chloride were used in the reaction to give reasonable yields (60-80%) compared to 60-70% for the durene analogues.[50, 63] It should be noted that the nitro compounds gave higher yields than the compounds without the nitro function.

The next step was the reduction of the keto functions to methylene groups.[79] Initially, diborane produced *in situ* (Section 2.3) was used. For the two diketones without nitro substituents, **37a** and **37b**, the reaction proceeded smoothly without any complication. But, for the nitro compounds **37c** and **37d**, problems arose and the yields were low (~57%). The products obtained by this method were so contaminated that they were brown colored. With this kind of method producing diborane *in situ*, too many species might exist in the reaction medium: $NaBH_4$, BF_3, B_2H_6 and B_2O_3 *etc.* It is generally believed that sodium borohydride alone does not affect nitro groups; only

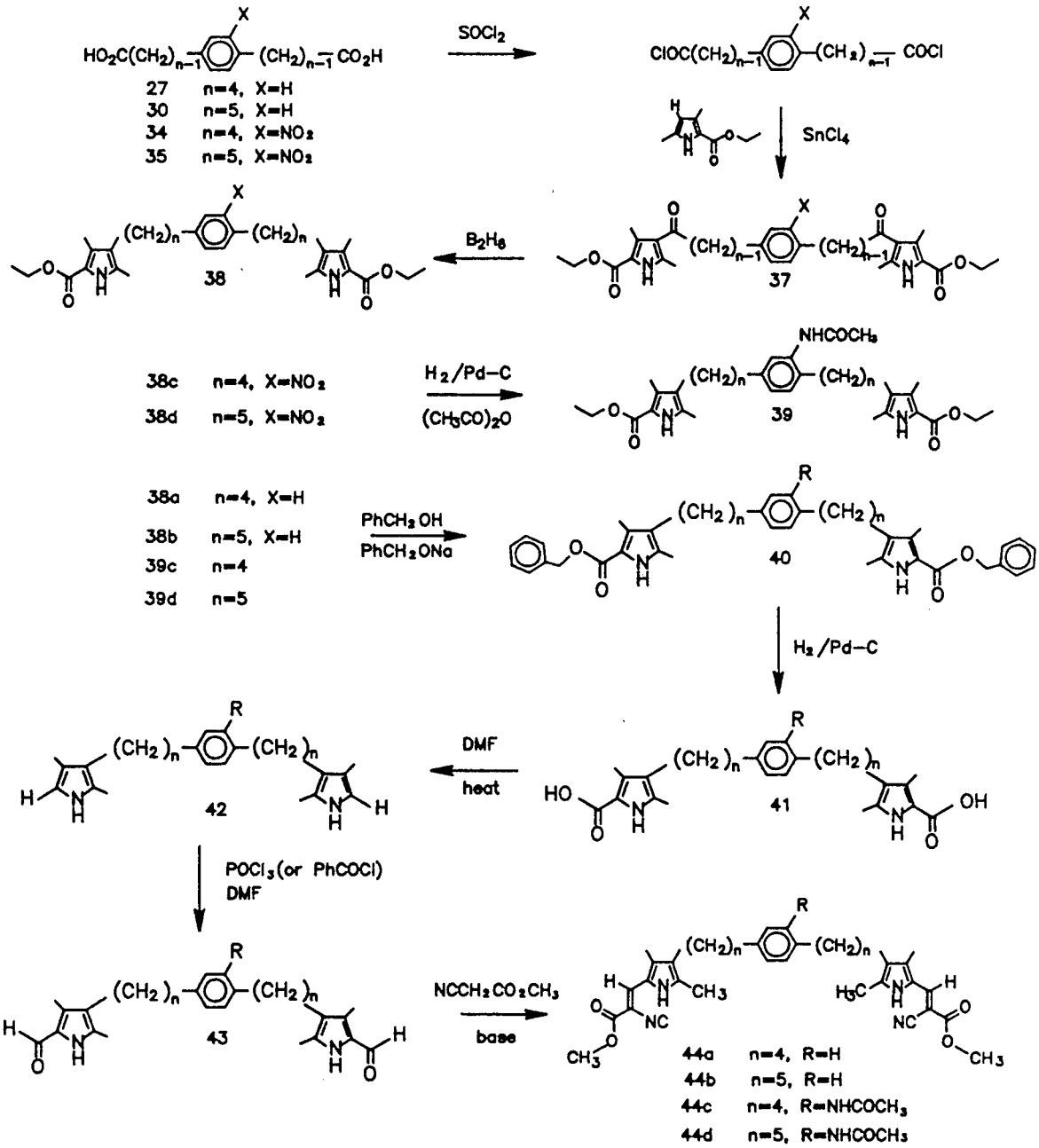

Fig. 2.5 Syntheses of chain linked bis pyrrolic intermediates

the combination of sodium borohydride with other catalysts such as palladized charcoal[80] can affect nitro functionality. However, there are some examples showing that the nitro groups of aromatic compounds can be reduced by sodium borohydride alone.[81, 82] In the latter case, the reaction has been considered to involve a 1,4 addition-elimination mechanism:

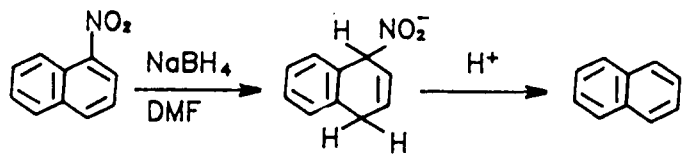

Since our starting material had many active sites, side reactions may have taken place and the possible attack on the nitro function by $NaBH_4$ may be one of them. In order to make the reaction cleaner, the borane-THF complex was used. The starting material was suspended in anhydrous THF, and addition of 1 M BH_3-THF complex caused the material to go into solution. Once the reaction was complete, it was quenched by adding methanol. A white, clean product was crystallized in high yield (~80%) from the concentrated solution upon addition of methanol. Since the reaction went well with the commercially available BH_3-THF complex, the reduction of diketones **37a-d** was finally completed with this reagent.

With the methylene chain of the desired length in the capping group, the next consideration in the synthetic plan was to change the α-ethyl ester to the synthetically useful α-formyl derivative. This included the removal of the ethyl ester functionality, thermal decarboxylation of the resulting diacid to give the α-free pyrrole, and transformation to the α-formyl derivative by a Vilsmeier reaction.[83] The direct saponification in strongly basic medium gave gelatinous solid products in low yields. In addition, the reaction went very slowly, requiring prolonged reflux with the risk of

subsequent decarboxylation to the air-sensitive α-free pyrrole which occurred in the synthesis of the durene analogue.[50, 63] Therefore, hydrogenolysis of the corresponding benzylester derivatives was chosen as the preferred route.[63] The transesterification, performed at high temperature, was a modification[84] of the procedure developed by Hayes *et al.*[85] Benzyl alcohol and the starting material were brought to reflux under a stream of nitrogen and a solution of sodium in benzyl alcohol was added in 1 mL portions. During each addition, vigorous evolution of ethanol and a simultaneous drop in temperature were observed. When no more ethanol was evolved, the hot solution was poured into a stirred mixture of acetic acid and methanol, the product was crystallized out by adding water. Because prolonged reflux would result in decomposition of the starting material and the product, the reaction time was minimized by immediately adding the catalyst once reflux occurred and quenching the mixture within a few minutes after the final addition of the catalyst. The solid product was filtered off as soon as possible because the decomposed materials in the solution tended to color the product pink; this colored material could only be removed by chromatography.

This transesterification method was suitable for diethylester **38a** and **38b**. It gave a clean reaction and the yield was high. But, for the two diethylesters with the nitro group, the reaction did not give any product. Reflux of the starting material in benzyl alcohol did not cause any problems; the solution was clear yellow at reflux. Upon addition of sodium benzyloxide catalyst, however, the solution turned dark red immediately without effervescence of ethanol. After work-up, no product could be crystallized out and a deep red solution remained. Evaporation of the solvents gave a reddish black residue which could not be dissolved in any solvent nor be scraped off from the reaction flask. By introduction of a nitro function on the benzene moiety, the

property of the compound towards strongly basic catalysts at high temperatures had changed dramatically so that the compound decomposed. This may be attributed to the increasing acidity of the molecule due to the nitro functionality. If the acidity of the benzylic protons increased after introduction of the nitro group, the benzylic protons may be able to dissociate from the starting material. A literature survey suggested this possibility. The pKa of benzyl alcohol in DMSO at 25°C[86] is 21.30 and the pKa of toluene in DMSO is ~42.[87] This means that at room temperature, toluene is a much weaker acid than benzyl alcohol, and it is not possible for the benzylic protons of toluene to react with the base, sodium benzyl alkoxide. After introduction of a nitro group, the pKa of 4-nitrotoluene in DMSO decreases to 22.5.[86] This value is comparable to that of benzyl alcohol. Even though the pKa of 2-nitrotoluene could not be found in the literature, one might expect that it should be lower than that of 4-nitrotoluene, considering inductive and conjugative effects. Therefore, in the reaction medium, some of the protons may dissociate and destruction of the starting material be initiated.

To avoid the transesterification step, a direct saponification of the ethyl ester in aqueous base had to be considered even though it did not give a clean product with similar compounds.[63] If the diacid could be obtained by this method, hydrogenolysis could be avoided. This seemed to be a better route for the synthesis. Saponification was investigated in a refluxing KOH solution of water and n-propanol. The amount and ratio of the materials (solvents, base) used in the reaction and reaction time were varied, but no product was obtained and the starting material was always destroyed. In most cases, some solid remained undissolved. As indicated by the appearance of the reddish colored material, decarboxylation might have taken placed under these strongly basic, high temperature conditions giving an air-sensitive α-free pyrrole derivative.

Because transesterification and saponification did not afford any product for the NO_2 substituted compounds, an alternative procedure was proposed (Fig. 2.6, p. 56). Instead of transforming the 5,5′-positions of the bis pyrrole derivatives to the α-formyl function, a 5-formyl simple pyrrole could be used in the coupling to the dipyrromethane dimer. This required the 2,2′-positions of bis pyrrolic derivatives to be unsubstituted, for coupling with the α-formylpyrrole. The resulting product of this route is the same as the dipyrromethane from the original synthetic plan. Transformation of a simple pyrrole to an α-free pyrrole is a well developed procedure[63] (Fig. 2.7), which could be adopted in our bis pyrrolic derivative. The reaction was investigated on a nmr scale.

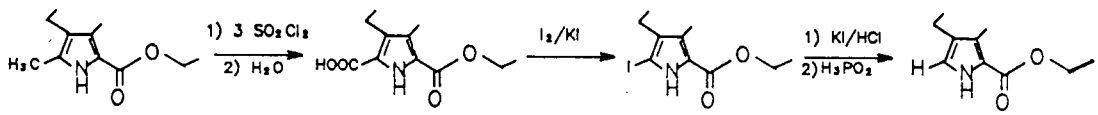

Fig. 2.7 Scheme for the synthesis of the α-free pyrrole

The nitroethylester **38d** (Fig. 2.5, p.51) dissolved in $CDCl_3$ in a nmr tube was treated with three equivalents of SO_2Cl_2 and the reaction monitored by nmr. The reaction proceeded very slowly. After two hours, nmr indicated that a large amount of the starting material still remained, but, peaks corresponding to the ethyl groups of the ethyl ester and the chain methylenes had changed. Some new peaks around 5-6 ppm and 1 ppm appeared. In addition, the pyrrole NH had split into two groups of peaks. As the reaction continued the nmr spectrum became more complicated. Finally, the 2,2′-CH_3 signal disappeared completely but the resulting compound was definitely not the desired α-trichlorinated derivative. Chlorination had taken place at other parts of the molecule. Therefore, this route was also not suitable.

Because the final purpose of this work was to make porphyrins with amide caps,

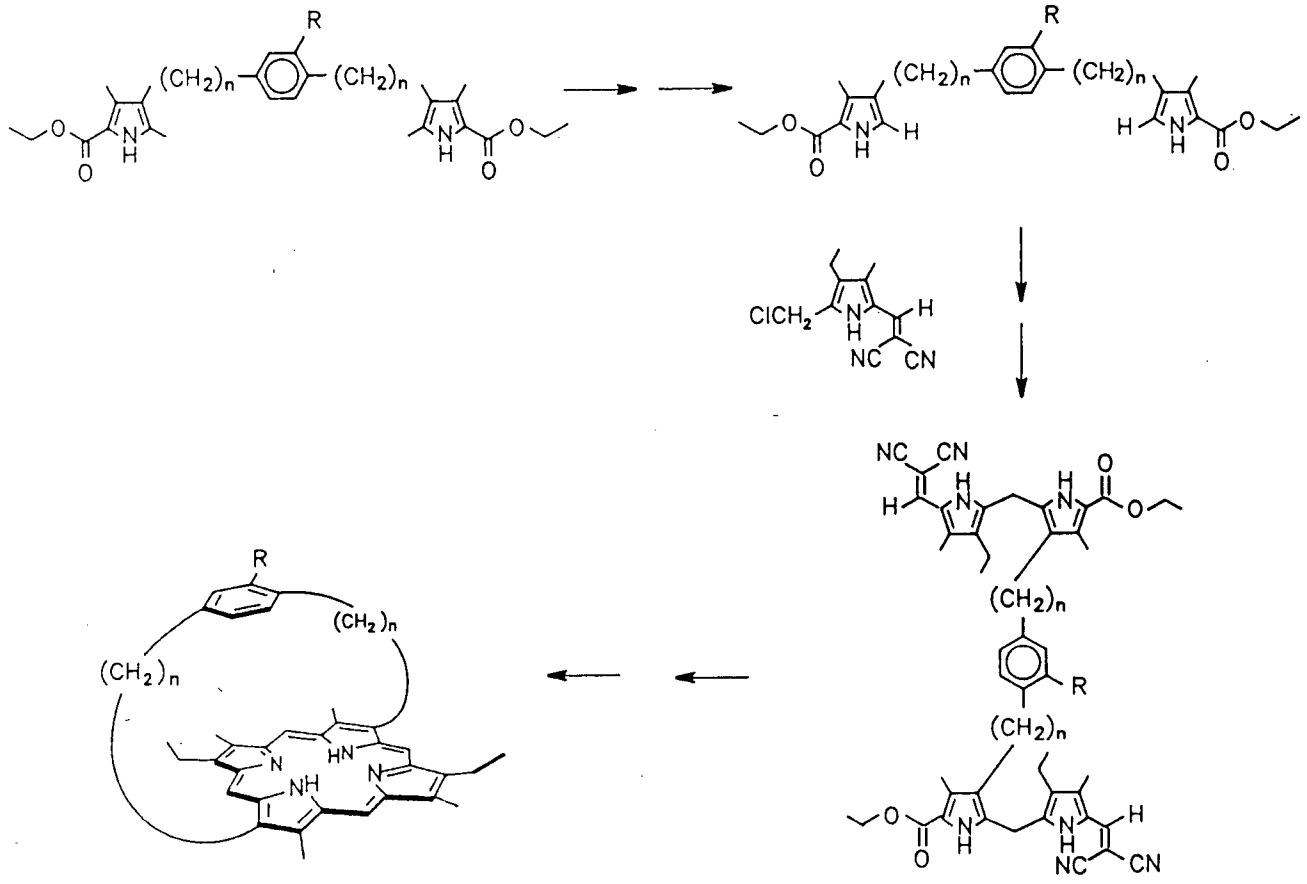

Fig. 2.6 The alternative procedure for the syntheses of the porphyrin

it was then decided that the nitro group should be transformed to amide at an early stage. The aromatic nitro function is one of the most active towards catalytic hydrogenation. It is generally presumed that nitroso compounds and hydroxyl amines are intermediates in the reduction. Both of these types of compounds give amines when treated with reducing agents:

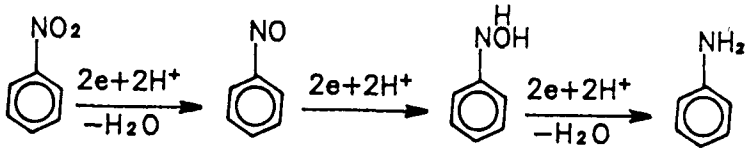

In our reaction, the starting material dissolved in THF was stirred with 10% Pd/C, acetic anhydride and sodium acetate under hydrogen. The amine produced was transformed to the amide *in situ.*

Now the amide substituted compounds were ready to undergo transesterification. To avoid the high temperature of boiling benzyl alcohol (205°C) which might cause decompose of the compounds, transesterification at 100°C and 12 mm Hg was employed as described by Kenner and coworkers.[88] Nitrogen had to be passed through the benzyl alcohol to exclude air before heating. Sodium was added followed by the starting material and the reaction vessel was evacuated so that any ethanol produced was pumped away to drive the reaction to the product side. After 5 hours of heating on a steam bath, most of the starting material had decomposed to a red colored material with only little product formed. The reaction time was reduced to 30 min which was found to be suitable for the reaction to go to completion. The solution was cooled, acidified by acetic acid and benzyl alcohol distilled off at 0.1 mm Hg in a boiling water bath. The impurities and the remaining benzyl alcohol were washed away with ethyl acetate and the white product was obtained in 60-70% yield.

The next consideration in the synthesis was hydrogenolytic debenzylation. The

reaction went smoothly at room temperature and 1 atm hydrogen. In the cases of the amide substituted benzylesters **40c** and **40d**, uptake of hydrogen was very slow at the beginning, but speeded up on addition of fresh catalyst. Removal of the catalyst by filtration, and evaporation of the solvent, produced a white solid.

The next major concern in the synthesis was to introduce a formyl function at the 2-positions of the pyrroles. The diacid was first decarboxylated by heating in DMF and formylation was carried out *in situ*. The diacid derivatives **41a-d** were directly used in the decarboxylation without purification. Decarboxylation was monitored by UV/visible spectrometry. The 282 nm band of the starting material was reduced to a shoulder after two hours refluxing. Continuous refluxing, however, did not remove the shoulder completely. The solution containing the α-free pyrrole was cooled in an ice bath under nitrogen for the next reaction.

Introduction of a formyl group into the chain linked bis pyrrole was achieved by a Vilsmeier reaction,[83, 62(b)] whereby the α-free pyrrole in the decarboxylation solvent was treated with either phosphorus oxychloride-DMF or benzoyl chloride-DMF.[89] The reactive intermediate (a) has been suggested for the phosphorus oxychloride reaction and the similar species (b) for the benzoyl chloride type reaction. The reaction is known to proceed via an iminium salt (c). The iminium salt was subsequently

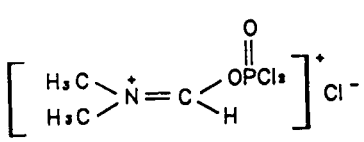

a

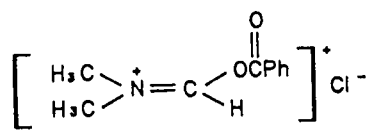

b

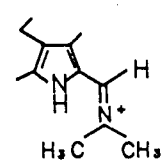

c

hydrolysed by using a weak aqueous base, sodium bicarbonate, to give the α-formylpyrrole.[63]

In the course of this work, it was found that formylation of the two compounds

without an amide substituent on the benzene moiety could be effected by phosphorus oxychloride. But for the two amide substituted analogues, phosphorus oxychloride gave little product. After addition of the Vilsmeier reagent to the amide substituted α-free pyrrole, the solution turned reddish purple and hydrolysis gave some intractable tars mixed with the product. In fact, modification of the Vilsmeier formylation procedure by substitution of benzoyl chloride for phosphorus oxychloride[89] is better for acid sensitive compounds. Eventually, formylation of the two amide substituted compounds was effected using benzoyl chloride-DMF as the Vilsmeier reagent. In all cases, the iminium salts were not isolated but hydrolysed directly in aqueous base.

The next stage in the synthetic scheme was to attach a second pyrrole to each end of the chain linked intermediates to give the desired dipyrromethane dimers. This required the use of sulphuryl chloride for α-methyl oxidation and acidic conditions for coupling. Protection of the formyl function was therefore essential. The most useful of these protecting groups was first used by Fischer and Hofelmann[90] and later by Woodward[91] in the synthesis of chlorophyll. These are the cyanovinyl derivatives, prepared by a Knoevenagel condensation of a formyl pyrrole with malononitrile or a cyanoacetate ester, under basic conditions.[9c] These compounds are usually crystalline, less soluble than the aldehyde counterparts and move well on silica gel, allowing the use of the Knoevenagel reagent to scavenge the crude aldehyde and then purify it by chromatography. Due to the extended conjugation, the products have absorption maxima in the 390-410 nm range, resulting in yellow to orange colors, and fluorescence under UV light.

However, strongly basic conditions, which are required for regenerating the aldehyde, limit the usefulness of these protecting groups to pyrroles bearing no ester groups. This was not a matter of concern in this work since this synthesis was

designated[63] to make the best use of the strongly basic conditions. When the protecting group was removed after formation of the dipyrromethane dimer, the use of alkali would not only regenerate the aldehyde function but also saponify the two ester functions and produce intermediate **48**.

The choice of which protecting group should be used depends on the nature of the compounds. Malononitrile gives the less soluble derivative, and its use should be

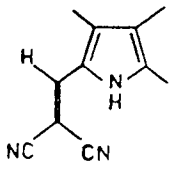

DICYANOVINYL

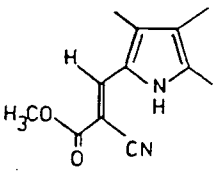

CYANOACRYLATE

avoided in systems of inherently low solubility. But the corresponding dipyrromethane dimer can be crystallized cleanly giving a pure product. The solubility of cyanoacrylates are much higher than dicyanovinyls and they can be deprotected more readily. But, in principle, Z and E isomers (four of them could result in this case, one with the two bulky ester groups being opposite to the pyrrole nucleus should predominate) could exist. Crystallization of the corresponding dipyrromethane dimers was impossible due to the existence of these isomers.

During the course of this synthesis, the two protecting groups were investigated in detail. Both reactions to form dicyanovinyl and cyanoacrylate derivatives proceeded smoothly in refluxing toluene with cyclohexylamine as catalyst. The reaction solvent had been chosen to prevent premature crystallization of the monoprotected aldehyde.[63] The reaction was monitored by TLC where the monoreacted derivative moved faster than the starting material, whereas, the diprotected derivative moved well ahead of both. It was found that within two hours, all of the starting material would be converted to

the diprotected derivative. The advantage of the dicyanovinyl derivatives was ease of purification on a silica gel column, which was essentially a filtration process using methylene chloride as the eluting solvent. Column chromatography of cyanoacrylate derivatives was more complicated, ethyl acetate or methanol in methylene chloride had to be used to move the product. Both dicyanovinyl and cyanoacrylate derivatives could be crystallized out giving lemon yellow, analytically pure products.

Both protected chain linked dipyrrolic derivatives were examined for pyrrole coupling reaction to make dipyrromethane dimers **47**. In the case of the cyanoacrylates, the reaction went well without any complication, but just as expected, the product **47** could not be crystallized. After the solvent was evaporated under vacuum, column chromatography was necessary to purify the product. In some cases, a second column of alumina or the use of the chromatotron with a silica gel rotor was necessary since impurities were very difficult to be removed. The purification of the dicyanovinyl analogue was relatively easy and the product could be crystallized. But a large volume of reaction solvent, methylene chloride, was needed since the solubility of the starting material was very low, especially in the case of the amide substituted dipyrromethanes. Changing of the solvent to 1,2-dichloroethane did not improve the solubility much. 40 mg of the starting material needed more than 200 mL of 1,2-dichloroethane to dissolve it completely. Therefore, a compromise had to be made and the cyanoacrylate protecting group was employed eventually in the synthesis.

2.5 Dipyrromethane dimers and porphyrins

With the dialdehyde protected, the next major concern was to couple the second pyrrole to make the synthetically useful intermediates: dipyrromethane dimers **47** which

could be then further transformed into porphyrin **49** (Fig. 2.8, p.63). This was achieved by coupling two α-free pyrrole nuclei to the chain linked derivatives of pyrrylcarbinyl cations. Pyrrylcarbinyl cations are highly stabilized by delocalization of the positive charge throughout the electron-rich pyrrole nucleus (Fig. 2.9), and as a result they are

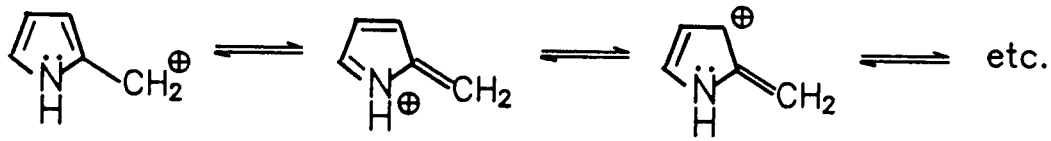

Fig. 2.9 Resonance structures of pyrrylcarbinyl cations

formed readily from a variety of precursors (**51**) by an S_N1 mechanism. Of the three commonly used pyrrylcarbinyl cation sources (bromide, chloride and acetoxy),

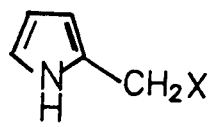

51

X = -Br, -Cl, $-OCH_3$, -OH,
$-OCOCH_3$, $-NR_3$, $-NHR_2$ *etc.*

chloromethylpyrrole was chosen to be the source of pyrrylcarbinyl cation in this synthesis because of its stability.

It is known that the α-methyl position can be selectively chlorinated over a β-methyl group when using sulphuryl chloride,[62(b)] but multichlorination at the α-methyl is possible. Usually this is controlled by the use of low temperatures and calculated amount of reagent. In addition, the presence of an electron withdrawing cyanoacrylate group deactivates the ring towards dichlorination. Since in the starting material, there were two positions to be chlorinated, two equivalents of the chlorination reagent must be used.

Compounds **44** contain a benzene moiety which is likely to undergo chlorination

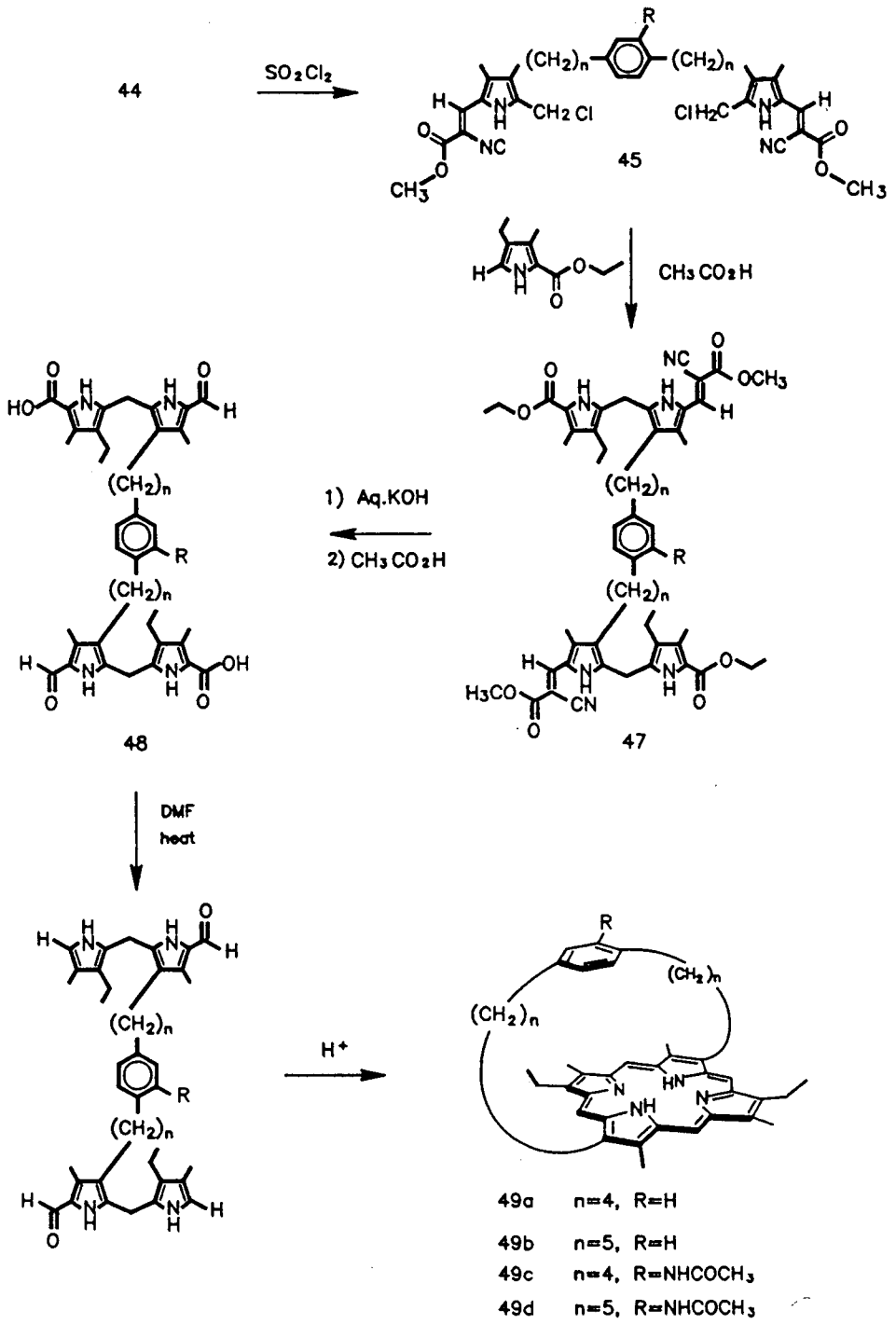

Fig. 2.8 Transformation of dipyrromethane dimers and cyclization to the porphyrins

as well under the reaction conditions. From the detailed discussion[63] of the mechanism of the pyrrole side chain chlorination, it is known that both electrophilic[93-95] and free radical[96] mechanisms are possible. Therefore, any attempt to chlorinate the pyrrolic side chain might chlorinate the benzene moiety. Wijesekera[63] has shown that exclusive pyrrole side chain chlorination takes place in the presence of a hexaalkyl substituted benzene during the reaction with sulphuryl chloride. It was expected that with compounds **44a** and **44b** there should not be any problem with this reaction. But, in the cases of amide substituted **44c** and **44d**, the electron donating amide might make the benzene ring active enough towards chlorination. Since a pyrrolic nucleus is known to be more reactive towards electrophilic attack, it was hoped that this reaction center could compete favorably with the amide benzene center and lead to only pyrrole chlorination.

In fact, treatment of the starting material in dry methylene chloride with slightly more than two equivalents of sulphuryl chloride led to exclusive α-chlorination at the pyrrole nucleus and a high yield of dipyrromethane dimer **47** was isolated. No benzene chlorinated material was observed. The α-chloromethyl derivative was isolated by evaporating the solvent under vacuum. The yellow powdery product was used for coupling with the α-free pyrrole **46**, without further purification.

A variety of conditions has been discussed for the coupling of pyrrole monoesters.[62(b), 63] In our synthesis, the coupling in acetic acid according to the procedure developed by Wijesekera[63] was adopted with success. The bis-α-chloro methylpyrrole derivative was suspended in glacial acetic acid together with the 2-ethoxycarbonyl-4-ethyl-3-methylpyrrole (**46**) and the mixture was warmed in a water bath. In order to prevent any oxidation of the α-free pyrrole at high temperature, a nitrogen atmosphere was provided for the reaction mixture. When the temperature

reached 70°C, the chloromethyl compound began to dissolve resulting in a transparent red solution. An aliquot was taken out for TLC analysis. There were two major spots existed which could be assigned to the product and the half coupled compound. After the mixture being heated at this temperature for 30 min, a TLC analysis exhibited only a single yellow spot with some impurities at the origin. This yellow spot could be colored reddish violet by bromine vapour which is characteristic for dipyrromethanes due to the ready oxidizability at the methane bridge.[97] Since no other spot on TLC plate was colored by bromine vapour, the two α-chloromethyl positions in a single starting material molecule had been attached to α-free pyrrole and no half coupling compound remained. Because of the possible isomers (up to four), crystallization of the product was impossible. The solvent was therefore removed completely by evaporating under vacuum, and the product was purified by chromatography. In all cases, silica gel was used. The product did not move on the column with methylene chloride alone, and either methanol or ethyl acetate had to be added to facilitate its elution. Even after column chromatography, the compounds **47a** and **47b** were still not pure, and separation in a chromatotron followed by an alumina column had to be performed to obtain an analytically pure sample. In spite of the difficulty of purification, the cyanoacrylate protecting group was still preferred because of the high yield (> 80%).

The final stage of the synthesis was to convert the dipyrromethane dimers to porphyrins. The first step here was to remove the cyanoacrylate protecting groups and the ethyl esters simultaneously. Since an amide is not as susceptible as an ester towards hydrolysis, it would be possible to hydrolyse the ester function and leave the amide unattacked by choosing proper reaction conditions. The reaction was therefore examined on a small scale. Dipyrromethane dimer **47c** was refluxed in aqueous n-

propanol/potassium hydroxide (10 equivalents) under nitrogen. Although cleavage of the cyanoacrylate function can be followed by UV/visible spectroscopy, complete formation of the acid from the ethyl ester was only guaranteed by prolonged reflux in a strongly basic medium. Prolonged refluxing might lead to decarboxylation of the acid function and possible hydrolysis of the amide function. After 2 hours at reflux, the reaction mixture was cooled, neutralized and the gelatinous precipitate isolated by filtration. The mass spectrum (FAB) gave the parent peak. The ^{1}H-nmr spectrum of this material indicated that no ester group remained and the other peaks, which were very complicated, could not be assigned. The product was carried forward. The α-acid function was decarboxylated in boiling DMF to give the α-free derivative. This solution diluted with methylene chloride was added slowly, to the reaction flask containing the acid catalyst, by syringe pump. Work-up afforded the porphyrin in extremely low yield (5%). During the addition of the α-free derivative, precipitation of some black tar was observed and the porphyrin obtained appeared to decompose. It was possible that the amide function might have partially hydrolysed during the deprotection step giving an unstable amine derivative. To avoid the problem, the material after hydrolysis was subjected to acetylation, by stirring with acetic anhydride for 20 min. Decarboxylation seemed to be unsuccessful; the band at 280 nm in the UV/visible changed, but, the system didn't behave like the previous reaction. In fact, no porphyrin was obtained after the cyclization reaction. When the amine was converted to the amide, the acid function was also affected by acetic anhydride, giving a mixed anhydride which could not be decarboxylated and therefore gave no porphyrin product.

The above results suggested that hydrolysis should be carried out under more controlled conditions. Therefore, various conditions, not only the concentration of the

base, but also its ratio to the reactants, were examined. With just enough base and time to deprotect the cyanoacrylate group, a large amount of ester function still existed. By a gradual increase of the amount of the base used, the amount of unsaponified compound decreased. Finally, a 30:1 molar ratio of base:starting material and a base concentration of 1.5 M in water and water:n-propanol of 2:1 were found to be optimal. The reaction was carried out under a nitrogen atmosphere in order to prevent the oxidation of any decarboxylated pyrrole derivative which was highly sensitive to the air. The reaction was followed by UV/visible spectroscopy. The starting material exhibited a strong band at 388 nm (due to the cyanoacrylate function), and a band of medium intensity at 280 nm. As reflux continued, the band at 388 nm decreased in intensity (also moving to lower wavelength) with a simultaneous increase in intensity of the band at lower wavelength and a growth of a new absorption at 324 nm (due to pyrrole aldehyde). The reaction appeared to have gone to completion within three hours. n-Propanol was boiled off and the mixture was allowed to cool to room temperature under nitrogen, at which time partial precipitation of some brown solid was observed. The solution was filtered off and the solid left on the filter paper was dissolved by adding water. The resulting clear solution was acidified and the product was collected by filtration. The yield of this reaction was high (over 80%) and the product was quite pure. Its mass and proton nmr spectra were in agreement with its proposed structure. However, a small peak at around 6 ppm was noted in the nmr spectrum, which indicated some decarboxylation during reflux. The product was not quite pure for this reason and an elemental analysis was therefore not obtained.

As discussed by Wijesekera,[63] decarboxylation can be carried out thermally under mildly acidic, neutral or weakly basic conditions. In practice the acidic decarboxylation approach gives considerably low yields of final porphyrin and should be avoided.[98] The

low yield might be due to premature condensation of the α-free and α-formyl functions which leads to intermolecular coupling. Decarboxylation of compounds **48a-d** was carried out in refluxing DMF under nitrogen. The reaction was monitored by UV/visible spectra again. In two hours, the absorption band at 280 nm (due to the carboxypyrrole group) was reduced to a shoulder and the solution was cooled and DMF evaporated under vacuo to give a small final reaction volume. Methylene chloride was added and the solution was extracted with water to remove the last trace amount of DMF. Even though precipitation of some black material during cyclization in the previous reaction had been attributed to decomposition of the amine derivative, it might also be caused by the low solubility of the compound in methylene chloride since this series of compounds had an inherently lower solubility than the durene systems. Therefore, methylene chloride was substituted for by THF to improve solubility. The methylene chloride solution containing the α-free derivative was dried over sodium sulphate, filtered and evaporated down to about 10 mL and then diluted with distilled THF to 200 mL and stored in a refrigerator for the subsequent cyclization procedure.

The dipyrromethane dimers bearing α-free and α-formyl functions were thus ready for the intramolecular cyclization to form the porphyrins via a b-bilene to porphodimethene (Fig. 2.10). The strain introduced by imposition of a short strap has less adverse effect on the more flexible porphodimethene, which is a non planar system, than on a porphyrin, and so that the initial cyclization step should proceed smoothly. Once formed, the porphodimethene undergoes rapid autoxidation where the net gain in resonance stabilization energy is the driving force for porphyrin formation. Furthermore the bilene-b can accommodate the diagonal strap, which also allows for correct orientation of the remaining α-formyl and α-free functions to undergo a second intramolecular coupling to the porphodimethene.[63] The reaction of an α-free with an α-

formyl group must occur in an intramolecular head-to-tail fashion. Intermolecular reaction between functions on different molecules will only cause polymerization without porphyrin formation. Therefore the acid-catalysed condensation must be carried out under high dilution in order to minimize intermolecular coupling.

Since the acid-catalysed rearrangement of dipyrromethanes is a well known

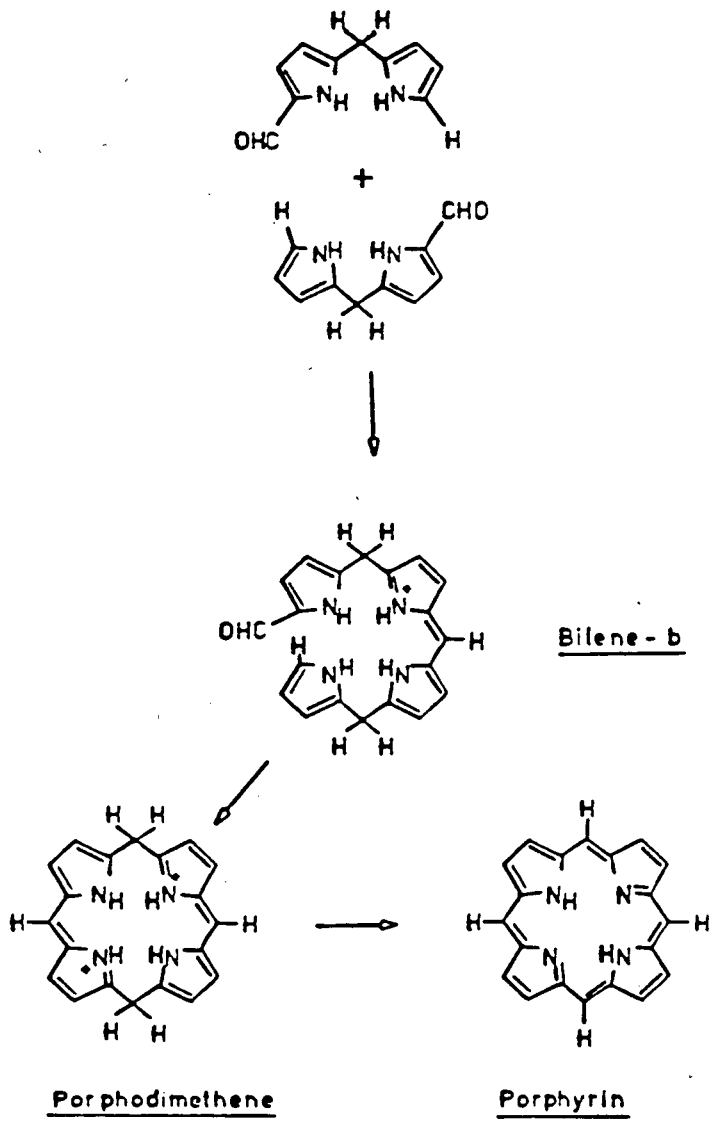

Fig. 2.10 Formation of a porphyrin via the acid-catalyzed cyclization of dipyrromethanes

phenomenon,[99] the acid used in the condensation has to be carefully selected. Toluene-p-sulphonic acid, first used by Kenner's group[100] and later used successfully by Wijesekera[63] in the synthesis of the durene-capped porphyrins, was employed in our work. The THF solution of the decarboxylated **48** was added extremely slowly to the acid catalyst using a syringe-pump. This is a device that is used to add a solution at a constant rate, by means of a hypodermic syringe. At the slowest speed of operation, the pump emptied a 50 mL syringe in approximately 9 hours. Two separate syringes were used to add the solution to two flasks, each containing toluene-p-sulphonic acid in methanol and methylene chloride.

Two stages of chromatography purification were needed to purify the porphyrins. Since the porphyrins were not easily eluted on silica gel, methanol was necessary to facilitate separation, resulting in the elution of some impurities. Chromatography on an alumina column was therefore used to remove these impurities and obtain pure **49a** and **49b**. In the cases of the amide substituted porphyrins **49c** and **49d**, the alumina column was not efficient, and thus chromatotron purification was needed.

The hemin chloride complexes were synthesized from the porphyrins and ferrous chloride.

2.6 Electronic absorption spectra of benzene and amidobenzene capped porphyrins

The electronic spectra of a typical porphyrin consists of an intense Soret band and four weak bands in the visible range. The Soret band, often recorded at around 400 nm with a molar extinction coefficient around 400,000, is characteristic of the macrocyclic conjugation of porphyrins. The two hydrogens in the center of the free-

base porphyrin break the conjugated ring symmetry, and give rise to two possible tautomeric forms.[101] It is generally considered that the Soret band is due to one π-π^* transition which is similar for both tautomers, and that the four bands at longer wavelengths (I, II, III, IV in the order of increasing energy) arise in pairs, two from each tautomer, from a second π-π^* transition.[101] The intensities of the four satellite visible bands are correlated to the nature of the side chains on porphyrins.[101(b)] The etio spectrum [Fig. 2.11(a)] is found in all porphyrins carrying alkyl side chains at six or more peripheral positions. The spectral pattern for the band intensities is IV>III>II>I. If a single carbonyl (aldehyde, ketone), a carboxylic acid, ester or an acrylic acid side chain is present, band III becomes more intense than band IV, affording a rhodo-spectrum. These strongly electron-withdrawing groups, which also cause shift of absorption to longer wavelengths, are termed "rhodofying" groups. Two rhodofying groups on adjacent 'pyrrole' subunits cancel each other's rhodofying effect, and an etio-spectrum results. But, two rhodofying groups on diagonally opposite rings enhance each other's effect and an oxorhodo spectrum is obtained [Fig. 2.11(c), III>II>IV>I]. Finally, if four or more peripheral positions are unsubstituted, the spectrum is of the phyllo-type.

Upon protonation of the free-base porphyrin, a dication results with a proton attached to each central nitrogen. Since the symmetry changes to D_{4h}, the four bands in the visible range collapse to two, the α-band and β-band. The Soret band in the absorption of dicationic porphyrins is displaced to longer wavelength compared to that in neutral species. Insertion of a metal at the porphyrin core also results in similar changes in spectra.

Since the porphyrins synthesised here have only alkyl substituents on the porphyrin periphery, one might expect the etio-type absorption spectra. This was

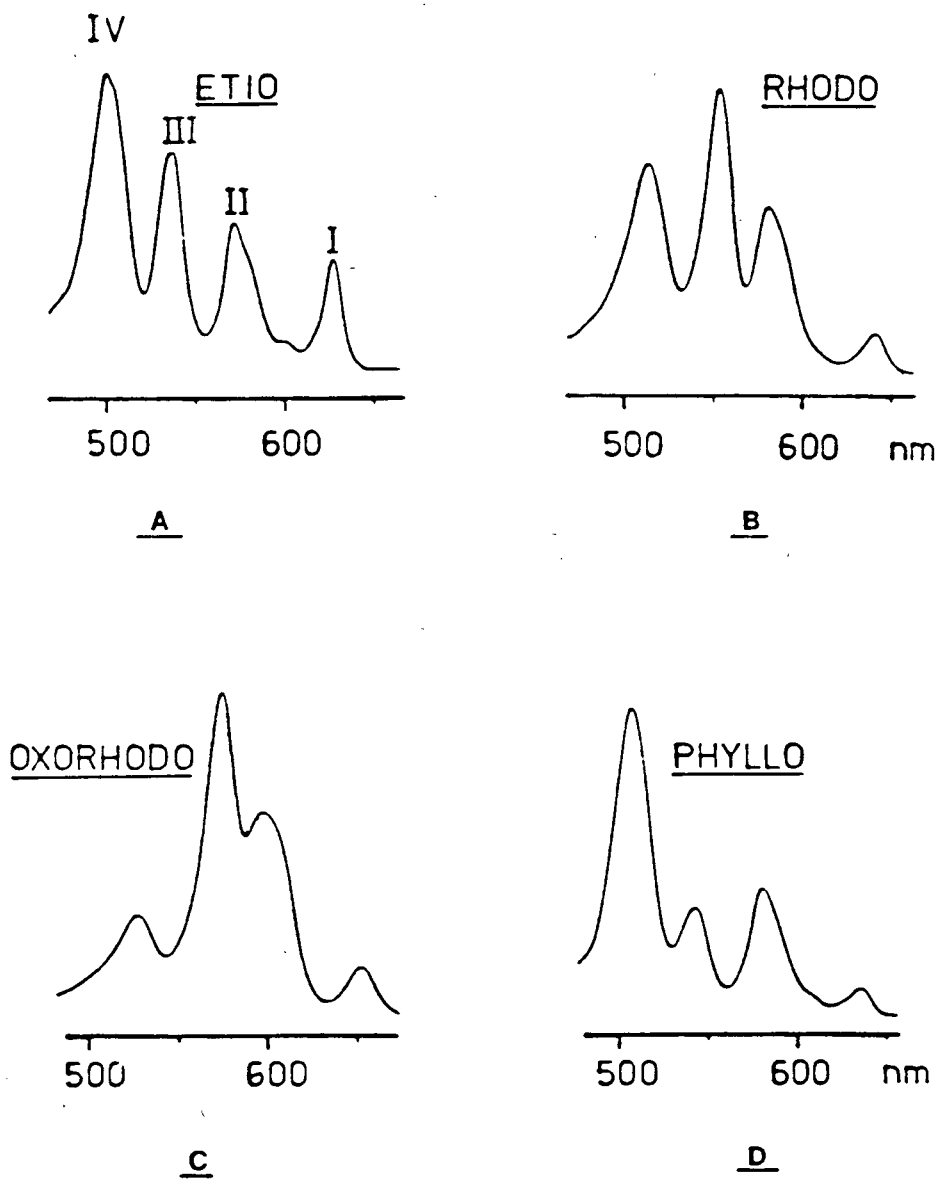

Fig. 2.11 Trends in visible spectra for various pyrrole-substituted porphyrins

indeed the case of the 5/5-methylene chain capped porphyrins. But, there has been evidence[63] showing that distortion of the porphyrin skeleton also leads to a change in intensities of the four visible bands. Our porphyrins also showed similar trends. As the chain length decreases from a 5/5-methylene chain (Figs. 2.13, 2.15) to a 4/4-chain (Figs 2.12, 2.14), the spectra changed from an etio-type to a typical rhodo-type with III>IV>II>I. This change in intensities is due to distortion of the porphyrin macrocycle as the chain becomes shorter.[63]

Table 2.1 Comparison of electronic absorption spectral data of the porphyrins in CH_2Cl_2

λ_{max} nm

(log ε)

Porphyrin	Soret	Band IV	Band III	Band II	Band I
Benzene-4,4 **49a**	404	506	542	572	626
	(5.26)	(4.08)	(4.10)	(3.91)	(3.60)
Benzene-5,5 **49b**	400	498	534	568	622
	(5.10)	(3.90)	(3.77)	(3.46)	(3.13)
Amidobenzene-4,4 **49c**	404	506	542	572	624
	(5.23)	(4.07)	(4.09)	(3.89)	(3.60)
Amidobenzene-5,5 **49d**	400	500	536	568	622
	(5.26)	(4.20)	(4.13)	(3.96)	(3.82)

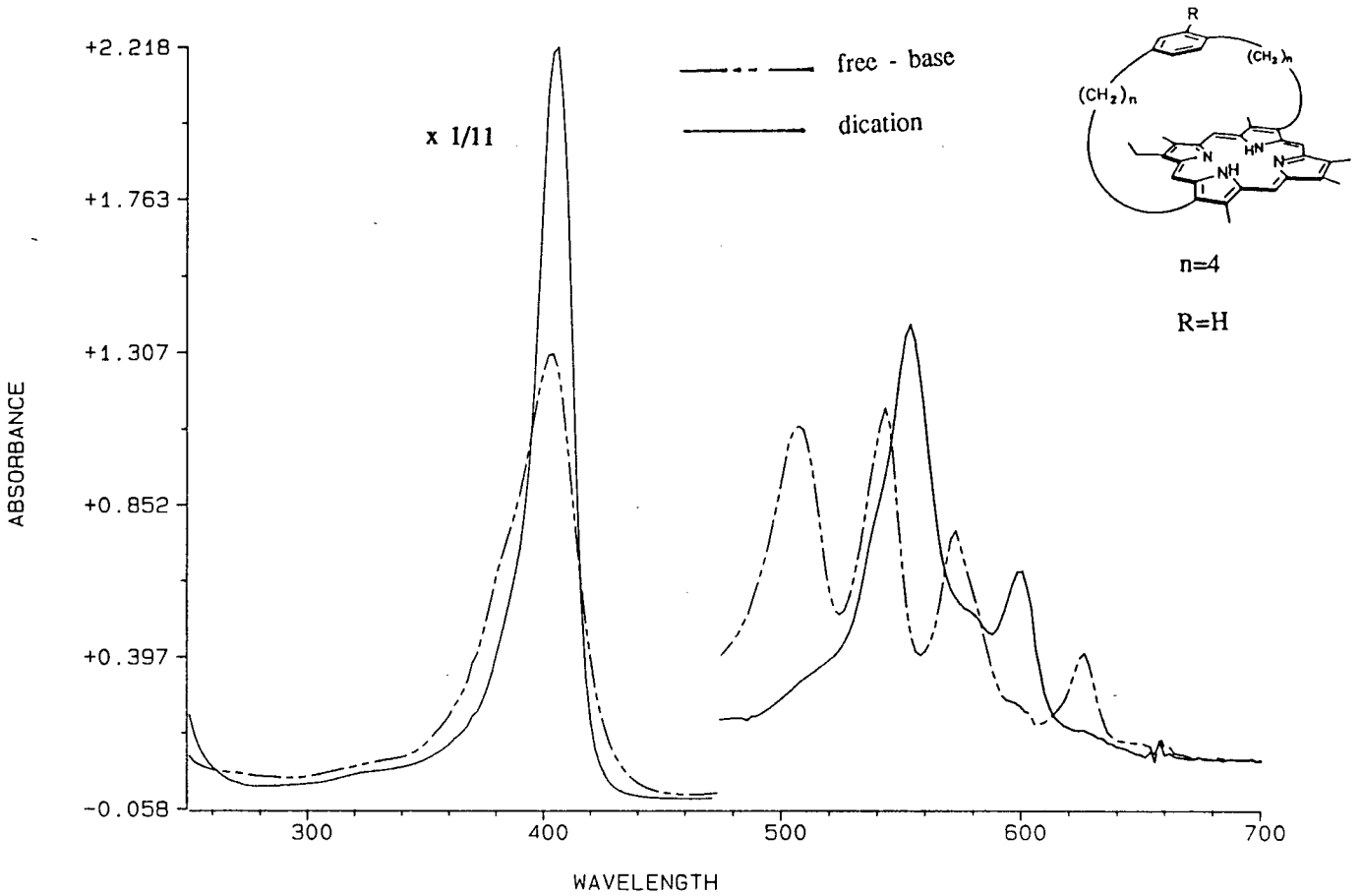

Fig. 2.12 UV-visible spectrum of the benzene-4/4 capped porphyrin **49a** in CH_2Cl_2

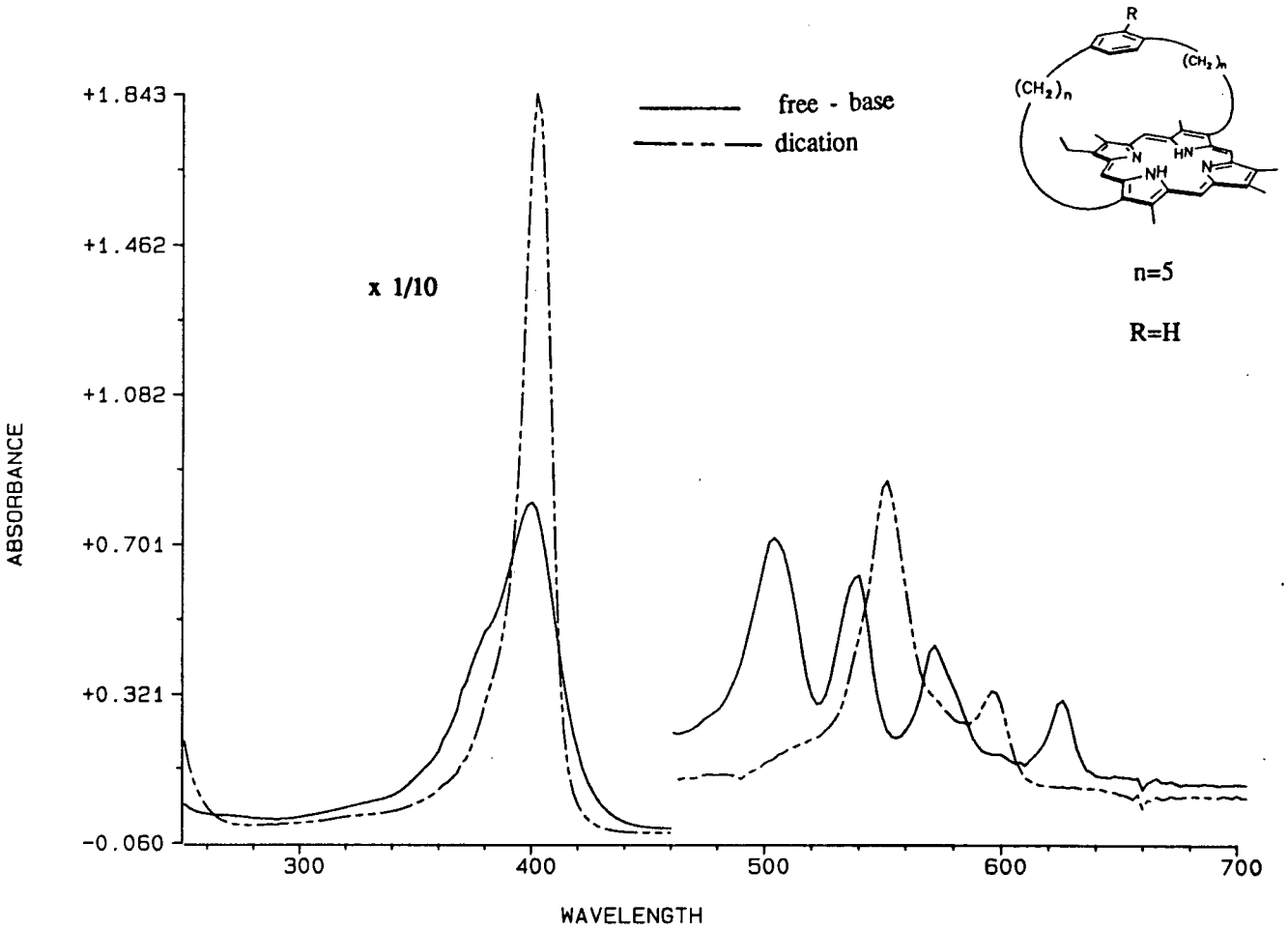

Fig. 2.13 UV-visible spectrum of the benzene-5/5 capped porphyrin **49b** in CH_2Cl_2

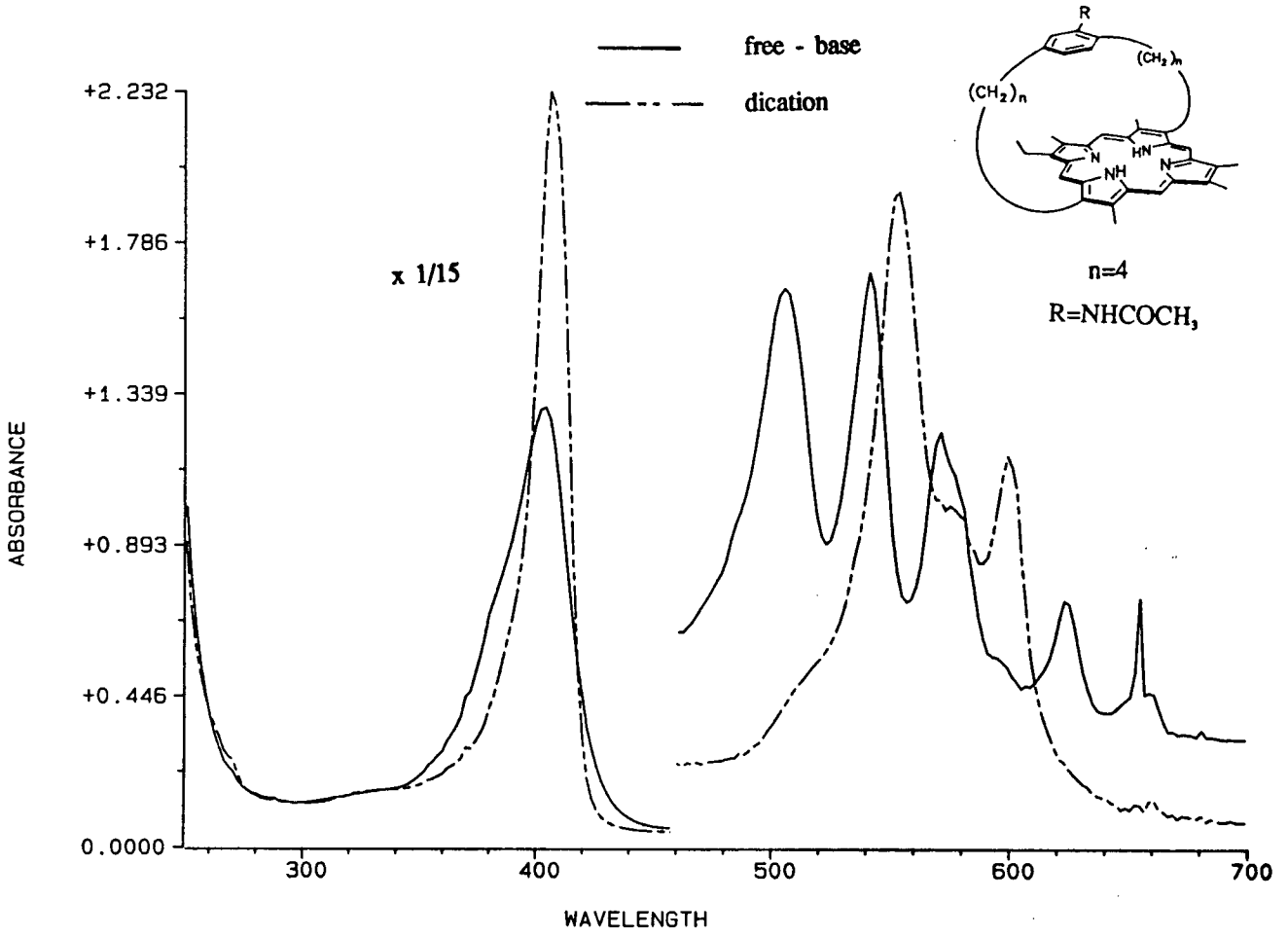

Fig. 2.14 UV-visible spectrum of the amidobenzene-4/4 capped porphyrin **49c** in CH_2Cl_2

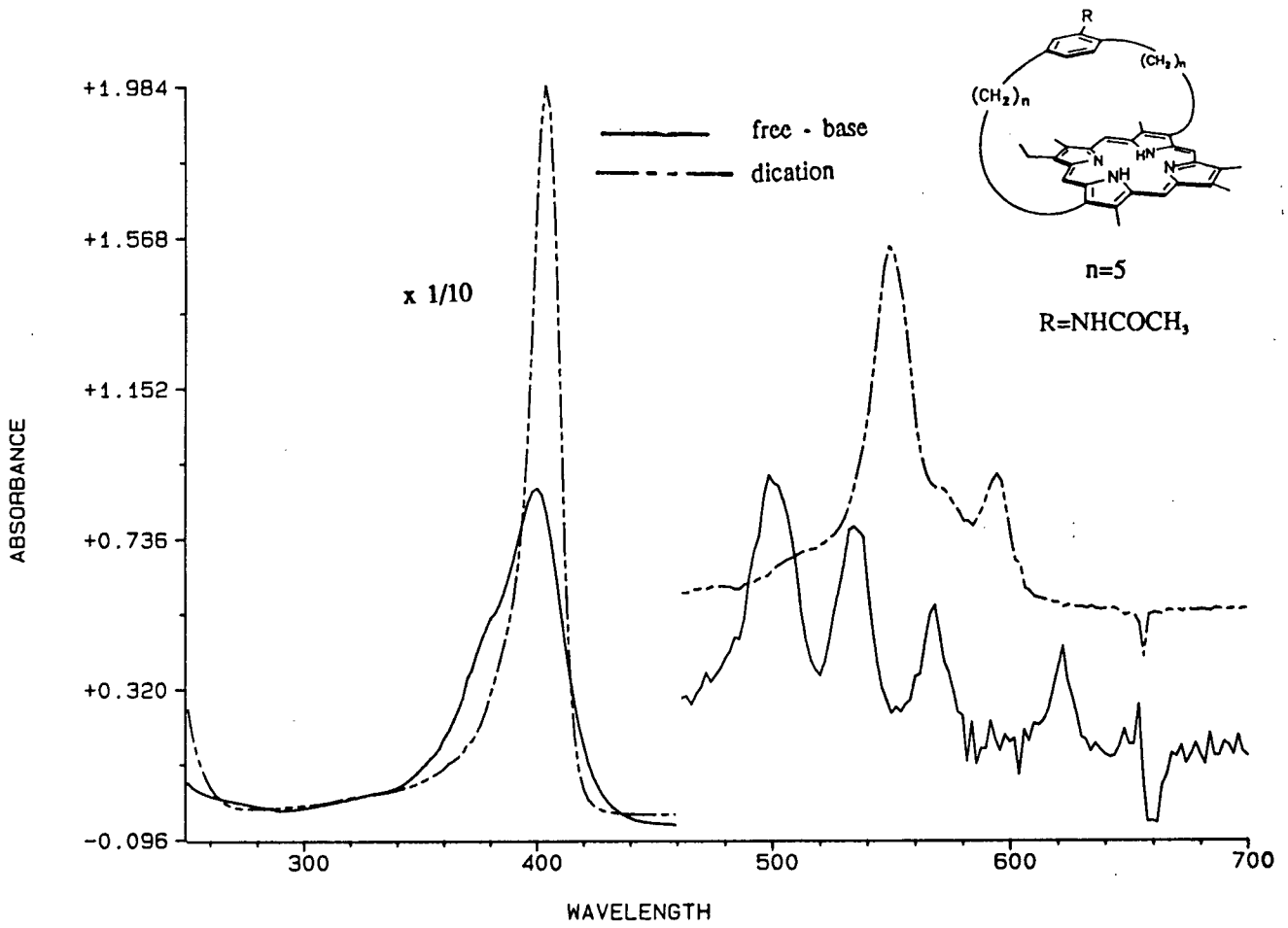

Fig. 2.15 UV-visible spectrum of the amidobenzene-5/5 capped porphyrin **49d** in CH_2Cl_2

2.7 Proton nmr spectral assignments of benzene and amidobenzene capped porphyrins

The ^{1}H-nmr spectra (Figs. 2.16 - 2.19) of the porphyrins were recorded at 400 MHz in deuterated methylene chloride. In order to minimize the variation of chemical shifts caused by aggregation of the porphyrin,[102] concentrations of the solutions were kept low and consistent (in all cases, concentrations of the porphyrins were ~0.01 M). The alkyl substitution pattern surrounding the porphyrin periphery of the system is essentially identical to that of etioporphyrin II (Fig. 2.20), except that the C_2H_5 groups at positions 3 and 13 are replaced by a methylene chain linking of the cap. As for several other similar strapped and capped porphyrins that have been synthesised, the simple ^{1}H-nmr spectrum of etio II porphyrin is used as a suitable reference.[50, 63, 64]

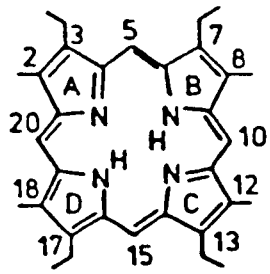

Fig. 2.20 Etioporphyrin II

The diamagnetic ring current of the highly delocalized porphyrin macrocycle causes protons associated with the periphery to experience a deshielding effect, and therefore these protons resonate further downfield from TMS. For etio II, the peripheral groups' resonances appear as four distinct groups of signals: the protons from all four equivalent methyl groups resonate at δ 3.62, the ethyl groups as a triplet and a quartet at δ 1.87 and δ 4.11 respectively, and the four methine protons (5, 10, 15,

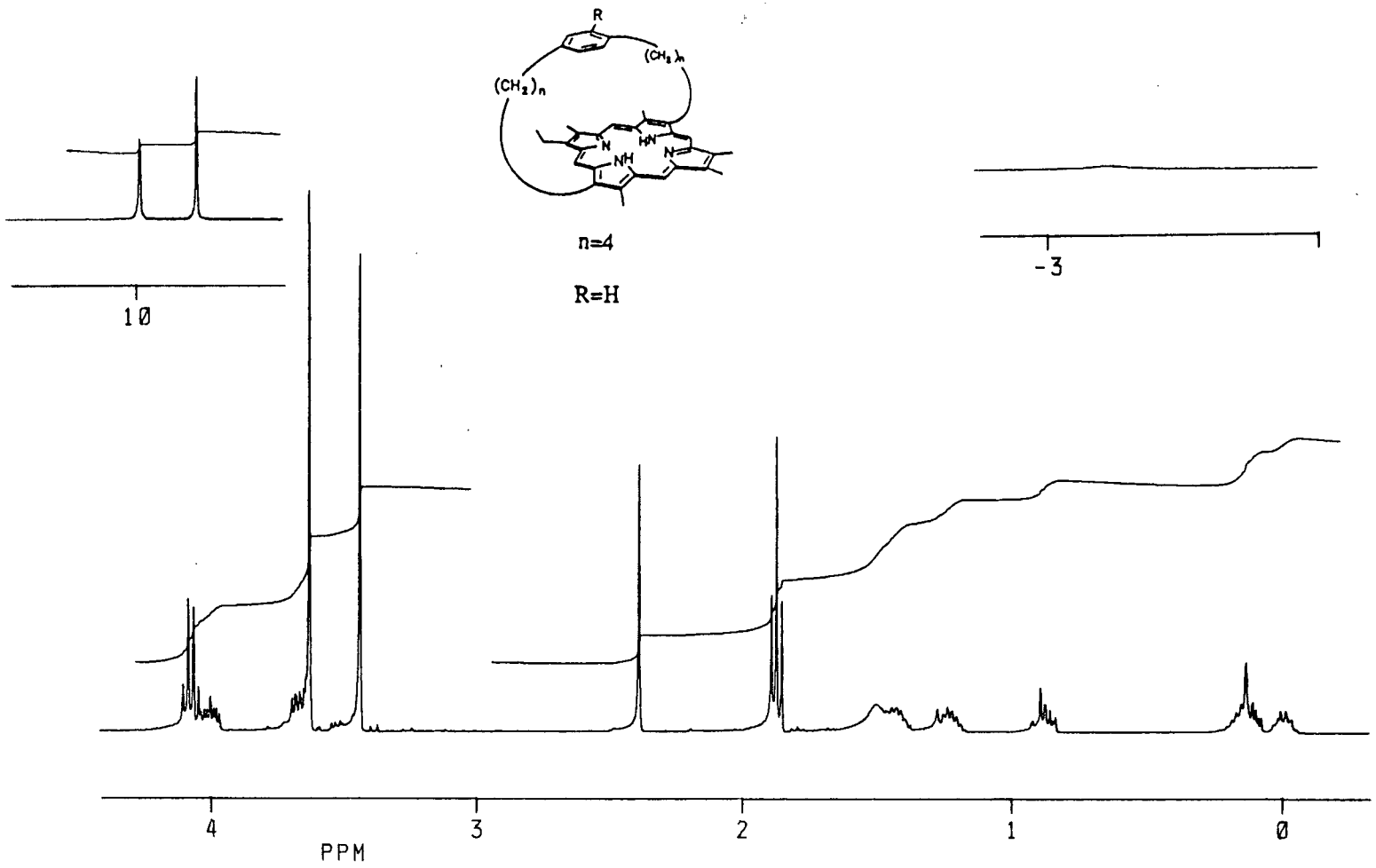

Fig. 2.16 ^{1}H-nmr spectrum of the benzene-4/4 capped porphyrin **49a** in CD_2Cl_2

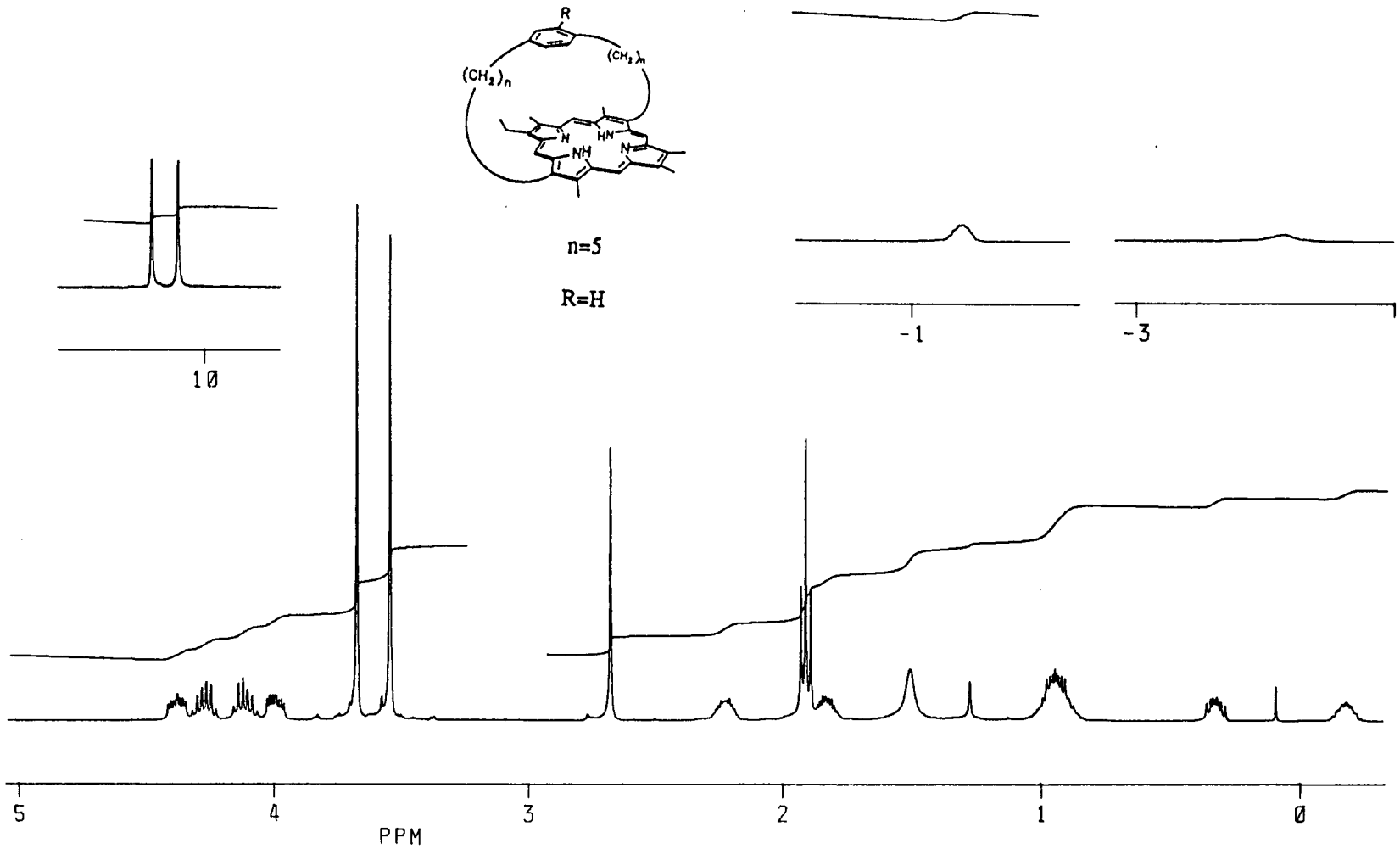

Fig. 2.17 ^{1}H-nmr spectrum of the benzene-5/5 capped porphyrin **49b** in CD_2Cl_2

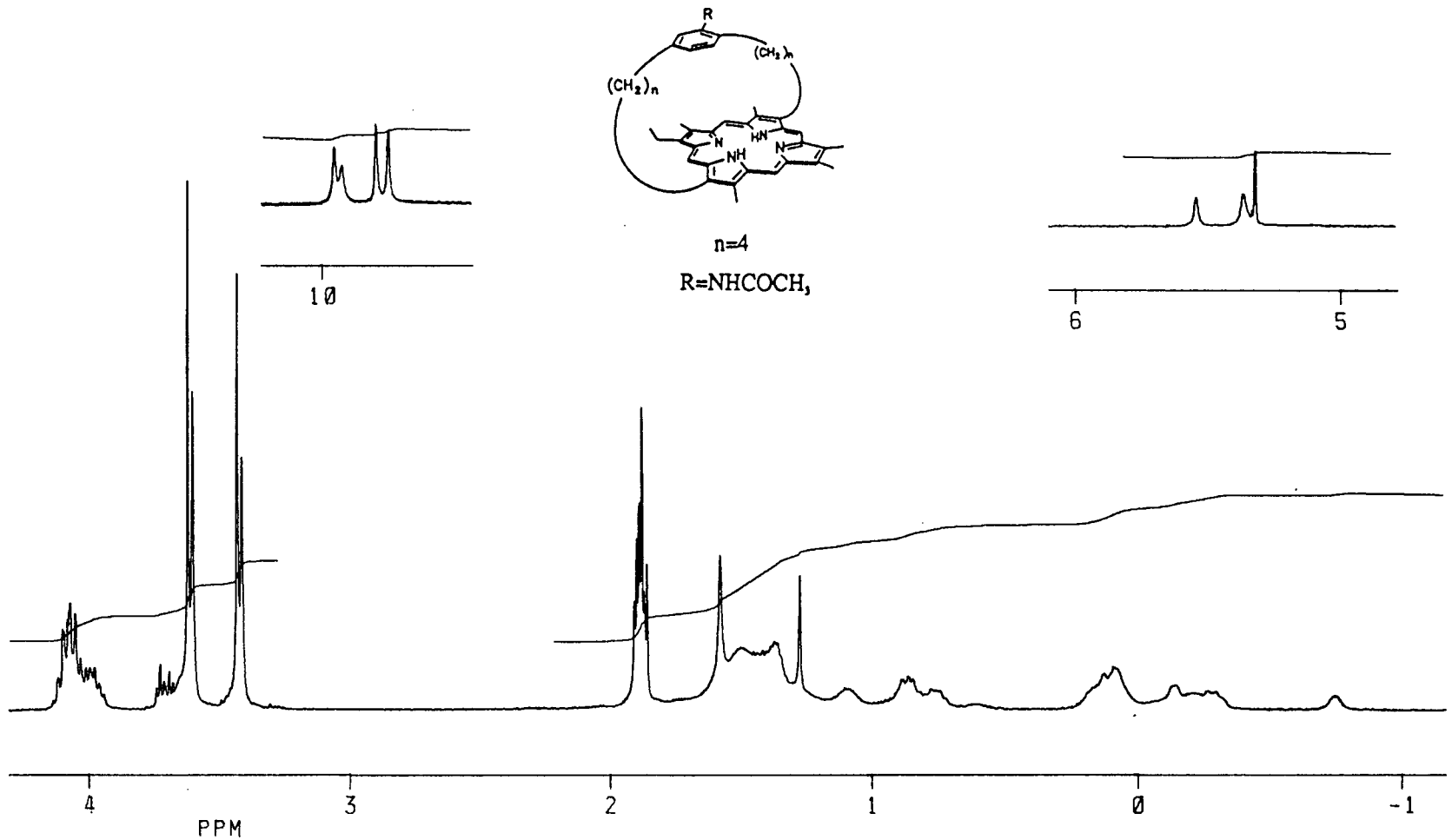

Fig. 2.18 ^{1}H-nmr spectrum of the amidobenzene-4/4 capped porphyrin **49c** in CD_2Cl_2

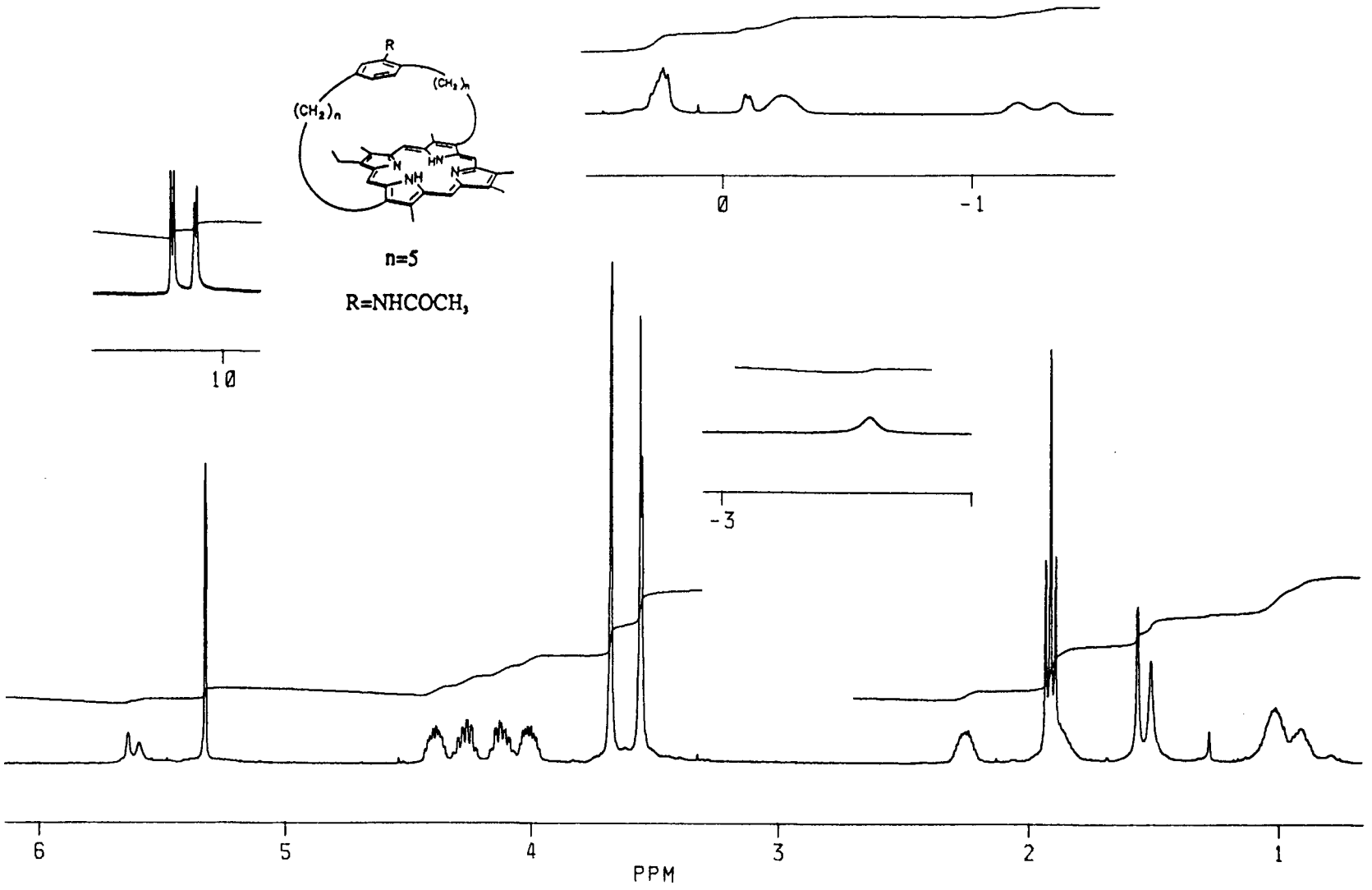

Fig. 2.19 ^{1}H-nmr spectrum of the amidobenzene-5/5 capped porphyrin **49d** in CD_2Cl_2

20) occur as a singlet at δ 10.11. The inner N-H protons appear upfield of TMS at approximately δ -3.78 due to extensive shielding by the porphyrin ring current.[103]

Introduction of a strap diagonally across one face of the porphyrin is equivalent to joining the ethyl groups at 3 and 13 positions of etio II and leads to asymmetry in the molecule. The asymmetry results in a splitting of the methyl and methine proton signals. It has been pointed out that the splitting of the methyl signals depends on the length of the strap.[63] The splitting of the methyl proton resonances for the long chain 5/5 system is smaller (0.13 ppm) than that of the shorter chain 4/4 system (0.19 ppm). As the chain length is decreased, both signals corresponding to the methyls are shifted upfield, because the distortion of rings A and C from the porphyrin plane[63, 64] towards the tight connecting strap. Such distortion affects the aromaticity of the porphyrin macrocycle and results in diminished deshielding for the methyl protons, thereby giving rise to an upfield shift. Within these shifts, the higher field signals shift more than low field ones, corresponding to methyl groups at the 2 and 12 positions.

A similar trend is found in the methine proton resonances. As the chain length decreases from 5/5 to 4/4, both meso signals are shifted upfield, with the peak at higher field being shifted more. Irradiation of the multiplet due to the 7 and 17 methylene protons (at 4.07 ppm in the case of 4/4-benzeneporphyrin) causes an enhancement in the intensity of the higher field meso-proton resonance, indicating that this signal corresponds to the protons at the 5 and 15 positions. It is these protons that are closer, in terms of carbon-carbon bonds, to the chain linked 3 and 13 ring positions. Distortion caused by a strap linking positions 3 and 13 is therefore expected to affect the 5 and 15 meso protons more than the 10 and 20 protons, thus giving rise to the increasing separation between their respective resonances.[50, 63, 64]

A reversal of this trend is displayed for the N-H protons in a downfield shift

relative to etio II. The shorter chain compounds have shifted more. Situated within the porphyrin core, these N-H protons experience extensive shielding from the porphyrin ring current that causes them to resonate at high field (δ -3.78 ppm for etio II). A disruption of the electron delocalization, caused by increasing distortion of the macrocycle from planarity, results in a diminished shielding effect and thus a gradual shift downfield.[50, 63, 64]

A striking feature of the ^{1}H-nmr spectra is the large upfield shifts observed for some of the proton resonances of the methylene straps which have previously been observed for various strapped porphyrin derivatives.[50, 63, 64, 104] Those protons positioned above the porphyrin macrocycle experience a strong shielding effect from the diamagnetic ring current, and thus have upfield shifts (relative to that of the free chain derivative). The protons associated with carbon atoms attached to the porphyrin periphery, however, experience the deshielding effect of the porphyrin ring current and thus resonate further downfield relative to those above the porphyrin macrocycle.

A series of double resonance experiments were carried out on the 4/4-benzene capped porphyrin in order to obtain a first-order assignment of the peaks arising from the chain methylene protons. The sixteen chain methylene protons appear as seven distinct multiplets, each consisting of two protons except the one at 0.13 ppm which consisted of four protons [Fig. 2.21(a)].

Figs. 2.21-2.25 illustrate the spectra obtained by a series of double resonance experiments carried out on the methylene chain protons of the 4/4-benzene capped porphyrin **49a**. The spectra were recorded in the same range and on the same expansion in order to give a direct comparison with the undecoupled spectrum. The seven resonances due to the chain methylene protons and the two signals from the peripheral ethyl groups have been labelled A to I, starting from the one at the lowest

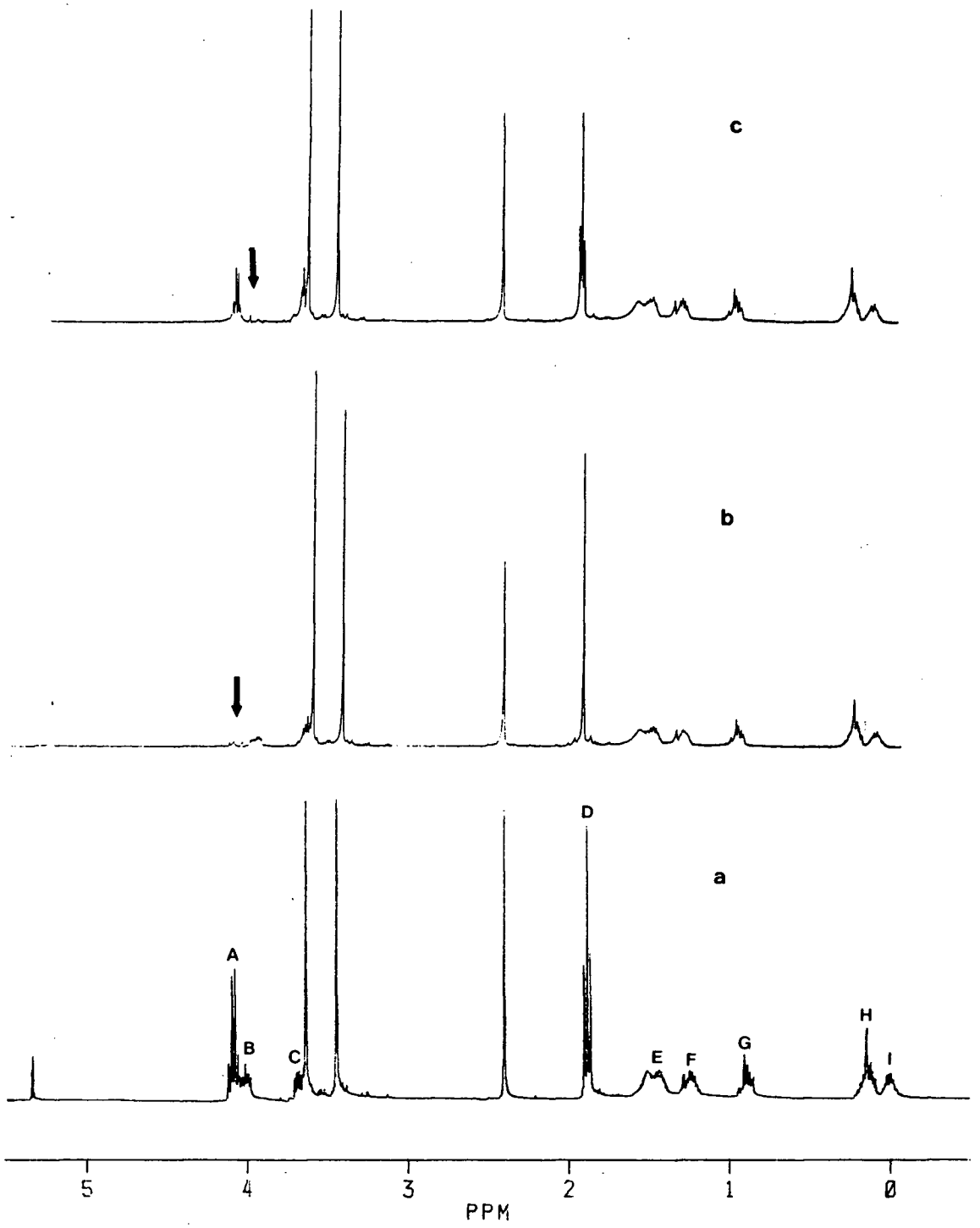

Fig. 2.21 Partial ^{1}H-nmr spectra of the benzene-4/4 capped porphyrin (**49a**)
(a) Normal spectrum
(b) Simultaneous irradiation at δ 4.07
(c) Simultaneous irradiation at δ 4.00

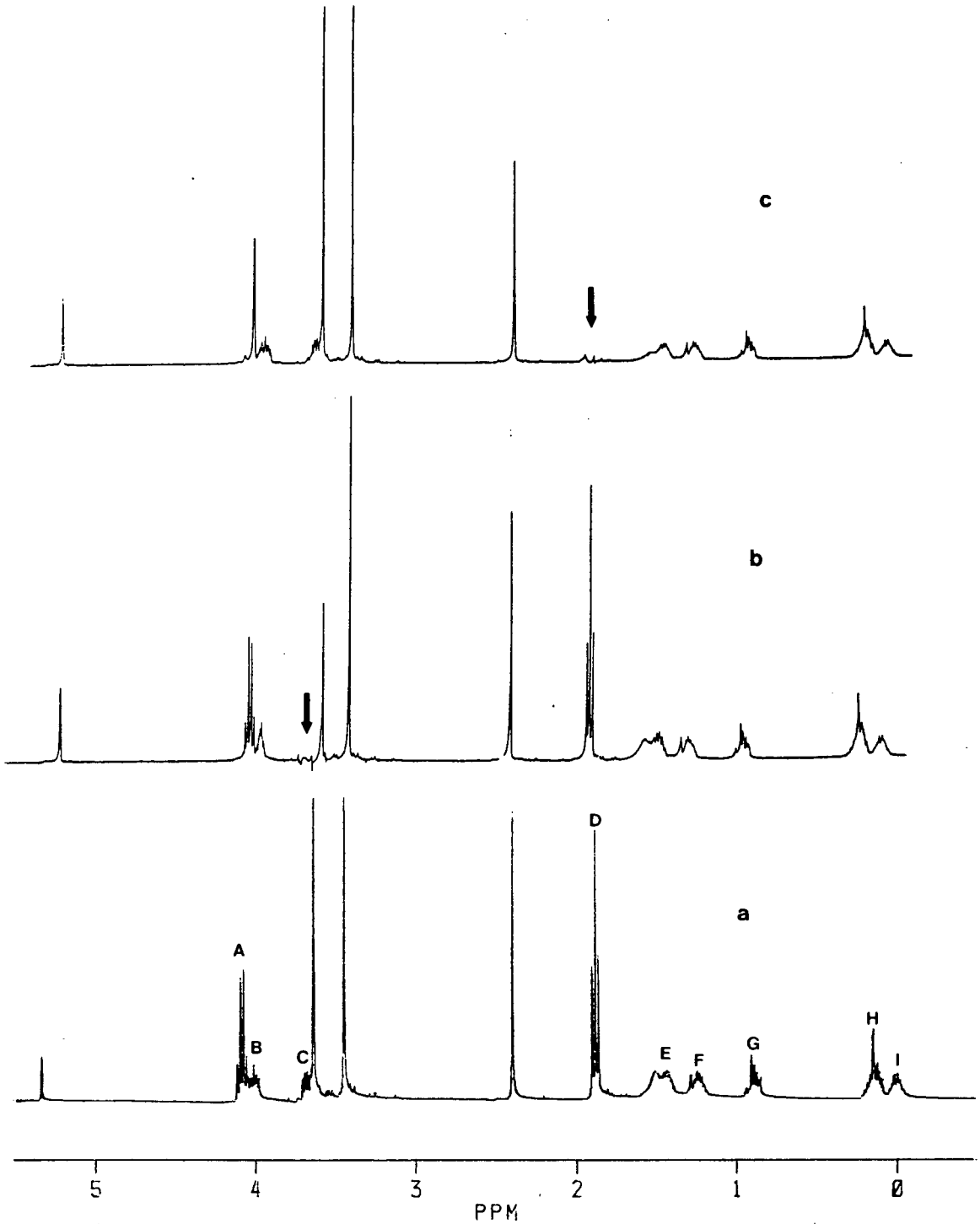

Fig. 2.22 Partial ^{1}H-nmr spectra of the benzene-4/4 capped porphyrin (**49a**)
(a) Normal spectrum
(b) Simultaneous irradiation at δ 3.86
(c) Simultaneous irradiation at δ 1.88

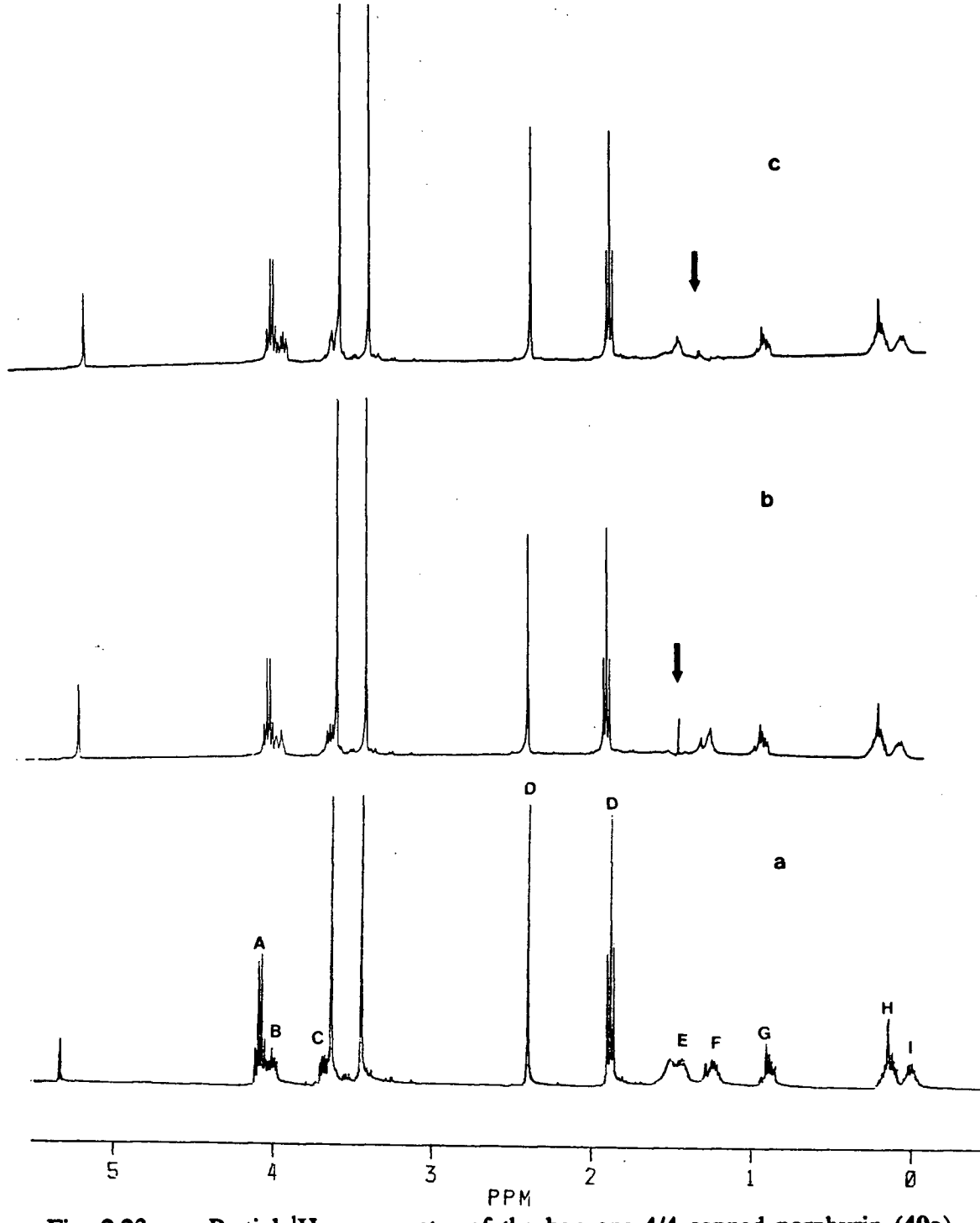

Fig. 2.23 Partial ^{1}H-nmr spectra of the benzene-4/4 capped porphyrin (**49a**)
(a) Normal spectrum
(b) Simultaneous irradiation at δ 1.44
(c) Simultaneous irradiation at δ 1.24

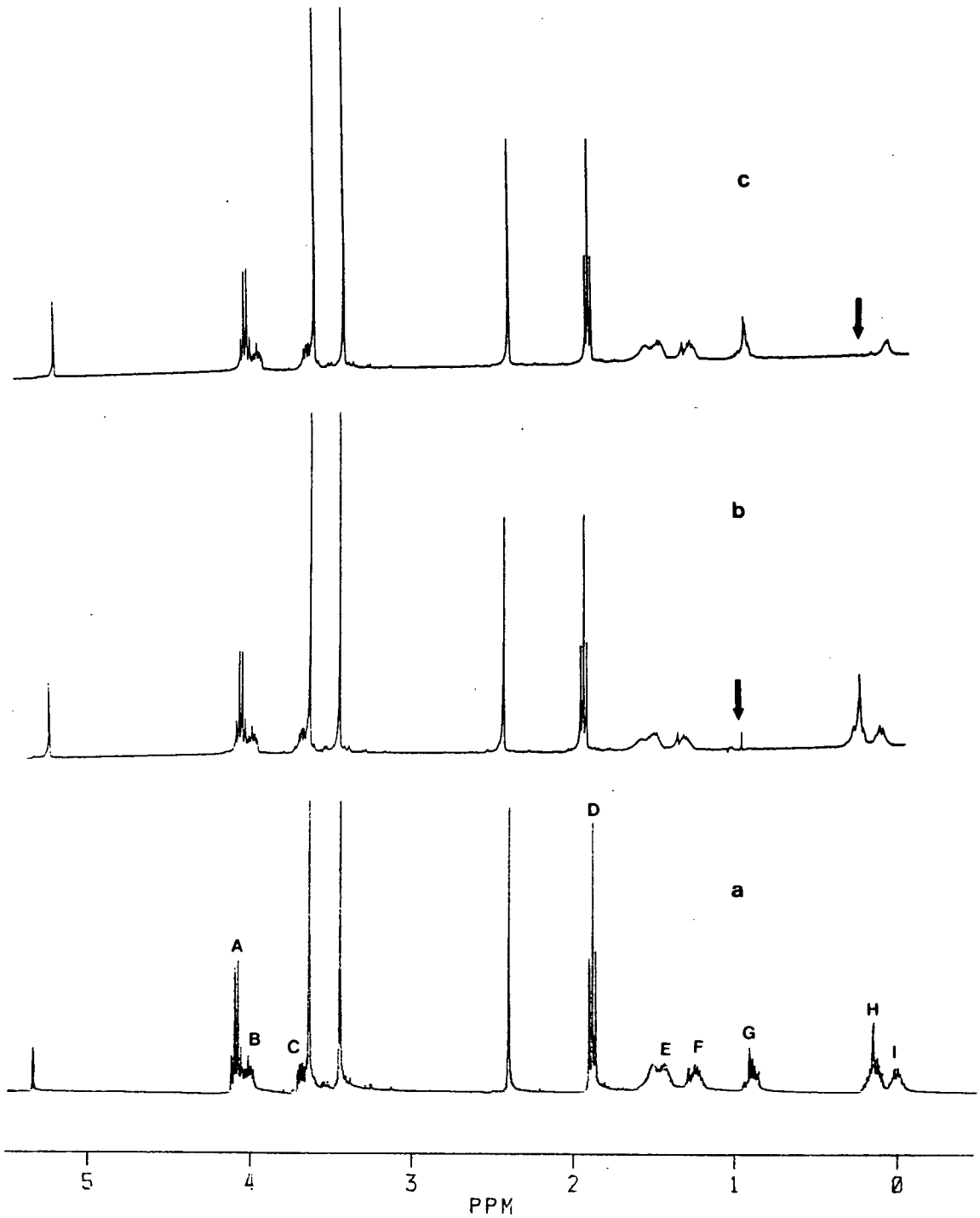

Fig. 2.24 Partial ^{1}H-nmr spectra of the benzene-4/4 capped porphyrin (**49a**)
(a) Normal spectrum
(b) Simultaneous irradiation at δ 0.88
(c) Simultaneous irradiation at δ 0.13

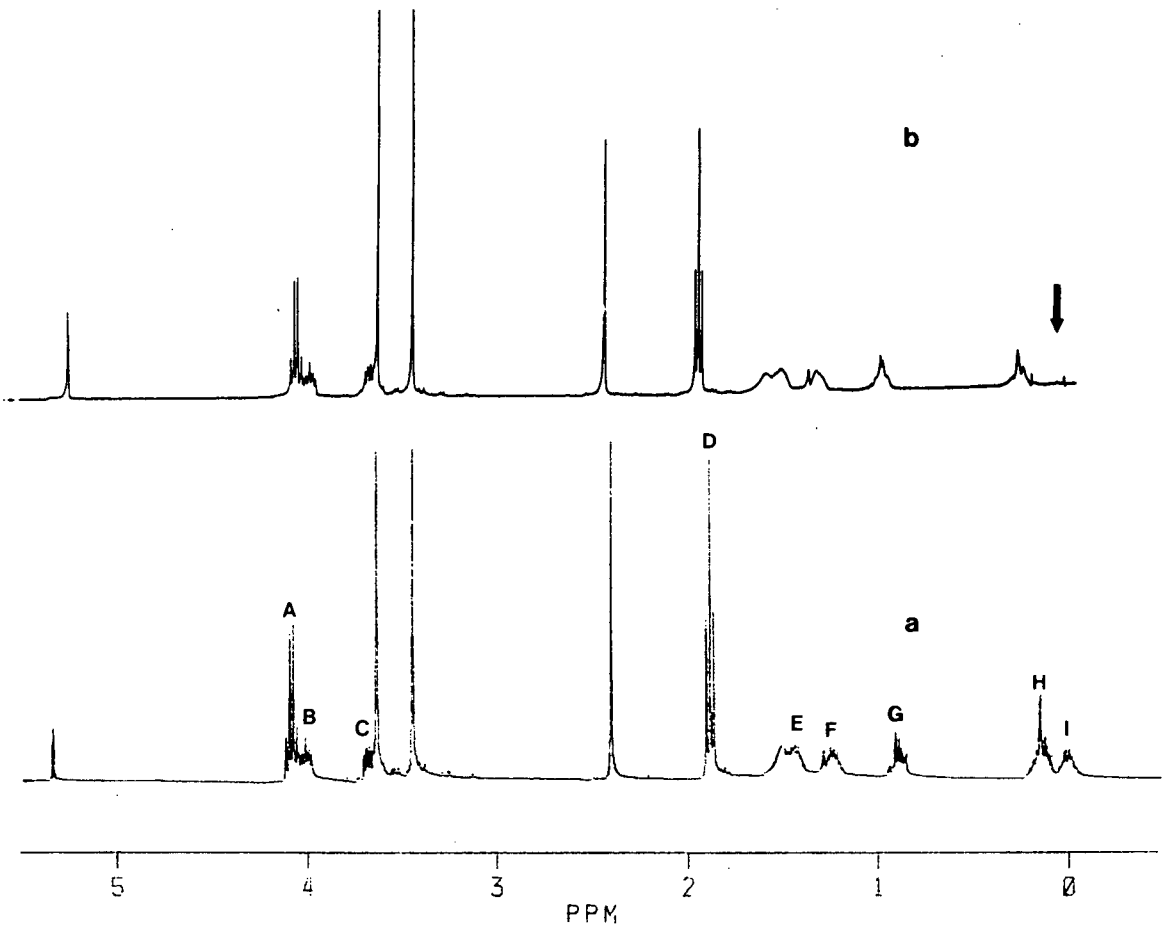

Fig. 2.25 Partial ^{1}H-nmr spectra of the benzene-4/4 capped porphyrin (**49a**)
(a) Normal spectrum
(b) Simultaneous irradiation at δ 0.00

field.

Among the two lowest field resonances A and B, the one at lower field is a quartet which contains four protons from the two CH_2 groups of the ethyl substituents. The one at higher field is a multiplet consisting of two protons assigned to the two protons at the chain termini (C-4 and C-4′). Being attached to the periphery of the porphyrin ring, these protons experience the largest deshielding effect due to the delocalized π-electron system of the macrocycle.

B at higher field corresponds to one proton each from C-4 and C-4′ of the chain,

and not two protons of the same carbon. This is identical with other systems.[63] Irradiation of the resonance A (Fig. 2.21b) resulted in the triplet at 1.87 ppm becoming a singlet while the other resonances remained unchanged. Irradiation at B (Fig. 2.21c) resulted in a significant change in the fine structure of the resonance C. In addition, this irradiation caused a change at resonance E and sharpening of the lines at resonance F, indicating that the protons at E and F are coupled to those at B. However, G, H and I are unaffected. Therefore, both E and F should consist of one proton each from C-3 and C-3′ of the chain and C, of one proton each from C-4 and C-4′. This assignment was further confirmed by irradiation at resonance C (Fig. 2.22b) which affected only B, E and F.

Irradiation at D (Fig. 2.22c) caused the quartet of A to turn into a singlet while the other resonances remained unaffected. This again confirmed that the signal A consisted of four protons from the ethyl groups.

Fig. 2.23b illustrates the result of decoupling of the protons at resonance E. As expected, changes were observed at B, C, F and I. However, the peak H was left unchanged, strongly suggesting that I and not H contains the two protons from C-2 and C-2′. Although G did not show any significant change, this was tentatively assigned to the other two protons of C-2 and C-2′. Irradiation at F (Fig. 2.23c) provided confirmation for the earlier assignment that G was due to the two protons of C-2 and C-2′.

Decoupling at G (Fig. 2.24b) caused changes in E (C-3, C-3′), F (C-3, C-3′), H and I (C-2, C-2′). From the previous decoupling, G had been assigned to the two C-2, C-2′ protons, thus suggesting that H corresponds to the four protons of C-1 and C-1′. Irradiation at I (Fig. 2.24c) changed E, F, G and H, confirming that I is due to C-2 and C-2′ not C-1 and C-1′. Finally, irradiation at H (Fig. 2.25b) affected G and I but not

E, F, indicating that it is from C-1 and C-1′.

Thus, the first order assignment of the protons at the different chain carbon atoms could be made as shown below:

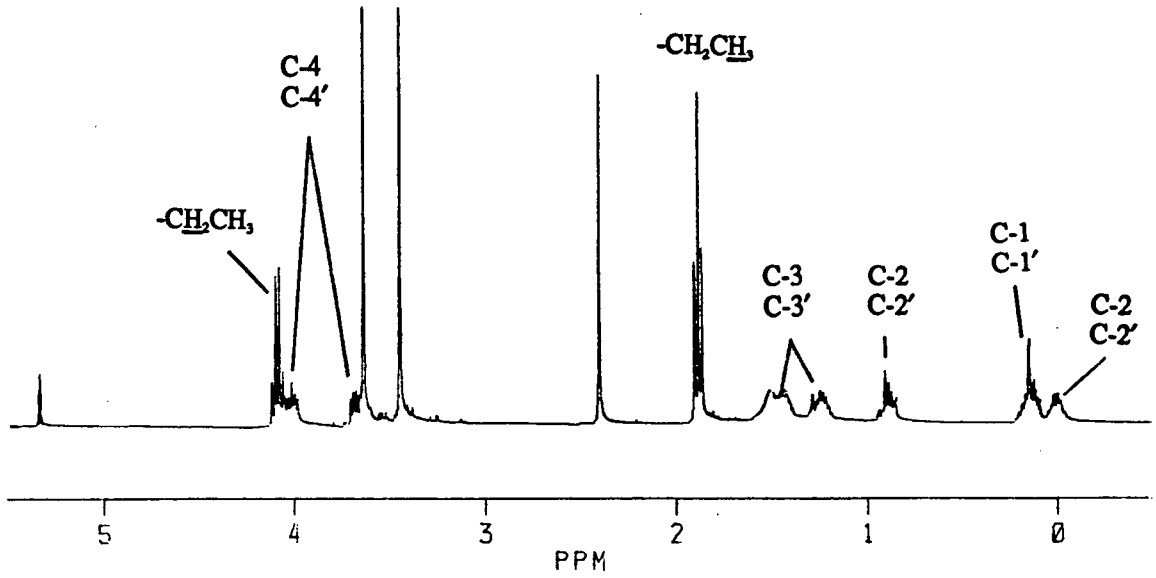

Similar decoupling experiments were carried out with the 5/5-benzene and 5/5-amidobenzene porphyrins. The assignments based on the analysis of the spectra are shown in Figs. 2.26 and 2.27.

In the case of the 5/5-benzene capped porphyrin, there is an overlap of signals from C-3,3′ and C-2,2′ or C-1,1′ at resonance H. Irradiation at I, J or K did not affect E and G (assigned to C-4,4′). Therefore, none of these is due to C-3,3′, suggesting that H consists of 4 protons from C-3,3′ and two protons from either C-2,2′ or C-1,1′. However, assignments for I, J and K were not possible since irradiation of any one of them caused changes in the other two and H. The only thing that can be decided is that they contain six protons from C-2,2′ and C-1,1′.

Another interesting feature observed in the spectra of the 5/5-benzene and 5/5-amidobenzene porphyrins is the existence of the methylene protons of the ethyl group as two complex multiplets rather than a simple quartet expected for the CH_2 protons of

an ethyl group as in etio porphyrin II. This inequivalence in nonmetallated systems has been interpreted in terms of the intrinsic asymmetry in the porphyrin molecule.[63, 105]

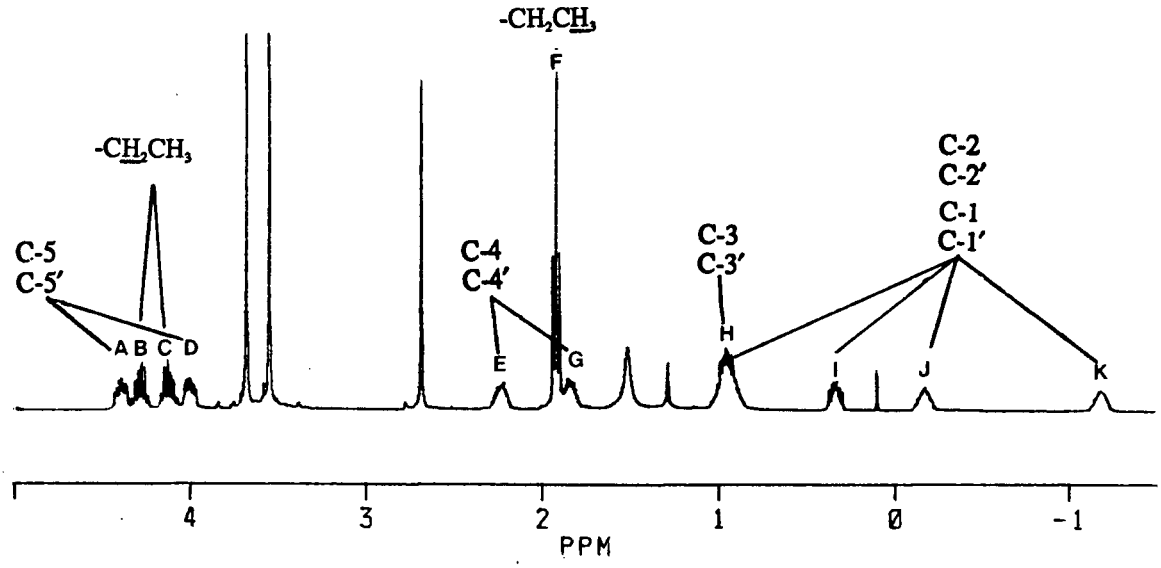

Fig. 2.26 The first-order assignment for the chain methylene protons of the 5/5-benzene capped porphyrin **49b**

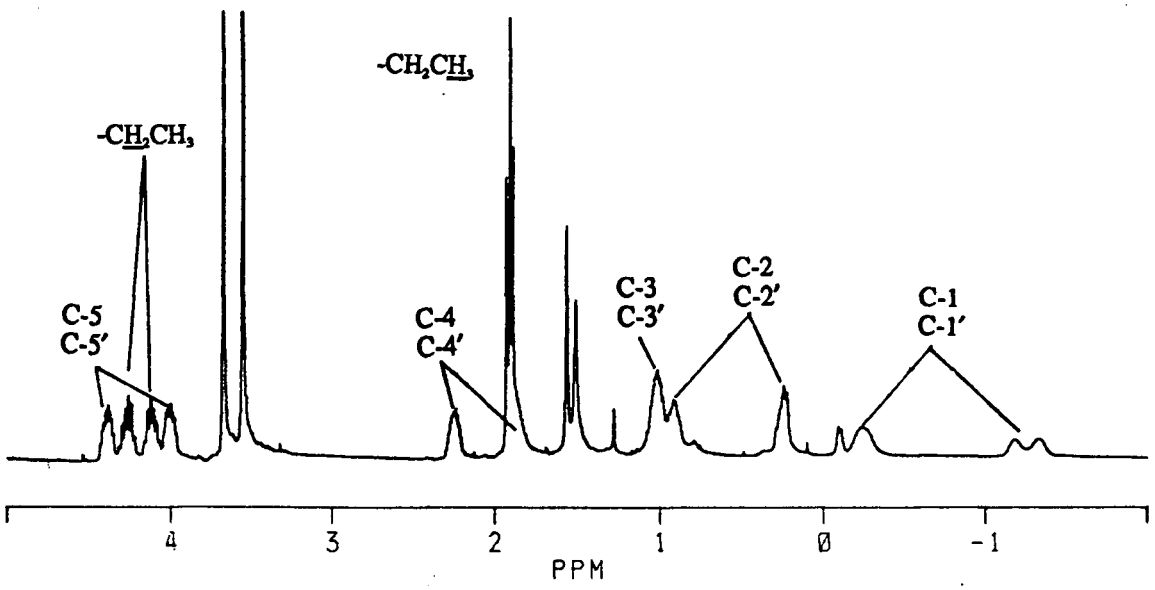

Fig. 2.27 The first order assignment for the chain methylene protons of the 5/5-amidobenzene capped porphyrin **49d**

The resonances from the methylene chain protons of the 4/4-amidobenzene capped porphyrin are either overlapped or very close, so that a first order assignment of the peaks arising from these protons through decoupling is precluded.

The resonances corresponding to the benzene protons in the porphyrins have been shifted upfield. The signals of the 4/4 and 5/5-benzene capped porphyrins have been shifted from ~7 ppm, for the normal aromatic protons, to 2.40 ppm for the 4/4 and 2.69 ppm for the 5/5 porphyrins respectively. The upfield shifts of the signals are easily explained by a strong shielding effect from the diamagnetic ring current due to the protons' positions above the porphyrin macrocycle. But, the reason for the 4/4 analogue having a larger upfield shift than that of the 5/5 is not so obvious. From the UV/visible spectrum of the 4/4-system, it is known that the porphyrin plane is distorted. The distortion would lower the aromaticity of the porphyrin system which should result in a reduced upfield shift. One possible reason for this reversal might possibly be the closer positioning of the benzene moiety in the benzene-4/4 capped porphyrin than that of the 5/5 analogue, to the porphyrin plane. The protons on the 4/4-benzene moiety would therefore experience a stronger shielding effect.

Chapter 3

Experimental for the porphyrin syntheses

3.1 General methods

Melting point determinations

Melting points were obtained using a Bristoline 6548-J17 microscope equipped with a Thomas Model 40 Micro Hot Stage, and are uncorrected.

Elemental analysis

Elemental analysis was performed by Mr. P. Borda of the Microanalytical Laboratory, U.B.C.

Nuclear magnetic resonance spectroscopy

The proton nmr spectra were recorded either at 300 MHz with a Varian XL-300 Fourier-transform spectrometer or at 400 MHz using a Bruker WH-400 spectrometer. In all cases the chemical shifts were recorded on the δ (ppm) scale with tetramethylsilane (TMS, δ = 0 ppm) as an internal or external standard.

Mass spectrometry

Mass spectra were recorded on a Varian Mat CH 4-B spectrometer or a Kratos/AEI MS-902 spectrometer. High resolution measurements were obtained on a

Kratos/AEI MS-50 spectrometer.

Electronic spectroscopy

A HP 8452A Diode Array Spectrophotometer was used to obtain UV/visible spectra.

Chromatography

Column chromatography was performed using silica gel obtained from Merck (70-230 mesh, activity I) and alumina from Fisher (neutral, 80-200 mesh, activity I). Thin layer chromatography (TLC) was performed using precoated silica gel plates (Analtech-Uniplate, 250 μ) and compounds were detected by UV light (254 nm). The chromatotron was a Harrison Research chromatotron apparatus with self-made silica gel rotors (Silica Gel PF-254 with $CaSO_4 \cdot 1/2H_2O$ type 60 TLC, Merck) and alumina rotors (Alumina GF-254 type E for TLC, Merck and Adsorbsil-Plus-2P, Applied Science).

Mixtures of solvents used in chromatography are expressed as volume/volume ratios.

Starting materials

The mono-pyrroles **36** and **46** were synthesized following methods described in detail by Wijesekera.[63] Terephthaldehyde **20** and all other reagents used were obtained commercially. Unless otherwise stated all solvents used were reagents grade.

3.2 Nomenclature of porphyrins and their intermediates

The nomenclature of the porphyrins is based on the IUPAC numbering system as shown below:

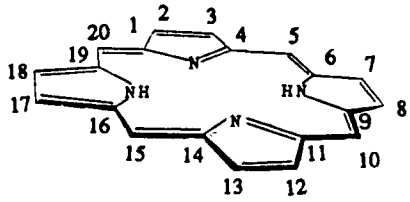

All intermediates have been labelled consistently as terminally bis-substituted-benzene, 2-nitrobenzene or 2-acetamidobenzene with the chain attached to position 3 of the pyrrole ring. For nitro- and amide-substituted compounds, the chain positions were labelled as 1, 2 and 1′, 2′ *etc.* as shown below:

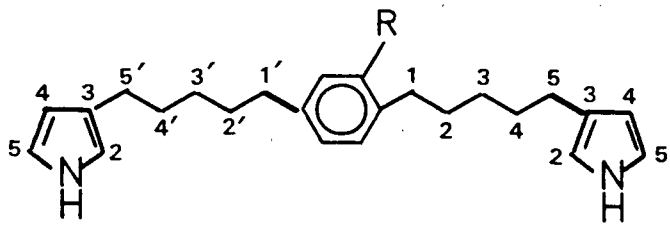

For dipyrromethanes the methane bridge is signified by the label '(pyrrole-2-yl)methylpyrrole'. The pyrrole nuclei of dipyrromethanes were numbered in such a way as to assign 2 and 2′ to the methane bridged α positions:

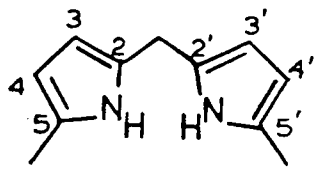

3.3 Syntheses of benzene and nitrobenzene diacid chain derivatives

1,4-Bis(2-carboxyethenyl)benzene **(21)**

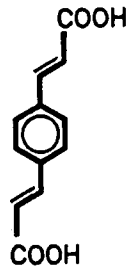

21

Malonic acid (125 g, 1.20 mol) was placed in a 2L-round-bottom flask containing pyridine (200 mL) and dissolved by warming and shaking on a steam bath. Terephthaldehyde **20** (70 g, 0.52 mol), toluene (200 mL) and piperidine (18 mL) were added. The flask, fitted with a reflux condenser, was moved to an oil bath and heated gradually to 80°C. The reaction mixture was maintained at this temperature overnight. During this time, a white solid precipitated and carbon dioxide was released.

After being cooled, the reaction mixture was poured into a large beaker containing a mixture of concentrated hydrochloric acid (250 mL) and water (250 mL). The white solid was filtered and washed with water till neutral, yield 108 g (95%).

M.P. = > 300°C (reported[106(a)] > 300°C).

Mol.wt. Calcd. for $C_{12}H_{10}O_4$: 218.0579; Found, by high resolution mass spectrometry: 218.0581.

Anal. Calcd. for $C_{12}H_{10}O_4$: C, 66.05; H, 4.62; Found: C, 65.78; H, 4.72.

^{1}H-nmr (80 MHz, δ, DMSO-d_6): 6.60(d, 2H, J=16Hz, side chain 2-CH), 7.60(d, 2H, J= 17Hz, side chain 1-CH), 7.73(s, 4H, benzene-H), 12.44(bs, 2H, -COOH).

Mass spectrum [m/e(relative intensity)]: 218(M^+, 100), 173(91), 155(32), 147(38), 127(56).

1,4-Bis(2-carboxyethyl)benzene (**22**)

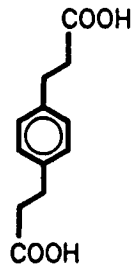

22

Potassium hydroxide (50 g) was dissolved in water (800 mL) in a 2L-wide-mouth-Erlenmeyer flask, followed by 1,4-bis(2-carboxyethenyl)benzene (**21**) (103.5 g, 0.47 mol) and the mixture was heated on a stirrer-hot plate until all of the material dissolved. To the warm solution was added Raney nickel-aluminum alloy (40 g) in small portions, over a period of 45-60 min to avoid too much frothing (if any excessive frothing occurred, a few drops of octyl alcohol was added). During addition of the alloy, the temperature of the mixture was kept around 80°C where it was held for an additional 3 h with stirring. The hot solution was then filtered using a steam-warmed buchner funnel, and the nickel residue was disposed of by pouring it into a mixture of nitric acid (50 mL) and water (100 mL). The filtrate was cooled and acidified by adding concentrated hydrochloric acid. The resulting mixture was allowed to stand overnight and the white solid was filtered off and washed with water. The solid was dried in air for a few days to give 98.5 g product (93.5%).

M.P. = 231.0 - 233.0°C (reported[106(b)] 223 - 224°C).

Mol.wt. Calcd. for $C_{12}H_{14}O_4$: 222.0892; Found: by high resolution mass spectrometry: 222.0894.

Anal. Calcd. for $C_{12}H_{14}O_4$: C, 64.85; H, 6.35; Found: C, 64.95; H, 6.52.

^{1}H-nmr (80 MHz, δ, DMSO-d_6): 2.05-2.78(m, 8H, side chain 1-CH_2 and 2-CH_2), 7.14(s, 4H, benzene-H), 12.09(bs, 2H, -COOH).

Mass spectrum [m/e(relative intensity)]: 222(M^+, 17), 204(6), 176(22), 162(38), 117(100), 91(34).

1,4-Bis(2-ethoxycarbonylethyl)benzene (**23**)

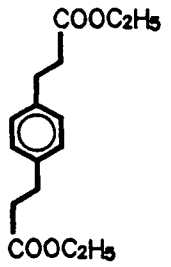

23

1,4-Bis(2-carboxyethyl)benzene (**22**) (96.4 g, 0.43 mol) was placed in a 1L-round-bottom flask and thionyl chloride (158 mL, 2.17 mol) was added. The mixture was refluxed on a steam bath with a calcium chloride drying tube on the top of the condenser. After 3 h, all of the diacid had reacted to give a yellow crystalline diacid

chloride in a brown reaction solution. The excess $SOCl_2$ was driven off by evaporating, in vacuo, and chased with carbon tetrachloride (2x50 mL).

Dry ethanol (150 mL) was added to dissolve the diacid chloride, with heat being generated by the partial formation of the ester. A 1:1 mixture (226 mL) of triethylamine and dry ethanol was added dropwise through a pressure equalizing funnel while the reaction flask was cooled in an ice bath. Once the addition was complete, the pale yellow crystalline diester started falling out of solution and the solution was stirred at room temperature overnight.

Acetic acid was added to acidify the reaction mixture. The pale yellow solid was filtered off and washed thoroughly with a 1:1 mixture of methanol and water to remove acetic acid. The product was dried in air, yield 101.6 g (84%).

M.P. = 70.3 - 72.0°C (reported[106(c)] 69°C).

Mol.wt. Calcd. for $C_{16}H_{22}O_4$: 278.1518; Found: by high resolution mass spectrometry: 278.1518.

Anal. Calcd. for $C_{16}H_{22}O_4$: C, 69.04; H, 7.97; Found: C, 69.14; H, 7.89.

^{1}H-nmr (300 MHz, δ, $CDCl_3$): 1.23(t, 6H, J=9Hz, -$OCH_2\underline{CH_3}$); 2.60(t, 4H, J=6Hz, 2-CH_2); 2.92(t, 4H, J=6Hz, 1-CH_2); 4.13(q, 4H, J=6Hz, -$O\underline{CH_2}CH_3$); 7.11(s, 4H, benzene-H).

Mass spectrum [m/e(relative intensity)]: 278(M^+, 24), 233(12), 204(62), 190(29), 159(22), 130(69), 117(100).

1,4-Bis(3-hydroxypropyl)benzene (**24**)

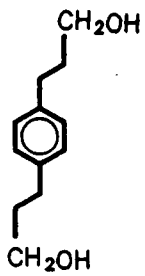

24

Sodium borohydride (41.1 g, 1.09 mol) was dissolved in diglyme (400 mL), under nitrogen, in an ice-cooled 1L-3-neck-round-bottom flask. The gas outlet of this flask was connected to a second ice-cooled 1L-3-neck-round-bottom flask which contained 1,4-bis(2-ethoxycarbonylethyl)benzene (**23**) (75.5 g, 0.27 mol) dissolved in anhydrous THF (400 mL). To the first magnetically stirred solution, boron trifluoride etherate (182.5 mL, 1.45 mol) was added slowly by dropping funnel. The B_2H_6 produced was introduced by N_2 to the second reaction flask. After addition of BF_3, the ice baths were removed and the reaction solution was stirred for a further 30 min. A TLC analysis of the reaction mixture showed a single spot, with a lower R_f value than that of the starting material indicating a complete reaction.

The excess diborane was destroyed with methanol and the reaction solution was filtered to remove some brown materials. The solvent was evaporated under reduced pressure and the remaining white compound was taken into CH_2Cl_2 (50 mL) and washed with water (3x50 mL). After removal of CH_2Cl_2, a white slurry was obtained which was dried on the vacuum line to give 46.36 g of the product (88%).

M.P. = 49.5 - 51.0°C (reported[106(d)] 55°C).

Mol.wt. Calcd. for $C_{12}H_{18}O_2$: 194.1307; Found, by high resolution mass spectrometry: 194.1307.

Anal. Calcd. for $C_{12}H_{18}O_2$: C, 74.19; H, 9.34; Found: C, 73.70; H, 9.32.

^{1}H-nmr (300 MHz, δ, $CDCl_3$): 1.61(s, 2H, -OH); 1.83-1.93(m, 4H, side chain 2-CH_2); 2.68(t, 4H, J=7.5Hz, side chain 1-CH_2); 3.67(t, 4H, J=6Hz, -CH_2OH); 7.14(s, 4H, benzene-H).

Mass spectrum [m/e(relative intensity)]: 194(M^+, 50), 176(18), 158(27), 148(17), 131(100), 117(89), 104(59), 91(75).

1,4-Bis(3-bromopropyl)benzene (**25**)

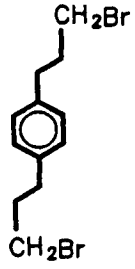

25

1,4-Bis(3-hydroxypropyl)benzene (**24**) (46.4 g, 0.24 mol) and 48% aqueous hydrobromic acid (200 mL) were heated at reflux under nitrogen. After 4 h, a TLC analysis indicated complete conversion of the starting material to a compound which moved faster on TLC plate. The emulsion was cooled to room temperature, methylene

chloride (100 mL) added and the acid extracted with water (3x50 mL) and saturated aqueous sodium bicarbonate (3x50 mL). The CH_2Cl_2 solution was extracted again with 0.1 M KOH aqueous solution (2x100 mL) to remove any trace amount of bromine and washed with water (2x100 mL).

The resulting solution was dried with anhydrous sodium sulphate, filtered and evaporated under reduced pressure to give a light yellow liquid product (72.6 g, 92.8%).

Mol.wt. Calcd. for $C_{12}H_{16}Br_2$: 317.9618-319.9598-321.9578; Found, by high resolution mass spectrometry: 317.9626-319.9611-321.9606.

Anal. Calcd. for $C_{12}H_{16}Br_2$: C, 45.03; H, 5.03; Found: C, 45.43; H, 5.19.

^{1}H-nmr (300 MHz, δ, $CDCl_3$): 2.25-2.34(m, 4H, side chain 2-CH_2), 2.89(t, 4H, J=7.5Hz, side chain 1-CH_2), 3.54(t, 4H, J=6Hz, -CH_2Br), 7.28(s, 4H, benzene-H).

Mass spectrum [m/e(relative intensity)]: 318-320-322(M^+, 28-60-28), 211-213(100-99), 172(17), 158(12), 131(28).

1,4-Bis(3-cyanopropyl)benzene (**26**)

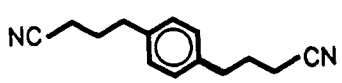

26

1,4-Bis(3-bromopropyl)benzene (**25**) (34.3 g, 0.107 mol) and potassium cyanide

(28 g, 0.43 mol) were refluxed in dry EtOH (500 mL) under nitrogen. After 7 h a TLC analysis showed only one spot, lower in R_f relative to the starting material. Water (1 L) was added to the reaction mixture while it was still warm to dissolve excess KCN. The solution was cooled with continuous stirring. The reaction mixture containing the yellow oil separated from the aqueous phase was extracted with CH_2Cl_2 (150 mL) and washed with water thoroughly. Methylene chloride was evaporated off under reduced pressure to give a quantitative yield of the product (22.6 g, 100%).

The solution containing KCN was treated with excess 5% sodium hypochlorite solution for 24 h and then poured into the drain in a fumehood.

M.P. = 54.3 - 56.0°C.

Mol.wt. Calcd. for $C_{14}H_{16}N_2$: 212.1314; Found, by high resolution mass spectrometry: 212.1313.

Anal. Calcd. for $C_{14}H_{16}N_2$: C, 79.21; H, 7.60; N, 13.20; Found: C, 79.27; H, 7.65; N, 13.00.

^{1}H-nmr (300 MHz, δ, $CDCl_3$): 2.03-2.13(m, 4H, side chain 2-CH_2), 2.44(t, 4H, J=7.5Hz, side chain 1-CH_2), 2.87(t, 4H, J=7.5Hz, side chain -CH_2CN), 7.50(s,4H,benzene-H).

Mass spectrum [m/e(relative intensity)]: 212(M^+, 12), 185(61), 172(46), 158(42), 131(65), 117(100).

1,4-Bis(3-carboxypropyl)benzene (**27**)

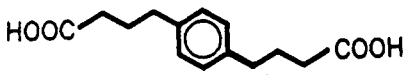

27

1,4-Bis(3-cyanopropyl)benzene (**26**) (23.8 g, 0.112 mol), potassium hydroxide (63 g, 1.12 mol) and ethanol (600 mL) were heated at reflux, under nitrogen, for 8 h. After this time the reaction flask was flushed with nitrogen, using a Claisen head adaptor, and the refluxing solution checked, with moist litmus, to ensure that the evolution of ammonia gas had ceased. Water (400 mL) was then added and the EtOH distilled off until the reflux temperature reached 100°C. The resulting clear solution was refluxed for another hour, and cooled; careful acidification with concentrated hydrochloric acid afforded the white diacid product **27** which was filtered and washed with water, yield 26 g (93%).

M.P. = 170.0 - 172.0°C (reported[106(e)] 176 - 177°C).

Mol.wt. Calcd. for $C_{14}H_{18}O_4$: 250.1205; Found, by high resolution mass spectrometry: 250.1207.

Anal. Calcd. for $C_{14}H_{18}O_4$: C, 67.18; H, 7.25; Found: C, 67.45; H, 7.35.

^{1}H-nmr (300 MHz, δ, 10% TFA/$CDCl_3$): 1.96-2.06(m, 4H, side chain 2-CH_2), 2.48(t, 4H, J=7.5Hz, side chain 3-CH_2), 2.69(t, 4H, J=9Hz, side chain 1-CH_2), 7.14(s, 4H, benzene-H).

Mass spectrum [m/e(relative intensity)]: 250(M^+, 21), 232(10), 214(30), 190(32), 130(67), 117(100).

1,4-Bis(3-ethoxycarbonylpropyl)benzene (**28**)

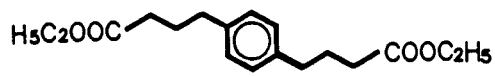

28

1,4-Bis(3-carboxypropyl)benzene (**27**) (19.3 g, 0.077 mol), ethanol (80 mL), toluene (120 mL) and p-toluene-sulphonic acid (0.5 g) were placed in a 250 mL Erlenmeyer flask fitted with a Dean-Stark trap surmounted by a reflux condenser. The solution was refluxed on a stirrer-hot plate for 4 days. During this period, the azeotrope collected in the trap was removed and more toluene and ethanol were added to the reaction flask.

After the reaction mixture was cooled, the solvents were removed under reduced pressure. The remaining yellow oil was taken into CH_2Cl_2 (100 mL) and extracted with saturated aqueous sodium bicarbonate (3x50 mL) and water (3x50 mL). The product was purified by silica gel (300 g) on a column with CH_2Cl_2 as the eluent to give 20.8 g of a colourless oil as product, yield 88%.

Mol.wt. Calcd. for $C_{18}H_{26}O_4$: 306.1831; Found, by high resolution mass spectrometry: 306.1840.

Anal. Calcd. for $C_{18}H_{26}O_4$: C, 70.56; H, 8.55; Found: C, 70.49; H, 8.60.

^{1}H-nmr (300 MHz, δ, $CDCl_3$): 1.26(t, 6H, J=9Hz, -$OCH_2\underline{CH_3}$), 1.88-1.98(m, 4H, side chain 2-CH_2), 2.32(t, 4H, J=10.5Hz, side chain 3-CH_2), 2.62(t, 4H, J=7.5Hz, side chain 1-CH_2), 4.12(q, 4H, J=10.5Hz, -$O\underline{CH_2}CH_3$), 7.10(s, 4H, benzene-H).

Mass spectrum [m/e(relative intensity)]: 306(M^+, 11), 260(13), 232(12), 215(58), 204(26), 173(96), 130(100), 117(92).

1,4-Bis(4,4-dicarboxybutyl)benzene (**29**)

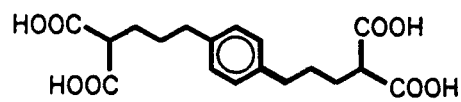

29

Freshly cut metallic sodium (5.7 g, 0.248 mol) was dissolved in anhydrous ethanol (200 mL), under nitrogen. Diethyl malonate (71.8 g, 0.448 mol) was added with stirring, followed by 1,4-bis(3-bromopropyl)benzene (**25**) (35.8 g, 0.112 mol) in anhydrous ethanol (100 mL), and the mixture refluxed for 2 h. A TLC analysis of the suspension indicated complete reaction of the starting material to a compound with a lower R_f.

Ethanol (~100 mL) was then distilled off and a solution of potassium hydroxide (75 g, 1.34 mol) in water (180 mL) added. The remaining ethanol was distilled off and the mixture refluxed at 100°C for a further 2 h. The hot aqueous solution was next treated dropwise with concentrated hydrochloric acid (100 mL). The white solid that precipitated when the solution became acidic was collected and washed with water to give 36.5 g (89%) of **29**.

M.P. = 140.0 - 141.5°C.

Anal. Calcd. for $C_{18}H_{22}O_8$: C, 59.01; H, 6.05; Found: C, 59.30; H, 6.24.

^{1}H-nmr (300 MHz, δ, 10%TFA/$CDCl_3$): 1.75-1.85(m, 4H, side chain 3-CH_2), 2.02-2.12 (m, 4H, side chain 2-CH_2), 2.70(t, 4H, J=6Hz, side chain 1-CH_2), 3.60[t, 2H, J=6Hz, C<u>H</u>$(COOH)_2$], 7.15(s, 4H, benzene-H).

Mass spectrum [m/e(relative intensity)]: 278[$(M-2CO_2)^+$, 8], 260(27), 242(100), 191(39), 145(51), 131(68).

1,4-Bis(4-carboxybutyl)benzene (**30**)

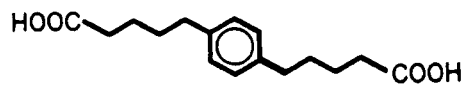

30

1,4-Bis(4,4-dicarboxybutyl)benzene (**29**) (36 g, 0.098 mol) was added slowly, in small portions to a refluxing solution of DMF (250 mL) in a 1L-Erlenmeyer flask. During addition, vigorous evolution of carbon dioxide was observed. The resulting white suspension was refluxed for a further 2 h to ensure complete decarboxylation, and then poured slowly into an aqueous solution of 6 M hydrochloric acid (300 mL). The white diacid product **30** was collected by filtration and washed with water, yield 26.3 g (96.5%).

M.P. = 149.0 - 151.0°C.

Mol.wt. Calcd. for $C_{16}H_{22}O_4$: 278.1518; Found, by high resolution mass spectrometry: 278.1519.

Anal. Calcd. for $C_{16}H_{22}O_4$: C, 69.04; H, 7.97; Found: C, 69.51; H, 7.82.

^{1}H-nmr (300 MHz, δ, 10% TFA/$CDCl_3$): 1.69-1.79(m, 8H, side chain 2- and 3-CH_2), 2.50(t, 4H, J=6Hz, side chain 4-CH_2), 2.65(t, 4H, J=7.5Hz, side chain 1-CH_2), 7.13(s, 4H, benzene-H).

Mass spectrum [m/e(relative intensity)]: 278(M^+, 11), 260(26), 242(100), 191(33), 145(67), 131(92).

1,4-Bis(4-ethoxycarbonylbutyl)benzene (**31**)

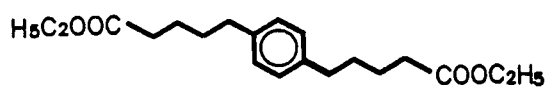

31

In a preparation analogous to that described for **28**, the diethylester **31** was obtained in 99% yield (15.8 g) from the diacid **30** (13.3 g, 0.048 mol).

Mol.wt. Calcd. for $C_{20}H_{30}O_4$: 334.2144; Found, by high resolution mass spectrometry: 334.2143.

Anal. Calcd. for $C_{20}H_{30}O_4$: C, 71.82; H, 9.04; Found: C, 71.56; H, 9.00.

^{1}H-nmr (300 MHz, δ, $CDCl_3$): 1.25(t, 6H, J=9Hz, -OCH_2CH_3), 1.61-1.70(m, 8H, side chain 2-, 3-CH_2), 2.32(t, 4H, J=6Hz, side chain 4-CH_2), 2.60(t, 4H, J=6Hz, side chain 1-CH_2), 4.11(q, 4H, J=6Hz, -OCH_2CH_3), 7.08(s, 4H, benzene-H).

Mass spectrum [m/e(relative intensity)]: 334(M^+, 13), 288(31), 242(100), 214(62), 186(65), 117(92).

1,4-Bis(3-ethoxycarbonylpropyl)-2-nitrobenzene (**32**)

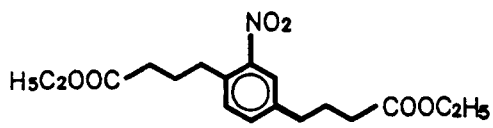

32

To a stirred ice cooled 500mL-Erlenmeyer flask, fitted with a $CaSO_4$ drying tube, were added 1,4-bis(3-ethoxycarbonylpropyl)benzene (**28**) (5.13 g, 0.0168 mol) and trifluoroacetic acid (50 mL), followed by sodium nitrite (2.33 g, 0.0336 mol). The resulting dark brown mixture was stirred in an ice bath until no brown gas came out of the solution (~24 h). The yellow solution was then poured onto crushed ice (50 g) and methylene chloride (50 mL) was added. The organic layer was extracted with saturated sodium bicarbonate (3x50 mL) and water (3x50 mL). The impure brown oil was purified using silica gel (50 g) in a column with 1% MeOH/CH_2Cl_2 as the eluent to give the yellow liquid product 4.3 g (73%).

Mol.wt. Calcd. for $C_{18}H_{25}N_1O_6$: 351.1682; Found, by high resolution mass spectrometry: 351.1671.

Anal. Calcd. for $C_{18}H_{25}N_1O_6$: C, 61.53; H, 7.17; N, 3.99; Found: C, 61.26; H, 7.20; N, 3.89.

^{1}H-nmr (300 MHz, δ, $CDCl_3$): 1.30(t, 6H, J=12Hz, -OCH_2CH_3), 1.97-2.07(m, 4H, side chain 2, 2′-CH_2), 2.34-2.43(m, 4H, side chain 3, 3′-CH_2), 2.74(t, 2H, J=7.5Hz, side chain 1′-CH_2), 2.92(t, 2H, J=6Hz, side chain 1-CH_2), 4.17(q, 4H, J=6Hz, -OCH_2CH_3), 7.32(d, 1H, J=9Hz, m-NO_2-benzene-H), 7.40(d, 1H, J=9Hz, p-NO_2-benzene-H), 7.76(s, 1H, o-NO_2-benzene-H).

Mass spectrum [m/e(relative intensity)]: 351(M^+, very weak), 306[$(M-OC_2H_5)^+$, 13], 276(29), 269(100), 242(23), 232(43), 172(47).

1,4-Bis(4-ethoxycarbonylbutyl)-2-nitrobenzene (**33**)

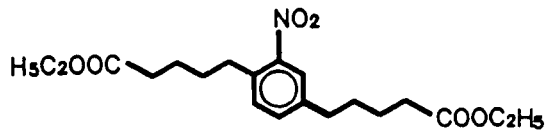

33

1,4-Bis(4-ethoxycarbonylbutyl)-2-nitrobenzene (**33**) was synthesized in 65.8% yield using the method described for compound **32**.

Anal. Calcd. for $C_{20}H_{29}N_1O_6$: C, 63.31; H, 7.70; N, 3.69; Found: C, 63.12; H, 7.63; N, 3.86.

^{1}H-nmr (300 MHz, δ, $CDCl_3$): 1.21(t, 6H, J=7.5Hz, -OCH_2CH_3), 1.60-1.70(m, 8H, side chain 2, 2′-, 3, 3′-CH_2), 2.28-2.31(m, 4H, side chain 4, 4′-CH_2), 2.64(m, 2H, side chain 1′-CH_2), 2.81(t, 2H, J=7.5Hz, side chain 1-CH_2), 4.08(q, 4H, J=7.5Hz, -OCH_2CH_3), 7.28(d, 1H, J=11.3Hz, m-NO_2-benzene-H), 7.35(d, 1H, J=7.5Hz, p-NO_2-benzene-H), 7.72(s, 1H, o-NO_2-benzene-H).

Mass spectrum [m/e(relative intensity)]: 349(40), 334[$(M-OC_2H_5)^+$, 100], 288(43), 274(71), 256(73), 246(98).

1,4-Bis(3-carboxypropyl)-2-nitrobenzene (**34**)

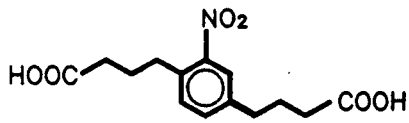

34

1,4-Bis(3-ethoxycarbonylpropyl)-2-nitrobenzene (**32**) (7.6 g, 0.022 mol) was dissolved in potassium hydroxide (7.5 g) solution of water (75 mL) and ethanol (225 mL) and refluxed under nitrogen. After 2 h, the condenser was removed and EtOH was distilled off until the temperature reached 100°C. The reaction mixture was cooled in an ice bath and acidified by adding concentrated hydrochloric acid. The off-white solid was collected by filtration and washed with water to give 5.97 g (92%) product.

M.P. = 157.0 - 159.0°C.

Anal. Calcd. for $C_{14}H_{17}N_1O_6$: C, 56.95; H, 5.80; N, 4.47; Found: C, 57.08; H, 5.82; N, 4.55.

^{1}H-nmr (300 MHz, δ, 10%TFA/$CDCl_3$): 1.91-2.09(m, 4H, side chain 2, 2′-CH_2), 2.48-2.58(m, 4H, side chain 3, 3′-CH_2), 2.76(t, 2H, J=9Hz, side chain 1′-CH_2), 2.95(t, 2H, J=9Hz, side chain 1-CH_2), 7.31(d, 1H, J=9Hz, m-benzene-NO_2-H), 7.41(d, 1H, J=7.5Hz, p-benzene-NO_2-H), 7.96(s, 1H, o-benzene-NO_2-H).

Mass spectrum [m/e(relative intensity)]: 277[$(M-H_2O)^+$, 2], 250(24), 232(19), 214(37), 190(48), 117(100).

1,4-Bis(4-carboxybutyl)-2-nitrobenzene (**35**)

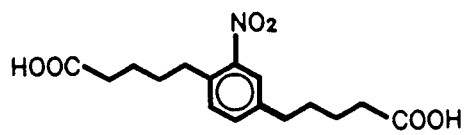

35

1,4-Bis(4-carboxybutyl)-2-nitrobenzene (**35**) was prepared according to the method described for compound **34** in a yield of 81%.

M.P. = 114.0 - 116.0°C.

Anal. Calcd. for $C_{16}H_{21}N_1O_6$: C, 59.43; H, 6.55; N, 4.33; Found: C, 58.93; H, 6.50; N, 4.07.

^{1}H-nmr (300 MHz, δ, 10% TFA/$CDCl_3$): 2.47-2.53(m, 4H, side chain 3, 3′-CH_2), 1.83-1.93(m, 8H, side chain 2, 2′-, 4, 4′-CH_2), 2.68-2.74(m, 2H, side chain 1'-CH_2), 2.90(t, 2H, J=7.5Hz, side chain 1-CH_2), 7.27(d, 1H, J=6Hz, m-NO_2-benzene-H), 7.37(d, 1H, J=6Hz, p-NO_2-benzene-H), 7.76(s, 1H, o-NO_2-benzene-H).

Mass spectrum [m/e(relative intensity)]: 305[$(M-H_2O)^+$, 13], 293(34), 270(22), 260(19), 246(100), 228(48), 218(79), 206(79).

3.4 Syntheses of benzene, nitrobenzene and amidobenzene bis pyrrole derivatives

3.4.1 The bis pyrrole diketones

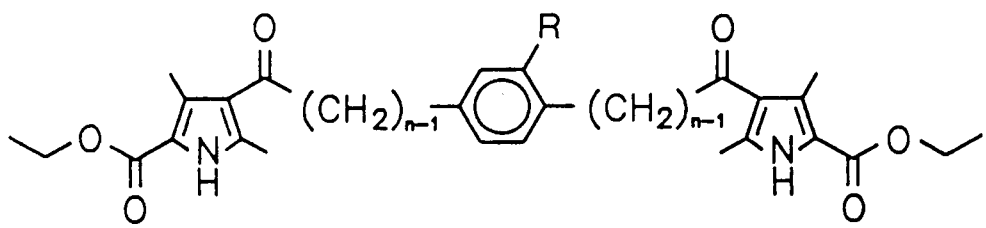

37a, n=4, R=H

37b, n=5, R=H

37c, n=4, R=NO_2

37d, n=5, R=NO_2

(a) 1,4-Bis[4-(5-ethoxycarbonyl-2,4-dimethylpyrrol-3-yl)-4-oxobutyl]benzene (**37a**)

1,4-Bis(3-carboxypropyl)benzene (**27**) (10 g, 0.04 mol) and thionyl chloride (19 g, 0.16 mol) were placed in a flask equipped with a reflux condenser and calcium chloride drying tube. The mixture was heated on a steam bath until all of solid went into solution (~30 min). The excess thionyl chloride was removed by evaporation under reduced pressure and chased with CCl_4 (4x25 mL). The dark red residue of the bis acid chloride was then taken up in distilled CH_2Cl_2 (30 mL) and transferred into a flask containing 2-ethoxy-3,5-dimethylpyrrole (**36**) (16.7 g, 0.1 mol), distilled CH_2Cl_2 (140 mL) and nitromethane (150 mL), under nitrogen. Anhydrous stannic chloride (41.7 g, 0.16 mol) was added rapidly and the reaction mixture was stirred overnight at room temperature. The dark brown solution was then poured into 0.1 M aqueous hydrochloric acid (100 mL) and stirred for ~15 min resulting in precipitation of the product. The yellow solid was filtered and washed with water, CH_2Cl_2 and methanol to give a creamy yellow product. The second crop was collected from the filtrate by evaporating all of the solvents and thoroughly washed with methanol. Overall yield was 12.5 g (57%).

An analytical sample was recrystallized by adding methanol to a concentrated solution of **37a** in CH_2Cl_2 and minimum trifluoroacetic acid.

M.P. = 185.0 - 186.5°C.

Mol.wt. Calcd. for $C_{32}H_{40}N_2O_6$: 548.2886; Found, by high resolution mass spectrometry: 548.2894.

Anal. Calcd. for $C_{32}H_{40}N_2O_6$: C, 70.05; H, 7.35; N, 5.11; Found: C, 70.00; H, 7.35; N, 5.24.

^{1}H-nmr (300 MHz, δ, 10% TFA/$CDCl_3$): 1.48(t, 6H, J=6Hz, -OCH_2CH_3), 1.99-2.09(m, 4H, side chain 2-CH_2), 2, 53(s, 6H, pyrrole 4-CH_3), 2.57(s, 6H, pyrrole 2-CH_3), 2.74(t, 4H, J=6Hz, side chain 1-CH_2), 2.90(t, 4H, J=6Hz, side chain 3-CH_2), 4.45(q, 4H, J= 6.2Hz, -OCH_2CH_3), 7.15(s, 4H, benzene-H), 10.25(bs, 2H, NH).

Mass spectrum [m/e(relative intensity)]: 548(M^+, 4), 340(17), 209(100), 194(66), 148(74).

(b) 1,4-Bis[5-(5-ethoxycarbonyl-2,4-dimethylpyrrol-3-yl)-5-oxopentyl]benzene (**37b**)

1,4-Bis[5-(5-ethoxycarbonyl-2,4-dimethylpyrrol-3-yl)-5-oxopentyl]benzene (**37b**) was synthesised in the manner described for **37a** from the diacid **30**. The product was isolated in two crops to give an overall yield of 70%.

M.P. = 175.0 - 177.0°C.

Mol.wt. Calcd. for $C_{34}H_{44}N_2O_6$: 576.3199; Found, by high resolution mass spectrometry: 576.3205.

Anal. Calcd. for $C_{34}H_{44}N_2O_6$: C, 70.81; H, 7.69; N, 4.86; Found: C, 70.90; H, 7.65; N, 4.97.

^{1}H-nmr (300 MHz, δ, 10% TFA/$CDCl_3$): 1.47(t, 6H, J=5.6Hz, -OCH_2CH_3), 1.75(b, 8H, side chain 2-, 3-CH_2), 2.56(s, 6H, pyrrole 4-CH_3), 2.59(s, 6H, pyrrole 2-CH_3), 2.61-

2.68(m, 4H, side chain 1-CH_2), 2.86-2.91(m, 4H, side chain 4-CH_2), 4.45(q, 4H, J=7.5Hz, -OC$\underline{H_2}CH_3$), 7.11(s, 4H, benzene-H), 10.16(bs, 2H, NH).

Mass spectrum [m/e(relative intensity)]: 576(M^+, 9), 530(2), 409(4), 363(4), 209(37), 194(67), 148(100).

(c)1,4-Bis[4-(5-ethoxycarbonyl-2,4-dimethylpyrrol-3-yl)-4-oxobutyl]-2-nitrobenzene (**37c**)

1,4-Bis[4-(5-ethoxycarbonyl-2,4-dimethylpyrrol-3-yl)-4-oxobutyl]-2-nitrobenzene **37c** was obtained according to the method for **37a** with a yield of 82%.

M.P. = 181.5 - 182.5°C.

Mol.wt. Calcd. for $C_{32}H_{39}N_3O_8$: 593.2723; Found, by high resolution mass spectrometry: 593.2747.

Anal. Calcd. for $C_{32}H_{39}N_3O_8$: C, 64.74; H, 6.62; N, 7.08; Found: C, 64.72; H, 6.52; N, 6.89.

^{1}H-nmr (300 MHz, δ, 10% TFA/$CDCl_3$): 1.40(t, 6H, J=7.5Hz, -$OCH_2\underline{CH_3}$), 1.96-2.06(m, 4H, side chain 2, 2′-CH_2), 2.48-2.54(m, 12H, pyrrole 2-, 4-CH_3), 2.73(t, 2H, J=5.6Hz, side chain 1′-CH_2), 2.83-2.96(m, 6H, side chain 1-, 3, 3′-CH_2), 4.39(q, 4H, J=7.5Hz, -OC$\underline{H_2}CH_3$), 7.29(d, 1H, J=7.5Hz, m-NO_2-benzene-$\underline{H}$), 7.31(d, 1H, J=7.5Hz, p-NO_2-

benzene-H), 7.74(s, 1H, o-NO_2-benzene-H), 10.21(bs, 2H, NH).

Mass spectrum [m/e(relative intensity)]: 593(M^+, 3), 576(4), 209(45), 194(78), 148(100).

(d)1,4-Bis[5-(5-ethoxycarbonyl-2,4-dimethylpyrrol-3-yl)-5-oxopentyl]-2-nitrobenzene(**37d**)

1,4-Bis[5-(5-ethoxycarbonyl-2,4-dimethylpyrrol-3-yl)-5-oxopentyl]-2-nitrobenzene (**37d**) was obtained in a yield of 74% from the diacid **35** according to the method described for **37a**.

M.P. = 193.5 - 194.5°C.

Mol.wt. Calcd. for $C_{34}H_{43}N_3O_8$: 621.3050; Found, by high resolution mass spectrometry: 621.3035.

Anal. Calcd. for $C_{34}H_{43}N_3O_8$: C, 65.68; H, 6.97; N, 6.76; Found: C, 64.53; H, 6.88; N, 6.24; Calcd. for $C_{34}H_{43}N_3O_8 \cdot CH_3OH$: C, 64.30; H, 7.25; N, 6.43.

^{1}H-nmr (300 MHz, δ, 10% TFA/$CDCl_3$): 1.43(t, 6H, J=9.2Hz, -OCH_2CH_3), 1.71-1.82(b, 8H, side chain 2, 2′-, 3, 3′-CH_2), 2.57-2.62(m, 12H, pyrrole 2-, 4-CH_3), 2.68-2.75(b, 2H, side chain 1′-CH_2), 2.86-2.95(m, 6H, side chain 1-, 4, 4′-CH_2), 4.42(q, 4H, J=7.7Hz, -OCH_2CH_3), 7.27(d, 1H, J=9Hz, m-NO_2-benzene-H), 7.38(d, 1H, J=9Hz, p-NO_2-benzene-H), 7.75(s, 1H, o-NO_2-benzene-H), 10.23(bs, 2H, NH).

Mass spectrum [m/e(relative intensity)]: 621(M^+, 2), 591(8), 209(10), 194(74), 148(100).

3.4.2 The bis pyrrole ethyl esters

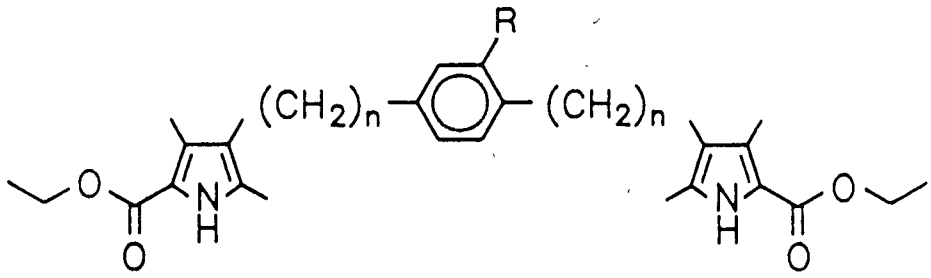

38a, n=4, R=H

38b, n=5, R=H

38c, n=4, R=NO_2

38d, n=5, R=NO_2

(a) 1,4-Bis[4-(5-ethoxycarbonyl-2,4-dimethylpyrrol-3-yl)butyl]benzene (**38a**)

The diketone **37a** (14 g, 0.0255 mol) was suspended in anhydrous THF (150 mL) in a 250 mL-two-neck-round-bottom flask which was kept closed with rubber septa; one needle was inserted into each septum allowing a very small flow of N_2. A 1 M borane-THF complex (10 mL) was injected in the solution and the resulting mixture was stirred for 1 h, during which time all of the white suspension had gone into solution. TLC analysis of an aliquot, quenched by acetic acid, indicated the reaction had not gone to completion. Another 10 mL of BH_3-THF solution was added and the mixture was stirred for another hour. TLC analysis, which showed a single spot with a higher R_f value than that of the starting material, indicated a complete reaction.

The excess BH_3 was destroyed by slowly adding methanol (20 mL) and the

solvents were evaporated off under reduced pressure and methanol was added to this concentrated solution to crystallize the white product, yield 10.6 g (80%).

M.P. = 162.0 - 163.0°C.

Mol.wt. Calcd. for $C_{32}H_{44}N_2O_4$: 520.3301; Found, by high resolution mass spectrometry: 520.3307.

Anal. Calcd. for $C_{32}H_{44}N_2O_4$: C, 73.81; H, 8.52; N, 5.38; Found: C, 73.69; H, 8.52; N, 5.45.

^{1}H-nmr (300 MHz, δ, $CDCl_3$): 1.35(t, 6H, J=7.5Hz, -$OCH_2\underline{CH_3}$), 1.44-1.51(m, 4H, side chain 3-CH_2), 1.58-1.68(m, 4H, side chain 2-CH_2), 2.18(s, 6H, pyrrole 2-CH_3), 2.26(s, 6H, pyrrole 4-CH_3), 2.38(t, 4H, J=7.5Hz, side chain 4-CH_2), 2.59(t, 4H, J=9.4Hz, side chain 1-CH_2), 4.30(q, 4H, J=7.5Hz, -$O\underline{CH_2}CH_3$), 7.08(s, 4H, benzene-H), 8.70(bs, 2H, NH).

Mass spectrum [m/e(relative intensity)]: 520(M^+, 19), 474(23), 428(13), 206(100), 180(71), 134(94).

(b) 1,4-Bis[5-(5-ethoxycarbonyl-2,4-dimethylpyrrol-3-yl)pentyl]benzene (**38b**)

The bis pyrrole ethylester **38b** was synthesised by the method described in detail for **38a**, yield 84%.

M.P. = 181.5 - 182.5°C.

Mol.wt. Calcd. for $C_{34}H_{48}N_2O_4$: 548.3614; Found, by high resolution mass spectrometry: 548.3612.

Anal. Calcd. for $C_{34}H_{48}N_2O_4$: C, 74.42; H, 8.82; N, 5.10; Found: C, 72.00; H, 8.72; N, 4.92; Calcd. for $C_{34}H_{48}N_2O_4 \cdot CH_3OH$: C, 72.38; H, 9.02; N, 4.82.

^{1}H-nmr (300 MHz, δ, $CDCl_3$): 1.37, 1.34-1.49(t, m, 14H, $-OCH_2\underline{CH_3}$, side chain 3-, 4-CH_2), 1.58-1.68(m, 4H, side chain 2-CH_2), 2.20(s, 6H, pyrrole 2-CH_3), 2.28(s, 6H, pyrrole 4-CH_3), 2.30-2.38(m, 4H, side chain 5-CH_2), 2.58(t, 4H, J=7.5Hz, side chain 1-CH_2), 4.31(q, 4H, J=7.5Hz, $-O\underline{CH_2}CH_3$), 7.08(s, 4H, benzene-H), 8.66(bs, 2H, NH).

Mass spectrum [m/e(relative intensity)]: 548(M^+, 17), 502(27), 180(90), 134(100).

(c) 1,4-Bis[4-(5-ethoxycarbonyl-2,4-dimethylpyrrol-3-yl)butyl]-2-nitrobenzene (**38c**)

The diketone **37c** was converted to the ethylester **38c** by the method described for **38a**, yield 83%.

M.P. = 137.0 - 138.5°C.

Mol.wt. Calcd. for $C_{32}H_{43}N_3O_6$: 565.3152; Found, by high resolution mass spectrometry:

565.3153.

Anal. Calcd. for $C_{32}H_{43}N_3O_6$: C, 67.94; H, 7.66; N, 7.43; Found: C, 67.43; H, 7.61; N, 7.62.

^{1}H-nmr (300 MHz, δ, $CDCl_3$): 1.33(t, 6H, J=7.5Hz, -OCH_2CH_3), 1.42-1.53(m, 4H, side chain 3, 3′-CH_2), 1.58-1.66(m, 4H, side chain 2, 2′-CH_2), 2.15(s, 6H, pyrrole 2-CH_3), 2.23(s, 6H, pyrrole 4-CH_3), 2.35(t, 4H, J=7.5Hz, side chain 4, 4′-CH_2), 2.63(t, 2H, J=9.4Hz, side chain 1′-CH_2), 2.83(t, 2H, J=7.5Hz, side chain 1-CH_2), 4.27(q, 4H, J=6.3Hz, -OCH_2CH_3), 7.19(d, 1H, J=7.5Hz, m-NO_2-benzene-H), 7.26(d, 1H, J=7.5Hz, p-NO_2-benzene-H), 7.65(s, 1H, o-NO_2-benzene-H), 8.54(bs, 2H, NH).

Mass spectrum [m/e(relative intensity)]: 565(M^+, 3), 535(5), 519(3), 428(6), 206(12), 180(60), 134(100).

(d) 1,4-Bis[5-(5-ethoxycarbonyl-2,4-dimethylpyrrol-3-yl)pentyl]-2-nitrobenzene (**38d**)

The product **38d** was obtained in 79% yield using the method described for **38a**.

M.P. = 137.5 - 138.0°C.

Mol.wt. Calcd. for $C_{34}H_{47}N_3O_6$: 593.3465; Found, by high resolution mass spectrometry: 593.3466.

Anal. Calcd. for $C_{34}H_{47}N_3O_6$: C, 68.78; H, 7.98; N, 7.08; Found: C, 68.99; H, 7.98; N.6.83.

^{1}H-nmr (300 MHz, δ, $CDCl_3$): 1.35, 1.32-1.50(t, m, 14H, $-OCH_2CH_3$, side chain 3, 3′-, 4, 4′-CH_2), 1.58-1.67(m, 4H, side chain 2, 2′-CH_2), 2.19(s, 6H, pyrrole 2-CH_3), 2.26(s, 6H, pyrrole 4-CH_3), 2.34-2.38(m, 4H, side chain 5, 5′-CH_2), 2.63(t, 2H, J=7.5Hz, side chain 1′-CH_2), 2.83(t, 2H, J=7.5Hz, side chain 1-CH_2), 4.29(q, 4H, J=7.5Hz, $-OCH_2CH_3$), 7.20(d, 1H, J=8Hz, m-NO_2-benzene-H), 7.29(d, 1H, J=9Hz, p-NO_2-benzene-H), 7.67(s, 1H, o-NO_2-benzene-H), 8.80(bs, 2H, NH).

Mass spectrum [m/e(relative intensity)]: 593(M^+, 7), 563(9), 547(5), 456(7), 206(7), 180(61), 134(100).

3.4.3 The amide bis pyrrole ethyl esters

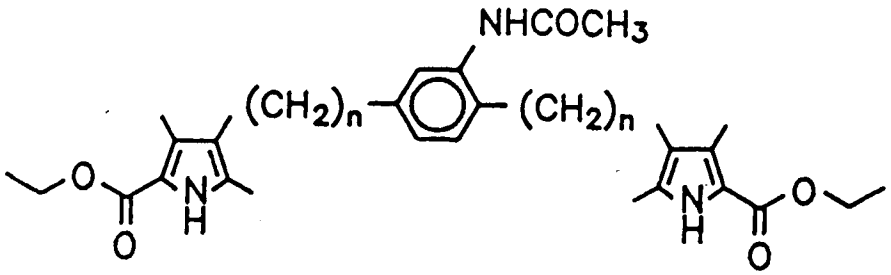

39a, n=4

39b, n=5

(c) 1,4-Bis[4-(5-ethoxycarbonyl-2,4-dimethylpyrrol-3-yl)butyl]-2-acetamidobenzene (**39c**)

1,4-Bis[4-(5-ethoxycarbonyl-2,4-dimethylpyrrol-3-yl)butyl]-2-nitrobenzene (**38c**) (7.3 g, 12.9 mmol) was dissolved in THF (200 mL), followed by 10% Pd/C (0.7 g), acetic anhydride (10 mL) and sodium acetate (0.5 g). The reaction flask was then connected to a hydrogenation apparatus and the solution was stirred under an H_2 atmosphere (1 atm) overnight. TLC analysis indicated that only part of the starting material had reacted. The catalyst was filtered off and fresh 10% Pd/C catalyst (0.7 g) was added and the reaction flask connected to the hydrogenator again. The mixture was stirred under an H_2 atmosphere overnight, when TLC analysis indicated a complete reaction.

The catalyst was filtered off and the white solid was crystallized out by concentrating the solution, in the presence of hexane, yield 90% (6.7 g).

M.P. = 215.5 - 216.5°C.

Mol.wt. Calcd. for $C_{34}H_{47}N_3O_5$: 577.3516; Found, by high resolution mass spectrometry: 577.3514.

Anal. Calcd. for $C_{34}H_{47}N_3O_5$: C, 70.68; H, 8.20; N, 7.27; Found: C, 70.44; H, 8.39; N, 7.07.

^{1}H-nmr (400 MHz, δ, $CDCl_3$): 1.27(t, 6H, J=8Hz, $-OCH_2\underline{CH_3}$), 1.35-1.58(m, 8H, side chain 2, 2′-, 3, 3′-CH_2), 2.10(s, 9H, pyrrole 2-CH_3, $NHCOC\underline{H_3}$), 2.18(s, 6H, pyrrole 4-CH_3), 2.28-2.34(m, 4H, side chain 4, 4′-CH_2), 2.44-2.54(m, 4H, side chain 1, 1′-CH_2), 4.22(q, 4H, J=6.7Hz, $-O\underline{CH_2}CH_3$), 6.83-6.87(s, d, 2H, $N\underline{H}COCH_3$, m-$NHCOCH_3$-benzene-$\underline{H}$), 7.00(d, 1H, J=8Hz, p-$NHCOCH_3$-benzene-$\underline{H}$), 7.48(s, 1H, o-$NHCOCH_3$-benzene-$\underline{H}$), 8.49(b, 2H, NH).

Mass spectrum [m/e(relative intensity)]: 577(M^+, 15), 531(18), 485(14), 206(16), 180(46), 134(100).

(d)1,4-Bis[5-(5-ethoxycarbonyl-2,4-dimethylpyrrol-3-yl)pentyl]-2-acetamidobenzene (**39d**)

The product was obtained in the same way described for **39c**, yield 96%.

M.P. = 167.0 - 169.0°C.

Mol.wt. Calcd. for $C_{36}H_{51}N_3O_5$: 605.3829; Found, by high resolution mass spectrometry: 605.3821.

Anal. Calcd. for $C_{36}H_{51}N_3O_5$: C, 71.37; H, 8.48; N, 6.94; Found: C, 71.39; H, 8.68; N, 6.84.

^{1}H-nmr (400 MHz, δ, $CDCl_3$): 1.33-1.48(t, m, 14H, -OCH_2CH_3, side chain 3, 3′-, 4, 4′-CH_2), 1.55-1.65(m, 4H, side chain 2, 2′-CH_2), 2.19(s, 9H, pyrrole 2-CH_3, $NHCOCH_3$), 2.26(s, 6H, pyrrole 4-CH_3), 2.34-2.38(m, 4H, side chain 5, 5′-CH_2), 2.50-2.60(m, 4H, side chain 1, 1′-CH_2), 4.30(q, 4H, J=6.7Hz, -OCH_2CH_3), 6.95(b, 2H, $NHCOCH_3$, m-$NHCOCH_3$-benzene-H), 7.08(d, 1H, J=8Hz, p-$NHCOCH_3$-benzene-H), 7.56(s, 1H, o-$NHCOCH_3$-benzene-H), 8.58(b, 2H, NH).

Mass spectrum [m/e(relative intensity)]: 605(M^+, 26), 587(47), 559(44), 541(14), 513(18), 180(61), 134(100).

3.4.4 The bis pyrrole benzyl esters

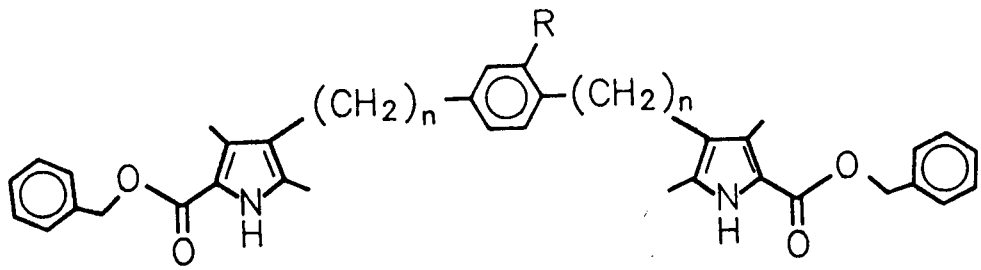

40a, n=4, R=H

40b, n=5, R=H

40c, n=4, R=NHCOCH$_3$

40d, n=5, R=NHCOCH$_3$

(a) 1,4-Bis[4-(5-benzyloxycarbonyl-2,4-dimethylpyrrol-3-yl)butyl]benzene (**40a**)

1,4-Bis[4-(5-ethoxycarbonyl-2,4-dimethylpyrrol-3-yl)butyl]benzene (**38a**) (7.8 g, 15 mmol) and distilled benzyl alcohol (100 mL) were heated under nitrogen. At the onset of reflux (205°C), a concentrated solution of sodium in benzyl alcohol was added, in 1 mL portions. During each addition, ethanol vapor was liberated and a simultaneous drop in temperature was observed; the mixture was allowed to attain reflux each time before further addition of the catalyst. After addition of 3 mL of the catalyst, no effervescence could be observed and the hot solution was carefully poured into methanol (150 mL) with sufficient acetic acid (10 mL) to quench the catalyst. Water was added slowly to precipitate the product, which was filtered and washed with 50% MeOH/water. The dibenzylester was obtained in 86% yield (8.3 g).

M.P. = 147.0 - 149.0°C.

Mol.wt. Calcd. for $C_{42}H_{48}N_2O_4$: 644.3614; Found, by high resolution mass spectrometry: 644.3610.

Anal. Calcd. for $C_{42}H_{48}N_2O_4$: C, 78.23; H, 7.50; N, 4.34; Found: C, 78.04; H, 7.59; N, 4.38.

^{1}H-nmr (400 MHz, δ, $CDCl_3$): 1.42-1.49(m, 4H, side chain 3-CH_2), 1.57-1.66(m, 4H, side chain 2-CH_2), 2.16(s, 6H, pyrrole 2-CH_3), 2.27(s, 6H, pyrrole 4-CH_3), 2.37(t, 4H, J=8Hz, side chain 4-CH_2), 2.58(t, 4H, J=8Hz, side chain 1-CH_2), 5.29(s, 4H, -$OCH_2C_6H_5$), 7.07(s, 4H, benzene-H), 7.31-7.43(m, 10H, -$OCH_2C_6H_5$), 8.54(bs, 2H, NH).

Mass spectrum [m/e(relative intensity)]: 644(M^+, 8), 536(4), 509(7), 401(10), 268(23), 108(31), 91(100).

(b) 1,4-Bis[5-(5-benzyloxycarbonyl-2,4-dimethylpyrrol-3-yl)pentyl]benzene (**40b**)

The dibenzylester **40b** was obtained with the method described for **40a**. The yield was 92%.

M.P. = 131.0 - 133.0°C.

Mol.wt. Calcd. for $C_{44}H_{52}N_2O_4$: 672.3927; Found, by high resolution mass spectrometry: 672.3923.

Anal. Calcd. for $C_{44}H_{52}N_2O_4$: C, 78.54; H, 7.79; N, 4.16; Found: C, 78.30; H, 7.95; N, 4.14.

^{1}H-nmr (400 MHz, δ, $CDCl_3$): 1.33-1.48(m, 8H, side chain 3-, 4-CH_2), 1.57-1.66(m, 4H, side chain 2-CH_2), 2.16(s, 6H, pyrrole 2-CH_3), 2.27(s, 6H, pyrrole 4-CH_3), 2.31-2.37(m, 4H, side chain 5-CH_2), 2.55(t, 4H, J=8Hz, side chain 1-CH_2), 5.29(s, 4H, -O$CH_2C_6H_5$), 7.07(s, 4H, benzene-H), 7.30-7.43(m, 10H, -$OCH_2C_6H_5$), 8.70(bs, 2H, NH).

Mass spectrum [m/e(relative intensity)]: 672(M^+, 12), 564(8), 537(10), 493(9), 429(14), 242(12), 108(56), 91(100).

(c)1,4-Bis[4-(5-benzyloxycarbonyl-2,4-dimethylpyrrol-3-yl)butyl]-2-acetamidobenzene(**40c**)

1,4-Bis[4-(5-ethoxycarbonyl-2,4-dimethylpyrrol-3-yl)butyl]-2-acetamidobenzene (**39c**) (1 g, 1.73 mmol) was placed in distilled benzyl alcohol (10 mL) and a small piece of metallic sodium (~0.05 g) was added. The resulting mixture was heated at 100°C under 12 mm Hg pressure controlled by a pumptable. After 30 min of heating, all of the starting material had dissolved resulting in a brownish yellow solution which was cooled to room temperature while still on the vacuum line.

Acetic acid was slowly added to the solution under nitrogen to neutralize the reaction mixture. When some pink color appeared, wet pH paper showed the solution was neutral and dry ice was added.

Benzyl alcohol was distilled off under 0.1 mm Hg at 70 - 100°C. The slightly

pink solid was then taken into methylene chloride (30 mL) and washed with water (3x30 mL) to remove salts. After evaporating the methylene chloride, the solid was taken into ethyl acetate (10 mL), warmed, shaken in a supersonic apparatus and cooled in a refrigerator at 4°C.

A white solid was filtered off and washed with cold ethyl acetate to give 0.91 g product (75%).

M.P. = 187.0 - 189.0°C.

Mol.wt. Calcd. for $C_{44}H_{51}N_3O_5$: 701.3829; Found, by high resolution mass spectrometry: 701.3834.

Anal. Calcd. for $C_{44}H_{51}N_3O_5$: C, 75.29; H, 7.32; N, 5.99: Found: C, 75.13; H, 7.50; N, 5.78.

^{1}H-nmr (400 MHz, δ, $CDCl_3$): 1.42-1.65(m, 8H, side chain 2, 2′-, 3, 3′-CH_2), 2.16(s, 9H, pyrrole 2-CH_3, NHCOCH_3), 2.27(s, 6H, pyrrole 4-CH_3), 2.35-2.41(m, 4H, side chain 4, 4′-CH_2), 2.52-2.61(m, 4H, side chain 1, 1′-CH_2), 5.29(s, 4H, -O$CH_2C_6H_5$), 6.86(b,1H, NHCOCH$_3$), 6.92(bd, 1H, m-NHCOCH$_3$-benzene-H), 7.06(bd, 1H, p-NHCOCH$_3$-benzene-H), 7.32-7.45(m, 10H, -OCH$_2$C$_6$$H_5$), 7.56(b, 1H, o-NHCOCH$_3$-benzene-$H$), 8.53(b, 2H, NH).

Mass spectrum [m/e(relative intensity)]: 701(M^+, 3), 593(3), 458(9), 108(69), 91(100).

(d) 1,4-Bis[5-(5-benzyloxycarbonyl-2,4-dimethylpyrrol-3-yl)pentyl]-2-acetamidobenzene (**40d**)

The diethylester **39d** (1.3 g, 2.15 mmol) was transesterified in 10 mL benzyl alcohol as described for the analogue **40c**.

The solution was neutralized by adding dry ice only and worked up as for **40a**. The yield was 59% (0.92 g).

M.P. = 164.0 - 166.0°C.

Mol.wt. Calcd. for $C_{46}H_{55}N_3O_5$: 729.4142; Found, by high resolution mass spectrometry: 729.4140.

Anal. Calcd. for $C_{46}H_{55}N_3O_5$: C, 75.69; H, 7.59; N, 5.76; Found: C, 75.38; H, 7.55; N, 5.56.

^{1}H-nmr (400 MHz, δ, $CDCl_3$): 1.33-1.49(m, 8H, side chain 3, 3′-, 4, 4′-CH_2), 1.56-1.65(m, 4H, side chain 2, 2′-CH_2), 2.17(s, 9H, pyrrole 2-CH_3, NHCOCH_3), 2.28(s, 6H, pyrrole 4-CH_3), 2.33-2.38(m, 4H, side chain 5, 5′-CH_2), 2.50-2.60(m, 4H, side chain 1, 1′-CH_2), 5.30(s, 4H, -OCH_2C$_6$H$_5$), 6.93(b, 2H, NHCOCH$_3$, m-NHCOCH$_3$-benzene-H), 7.07(b, 1H, p-NHCOCH$_3$-benzene-H), 7.32-7.44(m, 10H, -OCH$_2$C$_6$$H_5$), 7.56(b, 1H, o-NHCOCH$_3$-benzene-$H$), 8.60(b, 2H, NH).

Mass spectrum [m/e(relative intensity)]: 729(M^+, 7), 685(6), 621(10), 595(13), 486(17), 460(9), 108(100), 91(86).

3.4.5 The bis-formylpyrroles

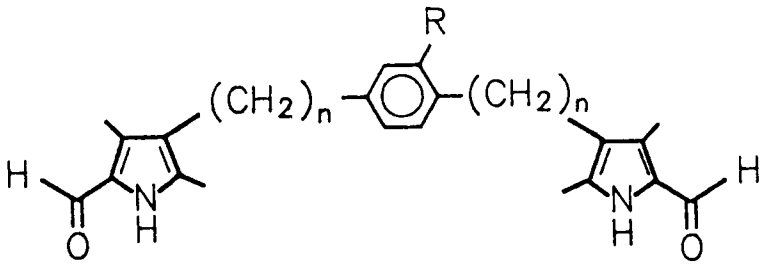

43a, n=4, R=H

43b, n=5, R=H

43c, n=4, R=$NHCOCH_3$

43d, n=5, R=$NHCOCH_3$

(a) 1,4-Bis[4-(5-formyl-2,4-dimethylpyrrol-3-yl)butyl]benzene (**43a**)

(i) Debenzylation of **40a**:

The dibenzylester **40a** (5 g, 9.62 mmol) and 10% Pd/C (0.5 g) were stirred under hydrogen (1 atm) in THF (150 mL) overnight. When the uptake of hydrogen ceased, the catalyst was filtered and the solution checked by TLC for any unconverted starting material. The solvents were then evaporated in vacuo, leaving the bis(carboxy)pyrrole **41a** as a white solid.

(ii) Decarboxylation of **41a**:

The crude bis(carboxy)pyrrole **41a** was refluxed in DMF (100 mL) under nitrogen. The UV absorption spectrum showed a reduction of the band at 282 nm to just a shoulder, within 2 h. No further change was then observed. The solution containing the bis α-free pyrrole **42a** was cooled in an ice bath and used directly in the next reaction.

(iii) Vilsmeier formylation of **42a**:

To an ice cooled solution of DMF (11 mL) in dry CH_2Cl_2 (40 mL), phosphorus oxychloride (9.8 mL) was added dropwise. The Vilsmeier reagent, thus prepared, was added rapidly to the chilled DMF solution of the bis α-free pyrrole **42a** prepared above. Once addition was complete, the solution was stirred for a further 30 min to ensure completion of the reaction, and then poured onto crushed ice (100 g). Solid sodium bicarbonate was added carefully until the solution became basic, and CH_2Cl_2 was then boiled off. Water (300 mL) was added and the mixture was heated at ~75°C for 1 h. The grey colored solid which crystallized out was filtered and washed with water. An overall yield of 85% of crude **43a** was obtained from the dibenzylester **40a**. An analytically pure sample of the bis formylpyrrole was prepared by deprotecting the cyanoacrylate derivative **44a** with aqueous potassium hydroxide in n-propanol.

M.P. = 217.0 - 219.0°C.

Mol.wt. Calcd. for $C_{28}H_{36}N_2O_2$: 432.2777; Found, by high resolution mass spectrometry: 432.2783.

Anal. Calcd. for $C_{28}H_{36}N_2O_2$: C, 77.74; H, 8.39; N, 6.48; Found: C, 77.57; H, 8.28; N, 6.32.

^{1}H-nmr (300 MHz, δ, $CDCl_3$): 1.40-1.51(m, 4H, side chain 3-CH_2), 1.58-1.68(m, 4H, side chain 2-CH_2), 2.21(s, 6H, pyrrole 2-CH_3), 2.25(s, 6H, pyrrole 4-CH_3), 2.38(t, 4H, J=7.5Hz, side chain 4-CH_2), 2.60(t, 4H, J=7.5Hz, side chain 1-CH_2), 7.07(s, 4H, benzene-H), 9.47(s, 4H, NH, HCO).

Mass spectrum [m/e(relative intensity)]: 432(M^+, 44), 404(34), 389(18), 296(10), 136(100), 108(58).

(b) 1,4-Bis[5-(5-formyl-2,4-dimethylpyrrol-3-yl)pentyl]benzene (**43b**)

This compound was prepared by the same procedure as that employed in the preparation of dialdehyde **43a**. The crude bis formylpyrrole was obtained in 88% yield from the dibenzylester **40b**.

M.P. = 152.0 - 154.0°C.

Mol.wt. Calcd. for $C_{30}H_{40}N_2O_2$: 460.3090; Found, by high resolution mass spectrometry: 460.3081.

Anal. Calcd. for $C_{30}H_{40}N_2O_2$: C, 78.22; H, 8.75; N, 6.08; Found: C, 77.90; H, 8.85; N, 6.13.

^{1}H-nmr (400 MHz, δ, $CDCl_3$): 1.32-1.40(m, 4H, side chain 3-CH_2), 1.43-1.51(m, 4H, side chain 4-CH_2), 1.57-1.65(m, 4H, side chain 2-CH_2), 2.22(s, 6H, pyrrole 2-CH_3), 2.25(s, 6H, pyrrole 4-CH_3), 2.37(t, 4H, J=8Hz, side chain 5-CH_2), 2.57(t, 4H, J=8Hz, side chain 1-CH_2), 7.06(s, 4H, benzene-H), 9.18(bs, 2H, NH), 9.48(s, 2H, HCO).

Mass spectrum [m/e(relative intensity)]: 460(M^+, 15), 432(17), 150(14), 136(100),

108(78).

(c) 1,4-Bis[4-(5-formyl-2,4-dimethylpyrrol-3-yl)butyl]-2-acetamidobenzene (**43c**)

The dibenzylester **40c** (3.6 g, 5.14 mmol) was debenzylated and decarboxylated according to the procedure described for **40a** and **41a**.

The ice cooled bis α-free pyrrole **42c** was treated dropwise with the Vilsmeier reagent, which was made by adding benzoyl chloride (5.4 mL) to a chilled mixture of DMF (5.8 mL) and dry CH_2Cl_2 (21 mL). Then, the resulting mixture was treated same way as described for **42a**. After being heated at 70°C for 1 h, the product was extracted with CH_2Cl_2 to give an impure greyish black **43c**. An analytical sample was prepared by deprotecting the cyanoacrylate derivative **44c** with aqueous potassium hydroxide in n-propanol.

M.P. = 206.5 - 208.5°C.

Mol.wt. Calcd. for $C_{30}H_{39}N_3O_3$: 489.2991; Found, by high resolution mass spectrometry: 489.2995.

Anal. Calcd. for $C_{30}H_{39}N_3O_3$: C, 73.59; H, 8.03; N, 8.58; Found; C, 73.23; H, 8.23; N, 8.55.

^{1}H-nmr (400 MHz, δ, $CDCl_3$): 1.44-1.67(m, 8H, side chain 2, 2′-, 3, 3′-CH_2), 2.18(s,

3H, NHCOC<u>H</u>$_3$), 2.20(s, 6H, pyrrole 2-CH_3), 2.24(s, 6H, pyrrole 4-CH_3), 2.36-2.41(m, 4H, side chain 4, 4′-CH_2), 2.53-2.62(m, 4H, side chain 1, 1′-CH_2), 6.88-6.93(b, 2H, N<u>H</u>COCH$_3$, m-NHCOCH$_3$-benzene-<u>H</u>), 7.05-7.07(b, 1H, p-NHCOCH$_3$-benzene-<u>H</u>), 7.55 (bs, 1H, o-NHCOCH$_3$-benzene-<u>H</u>), 8.87(bs, 2H, NH), 9.48, 9.52(s, s, 2H, <u>H</u>CO).

<u>Mass spectrum</u> [m/e(relative intensity)]: 4.89(M^+, 19), 461(23), 446(11), 169(40), 136(92), 108(100).

<u>(d) 1,4-Bis[5-(5-formyl-2,4-dimethylpyrrol-3-yl)pentyl]-2-acetamidobenzene</u> (**43d**)

The product **43d** was obtained according to the procedure employed in the synthesis of **43c**.

<u>M.P.</u> = 143.0 - 144.0°C.

<u>Mol.wt.</u> Calcd. for $C_{32}H_{43}N_3O_3$: 517.3304; Found, by high resolution mass spectrometry: 517.3303.

^{1}<u>H-nmr</u> (400 MHz, δ, $CDCl_3$): 1.31-1.65(m, 12H, side chain 2, 2′-, 3, 3′-, 4, 4′-CH_2), 2.19(s, 3H, NHCOC<u>H</u>$_3$), 2.20(s, 6H, pyrrole 2-CH_3), 2.25(s, 6H, pyrrole 4-CH_3), 2.34-2.38(m, 4H, side chain 5, 5′-CH_2), 2.50-2.58(m, 4H, side chain 1, 1′-CH_2), 6.91, 7.02-7.09, 7.56(b, m, b, 4H, N<u>H</u>COCH$_3$, benzene-H), 8.98(bs, 2H, NH), 9.48(b, 2H, HCO).

<u>Mass spectrum</u> [m/e(relative intensity)]: 517(M^+, 20), 498(8), 489(23), 474(10), 150(18),

136(81), 122(27), 108(100).

3.4.6 The bis cyanoacrylates

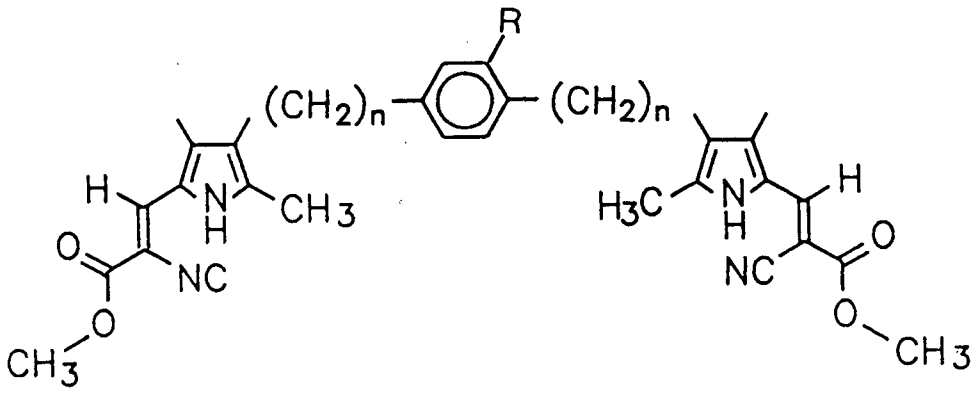

44a, n=4, R=H

44a, n=5, R=H

44a, n=4, R=$NHCOCH_3$

44a, n=5, R=$NHCOCH_3$

(a) 1,4-Bis{4-[5-(2-cyano-2-methoxycarbonylvinyl)-2,4-dimethylpyrrol-3-yl]butyl}benzene (**44a**)

The crude 1,4-bis[4-(5-formyl-2,4-dimethylpyrrol-3-yl)butyl]benzene (**43a**) (1 g, 2.31 mmol) was taken up in toluene (50 mL) with methyl cyanoacetate (0.56 g, 5.65 mmol) and cyclohexylamine (0.5 mL). The mixture was heated at reflux on a stirrer-hot plate under nitrogen. The reaction was monitored by TLC and was found to be complete in 2 h. The solvent was evaporated, in vacuo, and the residue was taken to dryness on a vacuum line.

The crude product was dissolved in CH_2Cl_2 and chromatographed on silica gel (50

g). The solvent polarity was gradually increased, 0.5% ethyl acetate/CH_2Cl_2 and then 1% ethyl acetate/CH_2Cl_2, to facilitate elution without causing the impurities to move. The bright yellow product was crystallized from the eluates by concentrating, in the presence of methanol, to yield 1.06 g (76.9%). The solid thus obtained was analytically pure.

M.P. = 198.3 - 200.3°C.

Mol.wt. Calcd. for $C_{36}H_{42}N_4O_4$: 594.3206; Found, by high resolution mass spectrometry: 594.3207.

Anal. Calcd. for $C_{36}H_{42}N_4O_4$: C, 72.70; H, 7.12; N, 9.42; Found: C, 72.87; H, 7.27; N, 9.32.

^{1}H-nmr (400 MHz, δ, $CDCl_3$): 1.43-1.50(m, 4H, side chain 3-CH_2), 1.58-1.66(m, 4H, side chain 2-CH_2), 2.15(s, 6H, pyrrole 4-CH_3), 2.28, 2.29(s, s, 6H, pyrrole 2-CH_3), 2.38-2.43(m, 4H, side chain 4-CH_2), 2.60(t, 4H, J=8Hz, side chain 1-CH_2), 3.86(s, 6H, -OCH_3), 7.07(s, 4H, benzene-H), 7.20, 7.91[s, s, 2H, C(H)=C(CN)$COOCH_3$], 9.48(bs, 2H, NH).

Mass spectrum [m/e(relative intensity)]: 594(M^+, 49), 562(14), 530(26), 217(68), 185(100).

(b) 1,4-Bis{5-[5-(2-cyano-2-methoxycarbonylvinyl)-2,4-dimethylpyrrol-3-yl]pentyl} benzene (**44b**)

The bright yellow product **44b** was synthesized according to the method described for **44a** in a yield of 81.8%.

M.P. = 168.5 - 170.0°C.

Mol.wt. Calcd. for $C_{38}H_{46}N_4O_4$: 622.3519; Found, by high resolution mass spectrometry: 622.3531.

Anal. Calcd. for $C_{38}H_{46}N_4O_4$: C, 73.28; H, 7.44; N, 9.00; Found: C, 73.32; H, 7.41; N, 8.98.

^{1}H-nmr (400 MHz, δ, $CDCl_3$): 1.32-1.41(m, 4H, side chain 3-CH_2), 1.41-1.50(m, 4H, side chain 4-CH_2), 1.59-1.67(m, 4H, side chain 2-CH_2), 2.15, 2.17(s, s, 6H, pyrrole 4-CH_3), 2.28, 2.30(s, s, 6H, pyrrole 2-CH_3), 2.37(t, 4H, J=8Hz, side chain 5-CH_2), 2.58(t, 4H, J=8Hz, side chain 1-CH_2), 3.86(s, 6H, -OCH_3), 7.07(s, 4H, benzene-H), 7.20, 7.92[s, s, 2H, C(H)=C(CN)$COOCH_3$], 9.49(bs, 2H, NH).

Mass spectrum [m/e(relative intensity)]: 622(M^+, 28), 590(7), 558(8), 217(54), 185(77).

(c) 1,4-Bis{4-[5-(2-cyano-2-methoxycarbonylvinyl)-2,4-dimethylpyrrol-3-yl]butyl}-2-acetamidobenzene (**44c**)

1,4-Bis[4-(5-benzyloxycarbonyl-2,4-dimethylpyrrol-3-yl)butyl]-2-acetamidobenzene (**40c**) (3.5 g, 5.0 mmol) was initially converted to the bis formylpyrrole **43c** in the manner described previously. The crude **43c** was then taken up in toluene (100 mL) containing methyl cyanoacetate (1.78 g, 18 mmol) and cyclohexylamine (1 mL), and the mixture refluxed under nitrogen for 2 h to reach completion.

The residue obtained after evaporating the solvent was chromatographed on silica gel (100 g, activity I) with 1% $MeOH/CH_2Cl_2$ as the eluent. The bright yellow powdery product was crystallized by concentrating the solution in the presence of methanol, yield 1.76 g (54.1% overall from the bis benzylester **40c**).

M.P. = 228.0 - 230.0°C.

Mol.wt. Calcd. for $C_{38}H_{45}N_5O_5$: 651.3421; Found, by high resolution mass spectrometry: 651.3440.

Anal. Calcd. for $C_{38}H_{45}N_5O_5$: C, 70.02; H, 6.96; N, 10.74; Found: C, 69.71; H, 6.88; N, 10.58.

^{1}H-nmr (400 MHz, δ, $CDCl_3$): 1.43-1.66(m, 8H, side chain 2, 2′-, 3, 3′-CH_2), 2.15(s, 6H, pyrrole 4-CH_3), 2.17(s, 3H, NHCOCH_3), 2.27, 2.30(s, s, 6H, pyrrole 2-CH_3), 2.37-2.42(m, 4H, side chain 4, 4′-CH_2), 2.52-2.61(m, 4H, side chain 1, 1′-CH_2), 3.85(s, 6H, -OCH_3), 6.89-6.93(m, 2H, NHCOCH$_3$, m-NHCOCH$_3$-benzene-H), 7.06(b, 1H, p-NHCOCH$_3$-benzene-H), 7.20, 7.54(bd, 1H, o-NHCOCH$_3$-benzene-H), 7.90, 7.92[s, s, 2H, C(H)=C(CN)COOCH$_3$], 9.49(bs, 2H, NH).

Mass spectrum [m/e(relative intensity)]: 651(M^+, 54), 619(12), 587(14), 245(25), 217(85), 185(100).

(d) 1,4-Bis{5-[5-(2-cyano-2-methoxycarbonylvinyl)-2,4-dimethylpyrrol-3-yl]pentyl}-2-acetamidobenzene (**44d**)

The bright yellow product was obtained in a yield of 53.4% from the bis benzyl ester **40d** using the method described for **44c**.

M.P. = 184.0 - 186.0°C.

Mol.wt. Calcd. for $C_{40}H_{49}O_5N_5$: 679.3733; Found, by high resolution mass spectrometry: 679.3734.

Anal. Calcd. for $C_{40}H_{49}O_5N_5$: C, 70.67; H, 7.26; N, 10.30; Found: C, 70.51; H, 7.30; N, 10.17.

^{1}H-nmr (400 MHz, δ, $CDCl_3$): 1.33-1.50(m, 8H, side chain 3, 3′-, 4, 4′-CH_2), 1.57-1.67(m, 4H, side chain 2, 2′-CH_2), 2.16(s, 6H, pyrrole 4-CH_3), 2.20(s, 3H, NHCOCH_3), 2.29, 2.31(s, s, 6H, pyrrole 2-CH_3), 2.35-2.40(m, 4H, side chain 5, 5′-CH_2), 2.52-2.60(m, 4H, side chain 1, 1′-CH_2), 3.87(s, 6H, -OCH_3), 6.93(b, 2H, NHCOCH$_3$, m-NHCOCH$_3$-benzene-H), 7.07(b, 1H, p-NHCOCH$_3$-benzene-H), 7.21, 7.58(b, 1H, o-NHCOCH$_3$-benzene-H), 7.91, 7.93[s, s, 2H, C(H)=C(CN)$COOCH_3$], 9.49(bs, 2H, NH).

Mass spectrum [m/e(relative intensity)]: 679(M^+, 53), 647(10), 615(12), 273(8), 217(83), 185(100).

3.5 Syntheses of benzene and amidobenzene linked dipyrromethane dimers

3.5.1 Preparation of 47

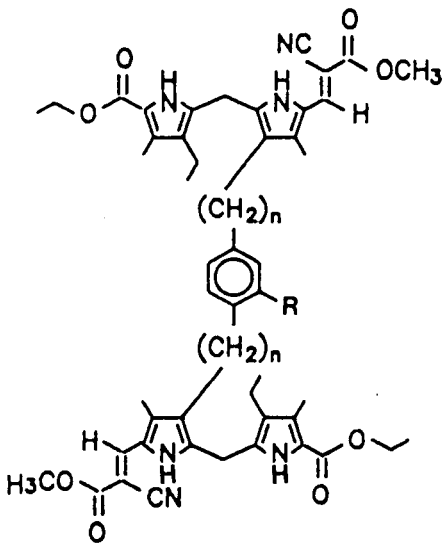

47a, n=4, R=H

47b, n=5, R=H

47c, n=4, R=$NHCOCH_3$

47d, n=5, R=$NHCOCH_3$

(a) 1,4-Bis{4-[2-((5-ethoxycarbonyl-3-ethyl-4-methylpyrrol-2-yl)methyl)-5-(2-cyano-2-methoxycarbonylvinyl)-4-methylpyrrol-3-yl]butyl}benzene (**47a**)

(i) Monochlorination of the α-methyl group in **44a**:

1,4-Bis{4-[5-(2-cyano-2-methoxycarbonylvinyl)-2,4-dimethylpyrrol-3-yl]butyl} benzene (**44a**) (0.44 g, 0.74 mmol) in dry methylene chloride (50 mL) was treated, dropwise, with a solution of sulfuryl chloride (0.22 g, 1.63 mmol) in methylene chloride (10 mL) over a period of 10 min at room temperature. The pale yellow solution which turned orange during addition was stirred for a further 0.5 h. The solvent was then removed completely in vacuo, and the yellow residue of the corresponding α-chloromethyl derivative **45a** was used directly in the next reaction without purification.

(ii) Condensation of **45a** with **46**:

The α-chloromethyl derivative **45a**, prepared above, was suspended in glacial acetic acid (50 mL) together with 2-ethoxycarbonyl-4-ethyl-3-methylpyrrole **46** (0.35 g, 1.9 mmol) and heated under nitrogen. When the temperature reached 70°C, all of the starting material went into solution resulting a clear dark red solution. After the reaction mixture was heated for a further 30 min, TLC analysis of the reaction mixture indicated the product as a single yellow spot, colored violet by bromine vapor. The mixture was evaporated to dryness in vacuo and the residue taken up in methylene chloride (50 mL). The remaining acid was removed by extraction with saturated aqueous sodium bicarbonate (3x50 mL) and water (3x50 mL). The dried methylene chloride solution was then chromatographed on silica gel (50 g). The excess α-free pyrrole starting material **46** was eluted with methylene chloride and the product was eluted with 5%-10% ethyl acetate/methylene chloride. Crystallization of the product was tried in several solvents system and all failed. The product was eventually isolated as a non-crystallisable glass, by evaporating the solvents, yield 0.65 g (92%). An analytically pure sample was obtained using a chromatotron (silica gel, 1 mm plate, 0.5% methanol/methylene chloride as the eluent).

M.P. = 244°C (decomp.).

Mol.wt. Calcd. for $C_{56}H_{68}N_6O_8$: 952.5099; Found, by high resolution mass spectrometry: 952.5090.

Anal. Calcd. for $C_{56}H_{68}N_6O_8$: C, 70.56; H, 7.19; N, 8.82; Found: C, 69.83; H, 7.36; N, 8.36; Calcd. for $C_{56}H_{68}N_6O_8 \cdot CH_3OH$: C, 69.49; H, 7.37; N, 8.53.

^{1}H-nmr (400 MHz, δ, $CDCl_3$): 1.01(t, 6H, J=8Hz, 3′-CH_2CH_3), 1.31, 1.29-1.40(t, m, 10H, -OCH_2CH_3, side chain 3-CH_2), 1.55-1.64(m, 4H, side chain 2-CH_2), 2.10, 2.11, 2.12(s, s, s, 6H, pyrrole 4-CH_3), 2.29(s, 6H, pyrrole 4′-CH_3), 2.33-2.43(m, 8H, 3′-CH_2CH_3, side chain 4-CH_2), 2.53-2.61(m, 4H, side chain 1-CH_2), 3.78, 3.83(s, s, 6H, -OCH_3 isomers), 3.87-4.20(m, 4H, bridge-CH_2), 4.24(q, 4H, J=8Hz, -OCH_2CH_3), 7.06(s, 4H, benzene-H), 7.20, 7.84, 7.85[s, s, s, 2H, C(H)=C(CN)$COOCH_3$ isomers], 9.00(b, 2H, 1′-NH), 9.37(b, 2H, 1-NH).

Mass spectrum [m/e(relative intensity)]: 952(M^+, 3), 906(15), 860(20), 698(29), 666(20).

(b) 1,4-Bis{5-[2-((5-ethoxycarbonyl-3-ethyl-4-methylpyrrol-2-yl)methyl)-5-(2-cyano-2-methoxycarbonylvinyl)-4-methylpyrrol-3-yl]pentyl}benzene (**47b**)

This compound was prepared by the same procedure as that employed in the preparation of compound **47a**. With 0.51 g (0.82 mmol) of the starting material **44b**, a yield of 85.8% was obtained. The product was purified by silica gel (50 g) first, then

by alumina (30 g) and was found to be analytically pure.

M.P. = 96.0 - 98.0°C.

Mol.wt. Calcd. for $C_{58}H_{72}N_6O_8$: 980.5412; Found, by high resolution mass spectrometry: 980.5394.

Anal. Calcd. for $C_{58}H_{72}N_6O_8$: C, 71.00; H, 7.40; N, 8.56; Found: C, 68.88; H, 7.43; N, 8.07; Calcd. for $C_{58}H_{72}N_6O_8 \cdot 1/2CH_2Cl_2$: C, 68.64; H, 7.19; N, 8.21.

Mass spectrum [m/e(relative intensity)]: 980(M^+, very weak), 934[$(M-CH_3CH_2OH)^+$, very weak], 374(41), 343(41).

(c) 1,4-Bis{4-[-2((5-ethoxycarbonyl-3-ethyl-4-methylpyrrol-2-yl)methyl)-5-(2-cyano-2-methoxycarbonylvinyl)-4-methylpyrrol-3-yl]butyl}-2-acetamidobenzene (**47c**)

Compound **44c** (0.42 g, 0.65 mmol), in dry methylene chloride (50 mL) was chlorinated using a solution of sulfuryl chloride (0.19 g, 1.4 mmol) in methylene chloride (10 mL) as described for **47a**. The bis α-chloromethyl derivative was then reacted with 2-ethoxycarbonyl-4-ethyl-3-methylpyrrole (**46**) (0.3 g, 1.66 mmol) in acetic acid (50 mL) to give the dipyrromethane dimer **47c**. The crude product was purified by silica gel (30 g, activity I), 1% MeOH/CH_2Cl_2 as the eluent, yield 0.58 g (89%).

M.P.= 132.0 - 134.0°C.

Mol.wt. Calcd. for $C_{58}H_{71}N_7O_9$: 1009.5313; Found, by high resolution mass spectrometry: 1009.5289.

Anal. Calcd. for $C_{58}H_{71}N_7O_9$: C, 68.96; H, 7.08; N, 9.71; Found: C, 68.58; H, 7.10; N, 9.18.

^{1}H-nmr (400 MHz, δ, $CDCl_3$): 0.96-1.03(m, 6H, 3′-CH_2CH_3), 1.26-1.35(m, 6H, -OCH_2CH_3), 1.35-1.50(m, 4H, side chain 3, 3′-CH_2), 1.50-1.68(m, 4H, side chain 2, 2′-CH_2), 2.11(s, 6H, pyrrole 4-CH_3), 2.16(s, 3H, $NHCOCH_3$), 2.27(s, 6H, pyrrole 4′-CH_3), 2.34-2.43(m, 8H, 3′-CH_2CH_3, side chain 4, 4′-CH_2), 2.48-2.63(m, 4H, side chain 1, 1′-CH_2), 3.71, 3.76, 3.78, 3.82(s, s, s, s, 6H, -OCH_3 isomers), 3.86-3.92(m, 4H, bridge-CH_2), 4.20-4.30(m, 4H, -OCH_2CH_3), 5.63-5.68(bd, 1H, $NHCOCH_3$), 6.92(bd, 1H, m-$NHCOCH_3$-benzene-H), 7.05(bd, 1H, p-$NHCOCH_3$-benzene-H), 7.43(b, 1H, o-$NHCOCH_3$-benzene-H), 7.17-7.20, 7.84, 7.86[b, s, s, 2H, C(H)=$C(CN)CO_2CH_3$], 8.92, 9.25(b, b, 2H, 1′-NH isomers), 9.36, 9.40(b, b, 2H, 1-NH isomers).

Mass spectrum [m/e(relative intensity)]: 1009(M^+, very weak), 963[$(M-CH_3CH_2OH)^+$, 2], 784(6).

(d) 1,4-Bis{5-[2-((5-ethoxycarbonyl-3-ethyl-4-methylpyrrol-2-yl)methyl)-5-(2-cyano-2-methoxycarbonylvinyl)-4-methylpyrrol-3-yl]pentyl}-2-acetamidobenzene (**47d**)

The product **47d** was synthesised using the same procedure as described for **47c**, yield 94%.

M.P. = 99 - 101°C.

Mol.wt. Calcd. For $C_{60}H_{75}N_7O_9$: 1037.5626; Found, by high resolution mass spectrometry: 1037.5535.

Anal. Calcd. For $C_{60}H_{75}N_7O_9$: C, 69.41; H, 7.28; N, 9.44; Found: C, 68.94; H, 7.32; N, 9.07.

^{1}H-nmr (400 MHz, δ, $CDCl_3$): 0.98-1.05(m, 6H, 3′-CH_2CH_3), 1.29-1.43(t, m, 14H, -OCH_2CH_3, side chain 3, 3′-CH_2, 4, 4′-CH_2), 1.52-1.63(m, 4H, side chain 2, 2′-CH_2), 2.14, 2.16(s, s, 6H, pyrrole 4-CH_3), 2.20(s, 3H, $NHCOCH_3$), 2.27, 2.29, 2.30(s, s, s, 6H, pyrrole 4′-CH_3), 2.34-2.45(m, 8H, 3′-CH_2CH_3, side chain 5, 5′-CH_2), 2.49-2.57(m, 4H, side chain 1, 1′-CH_2), 3.78-3.85(m, 6H, -OCH_3 isomers), 3.91(s, 4H, bridge-CH_2), 4.21-4.30(m, 4H, -OCH_2CH_3), 6.05-6.13(bd, 1H, $NHCOCH_3$), 6.91(bd, 1H, m-$NHCOCH_3$-benzene-H), 7.05(bd, 1H, p-$NHCOCH_3$-benzene-H), 7.14, 7.54(b, 1H, o-$NHCOCH_3$-benzene-H), 7.23, 7.89, 7.92[b, s, s, 2H, C(H)=C(CN)$COOCH_3$ isomers], 8.78, 8.94(b, b, 2H, 1′-NH isomers), 9.37, 9.40(b, b, 2H, 1-NH isomers).

Mass spectrum [m/e(relative intensity)]: 1037(M^+, very weak), 991[(M-CH_3CH_2OH), 2].

3.5.2 Hydrolysis of 47

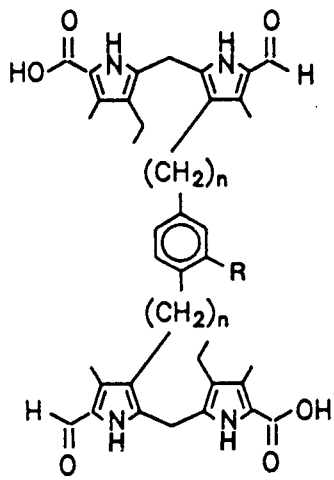

48a, n=4, R=H

48b, n=5, R=H

48c, n=4, R=$NHCOCH_3$

48d, n=5, R=$NHCOCH_3$

(a) 1,4-Bis{4-[2-((5-carboxy-3-ethyl-4-methylpyrrol-2-yl)methyl)-5-formyl-4-methylpyrrol-3-yl]butyl}benzene (**48a**)

In a 25 mL-round-bottom flask fitted with a Claisen adaptor, a nitrogen inlet and a reflux condenser, were placed 1,4-bis{4-[2-((5-ethoxycarbonyl-3-ethyl-4-methylpyrrol-2-yl)methyl)-5(2-cyano-2-methoxycarbonylvinyl)-4-methylpyrrol-3-yl]butyl}benzene (**47a**) (0.46 g, 0.48 mmol), KOH (0.81 g, 14.5 mmol) and water (9.6 mL). The magnetically stirred suspension was heated to reflux and n-propanol (4.8 mL) was added. The yellow solid starting material went into solution immediately resulting in a pale brown solution. Refluxing was continued and every half an hour an aliquot was removed, diluted with water and its UV/visible spectrum was recorded. This spectrum was compared to that of the starting material which showed a strong absorption at 388 nm

and a moderately intense absorption at 280 nm. During the reaction, the peak at 388 nm diminished with a simultaneous increase in the intensity of the peak at lower wavelength and a new peak appeared at 324 nm. In 3 h, the peak at 388 nm disappeared completely, indicating complete removal of the cyanoacrylate protecting groups. The lower wavelength bands (now at 268 nm and 322 nm) were very intense.

The condenser was removed at this time to evaporate off n-propanol until the temperature reached 100°C. The solution was cooled to room temperature, while under nitrogen, when the product partially separated out as a brown slimy material. The solution was filtered under suction and the brown material was dissolved by adding water while on the filter paper. The clear solution was then cooled in ice and acidified with glacial acetic acid. The brown powder was collected by filtration and washed with water. The final product was dried in a vacuum desiccator over KOH for 2 days, yield 0.33 g (93%).

M.P. = 179.0 - 181.0°C.

^{1}H-nmr (300 MHz, δ, DMSO-d_6): 0.90(m, 6H, 3′-CH_2CH_3), 1.04-1.60(b, 8H, side chain 2-, 3-CH_2), 2.12(s, 12H, pyrrole 4, 4′-CH_3), 2.20-2.36(m, 8H, side chain 4-CH_2, 3′-CH_2CH_3), 2.40-2.56(m, 4H, side chain 1-CH_2), 3.80(s, 4H, bridge-CH_2), 7.00(s, 4H, benzene-H), 9.44(s, 2H, HCO), 11.06-11.48(m, 4H, pyrrole NH).

Mass spectrum [m/e(relative intensity)]: 734(M^+, from FAB), 646[$(M-2COO)^+$, 3], 617(3), 508(5), 169(11), 122(42), 109(58), 94(100).

(b) 1,4-Bis{5-[2-((5-carboxy-3-ethyl-4-methylpyrrol-2-yl)methyl)-5-formyl-4-methylpyrrol-3-yl]pentyl}benzene (**48b**)

A brown powdery product was obtained by the same method described for compound **48a** in a yield of 86%.

M.P. = 250.0 - 252.0°C.

^{1}H-nmr (300 MHz, δ, DMSO-d_6): 0.90(t, 6H, 3′-CH_2CH_3), 1.04-1.36(m, 8H, side chain 3-, 4-CH_2), 1.36-1.58(b, 4H, side chain 2-CH_2), 2.14(s, 12H, pyrrole 4, 4′-CH_3), 2.22-2.30 (m, 4H, side chain 5-CH_2), 2.30-2.48(m, 8H, side chain 1-CH_2, 3′-CH_2CH_3), 3.80(s, 4H, bridge-CH_2), 7.00(s, 4H, benzene-H), 9.44, 9.52(s, s, 2H, HCO), 11.04-11.60(m, 4H, pyrrole NH).

Mass spectrum [m/e(relative intensity)]: 761[$(M-H)^+$, from FAB], 674[$(M-2COO)^+$, 2], 645(3), 536(3), 524(7), 122(30), 109(56), 94(100).

(c) 1,4-Bis{4-[2-((5-carboxy-3-ethyl-4-methylpyrrol-2-yl)methyl)-5-formyl-4-methylpyrrol-3-yl]butyl}-2-acetamidobenzene (**48c**)

The procedure used for the synthesis of this compound was the same as that employed in the preparation of **48a**. The quantities of the reagent and solvents used for 0.33 g (0.33 mmol) starting material **47c** were, potassium hydroxide (0.55 g), water (6.5 mL) and n-propanol (3.2 mL). The brown powdery product was obtained in a yield of 89% (0.23 g).

M.P. = 165.0 - 167.0°C.

^{1}H-nmr (300 MHz, δ, DMSO-d_6): 0.94(m, 6H, 3′-CH_2CH_3), 1.12-1.64(m, b, 8H, side chain 2, 2′-, 3, 3′-CH_2), 2.02(s, 3H, $NHCOCH_3$), 2.18(s, 12H, pyrrole 4, 4′-CH_3), 2.24-2.40(m, 8H, side chain 4, 4′-CH_2, 3′-CH_2CH_3), 2.40-2.62(m, 4H, side chain 1, 1′-CH_2), 3.80(s, 4H, bridge-CH_2), 6.88-7.20(m, 3H, benzene-H), 9.24, 9.50, 9.58(d, s, s, 2H, HCO), 11.10-11.50(m, 4H, pyrrole NH).

Mass spectrum [m/e(relative intensity)]: 791(M^+, from FAB), 703[$(M-2COO)^+$, 4], 674(4), 568(8), 122(24), 109(48), 94(100).

(d) 1,4-Bis{5-[2-((5-carboxy-3-ethyl-4-methylpyrrol-2-yl)methyl)-5-formyl-4-methylpyrrol-3-yl]pentyl}-2-acetamidobenzene (**48d**)

The product was synthesised by the same method described for **48a**. The quantities of the reagent and solvents used for 0.45 g (0.43 mmol) starting material **47d** were, potassium hydroxide (0.73 g), water (8.7 mL) and n-propanol (4.4 mL), yield 85.4% (0.303 g).

M.P. = 159.0 - 161.0°C.

^{1}H-nmr (300 MHz, δ, DMSO-d_6): 0.80-0.96(m, 6H, 3′-CH_2CH_3), 1.12-1.36(b, 8H, side chain 3, 3′-, 4, 4′-CH_2), 1.38-1.56(b, 4H, side chain 2, 2′-CH_2), 2.00(s, 3H, $NHCOCH_3$),

2.16, 2.20(s, s, 12H, pyrrole 4, 4′-CH_3), 2.30(b, 8H, 3′-$\underline{CH_2}CH_3$, side chain 5, 5′-CH_2), 2.48(b, 4H, side chain 1, 1′-CH_2), 3.90(s, 4H, bridge-CH_2), 6.92-7.14(m, 3H, benzene-H), 9.20, 9.48(s, s, 2H, $\underline{H}CO$), 11.08(s, 2H, 1-NH), 11.50(s, 2H, 1′-NH).

Mass spectrum [m/e(relative intensity)]: 819(M^+, very weak), 775[$(M-COO)^+$, 2], 731[$(M-2COO)^+$, 3], 702(4), 593(9), 122(70), 109(58), 94(100).

3.6 Cyclization to the capped porphyrins

(a) 7,17-Diethyl-2,8,12,18-tetramethyl-3,13-[phenylene-1,4-bis(tetramethylene)]porphyrin (**49a**)

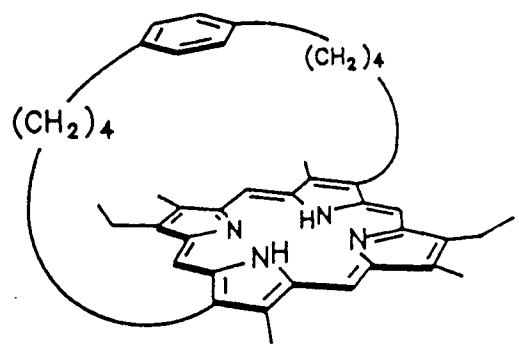

49a

(i) Decarboxylation of **48a**:

The dipyrromethane derivative **48a** (0.31 g, 0.42 mmol) was dissolved in DMF (100 mL) in a 250 mL Erlenmeyer flask, fitted with a Claisen adapter and a nitrogen inlet. The UV/visible spectrum of a drop of this solution, diluted with methylene chloride, showed two bands, one at 280 nm and the other at 318 nm. The magnetically

stirred DMF solution was heated at its reflux temperature (153°C). At regular intervals, an aliquot was removed into methylene chloride and its UV/visible spectrum recorded. The intensity of the 280 nm band decreased considerably relative to that of the 318 nm band. This was taken as an indication of the extent of decarboxylation. In 2 h, the 280 nm band was reduced to a shoulder.

The solution was cooled to room temperature under nitrogen and the DMF evaporated in vacuo to ~10 mL. Methylene chloride (100 mL) was added. The solution was then extracted with water (3x50 mL), dried with anhydrous sodium sulphate, filtered and evaporated to ~10 mL. Distilled THF was added to dilute the solution to 200 mL and the solution was stored in a refrigerator for the subsequent cyclization reaction.

(ii) Intramolecular 2+2 coupling:

The cyclization was carried out in two 2-Litre Erlenmeyer flasks, covered with aluminum foil, each flask containing toluene-p-sulphonic acid (4.0 g), dissolved in methanol (25 mL) and diluted with distilled methylene chloride (600 mL). The dipyrromethane derivative prepared above was added very slowly to the magnetically stirred acid catalyst solution by means of a syringe pump. The syringe pump, operating at its slowest speed, took approximately 9 h to empty one 50 mL syringe.

Once addition was complete (~20 h), the reddish-violet solution was concentrated down to ~10 ml and taken into methylene chloride (100 mL) and extracted with saturated aqueous sodium bicarbonate (3x50 mL) to remove the acid catalyst. With removal of the acid the solution turned to dark brown but was fluorescent under 366 nm light. It was then taken to dryness in vacuo and the residue was chromatographed as described below.

(iii) Chromatographic purification of the porphyrin

The crude porphyrin was first chromatographed on silica gel (120 g, activity I) using methylene chloride as the solvent. Some pink materials which eluted down first were discarded. The solvent was then changed to 1% $MeOH/CH_2Cl_2$ and the porphyrin eluted down with some brown impurities.

The partially purified porphyrin was chromatographed again on alumina (30 g, 4% water added) with methylene chloride as the eluting solvent. Some brown, fast moving impurities initially eluted out, and then, the porphyrin eluted down cleanly, leaving all other impurities adsorbed at the origin. Crystallization from a solution of $MeOH/CH_2Cl_2$ afforded 89.2 mg (34.8%) of the purple porphyrin.

M.P. > 300°C.

Mol.wt. Calcd. For $C_{42}H_{48}N_4$: 608.3879; Found, by high resolution mass spectrometry: 608.3883.

Anal. Calcd. for $C_{42}H_{48}N_4$: C, 82.85; H, 7.95; N, 9.20; Found: C, 82.40; H, 7.87; N, 8.95.

^{1}H-nmr (400 MHz, δ, CD_2Cl_2): 9.98(s, 2H, methine protons 10-H and 20-H), 9.77(s, 2H, methine protons 5-H and 15-H), 4.08(q, 4H, J=6.7Hz, $-CH_2CH_3$), 3.96-4.05(m, 2H, one proton each at chain termini), 3.63-3.70(m, 2H, one proton each at chain termini), 3.63(s, 6H, $2CH_3$), 3.44(s, 6H, $2CH_3$), 2.38(s, 4H, benzene-H), 1.87(t, 6H, J=8Hz, $-CH_2CH_3$), 1.36-1.50(m, 2H, chain protons), 1.18-1.27(m, 2H, chain protons), 0.83-0.91(m, 2H, chain protons), 0.07-0.18(m, 4H, chain protons), -0.08-0.02(m, 2H, chain protons), -3.26(bs, 2H, NH).

Visible spectrum (CH_2Cl_2):

λ_{max} (nm),	404	506	542	572	626
log ε,	5.26	4.08	4.10	3.91	3.60

(b) 7,17-Diethyl-2,8,12,18-tetramethyl-3,13-[phenylene-1,4-bis(pentamethylene)]porphyrin (**49b**)

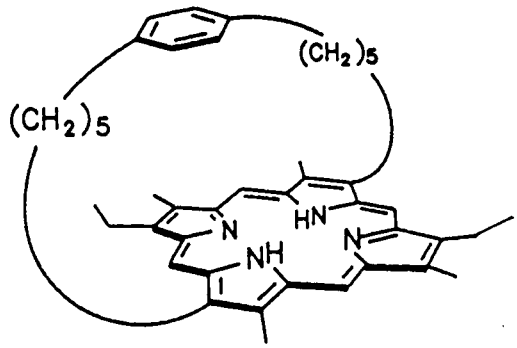

49b

This porphyrin was prepared and purified in the same way as described for porphyrin **49a**. The yield was 19.1%.

M.P. > 300°C.

Mol.wt. Calcd. for $C_{44}H_{52}N_4$: 636.4192; Found, by high resolution mass spectrometry: 636.4189.

Anal. Calcd. for $C_{44}H_{52}N_4$: C, 82.97; H, 8.23; N, 8.80; Found: C, 80.72; H, 8.62; N, 8.57; Calcd. for $C_{44}H_{52}N_4 \cdot CH_3OH$: C, 80.80; H, 8.44; N, 8.38.

^{1}H-nmr (400 MHz, δ, CD_2Cl_2): 10.19(s, 2H, methine protons 10-H and 20-H), 10.09(s, 2H, methine protons 5-H and 15-H), 4.34-4.41(m, 2H, one proton each at chain termini), 4.22-4.32(m, 2H, -$C\underline{H}_2CH_3$), 4.06-4.15(m, 2H, -$C\underline{H}_2CH_3$), 3.95-4.05(m, 2H, one proton each at chain termini), 3.67(s, 6H, $2CH_3$), 3.54(s, 6H, $2CH_3$), 2.68(s, 4H, benzene-H), 2.17-2.27(m, 2H, chain protons), 1.91, 1.87-1.91(t, m, 8H, -$CH_2C\underline{H}_3$, chain protons), 0.86-0.97(m, 6H, chain protons), 0.28-0.35(m, 2H, chain termini), -0.13- -0.24(m, 2H, chain protons), -1.13(m, 2H, chain protons), -3.58(bs, 2H, NH).

Visible spectrum (CH_2Cl_2):

λ_{max} (nm),	400	498	534	568	622
log ε,	5.10	3.90	3.77	3.46	3.13

(c) 7,17-Diethyl-2,8,12,18-tetramethyl-3,13-[2-acetamido-phenylene-1,4-bis(tetramethylene)]porphyrin (**49c**)

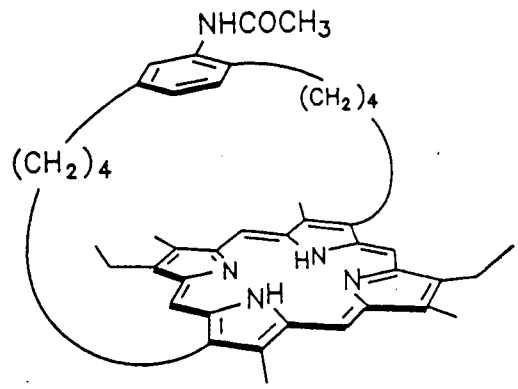

49c

The procedure used in preparation of this porphyrin was the same as that employed in preparation of porphyrin **49a**.

This porphyrin was found to be adsorbed onto silica gel more strongly than **49a** and **49b**. For activity I silica gel, 2% MeOH/CH_2Cl_2 was necessary to move the porphyrin. The porphyrin eluate which containing some impurities was purified again using a chromatotron with a 1 mm Al_2O_3 plate and 50%-25%hexane/CH_2Cl_2 as the eluting solvents. The porphyrin was found to be quite clean by an UV/visible spectrum and the product was obtained by evaporating the solvents. The residue was dried under vacuum for 3 days to give 44.8% yield. Crystallization was achieved by evaporating a hexane/CH_2Cl_2 solution of the porphyrin.

M.P. > 300°C

Mol.wt. Calcd. for $C_{44}H_{51}N_5O$: 665.4094; Found, by high resolution mass spectrometry: 665.4093.

^{1}H-nmr (400 MHz, δ, CD_2Cl2): 9.94(d, 2H, J=16Hz, methine protons 10-H and 20-H), 9.77(d, 2H, J=16Hz, methine protons 5-H and 15-H), 5.54, 5.36(s, s, 2H, benzene-H), 3.94-4.14(m, 6H, -CH_2CH_3, one proton each at chain termini), 3.60-3.74(m, d, 9H, one proton each at chain termini, two CH_3, one benzene-H)), 3.41(d, 6H, two CH_3), 1.86-1.92(m, 6H, -CH_2CH_3), 1.59(s, 3H, NHCOCH_3), 1.31-1.59(m, 2H, chain protons), 1.50(s, 1H, NHCOCH_3), 0.70-0.95(m, 2H, chain protons), 0.01-0.20(b, 4H, chain protons), -0.10- -0.35(b, 4H, chain protons), -3.30(b, 2H, NH).

Visible spectrum (CH_2Cl_2):

λ_{max} (nm),	404	506	542	572	624
log ε,	5.23	4.07	4.09	3.89	3.60

(d) 7,17-Diethyl-2,8,12,18-tetramethyl-3,13-[2-acetamido-phenylene-1,4-bis(pentamethylene)]porphyrin (**49d**)

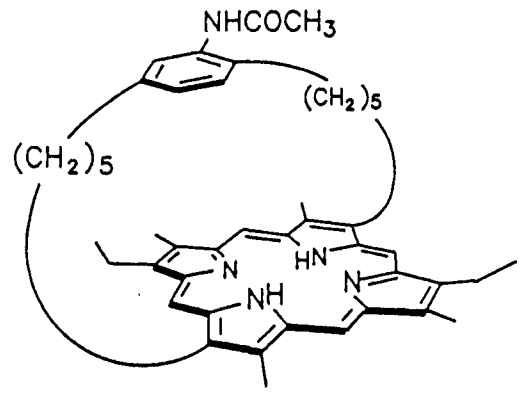

49d

This compound was obtained by the same method described for **49c**. The yield was 28.6%.

M.P. > 300°C

Mol.wt. Calcd. $C_{46}H_{55}N_5O$: 693.4407; Found, by high resolution mass spectrometry: 693.4423.

Anal. Calcd. for $C_{46}H_{55}N_5O$: C, 79.61; H, 7.99; N, 10.09; Found: C, 79.44; H, 8.09; N, 9.86.

^{1}H-nmr (400 MHz, δ, CD_2Cl_2): 10.17(d, 2H, methine protons 10-H and 20-H), 10.07(d, 2H, methine protons 5-H and 15-H), 5.62(m, 1H, benzene-H), 4.32-4.42(m, 2H, one proton each at chain termini), 4.21-4.32(m, 2H, -C<u>H</u>$_2$CH$_3$), 4.05-4.16(m, 2H, -C<u>H</u>$_2$CH$_3$), 3.95-4.05(m, 2H, one proton each at chain termini), 3.68(s, 6H, 2CH$_3$), 3.54(s, 8H,

$2CH_3$, two benzene-H), 2.22(b, 2H, chain protons), 1.86, 1.91(m, t, 8H, $-CH_2\underline{CH_3}$ and chain protons), 1.55(s, 3H, $NHCOC\underline{H_3}$), 1.50(s, 1H, $N\underline{H}COCH_3$), 0.83-1.03(m, 6H, chain protons), 0.10-0.24(m, 2H, chain protons), -0.23(m, 2H, chain protons), -1.23, -1.38(b, b, 2H, chain protons), -3.82(b, 2H, NH).

Visible spectrum (CH_2Cl_2):

λmax (nm),	400	500	536	568	622
log ε,	5.26	4.20	4.13	3.96	3.82

3.7 Syntheses of the benzene and amidobenzene-hemin chloride complexes

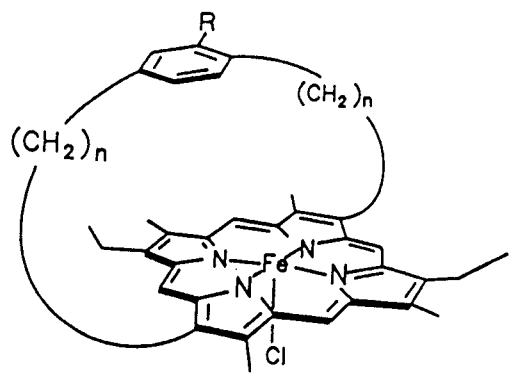

(50a)Cl, n=4, R=H

(50b)Cl, n=5, R=H

(50c)Cl, n=4, R=$NHCOCH_3$

(50d)Cl, n=5, R=$NHCOCH_3$

The free base porphyrin (**49a-d**, 0.035 mmol), dissolved in THF (20 mL), was bubbled with nitrogen for 30 min, and then added rapidly to a stirred solution of

ferrous chloride (0.35 mmol) in methanol (20 mL) which was previously purged by nitrogen. The mixture was refluxed under nitrogen for 1.5 h. After this time an UV/visible spectrum indicated complete conversion to the hemin chloride. The solution was cooled and stirred in air for 30 min to ensure complete conversion of Fe(II) to Fe(III). The solvent was then evaporated in vacuo, the residue taken up in methylene chloride, washed with water and chromatographed on alumina (30 g, 4% H_2O added) using methylene chloride as the solvent. The green μ-oxo dimer, eluting from the column, was shaken with aqueous hydrochloric acid (0.2 M, 30 mL) to effect conversion back to the hemin chloride. The solution was evaporated in vacuo and methanol added to crystallize the hemin chloride (yield 80%).

(a) Benzene-4/4 hemin chloride **(50a)Cl**

Mol.wt. Calcd. for $FeC_{42}H_{46}N_4Cl$: 697.2760; Found, by high resolution mass spectrometry: 697.2756.

Visible spectrum (toluene):

λ_{max} (nm),	374	402(sh)	508	528	630
log ε,	4.74	4.67	3.80	3.82	3.56

(b) Benzene-5/5 hemin chloride **(50b)Cl**:

Mol.wt. Calcd. for $Fe_{44}H_{50}N_4Cl$: 725.3073; Found, by high resolution mass spectrometry:

725.3098.

Visible spectrum (toluene):

λ_{max} (nm),	380	400(sh)	508	532	632
log ε,	4.86	4.77	3.73	3.77	3.33

(c) Amidobenzene-4/4 hemin chloride (**50c**)Cl:

Mol.wt. Calcd. for $FeC_{44}H_{49}N_5OCl$: 754.2975; Found, by high resolution mass spectrometry: 754.2977.

Visible spectrum (toluene):

λ_{max} (nm),	380	402(sh)	494	534	630
log ε	4.78	4.70	3.98	3.85	3.60

(d) Amidobenzene-5/5 hemin chloride (**50d**)Cl:

Mol.wt Calcd. for $FeC_{46}H_{53}N_5Cl$: 782.3288; Found, by high resolution mass spectrometry: 782.3267.

Visible spectrum (toluene):

λ_{max}(nm),	380	400	508	532	632
log ε	4.88	4.79	3.78	3.82	3.43

Chapter 4

Interaction of the capped hemes with CO and O_2

4.1 Materials and apparatus

4.1.1 General

Toluene (1 L) was washed with c. H_2SO_4 (2 x 200 mL) followed by water (2 x 100 mL), and distilled over CaH_2.

Sodium dithionite (sodium hydrosulphite) was purchased from Aldrich.

1,5-Dicyclohexylimidazole (DcIm) was purchased from Aldrich and recrystallized from heptane, m.p. = 113-114°C.

Carbon monoxide (99.5%) and dioxygen (99.99%) were passed through KOH columns prior to use. Argon (99.99%) was initially passed through a Redox column and then dried over molecular sieves (3 Å) and KOH.

The solubilities of CO and O_2 in toluene used were 1.0 x 10^{-5} M/torr and 1.2 x 10^{-5} M/torr respectively, at 20°C.[107]

4.1.2 Thermostatting equipment

(a) For temperatures down to 4°C

A thermostatted cell-holder (Fig. 4.1), constructed in the Chemistry Department Mechanical Shop, U.B.C., was used to maintain a constant temperature. It was

connected to a Haake (model FK) circulating thermostatting bath filled with 50% EtOH/H_2O by tygon tubing (Fig. 4.1). The circulating ethanolic solution was thermally equilibrated with the copper block of the cell-holding compartment. A tonometer (with cell path length 1 cm) could be firmly inserted into the cell-holder. Then, the solution inside the cell was equilibrated to the temperature of the surrounding copper block. The cell-holder could be fixed at the proper position of the UV/visible instrument for the recording of spectra.

(b) For low temperature: -45°C

A 6 cm path length quartz cell mounted inside a small Dewar (Fig. 4.2) was used for low temperature work. The Dewar was filled with a chlorobenzene-liquid nitrogen slush bath (-45°C).

4.1.3 Electronic absorption spectra

A Hewlett Packard 8452A Diode Array Spectrophotometer was used to record all UV/visible spectra in the range of 250-700 nm.

4.2 Solution preparation

All solution studies were performed in toluene. The major concern in choosing a suitable solvent is its ability to sustain a six-coordinate heme-O_2 adduct, during oxygen equilibria studies. Toluene, providing a relatively non-polar environment of dielectric constant 2.38, increases the stability of the oxygen adduct by reducing the rate of its autoxidation (section 1.5.1). For the purpose of consistency, toluene was also employed in the CO binding studies.

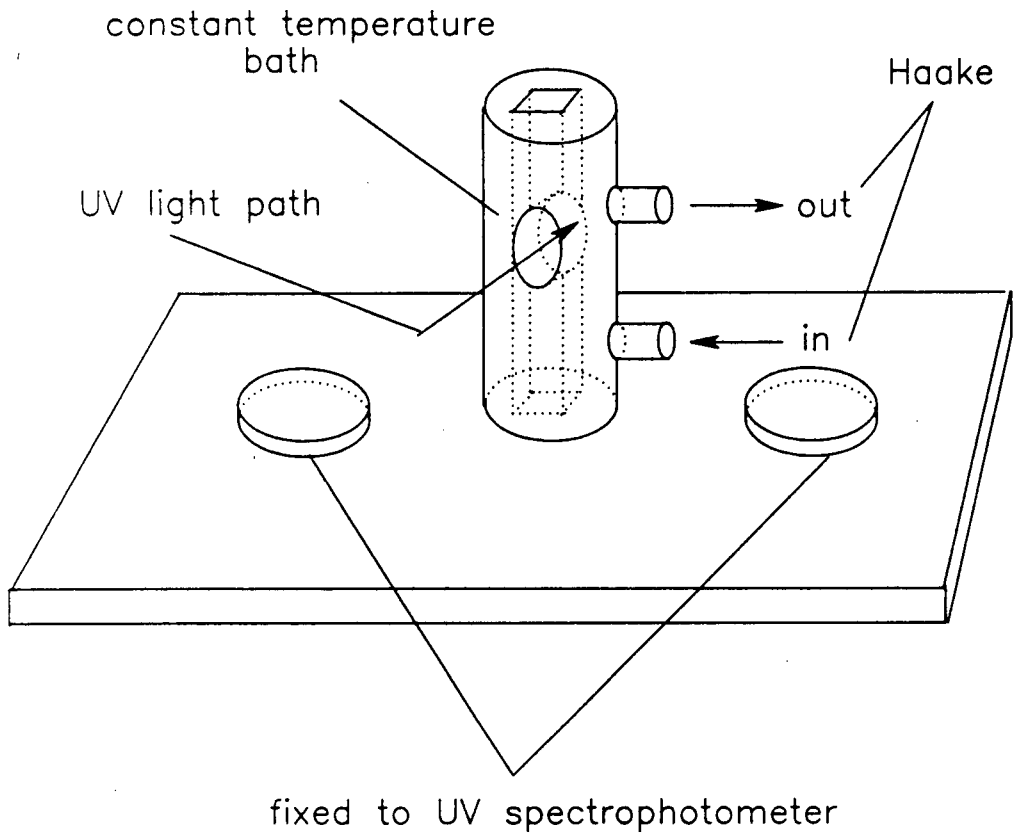

Fig. 4.1 Thermostatted cell-holder for temperatures above 4°C

Because of the tendency for Fe(II) to be oxidized to Fe(III) in the presence of trace dioxygen, preparation of the Fe(II) five-coordinate complexes and binding experiments must be carried out with complete exclusion of air. The aqueous dithionite reduction method of S. K. David,[50] was used to reduce the hemin chloride to the corresponding heme. A solution of the hemin chloride and 1,5-dicyclohexylimidazole, of required concentrations, in toluene (6 mL), was placed in flask A of a set up as shown in Fig. 4.3.A. The entire three flask system and hemin solution were deoxygenated by means of freeze-thaw cycles performed four times; Ar gas was admitted and tap 4 closed. A small volume (~0.5 mL) of freshly prepared

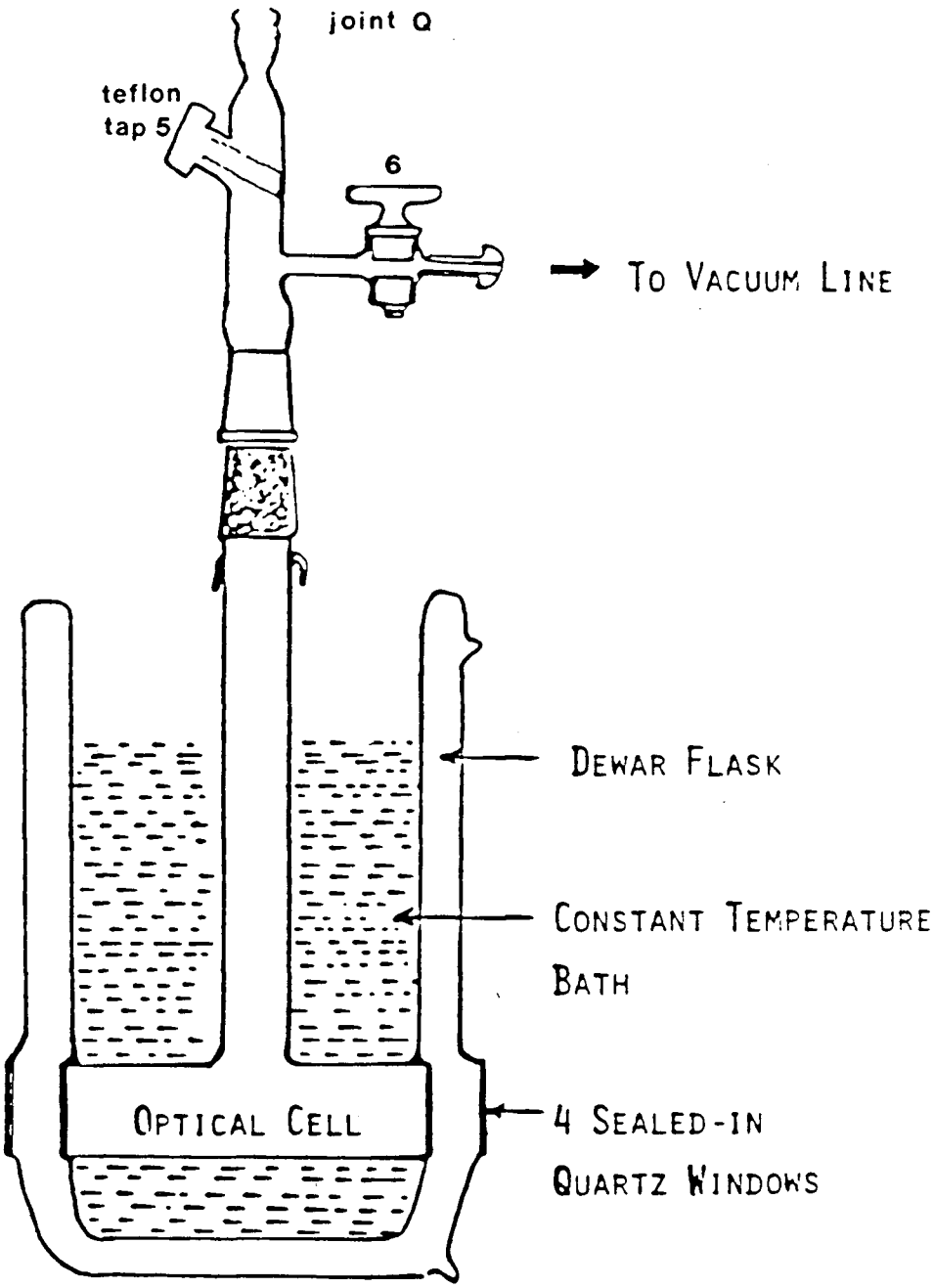

Fig. 4.2 6 cm path-length quartz cell[50(a)]

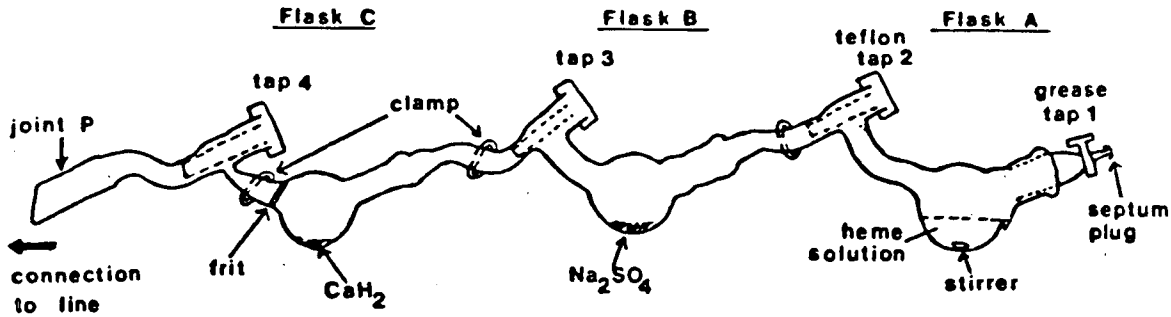

A

Fig. 4.3 (A) Apparatus used for reducing Fe^{III}(Por) to Fe^{II}(Por) using aqueous dithionite[50(a)]

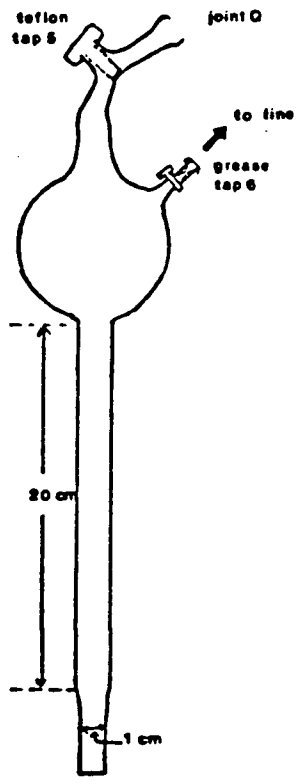

(B) Tonometer for measuring ligand binding constants of five-coordinate hemes, Fe^{II}(Por)(DcIm)[50(a)]

B

deoxygenated aqueous $Na_2S_2O_4$ (saturated) was cannulated into the hemin solution via tap 1, by means of a 2′ long double-ended needle and a stream of argon. The mixture was stirred for 30 min, during which time reduction to the five-coordinate, Fe^{II}(Por)(DcIm), complex was complete. The toluene layer was then decanted into flask B and partially dried over anhydrous Na_2SO_4 for 15 min. The solution was finally poured into flask C and dried over CaH_2 for 30 min. At this stage, tap 3 was closed and flask A disconnected for convenience.

The flask system was then connected to a tonometer (Fig. 4.3.B) by attaching joints P and Q, and the tonometer evacuated completely, keeping taps 5 and 6 open. With tap 6 closed, tap 4 was then opened and the solution allowed to filter through the frit into the tonometer. Tap 5 was closed, the flasks removed, and argon admitted through tap 6. During the titration experiment, aliquots of gaseous ligand could be introduced into the tonometer by connecting tap 6 to the vacuum line.

4.3 Mathematical analyses

The equilibrium constant for the reaction of a five-coordinate heme with a ligand as shown in eq. (4.1),

$$Fe^{II}(Por)(DcIm) + L \underset{L = CO \text{ or } O_2}{\overset{K^L}{\rightleftharpoons}} Fe^{II}(Por)(DcIm)(L) \qquad (4.1)$$

is defined by:

$$K^L = \frac{[Fe(Por)(DcIm)(L)]}{[Fe(Por)(DcIm)][L]} \qquad (4.2)$$

The equilibrium constant K^L is a measure of the affinity of the reactant, the heme

complex, towards the ligand L, and is given by the inverse of the concentration of L required to convert half of the reactant heme to the product.[108] In the experimental determination of K^L, excess imidazole blocks the unhindered side of the heme, while its binding on the capped side is inhibited for steric reasons. Therefore, the binding constant (K^L) corresponds exclusively to the coordination of L on the capped face. Eq. (4.2) may be re-written in a form such as:

$$K^L[L] = \frac{\text{fraction of product}}{\text{fraction of reactant}} = \frac{y}{1-y} \qquad (4.3)$$

If the reaction is followed spectrophotometrically, y can be determined from:

$$y = \frac{A - A_o}{A_\infty - A_o} \qquad (4.4)$$

where A_o = initial absorbance of reactant

A_∞ = final absorbance of product

and A = absorbance at a specific [L]

The logarithmic conversion of eq. (4.3) gives the Hill equation:[109]

$$\log\left(\frac{y}{1-y}\right) = \log[L] + \log K^L \qquad (4.5)$$

A plot of $\log\left(\frac{y}{1-y}\right)$ versus log[L] should result in a straight line of slope 1.0 for the

coordination of one ligand at the heme, and the equilibrium constant K^L may be determined from the x- or y- axis intercept of the log : log plot. In general, when the value of the slope is not exactly 1.0, the x-axis intercept is used to give a direct estimation of $K^L = \frac{1}{[L]}$. For the gaseous ligands CO or O_2, the ligand concentration [L] is commonly expressed in terms of partial pressure of the gas over the solution P^L. The equilibrium constant for the binding of a gas can then be written as:

$$K(torr^{-1}) = \frac{1}{P^L_{1/2}} \qquad (4.6)$$

Where $P^L_{1/2}$ = the partial pressure of gas (L) required to convert half of the five-coordinate heme into the six-coordinate ligated species.

Equilibrium constant determinations for CO binding to the benzene-4/4, and the amidobenzene-4/4 heme systems were carried out at varied temperatures. Van't Hoff plots of ln K versus 1/T(°K), eq. (4.7), afforded the thermodynamic constants ΔH° and ΔS° from the slope and y-intercept, respectively.[108]

$$\ln K = -\frac{\Delta H^\circ}{RT} + \frac{\Delta S^\circ}{R} \qquad (4.7)$$

4.4 Results

Binding studies of the durene systems have shown[50] that binding of the small 1-methylimidazole (MeIm) occurs under the large caps of the durene-7/7 and -5/5 systems. For the 7/7-heme particularly, a typical six-coordinate hemochrome,[110] was formed even with a very low [MeIm]. In the case of the 5/5-durene heme, binding under the cap was much weaker, but at the high [MeIm] required for studying CO and O_2 binding equilibria, a considerable amount of six-coordination was observed. This excluded MeIm as an axial base for the binding studies of these large capped systems. Based on the studies of the durene[50] and other systems,[111] DcIm was considered unlikely to coordinate under the large caps because of steric reasons. Therefore, the bulky DcIm was chosen as the base in the CO and O_2 binding studies for our systems.

4.4.1 Carbon monoxide binding to the five-coordinate hemes: K^{CO} values

(a) Solution preparation and the method of CO addition

The five-coordinate heme complexes Fe(Por)(DcIm) were prepared and transferred into a tonometer according to the method described in Section 4.2. The 5/5-hemes were found to bind CO too strongly to allow K^{CO} determination using pure CO ($P^{CO}_{1/2}$ ~0.03 - 0.06 torr). Even for the 4/4-hemes, $P^{CO}_{1/2}$ were several torr and accurate addition of pure CO during titration was difficult. Therefore diluted CO/Ar mixtures prepared in a glass bulb, attached to a manometer, were used for titrations (Fig. 4.4).[50] Initially a suitable amount (measured accurately) of CO was admitted into an evacuated bulb, and Ar added to barometric pressure. The total pressure in the bulb was then reduced roughly to half by evacuation (measured accurately on the manometer), and the bulb again filled with Ar. This evacuation procedure was repeated several times until a

desired partial pressure of CO remained in the bulb.

After being connected to the tonometer containing the five-coordinate heme, the system was completely degassed (taps 1 and 5 closed, taps 3 and 4 open, Fig. 4.4). The line and manometer were allowed to equilibrate to the partial pressure of toluene (tap 4 closed). Appropriate pressures of the prepared CO/Ar mixture were admitted into the tonometer from the bulb, by slowly opening and closing tap 1. The heme solution was stirred briefly and the tonometer disconnected (tap 5 closed). By this

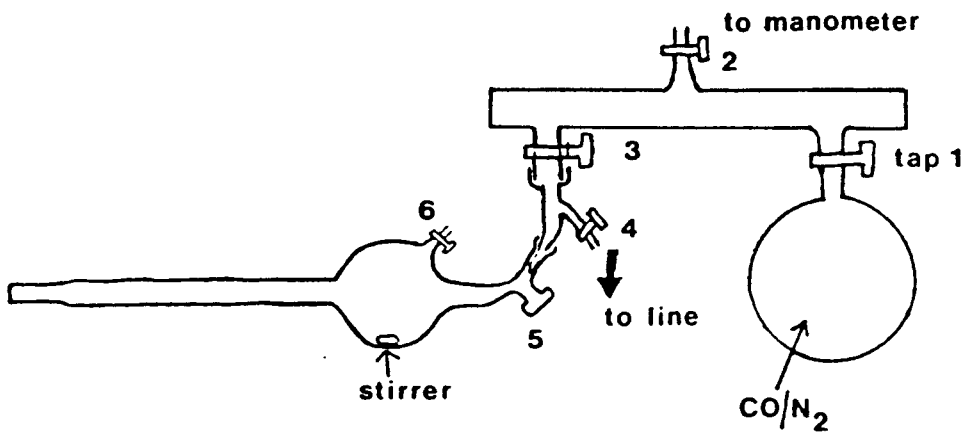

Fig. 4.4 Vacuum line set-up used for preparing and admitting CO/Ar mixtures into a tonometer[50(a)]

method, CO/Ar mixtures could be prepared in advance, allowing very low partial pressures of CO (~10^{-3} torr, within ± 10% error) to be admitted into the tonometer.

During the titration, a large excess of DcIm was maintained in solution, so that K_{DcIm}[DcIm] >> K^{CO}[CO]. Thus the equilibrium constant K^{CO} obtained for each heme corresponds exclusively to the binding of CO on the capped side of the heme, without any complication caused by the displacement of the DcIm axial base.

(b) Equilibrium constant determination, K^{CO}

The spectral properties of the four-, five- and six-coordinate Fe(benzene-4/4) systems are shown in Fig. 4.5.

All of the K^{CO} values were obtained via addition of CO/Ar mixtures to the five-coordinate hemes, according to the eq. (4.8):

$$\text{Fe(Por)(DcIm)} + \text{CO} \overset{K^{CO}}{\rightleftharpoons} \text{Fe(Por)(DcIm)(CO)} \qquad (4.8)$$

An example of the isosbestic spectral changes observed for CO binding is shown in Fig. 4.6. The extent of CO binding to the heme is dependent on the partial pressure of the gas, P^{CO}, over the toluene solution. For suitable ranges of P^{CO} (P^{CO} = 1-10^2 torr for the 4/4-pair and P^{CO} = 0.001-0.1 torr for the 5/5-pair), $\log(A-A_0)/(A_\infty-A)$ values were found to be linearly dependent on $\log P^{CO}$, with a slope ~1.0. After each addition of CO, the solution in the tonometer was shaken vigorously for 5-10 min to ensure equilibration and the tonometer then thermostatted to 20°C for a further 10 min. The volume ratio of solution : tonometer was small (3 : 300 mL), so that changes in P^{CO} with dissolution in the toluene phase were considered negligible. In all cases, the data were analyzed according to the Hill equation[109] (Appendix IIA). The K^{CO} values together with those of the durene series and open chelated systems are quoted in Table 4.1. A detailed analysis for the Fe(benzene-4/4)(DcIm)(CO) system, corresponding to the spectral changes shown in Fig. 4.6 is given in Appendix IIA(1) and the Hill plot is shown in Fig. 4.7.

(c) Temperature variation equilibria: ΔH^{o}_{CO}, ΔS^{o}_{CO} values

For the Fe(benzene-4/4)(DcIm) and Fe(amidobenzene-4/4)(DcIm) systems, K^{CO} values were measured at different temperatures within the range 0-30°C (Appendix IIB).

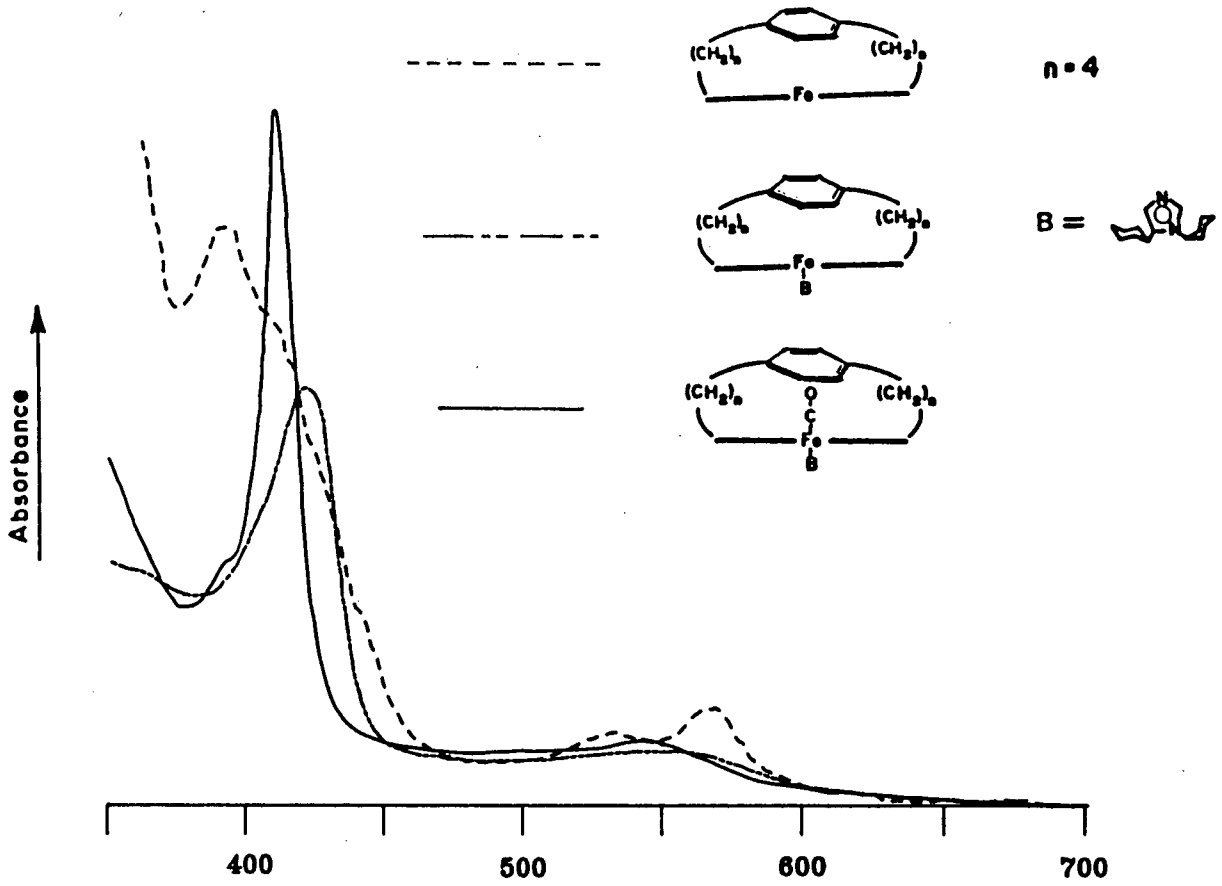

Fig. 4.5 Spectral trends for Fe^{II}(benzene-4/4), Fe^{II}(benzene-4/4)(DcIm) and Fe^{II}(benzene-4/4)(DcIm)(CO) systems in toluene

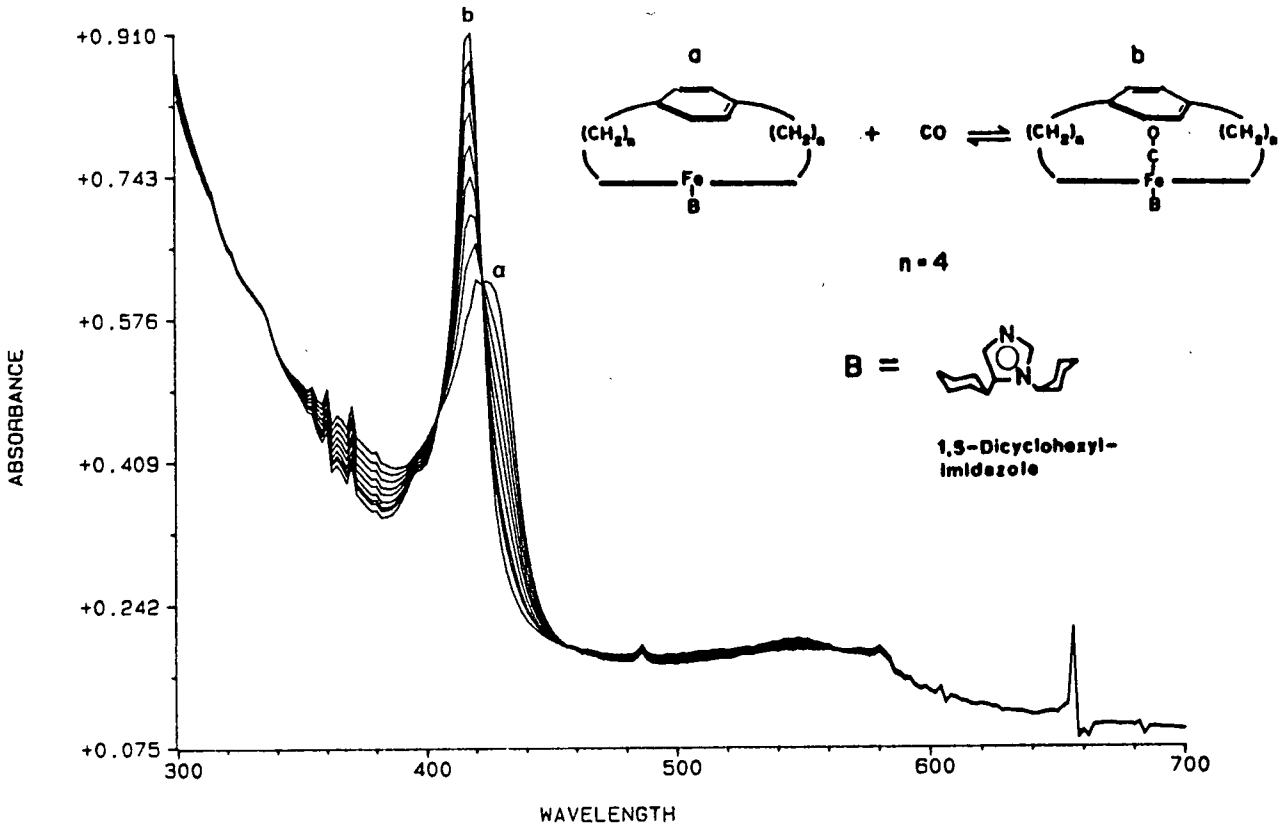

Fig. 4.6 Isosbestic spectral changes for:
Fe^{II}(Por)(DcIm) + CO $\rightleftharpoons$ Fe^{II}(Por)(DcIm)(CO) at 20°C in toluene
Por = the benzene-4/4 porphyrin **49a**; added P^{CO} = 1.99, 4.30, 7.55, 11.60, 19.03, 34.64 and 51.87 torr in the 300 - 700 nm range; final P^{CO} = 1 atm

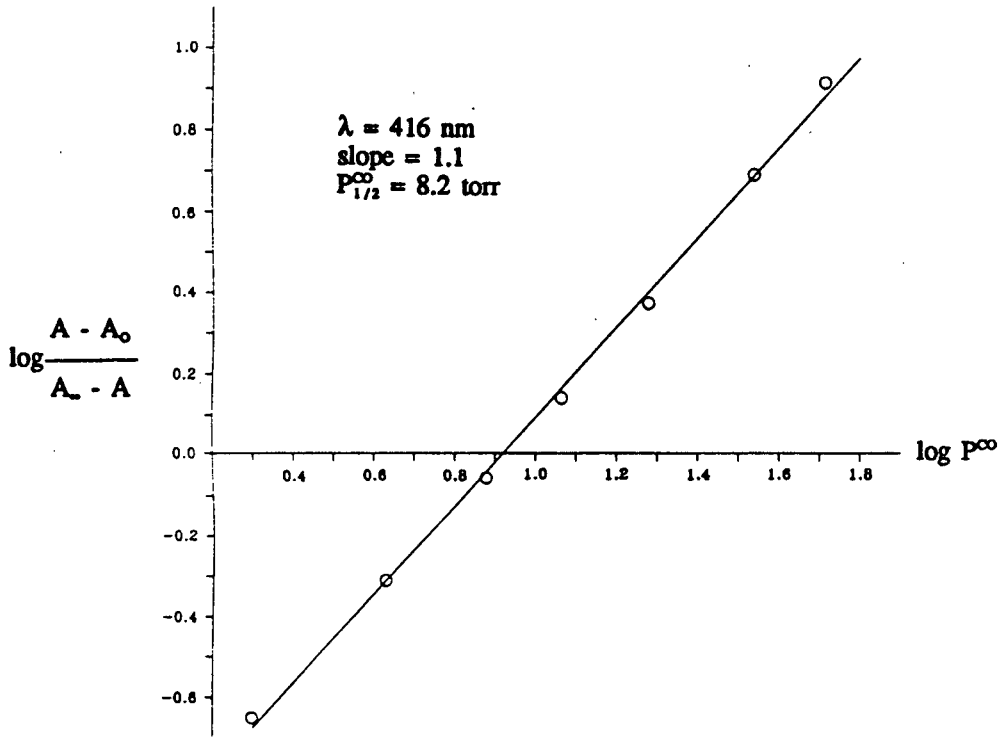

Fig. 4.7 Hill plot for Fe^{II}(benzene-4/4)(DcIm) + CO $\rightleftharpoons$ Fe^{II}(benzene-4/4)(DcIm)(CO) at 20°C

Van't Hoff plots of ln K^{CO} vs. 1/T(°K), shown in Figs. 4.8 and 4.9, provided the thermodynamic constants, ΔH^{o}_{co} and ΔS^{o}_{co} (see Appendix IIC and Table 4.3, p.184).

4.4.2 Dioxygen binding to the five-coordinate hemes, K^{O2}

(a) Ambient temperature

The five-coordinate heme Fe(II)(Por)(DcIm) solution in toluene (6 mL) was prepared and transferred into a tonometer (Fig. 4.3.B) by the method described in Section 4.2. In order to ensure no moisture remained, a small volume of toluene

Table 4.1 Equilibrium constants for CO binding to the capped hemes compared to those for chelated open hemes in toluene at 20°C

Heme	K^{CO} (M^{-1})	Heme	K^{CO} (M^{-1})
chelated protoheme[a]	4×10^8	benzene-4/4(DcIm) (**50a**)(DcIm)[c]	1.2×10^4
chelated mesoheme[a]	2×10^8	benzene-5/5(DcIm) (**50b**)(DcIm)[c]	1.6×10^6
durene-7/7(DcIm) (**13b**)(DcIm)[b]	6.6×10^7	amidobenzene-4/4(DcIm) (**50c**)(DcIm)[c]	2.8×10^4
durene-5/5(DcIm) (**12b**)(DcIm)[b]	8.6×10^7	amidobenzene-5/5(DcIm) (**50d**)(DcIm)[c]	3.3×10^6
durene-4/4(DcIm) (**11b**)(DcIm)[b]	4.3×10^6		

a Ref. 112; Solvent toluene-CH_2Cl_2 (90 : 10)
b Ref. 50
c Errors $\leq \pm 5\%$

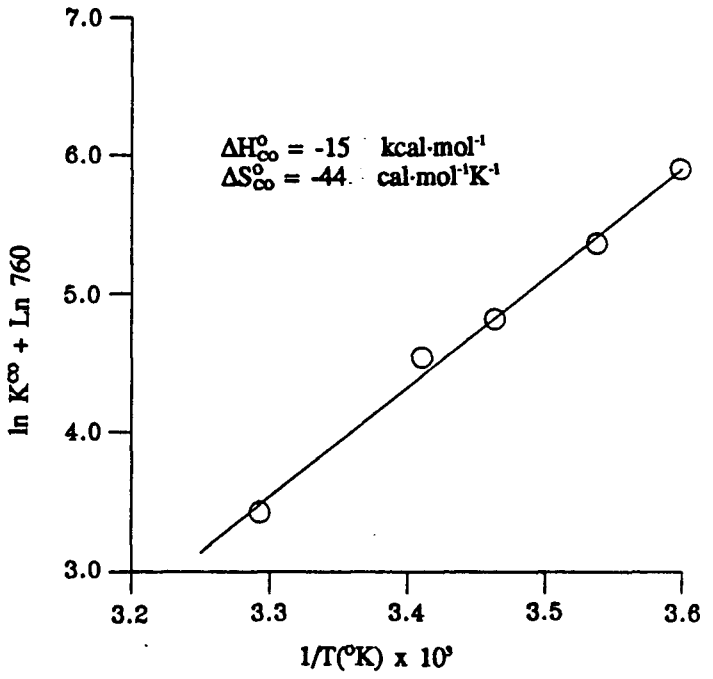

Fig. 4.8 Van't Hoff plot for:
Fe^{II}(benzene-4/4)(DcIm) + CO $\rightleftharpoons$ Fe^{II}(benzene-4/4)(DcIm)(CO)

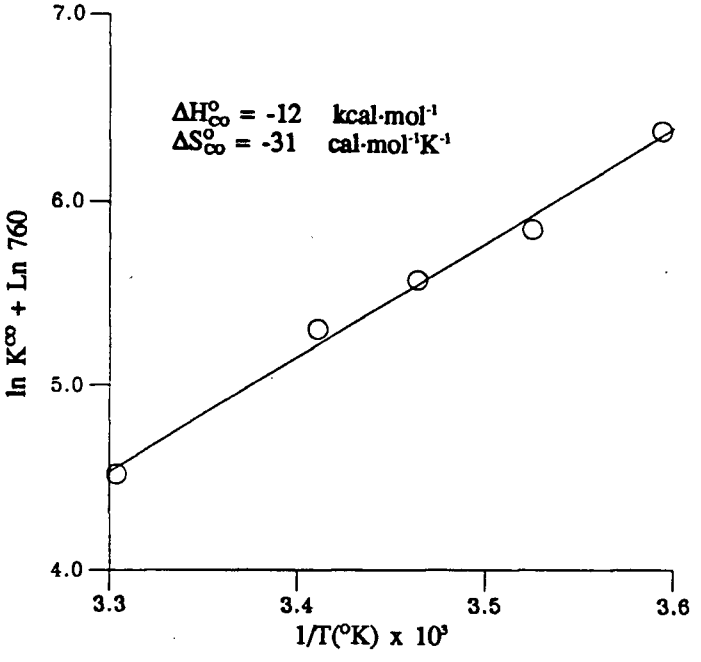

Fig. 4.9 Van't Hoff plot for:
Fe^{II}(amidobenzene-4/4)(DcIm) + CO $\rightleftharpoons$ Fe^{II}(amidobenzene-4/4)(DcIm)(CO)

(~1 mL) was pumped off, while the solution was stirred inside the tonometer. Pure dioxygen was admitted into the tonometer by the procedure outlined in Section 4.2. The UV/visible spectrum was taken immediately. For all of the four hemes, the oxidation of the five-coordinate species was instantaneous and the UV/visible spectrum showed that μ-oxo dimer had been formed (Fig. 4.10). Therefore, the studies had to be carried out at lower temperature.

(b) Low temperature equilibria: K^{O2} values

Several temperatures were examined and -45°C was found suitable. A solution of the five-coordinate heme Fe(II)(Por)(DcIm) in toluene (17 mL) was prepared as described in Section 4.2 and transferred into the cell mounted inside a Dewar (Fig. 4.2). During the transfer, the flask system in Fig. 4.3.A was attached to the cell by connecting joints P and Q, and the system evacuated with taps 5 and 6 open (tap 4 closed). With tap 6 then closed and tap 4 opened, the solution was allowed to flow into the cell. Finally, taps 5 and 6 were closed off and the flasks disconnected. The Dewar flask was filled with a slush bath of chlorobenzene-liquid nitrogen, and the solution degased completely by opening tap 6.

Dioxygen was admitted into the cell via a flexible stainless steel tube attached to joint Q and the vacuum line. The volume of the solution was maintained well below the narrow neck of the cell, in order to agitate the solution sufficiently by shaking the cell (5 min), to effect equilibration of O_2 between the solution and gas phases. The Dewar was then disconnected from the vacuum line (taps 5 and 6 closed), taken to the UV/visible instrument and the spectral changes recorded. Prolonged exposure to O_2 should be avoided in order to minimize oxidation of the hemes by O_2; therefore, the spectral changes for only four titrations were measured. A large excess of DcIm had to

be maintained, ([DcIm] : [heme]~10^4:1), in all cases to effectively thwart irreversible oxidation to the μ-oxo dimer.

Spectra of the μ-oxo dimer, five-coordinate and O_2-adduct for the Fe(benzene-5/5) system are shown in Fig. 4.10. O_2 titration for all of the five-coordinate hemes gave absorbance changes with clean isosbestic points, indicating a clean conversion to the oxy-species according to the equation:

$$\text{Fe(Por)(DcIm)} + O_2 \overset{K^{O2}}{\rightleftharpoons} \text{Fe(Por)(DcIm)}(O_2) \qquad (4.9)$$

Deoxygenation, by pumping, after full formation of the O_2-complex regenerated the five-coordinate heme with negligible heme oxidation. The data were analyzed according to the Hill equation[109] (Appendix IID). An example of the isosbestic spectral changes for O_2 binding is shown in Fig. 4.11 and a typical plot of log $(A-A_o)/(A_\infty-A)$ versus P^{O2} in Fig. 4.12. The affinity constants for O_2 binding to our systems together with those for the durene systems are quoted in Table 4.2.

4.5 Discussion

The five-coordinate high spin Fe(II) system is characterized by a broad absorption in both the visible and Soret region.[110] Coordination of CO as the sixth ligand gives rise to a sharp Soret band (Fig. 4.5), whereas the Soret band of the O_2-adduct has almost the same shape as that of the five-coordinate species (Fig. 4.10).

4.5.1 Carbon monoxide binding: K^{CO}

The data in Table 4.1 show that there has been a remarkable reduction of CO affinities with our systems compared to the "open" chelated meso- and proto-heme

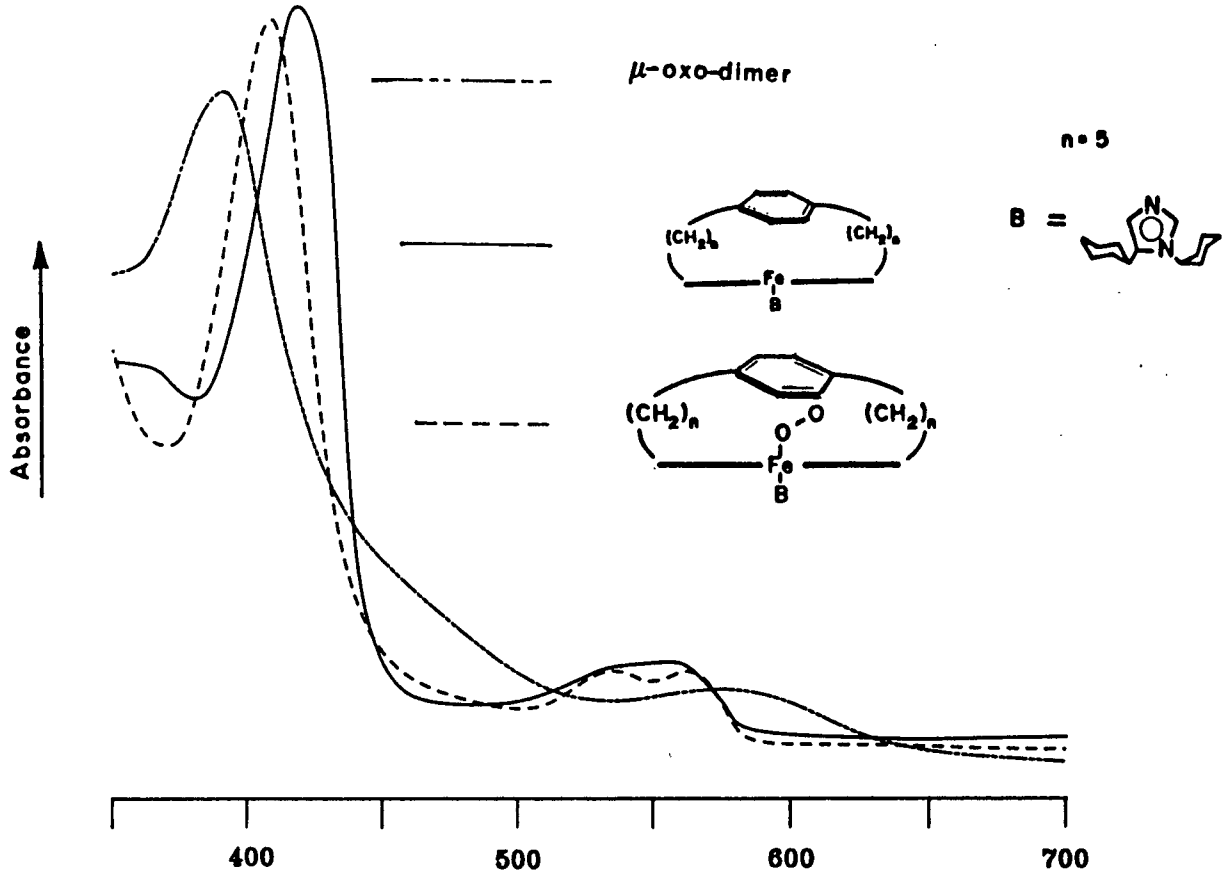

Fig. 4.10 Spectral trends for Fe^{II}(benzene-5/5)(DcIm), Fe^{II}(benzene-5/5)(DcIm)(O_2) and μ-oxo-dimer of the Fe^{II}(benzene-5/5)(DcIm) systems in toluene

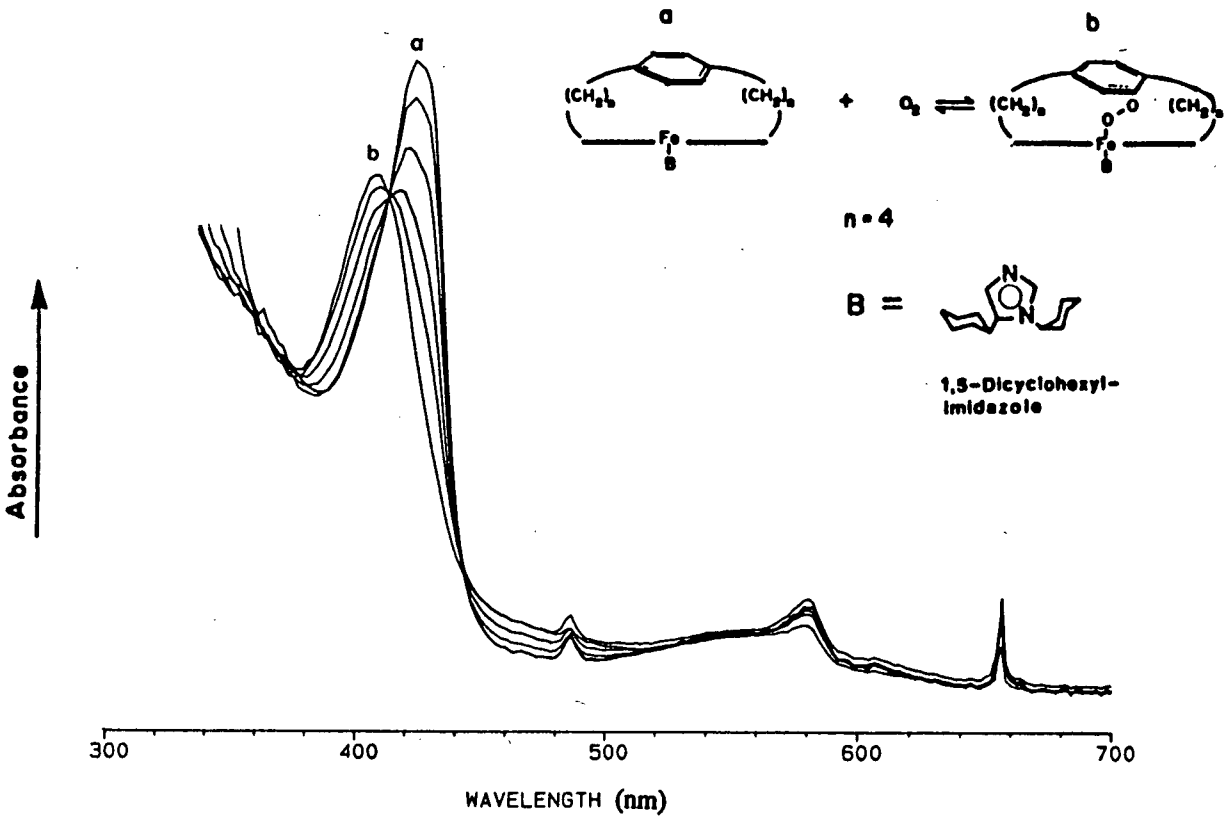

Fig. 4.11 Isosbestic spectral changes for:
$Fe^{II}(Por)(DcIm) + O_2 \rightleftharpoons Fe^{II}(Por)(DcIm)(O_2)$ at -45°C in toluene
Por = the benzene-4/4 porphyrin **49a**; added P^{O2} = 9.76, 30.95, 77.16 and 163.69 torr in the 300 - 700 nm range; final P^{O2} = 1 atm

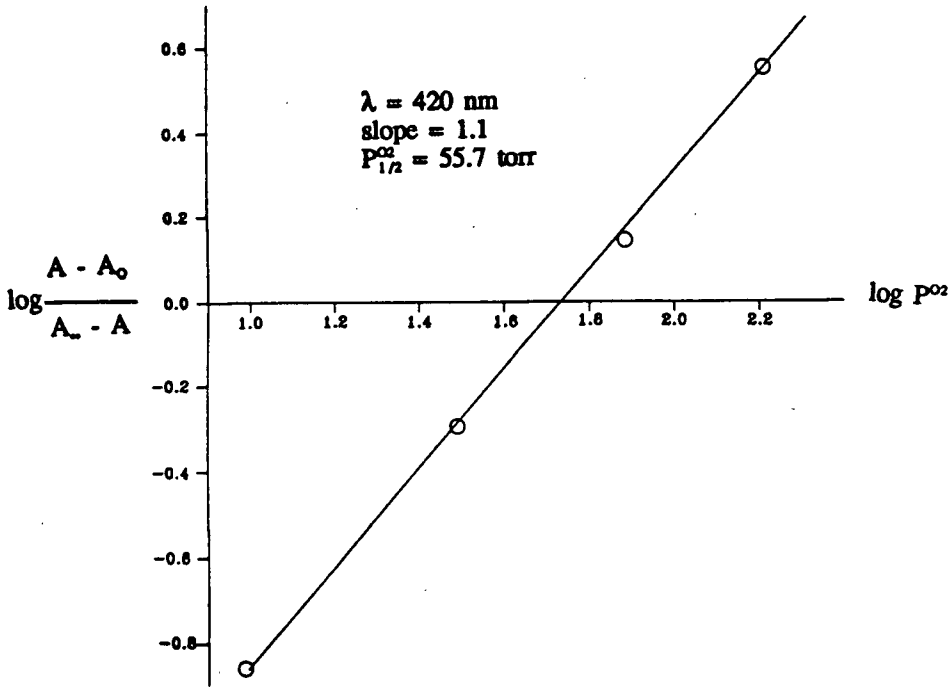

Fig. 4.12 Hill plot for Fe^{II}(benzene-4/4)(DcIm) + $O_2 \rightleftharpoons$ Fe^{II}(benzene-4/4)(DcIm)(O_2) at -45°C

systems and the corresponding durene series (**11b, 12b, 13b**). The 5/5- capped complexes exhibit a 100-fold reduction in CO affinities and the 4/4- capped complexes a 10^4-fold reduction compared to those of the "open" chelated hemes. The CO-complexes of the 4/4-series are so unstable that the 5-coordinate species can be regenerated by pumping. Compared to the durene series, the reduction in CO affinity is still as large as 50- and 350-fold for the 5/5 and 4/4 systems, respectively. The results were unexpected because the caps of the durene systems should be more crowded and access to the central metal should be hindered. However, placement of a more rigid diagonal strap (*ie.* the durene moiety), relative to the benzene and amidobenzene analogues, presumably induces doming of the porphyrin skeleton and

Table 4.2 $P_{1/2}$ values for dioxygen binding to the capped hemes in toluene

Heme	$P_{1/2}$ (20°C, torr)	$P_{1/2}$ (-45°C, torr)
Fe(durene-7/7)(DcIm) (**13b**)(DcIm)[a]	~64	
Fe(durene-5/5)(DcIm) (**12b**)(DcIm)[a]	~64	
Fe(durene-4/4)(DcIm) (**11b**)(DcIm)[a]	167	0.094[b]
Fe(durene-4/4)(MeIm) (**11b**)(MeIm)[a]	82.6	
Fe(benzene-5/5)(DcIm) (**50b**)(DcIm)		22.7
Fe(benzene-4/4)(DcIm) (**50a**)(DcIm)		55.7
Fe(amidobenzene-5/5) (**50d**)(DcIm)		2.8
Fe(amidobenzene-4/4) (**50c**)(DcIm)		9.5

a Ref. 50
b Extrapolated from thermodynamic data

resulting in a greater accessibility for an incoming ligand to the Fe(II) atom (Fig. 4.13.A). This would effectively result in an enhanced K^{CO}. On the other hand, the benzene and the amidobenzene moieties are more flexible and may prefer a "squashed"

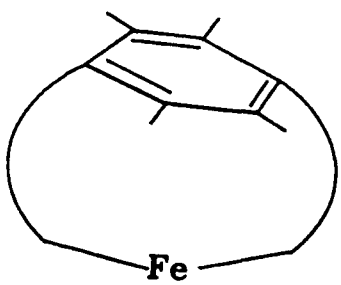

A

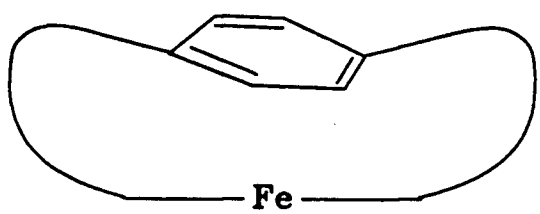

B

Fig. 4.13 (A) "Basket-shaped" conformation of the distorted durene-5/5 and -4/4 systems; (B) "Squashed" conformation of the benzene-5/5 system

cap conformation in which the rotating benzene moiety is suspended close to the center of the porphyrin plane (Fig. 4.13.B). Ligand coordination to the sixth position would then be retarded by the benzene moiety. A similar explanation has been proposed for the durene-7/7 complex's low CO association rate relative to those of the smaller 4/4- and 5/5-durene complexes.[50]

Within our systems, each 5/5- complex has ~100-fold higher CO affinity than that of the corresponding 4/4-complex. This is easily explained by the increased distortion of the porphyrin skeleton and a more crowded distal side (Section 1.2.2) of the 4/4-complexes. The shorter strap over the distal side of the 4/4-hemes should block access to the sixth position and the more distorted porphyrin plane would result in a more "T-state" character, therefore, CO affinity should be lower. Compared to the analogues without amide substitution, the amide groups in the amidobenzene hemes probably fix the distal moiety in a manner similar to the durene system (Fig. 4.13.A), creating a greater accessibility for an incoming ligand to the Fe atom, and therefore an increased CO affinity (~2-fold) results.

4.5.2 Thermodynamic considerations for CO-binding

Table 4.3 shows the thermodynamic data for CO binding of the benzene- and the amidobenzene-4/4 hemes together with data for the durene series. It is obvious that the relative decrease in CO affinity in our system results from the contribution of the more unfavorable entropy change. The large entropy loss suggests more rigidity of the CO complexes of the 4/4-benzene and amidobenzene hemes relative to those of the durene systems. After formation of the CO-complex, perhaps the previously flexible benzene moiety might become fixed. The relatively large overall loss of translational entropy (more negative ΔS°) between reacting species for binding of CO therefore can be

rationalized for our systems.

Table 4.3 Thermodynamic constants for CO binding[a]

Heme	ΔH^{o}_{co} (kcal·mol^{-1})	ΔS^{o}_{co} (cal·mol^{-1}K^{-1})[b]
chelated protoheme[c]	-17.5	-34
Fe(PocPiv)(1,2-Me_2Im)[d]	-13.9	-28
Fe(TPP)(1,2-Me_2Im)[d]	-12.8	-26.1
Fe(durene-4/4)(DcIm) (**11b**)(DcIm)[e]	-9	-12
Fe(durene-4/4)(1,2-Me_2Im) (**11b**)(1,2-Me_2Im)[e]	-14	-32
Fe(benzene-4/4)(DcIm) (**50a**)(DcIm)	-16	-44
Fe(amidobenzene-4/4)(DcIm) (**50c**)(DcIm)	-12	-32

a solvent system is toluene for all model systems with the exception of chelated protoheme.
b standard state 1 atm
c Ref. 113; aqueous suspension, pH 7
d Ref. 114
e Ref. 50

4.5.3 Dioxygen binding

The benzene and amidobenzene capped hemes cannot bind dioxygen reversibly at room temperature. The oxidation of the five-coordinate hemes in the presence of O_2 is instantaneous. This might result from a more flexible cap being able to swing to one side thus allowing for μ-oxo dimer formation. At -45°C, however, the oxidation can be prevented successfully and reversible O_2 binding achieved. The Fe(II) five-coordinate species could be regenerated by pumping on solutions of the O_2-complex. Table 4.2 shows the strikingly high $P_{1/2}$ values for our system at low temperature (-45°C). But,

within each pair of the benzene- and amidobenzene-hemes, a 6-8 fold increase in O_2 affinity is observed for the amide substituted complexes (a free energy gain of 949 cal/mol for the amidobenzene-4/4 heme and 802 cal/mol for the amidobenzene-5/5 heme, relative to their corresponding nonamido-hemes), suggesting a possible hydrogen bonding stabilization of the O_2-complex.

In the durene heme series, a hydrophobic "cap" provides a relatively non-polar distal environment, so that (lack of) polarity effects experienced by the bound dioxygen should be identical for all the three durene hemes. Any difference in O_2 affinities, should therefore, be caused by steric effects alone. Examination of the durene heme systems reveals that at 20°C the K^{O_2} values of the Fe(durene-7/7)(DcIm) and Fe(durene-5/5)(DcIm) systems are identical and the difference of K^{O_2} values between the Fe(durene-5/5)(DcIm) and Fe(durene-4/4)(DcIm) is only 2-fold,[50] indicating very small steric effects on O_2 binding in spite of the different cap sizes.

In the benzene- and amidobenzene-heme systems at -45°C, there is a very small (2- to 3-fold) increase in O_2 affinity for the 5/5- capped hemes relative to the 4/4-capped hemes. This is consistent with the trend found in the durene series. Perhaps the reduced accessibility to the sixth coordination site due to the smaller cap and the distortion (doming) of the 4/4-hemes could account for this decreased K^{O_2}. Porphyrin skeletal doming of this type may be viewed as imparting considerable "T-state" character on the five-coordinate heme complex and therefore leading to the low O_2 affinity.

As the CO binding affinities of the corresponding benzene- and amidobenzene-heme complexes are different (~2 fold increase for the amide-substituted analogues), the possible influence of this steric effect (Fig. 13.A) can be excluded as the only source for the higher O_2 affinity of the amide substituted analogues. The O_2 affinity

enhancement in the amide analogues is 6-8 fold, too large to be accounted for by the steric effect. Therefore, either the polarity of the distal cage or a direct interaction of the amide proton with bound dioxygen contributes partly to this increased O_2 affinity for the amidobenzene-hemes.

Within each pair of the benzene and amidobenzene hemes, the only difference in structure is the amide functionality. The partial double bond character of the bond between the carbonyl carbon and the nitrogen of an amide due to the resonance structures makes the nitrogen more electropositive. Therefore, the N-H of the amide is capable of forming a strong hydrogen-bonding with bound dioxygen. This electronic effect (or electrostatic effect as often cited in literature) would greatly influence the O_2-complex stability. In the free-base amide substituted porphyrin, the N-H of the amide group has been shifted upfield in the nmr spectrum compared to normal aromatic amide protons. It indicates that the H is situated near the center of the porphyrin plane, suggesting that a direct interaction of amide-H with bound O_2 (H-bonding) is likely in the heme.

Compared to the basket handle models **7** of Momenteau *et al.*[60] (Table 1.4, p. 26) and Chang's porphyrin naphthoic acid series **6**[58] (Table 1.3, p. 25), the O_2 stability gain (6-8 fold) of the amidobenzene-hemes due to an amide group is not so large. The basket handle model has a 10-fold increased O_2 affinity and the porphyrin naphthoic acid series has even larger increased O_2 affinity. The smaller O_2 affinity increase of our systems can be explained perhaps in terms of H-bonding strength. The strength of a hydrogen bond is largely dependent on steric constraints. For an effective hydrogen bonding to take place, it is essential to minimize the distance and the freedom of motion between the proton source and the acceptor. Only when a close encounter of the H source and the acceptor is realized, and both elements point towards each other,

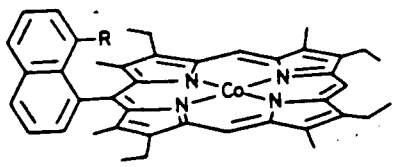

6a R=H

6b R=CO_2H

6c R=$CONH_2$

6d R=CH_2OH

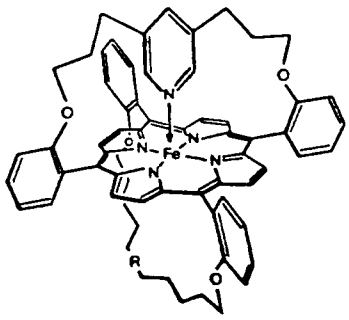

7a R=$(CH_2)_{12}$

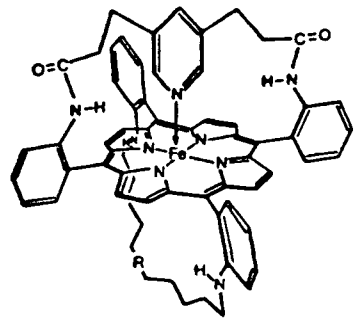

7b R=$CO(CH_2)_{10}CO$

can a strong H-bonding result. Various conformational characteristics of each "cap" can influence the direction in which a polar amide function points within the distal cavity. In our systems, space-filling (CPK) models indicate a close encounter of the two groups, but the N-H···O is not in a linear array. The close encounter demonstrates the possibility of H-bonding, but the steric pattern of the N-H···O suggests a relatively weak H-bonding and a relatively small enhancement of O_2 affinity in the system. Confirmation of this explanation awaits a crystal structure determination.

In conclusion, introduction of an amide functionality to the distal side of the heme increases the O_2 affinity due to the possible hydrogen bonding between the polar amide function and the bound dioxygen. The benzene- and amidobenzene-hemes, therefore, give quantitative support for the hypothesis that hydrogen bonding plays an important role in differential binding of CO and O_2 by hemoglobin and myoglobin.

References

1. (a) J. L. Hoard, in Porphyrins and Metalloporphyrins, K. M. Smith, Ed., American Elsevier, New York, N. Y., 1975, p. 317.

   (b) R. Bonnett, in The Porphyrins, Vol. I, D. Dolphin, Ed., Academic Press, 1978, p. 1.

2. A. L. Lehninger, Biochemistry, 3rd Ed., Worth Publishers Inc., New York, N.Y., 1975, p. 489.

3. T. P. Wijesekera, J. B. Paine III, D. Dolphin, F. W. B. Einstein & T. Jones, J. Am. Chem. Soc., 105, 6747 (1983).

4. W. R. Scheidt & C. A. Reed, Chem. Rev., 81, 543 (1981).

5. (a) M. F. Perutz, Nature, 228, 726 (1970).

   (b) M. F. Perutz, Br. Med. Bull., 32, 195 (1976).

   (c) M. F. Perutz, Scientific Am., 239 (6), 92 (1978).

6. M. F. Perutz, Ann. Rev. Biochem., 48, 327 (1979).

7. J. M. Baldwin, Br. Med. Bull., 32, 213 (1976).

8. J. V. Kilmartin, Br. Med. Bull., 32, 209 (1976).

9. J. V. Kilmartin, FEBS Lett., 38, 147 (1974).

10. J. C. Kendrew, R. E. Dickerson, B. E. Standberg, R. G. Hart, D. R. Davis, D. C. Phillips & V. C. Shore, Nature, 185, 422 (1960).

11. J. Baldwin & C. Chothia, J. Mol. Biol., 129, 175 (1979).

12. G. Fermi, M. F. Perutz, B. Shaanan & R. Fourme, J. Mol. Biol., 175, 159 (1984).

13. (a) B. R. Gelin & M. Karplus, Proc. Natl. Acad. Sci. USA, 74, 801 (1977).

    (b) B. R. Gelin, A. W.-M. Lee & M. Karplus, J. Mol. Biol., 171, 489 (1983).

14. A. Brzozowski, Z. Derewenda, E. Dodson, G. Dodson, M. Grabowski, R. Liddington, T. Skarzynski & D. Vallely, Nature, 307, 74 (1984).

15. R. Liddington, Z. Derewenda, G. Dodson & D. Harris, Nature, 331, 725 (1988).

16. B. Shaanan, J. Mol. Biol., 171, 31 (1983).

17. L. Pauling, Nature, 203, 182 (1964).

18. (a) C. H. Barlow, J. C. Maxwell, W. J. Wallace & W. S. Caughey, Biochem. Biophys. Res. Commun., 55, 91 (1973).

(b) J. C. Maxwell, J. A. Volpe, C. H. Barlow & W. S. Caughey, Biochem. Biophys. Res. Commun., 58, 166 (1974).

19. M. Tsubaki & N.-T. Yu, Proc. Natl. Acad. Sci. USA, 78, 3581 (1981).

20. M. P. Mims, A. G. Porras, J. S. Olson, R. W. Noble & J. A. Peterson, J. Biol. Chem., 258, 14219 (1983).

21. T. Yonetani, H. Yamamoto & T. Iizuka, J. Biol. Chem., 249, 2168 (1974).

22. F. A. Walker & J. Bowen, J. Am. Chem. Soc., 107, 7632 (1985).

23. M. Ikeda-Saito, T. Iizuka, H. Yamamoto, F. J. Kayne & T. Yonetani, J. Biol. Chem., 252, 4882 (1977).

24. S. E. V. Phillips & B. P. Schoenborn, Nature, 292, 81 (1981).

25. B. Shaanan, Nature, 296, 683 (1982).

26. J. M. Baldwin, J. Mol. Biol., 136, 103 (1980).

27. J. S. Olson, A. J. Mathews, R. J. Rohlfs, B. A. Springer, K. D. Egeberg, S. G. Sligar, J. Tame, J.-P. Renaud & K. Nagai, Nature, 336, 265 (1988).

28. Z. Derewenda, G. Dodson, P. Emsley, D. Harris, K. Nagai, M. F. Perutz & J. -P. Renaud, J. Mol. Biol., 211, 515 (1990).

29. K. Kim, J. Fettinger, J. L. Sessler, M. Cyr, J. Hugdahl, J. P. Collman & J. A. Ibers, J. Am. Chem. Soc., 111, 403 (1989).

30. B. A. Springer, K. D. Egeberg, S. G. Sligar, R. J. Rohlfs, A. J. Mathews, T. E. Carver & J. S. Olson, J. Biol. Chem., 265, 3168 (1990).

31. M. F. Perutz, Quarterly Reviews of Biophysics, 22, 139 (1989).

32. L. Pauling & C. D. Coryell, Proc. Natl. Acad. Sci. USA, 22, 210 (1936).

33. J. J. Weiss, Nature, 202, 83 (1964).

34. (a) H. P. Misra & I. Fridovich, J. Biol. Chem., 247, 6960 (1972).

(b) L. S. Demma & J. M. Salhany, J. Biol. Chem., 252, 1226 (1977).

35. A. S. Koster, J. Chem. Phys, 63, 3284 (1975).

36. (a) W. A. Goddard & B. D. Olafson, Proc. Natl. Acad. Sci. USA, 72, 2335 (1975).

(b) C. A. Reed & S. K. Cheung, Proc. Natl. Acad. Sci. USA, 74, 1780 (1977).

37. I. P. Gerothanassis & M. Momenteau, J. Am. Chem. Soc., 109, 6944 (1987).

38. I. J. Solomon, J. N. Keith, A. J. Kacmarek & J. K. Raney, J. Am. Chem. Soc., 90, 5408 (1968).

39. S. E. V. Phillips, J. Mol. Biol., 142, 531 (1980).

40. F. A. Cotton & G. Wilkinson, Advanced Inorganic Chemistry, 4th Ed., Wiley, New York, N. Y., 1980, p. 82.

41. S.-M. Peng & J. A. Ibers, J. Am. Chem. Soc., 98, 8032 (1976).

42. J. Kuriyan, S. Wilz, M. Karplus & G. A. Petsko, J. Mol. Biol., 192, 133 (1986).

43. (a) E. A. Padlan & W. E. Love, J. Biol. Chem., 249, 4067 (1974).

(b) J. C. Norvell, A. C. Nunes & B. P. Schoenborn, Science, 190, 568 (1975).

(c) E. J. Heidner, R. C. Ladner & M. F. Perutz, J. Mol. Biol., 104, 707 (1976).

44. T. Asakura, P. W. Lau, M. Sono, K. Adachi, J. J. Smith & J. A. McGray, in Hemoglobin and Oxygen Binding, Chien Ho, Ed., Elsevier, New York, N. Y., 1982, p. 177.

45. (a) R. H. Austin, K. W. Beeson, L. Eisenstein, H. Frauenfelder & I. C. Gunsalus, Biochemistry, 14, 5355 (1975).

(b) N. Alberding, S. S. Chan, L. Eisenstein, H. Frauenfelder, D. Good, I. C. Gunsalus, T. M. Nordlund, M. F. Perutz, A. H. Reynolds & L. B. Sorensen, Biochemistry, 17, 43 (1978).

(c) D. A. Case & M. Karplus, J. Mol. Biol., 132, 343 (1979).

46. R. D. Jones, D. A. Summerville & F. Basolo, Chem. Rev., 79, 139 (1979).

47. (a) N. Sadasivan, H. I. Eberspaecher, W. H. Fuchsman & W. S. Caughey, Biochem., 8, 534 (1969).

(b) A. L. Balch, Y.-W. Chan, R.-J. Cheng, G. N. La Mar, L. Latos-Grazynski & M. W. Renner, J. Am. Chem. Soc., 106, 7779 (1984).

48. (a) W. J. Wallace, J. C. Maxwell & W. S. Caughey, Biochem. Biophys. Res. Commun., 57, 1104 (1974).

(b) W. J. Wallace, R. A. Houtchens, J. C. Maxwell & W. S. Caughey, J. Biol. Chem., 257, 4966 (1982).

49. I. P. Gerothanassis, M. Momenteau & B. Loock, J. Am. Chem. Soc., 111, 7006 (1989).

50. (a) S. K. David, Ph. D Thesis, University of British Columbia, 1985.

(b) S. K. David, B. R. James & D. Dolphin, J. Inorg. Biochem., 28, 125 (1986).

(c) S. K. David, D. Dolphin & B. R. James, Front. Bioinorg. Chem., A. V. Xavier, Ed., VCH: Weinheim, Fed. Rep. Ger., 1986.

51. R. S. Drago, J. P. Cannady & K. A. Leslie, J. Am. Chem. Soc., 102, 6014 (1980).

52. (a) J. P. Collman, R. R. Gagne, T. R. Halbert, J.-C. Marchon & C. A. Reed, J. Am. Chem. Soc., 95, 7868 (1973).

(b) J. P. Collman, R. R. Gagne, C. A. Reed, T. R. Halbert, G. Lang & W. T. Robinson, J. Am. Chem. Soc., 97, 1427 (1975).

53. G. B. Jameson, G. A. Rodley, W. T. Robinson, R. R. Gagne, C. A. Reed & J. P. Collman, Inorg. Chem., 17, 850 (1978).

54. G. B. Jameson & R. S. Drago, J. Am. Chem. Soc., 107, 3017 (1985).

55. L. Leiserowitz & G. M. J. Schmidt, J. Chem. Soc. A, 2372 (1969).

56. L. Leiserowitz & A. C. Tuval, Acta. Crystallogr. Sect. B34, 1230 (1978).

57. C. K. Chang, B. Ward, R. Young & M. Kondylis, J. Macromol. Sci.-Chem., A25, 1307 (1988).

58. C. K. Chang & M. P. Kondylis, J. Chem. Soc., Chem. Commun., 316 (1986).

59. E. N. Guryanova, I. P. Goldshtein & T. I. Perepelkova, Russ. Chem. Rev., 45, 792 (1976).

60. (a) M. Momenteau & D. Lavalette, J. Chem. Soc., Chem. Commun., 341 (1982).

(b) D. Lavalette, C. Tetreau, J. Mispelter, M. Momenteau & J.-M. Lhoste, Eur. J. Biochem., 145, 555 (1984).

61. J. Mispelter, M. Momenteau, D. Lavalette & J.-M. Lhoste, J. Am. Chem. Soc.,

105, 5165 (1983).

62. (a) J. B. Kim, A. D. Alder & F. R. Longo in The Porphyrins, Vol. I, D. Dolphin, Ed., Academic Press, 1978, p. 85.

(b) J. B. Paine III in The Porphyrins, Vol. I, D. Dolphin, Ed., Academic Press, 1978, p.101.

(c) A. W. Johnson in The Porphyrins, Vol. I, D. Dolphin, Ed., Academic Press, 1978, p.235.

63. (a) T. P. Wijesekera, Ph. D. Thesis, University of British Columbia, 1979.

(b) T. P. Wijesekera, J. B. Paine III & D. Dolphin, J. Org. Chem., 53, 1345 (1988)

(c) T. P. Wijesekera, S. K. David, J. B. Paine III, B. R. James & D. Dolphin, Can. J. Chem., 66, 2063 (1988).

64. B. Morgan, Ph. D. Thesis, University of British Columbia, 1984.

65 T. P. Wijesekera & D. Dolphin, Synlett, 5, 235 (1990).

66. (a) A. D. Adler, F. R. Longo & W. Shergalis, J. Am. Chem. Soc., 86, 3145 (1964).

(b) A. D. Adler, F. R. Longo, J. D. Finarelli, J. Goldmacher, J. Assour & L. Korsakoff, J. Org. Chem., 32, 476 (1967).

67. J. E. Baldwin, M. J. Crossley & J. Debernardis, Tetrahedron, 38, 685 (1982).

68. G. Jones, Organic Reactions, 15, 204 (1967).

69. Organic Syntheses Collective, Vol. III, p.742.

70. W. Carruthers, Some Modern Methods of Organic Synthesis, 2nd Ed.; Cambridge University Press, 1978, p.6.

71. W. M. Weaver in The Chemistry of the Nitro and Nitroso Groups, Part II, Feuer Ed; Interscience Publishers, New York, 1970; pp. 1-48.

72. G. A. Olah & S. J. Kuhn, J. Am. Chem. Soc., 84, 3684 (1962).

73. (a) C. L. Coon, W. G. Blucher & M. E. Hill, J. Org. Chem., 38, 4243 (1973).

(b) Effenberger & Geke, Synthesis, 40 (1975).

74. U. A. Spitzer & R. Stewart, J. Org. Chem., 39, 3936 (1974).

75. The Sadtler Standard N.M.R. Spectra, Vol. 19, 12083M.

76. S. Uemura, A. Toshimitsu & M. Okano, J. C. S. Perkin I, 1076 (1978).

77. E. S. Gould in Mechanism and Structure in Organic Chemistry, Holt, Rinehart & Winston, New York, 1959; pp. 710-711.

78. J. B. Paine III & D. Dolphin, Can. J. Chem., 56, 1710 (1978).

79. H. W. Whitlock & R. Hanauer, J. Org. Chem., 33, 2169 (1968).

80. T. Neilson, H. C. S. Wood & A. G. Wylie, J. Chem. Soc., 371 (1962).

81. T. Severin, R. Schmitz & H.-L. Temme, Chem. Ber., 96, 2499 (1963).

82. P. Kniel, Helv. Chim. Acta., 51, 371 (1968).

83. E. J-H. Chu & T. C. Chu, J. Org. Chem., 19, 266 (1954).

84. A. R. Battersby, E. Hunt, E. McDonald, J. B. Paine III & J. Saunders, J. Chem. Soc. Perkin Trans. I, 1008 (1976).

85. A. Hayes, G. W. Kenner & N. R. Williams, J. Chem. Soc., 3779 (1958).

86. J.-J. Delpuech & D. J. Nicole, J. C. S. Perkin I, 570 (1977).

87. P. G. Farrell, F. Terrier & R. Schaal, Tetrahedron Letters, 26, 2435 (1985).

88. G. W. Kenner, J. Rimmer, K. M. Smith & J. F. Unsworth, J. C. S. Perkin I, 332 (1977).

89. R. Chong, P. S. Clezy, A. J. Liepa & A. W. Nichol, Aust. J. Chem., 22, 229 (1969).

90. H. Fischer and H. Hofelmann, Justus Liebigs Ann. Chem., 216, 533 (1938).

91. R. B. Woodward, Angew. Chem., 72, 651 (1960).

92. J. B. Paine III, R. B. Woodward & D. Dolphin, J. Org. Chem., 41, 2826 (1976).

93. E. Baciocchi & G. Illuminati, Tet. Lett., 15, 637 (1962).

94. E. Baciocchi, A. Clana, G. Illuminati & C. Pasini, J. Am. Chem. Soc., 87, 3953 (1965).

95. E. Baciocchi & G. Illuminati, Prog. Phys. Org. Chem., 5, 1 (1967).

96. K. H. Lee, Tetrahedron, 25, 4363 (1969).

97. P. S. Clezy & A. J. Liepa, Aust. J. Chem., 23, 2443 (1970).

98. P. S. Clezy, F. D. Looney, A. W. Nichol & G. A. Smythe, Aust. J. Chem., 19, 1481 (1966).

99. A. Treibs & H. G. Kolm, Liebigs Ann. Chem., 199, 614 (1958).

100 J. A. S. Cavaleiro, A. M. d'A. R. Gonsalves, G. W. Kenner & K. M. Smith, J. Chem. Soc. Perkin Trans I, 1771 (1974).

101. (a) R. J. P. Williams, Chem. Rev., 56, 299 (1956).

(b) K. M. Smith in "Porphyrins and Metalloporphyrins", K. M. Smith Ed., American Elsevier, New York, N. Y.,1975, p3.

102. (a) R. J. Abraham, P. A. Burbidge, A. H. Jackson & D. B. Macdonald, J. Chem. Soc. B, 620 (1966).

(b) T. R. Janson & J. J. Kate, J. Mag. Res., 6, 209 (1972).

103. (a) W. S. Caughey & W. S. Koski, Biochemistry, 1, 923 (1962).

(b) W. S. Caughey & P. K. Iber, J. Org. Chem., 28, 269 (1963).

104. (a) A. R. Battersby & A. Hamilton, J. Chem. Soc. Chem. Commun., 117 (1980).

(b) T. G. Traylor, C. K. Chang, J. Geibel, A. Berzinis, T. Mincey & J. Cannon, J. Am. Chem. Soc., 101, 6716 (1979).

105. (a) R. J. Abraham & K. M. Smith, Tet. Lett., 36, 3335 (1971).

(b) C. A. Busby & D. Dolphin, J. Magn. Res., 23, 211 (1976).

106. Beilsteins Handbuch der Organischen Chemie, Springer-Verlag.

(a) 9, 914d

(b) 9, 888c

(c) 9, III, 4324

(d) 6, III, 4724

(e) 9, IV, 3436

107. W. R. Linke & A. Seidell, Solubilities of Inorganic and Metal Organic Compounds, Van Nostrand: Princeton, N. J., 1958.

108. R. S. Drago, Physical Methods in Chemistry, W. B. Saunders, Philadelphia,

1977.

109. (a) A. V. Hill, J. Physiol (London), 40, IV-VII, (1910).

(b) P. E. Ellis, J. E. Linard, T. Szymanski, R. D. Jones, J. R. Budge & F. Basolo, J. Am. Chem. Soc., 102, 1889 (1980).

110. D. Brault & M. Rougee, Biochemistry, 13, 4598 (1974).

111. (a) T. G. Traylor, S. Tsuchiya, D. Campbell, M. Mitchell, D. Stynes & N. Koga, J. Am. Chem. Soc., 107, 604 (1985).

(b) B. Ward, C. Wang & C. K. Chang, J. Am. Chem. Soc., 103, 5236 (1981).

(c) T. Hashimoto, R. L. Dyer, M. J. Crossley, J. E. Baldwin & F. Basolo, J. Am. Chem. Soc., 104, 2101 (1982).

112. T. G. Traylor, M. J. Mitchell, S. Tsuchiya, D. H. Campbell, D. V. Stynes & N. Koga, J. Am. Chem. Soc., 103, 5234 (1981).

113. T. G. Traylor & A. P. Berzinis, Proc. Natl. Acad. Sci. U. S. A., 77, 3171 (1980)

114 J. P. Collman, J. I. Brauman, B. L. Iverson, J. L. Sessler, R. M. Morris & Q. H. Gibon, J. Am. Chem. Soc., 105, 3052 (1983).

Appendices

Appendix I Spectral data for the iron(II) capped systems

Fe(benzene-4/4)(DcIm)

λ_{max}(nm),	424	556
log ε,	4.74	3.94

Fe(benzene-5/5)(DcIm)

λ_{max}(nm),	420	548
log ε,	4.98	4.16

Fe(amidobenzene-4/4)(DcIm)

λ_{max}(nm),	424	548
log ε,	4.83	4.20

Fe(amidobenzene-5/5)(DcIm)

λ_{max}(nm),	424	548
log ε,	4.92	4.30

Fe(benzene-4/4)(DcIm)(CO)

λ_{max}(nm),	416	548
log ε,	4.93	4.00

Fe(benzene-5/5)(DcIm)(CO)

λ_{max}(nm),	416	534
log ε	5.31	4.14

Fe(amidobenzene-4/4)(DcIm)(CO)

λ_{max}(nm),	416	548	
log ε,	5.00	4.22	

Fe(amidobenzene-5/5)(DcIm)(CO)

λ_{max}(nm),	416	548	
log ε,	5.21	4.30	

Fe(benzene-4/4)(DcIm)(O_2)

λ_{max}(nm),	406	578	
log ε,	4.67	3.95	

Fe(benzene-5/5)(DcIm)(O_2)

λ_{max}(nm),	408	536	564
log ε,	4.96	4.12	4.13

Fe(amidobenzene-4/4)(DcIm)(O_2)

λ_{max}(nm),	406	580	
log ε,	4.79	4.17	

Fe(amidobenzene-5/5)

λ_{max}(nm),	408	536	564
log ε,	4.90	4.05	4.03

Appendix II Raw data for the binding of CO and O_2 to the capped hemes

The data were processed by least-squares analysis in all cases.

A CO affinity constant determination, K^{CO} in toluene at 20°C

[heme] ~ 3 x 10^{-6} M, [DcIm] ~ 0.3 M

(1) Fe(benzene-4/4)(DcIm) + CO

Preparation of CO/Ar mixture in glass bulb:

P^{CO} = 84 torr, P_{total} = 821 torr

λ_{max} = 416 nm, A_O = 0.574, A_∞ = 0.903

A	A_O - A	A - A_∞	$\log\frac{A_O - A}{A - A_\infty}$	P_{total} (torr)	P^{CO} (torr)	$\log P^{CO}$
0.634	0.060	0.269	-0.652	19.4	1.985	0.298
0.682	0.108	0.221	-0.311	42.1	4.297	0.633
0.728	0.154	0.175	-0.056	738	7.551	0.878
0.765	0.191	0.138	0.141	113.4	11.602	1.065
0.805	0.231	0.098	0.372	186.0	19.030	1.279
0.847	0.273	0.056	0.688	338.6	34.644	1.540
0.867	0.293	0.036	0.911	507.0	51.873	1.715

slope = 1.1 $P^{CO}_{1/2}$ = 8.2 torr

(2) Fe(benzene-5/5)(DcIm) + CO

Preparation of CO/Ar mixture in glass bulb:

Initial P^{CO} = 25 torr, P_{total} = 816 torr

Evacuation procedure:

P_{total}(after evacuation) (torr)	P_{total}(after refilling Ar)(torr)
296.4	827.0
307.6	814.0
281.0	823.6
293.6	821.0
290.0	817.6

Final P^{CO} = 0.1468 torr P_{total} = 817.6 torr

λ_{max} = 416 nm, A_O = 0.668, A_∞ = 1.194

A	A_O - A	A - A_∞	$\log\frac{A_O - A}{A - A_\infty}$	P_{total} (torr)	P^{CO} (torr)	$\log P^{CO}$
0.698	0.030	0.496	-1.218	20.6	0.00307	-2.432
0.737	0.069	0.457	-0.821	54.0	0.00970	-2.013
0.799	0.131	0.395	-0.479	120.6	0.0217	-1.664
0.876	0.208	0.318	-0.184	227.4	0.0408	-1.389
0.933	0.265	0.261	0.00661	342.0	0.0614	-1.212
0.984	0.316	0.210	0.177	497.0	0.0892	-1.049

slope = 1.0 $P^{CO}_{1/2}$ = 0.061 torr

(3) Fe(amidobenzene-4/4)(DcIm) + CO

Preparation of CO/Ar in glass bulb:

P^{CO} = 26 torr, P_{total} = 830 torr

λ_{max} = 416 nm, A_o = 0.534, A_∞ = 0.910

A	$A_o - A$	$A - A_\infty$	$\log\frac{A_o - A}{A - A_\infty}$	P_{total} (torr)	P^{CO} (torr)	$\log P^{CO}$
0.589	0.055	0.321	-0.766	20.4	0.639	-0.194
0.659	0.125	0.251	-0.303	59.0	1.848	0.267
0.747	0.213	0.163	0.116	157.4	4.31	0.63
0.789	0.255	0.121	0.324	245.4	7.687	0.886
0.816	0.282	0.094	0.477	344.8	10.801	1.033
0.848	0.314	0.062	0.705	527.4	16.521	1.218

slope = 1.0 $P^{CO}_{1/2}$ = 3.6 torr

(4) Fe(amidobenzene-5/5)(DcIm) + CO

Preparation of CO/Ar mixture in glass bulb:

Initial P^{CO} = 29 torr, P_{total} = 873 torr

Evacuation procedure:

P_{total}(after evacuation)(torr)	P_{total}(after refilling Ar)(torr)
320	816
287	816
377	828
292	818
283	812

Final P^{CO} = 0.2107 torr, P_{total} = 812 torr

λ_{max} = 416 nm, A_o = 0.495, A_∞ = 0.937

A	$A_o - A$	$A - A_\infty$	$\log\frac{A_o - A}{A - A_\infty}$	P_{total} (torr)	P^{CO} (torr)	$\log P^{CO}$
0.564	0.069	0.373	-0.733	20.0	0.0052	-2.285
0.641	0.146	0.296	-0.307	53.0	0.0138	-1.862
0.728	0.233	0.209	0.047	122.0	0.0317	-1.500
0.776	0.281	0.161	0.242	208.0	0.0540	-1.268
0.816	0.321	0.121	0.424	325.0	0.0843	-1.074
0.851	0.356	0.086	0.617	536.0	0.1391	-0.857

slope = 0.9 $P^{CO}_{1/2}$ = 0.03 torr

B CO affinity constant determination, K^{CO}, in toluene at varied temperatures

[heme] ~ 3 x 10^{-6} M, [DcIm] ~ 0.3 M

(1) Fe(benzene-4/4)(DcIm) + CO

(i) At 30.5°C, P^{CO} in glass bulb = 108.4 torr, P_{total} = 834 torr

λ = 418 nm, A_o = 0.519, A_∞ = 0.851

A	$A_o - A$	$A - A_\infty$	$\log\frac{A_o - A}{A - A_\infty}$	P_{total} (torr)	P^{CO} (torr)	$\log P^{CO}$
0.545	0.026	0.306	-1.017	21.4	2.78	0.444
0.572	0.053	0.279	-0.721	41.8	5.43	0.735
0.620	0.101	0.231	-0.359	85.4	11.10	1.045
0.654	0.135	0.197	-0.164	128.6	16.71	1.223
0.682	0.163	0.169	-0.016	186.2	24.20	1.384
0.766	0.247	0.085	0.463	532.0	69.15	1.840

slope = 1.1, $P^{CO}_{1/2}$ = 24.9 torr

(ii) At 15.5°C, P^{CO} in glass bulb = 58 torr, P_{total} = 822.8 torr

λ = 418 nm, A_o = 0.520, A_∞ =0.894

A	$A_o - A$	$A - A_\infty$	$\log\frac{A_o - A}{A - A_\infty}$	P_{total} (torr)	P^{CO} (torr)	$\log P^{CO}$
0.591	0.071	0.303	-0.630	22.8	1.607	0.206
0.627	0.107	0.267	-0.397	37.6	2.650	0.423
0.697	0.177	0.197	-0.046	80.0	5.639	0.751
0.774	0.254	0.120	0.326	184.0	12.970	1.113
0.813	0.293	0.081	0.558	291.0	20.513	1.312
0.846	0.326	0.048	0.832	515.6	36.345	1.560

slope = 1.1, $p^{CO}_{1/2}$ = 6.2 torr

(iii) At 9.7°C, P^{CO} in glass bulb = 39.4 torr, P_{total} = 841.8 torr

λ = 418 nm, A_o = 0.334, A_∞ = 0.600

A	$A_o - A$	$A - A_\infty$	$\log\frac{A_o - A}{A - A_\infty}$	P_{total} (torr)	P^{CO} (torr)	$\log P^{CO}$
0.375	0.041	0.225	-0.739	17.0	0.796	-0.099
0.436	0.102	0.164	-0.206	51.8	2.424	0.385
0.489	0.155	0.111	0.145	109.0	5.102	0.708
0.526	0.192	0.074	0.414	198.0	9.267	0.967
0.550	0.216	0.050	0.635	325.0	15.211	1.182
0.564	0.230	0.036	0.805	486.2	22.756	1.357

slope = 1.1, $P^{CO}_{1/2}$ = 3.8 torr

(iv) At 4.7°C, P^{CO} in glass bulb = 16.41 torr, P_{total} = 836.6 torr

λ = 418 nm, A_o = 0.414, A_∞ = 0.751

A	$A_o - A$	$A - A_\infty$	$\log\frac{A_o - A}{A - A_\infty}$	P_{total} (torr)	P^{CO} (torr)	$\log P^{CO}$
0.458	0.044	0.293	-0.823	16.8	0.329	-0.482
0.536	0.122	0.215	-0.246	62.6	1.228	0.089
0.577	0.163	0.174	-0.028	107.0	2.098	0.322
0.619	0.205	0.132	0.191	173.2	3.397	0.531
0.665	0.251	0.086	0.465	303.0	5.942	0.774
0.701	0.287	0.050	0.759	554.4	10.872	1.036

slope = 1.0, $P^{CO}_{1/2}$ = 2.1 torr

(2) Fe(amidobenzene-4/4)(DcIm) + CO

(i) At 5.10°C, P^{CO} in glass bulb = 10.7 torr, P_{total} = 831.0 torr

λ = 416 nm, A_o = 0.376, A_∞ = 0.734

A	$A_o - A$	$A - A_\infty$	$\log\frac{A_o - A}{A - A_\infty}$	P_{total} (torr)	P^{CO} (torr)	$\log P^{CO}$
0.433	0.057	0.301	-0.723	17.2	0.221	-0.655
0.510	0.134	0.224	-0.223	60.4	0.778	-0.109
0.589	0.213	0.145	0.167	134.0	1.725	0.237
0.628	0.252	0.106	0.376	241.4	3.108	0.493
0.648	0.272	0.086	0.500	333.2	4.290	0.632
0.674	0.298	0.060	0.696	500.4	6.443	0.809

slope = 0.97, $P^{CO}_{1/2}$ = 1.3 torr

(ii) At 10.5°C, P^{CO} = 35.8 torr, P_{total} = 835.2 torr

λ = 416 nm, A_o = 0.416, A_∞ = 0.749

A	$A_o - A$	$A - A_\infty$	$\log\frac{A_o - A}{A - A_\infty}$	P_{total} (torr)	P^{CO} (torr)	$\log P^{CO}$
0.475	0.059	0.274	-0.667	14.0	0.600	-0.222
0.545	0.129	0.204	-0.199	33.6	1.440	0.158
0.609	0.193	0.140	0.139	66.8	2.863	0.457
0.659	0.243	0.090	0.431	120.4	5.161	0.713
0.699	0.283	0.050	0.753	244.2	10.467	1.020
0.729	0.313	0.020	1.195	513.6	22.015	1.343

slope = 1.2, $P^{CO}_{1/2}$= 2.2 torr

(iii) At 15.5°C, P^{CO} in glass bulb = 35.4 torr, P_{total} = 820.0 torr

λ = 416 nm, A_o = 0.439, A_∞ = 0.813

A	$A_o - A$	$A - A_\infty$	$\log\frac{A_o - A}{A - A_\infty}$	P_{total} (torr)	P^{CO} (torr)	$\log P^{CO}$
0.511	0.072	0.302	-0.623	16.8	0.725	-0.140
0.564	0.125	0.249	-0.299	35.0	1.511	0.179
0.622	0.183	0.191	-0.019	64.8	2.797	0.447
0.684	0.245	0.129	0.279	126.0	5.440	0.736
0.732	0.293	0.081	0.558	229.0	9.886	0.995
0.777	0.338	0.036	0.973	509.0	21.974	1.342

slope = 1.1, $P^{CO}_{1/2}$ = 2.9 torr

(iv) At 29.5°C, P^{CO} in glass bulb = 100 torr, P_{total} = 846.6 torr

λ = 416 nm, A_o = 0.590, A_∞ = 1.002

A	$A_o - A$	$A - A_\infty$	$\log\frac{A_o - A}{A - A_\infty}$	P_{total} (torr)	P^{CO} (torr)	$\log P^{CO}$
0.627	0.037	0.375	-1.006	7.8	0.921	-0.036
0.725	0.135	0.277	-0.312	42.0	4.961	0.696
0.785	0.195	0.217	-0.046	71.0	8.386	0.924
0.847	0.257	0.155	0.220	120.0	14.174	1.152
0.928	0.338	0.074	0.660	280.6	33.144	1.520
0.970	0.380	0.032	1.075	508.8	60.099	1.779

slope = 1.1, $P^{CO}_{1/2}$ = 8.3 torr

C Van't Hoff plots for CO binding to Fe(benzene-4/4)(DcIm) and Fe(amidobenzene-4/4)(DcIm) systems

(1) Fe(benzene-4/4)(DcIm) + CO

K($torr^{-1}$)	ln K + ln 760	T(°C)	1/T(°K) x 10^3
0.0402	3.418	30.5	3.293
0.122	4.529	20.0	3.411
0.161	4.809	15.5	3.464
0.263	5.298	9.7	3.535
0.476	5.891	4.7	3.599

slope = $-\Delta H^o/R = 7.84 \times 10^3$

$\Delta H^o = -16 \pm 2$ kcal·mol^{-1}

Y-intercept = $\Delta S^o/R$ = -22.34

$$\Delta S^o = -44 \pm 7 \text{ cal·mol}^{-1}\text{K}^{-1}$$

(2) Fe(amidobenzene-4/4)(DcIm) + CO

K(torr^{-1})	ln K + ln 760	T(°C)	1/T(°K) x 10^3
0.7692	6.371	5.10	3.594
0.4545	5.845	10.50	3.525
0.3448	5.569	15.50	3.464
0.2632	5.298	20.00	3.411
0.1205	4.517	29.50	3.304

slope = $-\Delta H^o/R = 6.2 \times 10^3$

$$\Delta H^o = -12 \pm 3 \text{ kcal·mol}^{-1}$$

Y-intercept = $\Delta S^o/R$ = -15.9

$$\Delta S^o = -32 \pm 11 \text{ cal·mol}^{-1}\text{K}^{-1}$$

D O_2 affinity constant determination, K^{O2}, in toluene at -45°C

[heme] ~ 10^{-6} M, [DcIm] ~ 0.1 M

(1) Fe(benzene-4/4)(DcIm) + O_2

Preparation of O_2/Ar mixture in glass bulb:

P^{O2} = 267.4 torr, P_{total} = 838.0 torr

λ = 420 nm, A_o = 1.039, A_∞ = 0.652

A	$A_o - A$	$A - A_\infty$	$\log\frac{A_o - A}{A - A_\infty}$	P_{total} (torr)	P^{O2} (torr)	$\log P^{O2}$
0.992	0.047	0.340	-0.859	30.6	9.76	0.990
0.909	0.130	0.257	-0.296	97.0	30.95	1.491
0.814	0.225	0.162	0.143	241.8	77.16	1.887
0.737	0.302	0.085	0.551	513.0	163.69	2.214

slope = 1.1, $P^{O2}_{1/2}$ = 55.7 torr

(2) Fe(benzene-5/5)(DcIm) + O_2

Preparation of O_2/Ar mixture in glass bulb:

P^{O2} = 265.2 torr, P_{total} = 828.8 torr

λ = 420 nm, A_o = 1.182, A_∞ = 0.808

A	$A_o - A$	$A - A_\infty$	$\log\frac{A_o - A}{A - A_\infty}$	P_{total} (torr)	P^{O2} (torr)	$\log P^{O2}$
1.075	0.107	0.267	-0.397	28.0	9.0	0.952
0.947	0.235	0.139	0.228	119.8	38.3	1.584
0.893	0.289	0.085	0.531	249.2	79.7	1.902
0.858	0.324	0.050	0.812	469.8	150.3	2.177

slope = 0.98, $P^{O2}_{1/2}$ = 22.7 torr

(3) Fe(amidobenzene-4/4)(DcIm) + O_2

Preparation of O_2/Ar mixture in glass bulb:

P^{O2} = 150.0 torr, P_{total} = 822.6 torr

λ = 420 nm, A_o = 0.850, A_∞ = 0.543

A	$A_o - A$	$A - A_\infty$	$\log\frac{A_o - A}{A - A_\infty}$	P_{total} (torr)	P^{O2} (torr)	$\log P^{O2}$
0.742	0.108	0.199	-0.265	28.6	5.22	0.717
0.662	0.188	0.119	0.199	81.0	14.77	1.169
0.598	0.252	0.055	0.661	231.0	42.12	1.625
0.570	0.280	0.027	1.016	483.6	88.18	1.945

slope = 1.0, $P^{O2}_{1/2}$ = 9.5 torr

(4) Fe(amidobenzene-5/5)(DcIm) + O_2

Preparation of O_2/Ar mixture in glass bulb:

P^{O2} = 28.6 torr, P_{total} = 829.8 torr

λ = 420 nm, A_o = 1.137, A_∞ = 0.763

A	$A_o - A$	$A - A_\infty$	$\log\frac{A_o - A}{A - A_\infty}$	P_{total} (torr)	P^{O2} (torr)	$\log P^{O2}$
1.038	0.099	0.275	-0.444	27.2	0.937	-0.028
0.966	0.171	0.203	-0.074	66.8	2.302	0.362
0.885	0.252	0.122	0.315	174.8	6.025	0.780
0.837	0.300	0.074	0.608	363.2	12.518	1.098

slope = 0.93, $P^{O2}_{1/2}$ = 2.8 torr